Unione europea
Fondo sociale europeo

REGIONE AUTONOMA DELLA SARDEGNA

FSE 2007-2013
POR SARDEGNA
obiettivo competitività regionale e occupazione

Università degli Studi di Cagliari

DOTTORATO DI RICERCA

IN PROGETTAZIONE MECCANICA

Ciclo: XXVIII

TITOLO TESI

EXPERIMENTAL AND NUMERICAL INVESTIGATIONS TO ASSESS THE BEHAVIOUR OF A BURIED PIPELINE IN AREAS WITH HIGH GEOLOGICAL INSTABILITY

Settore/i scientifico disciplinari di afferenza

ING-IND/14

Presentata da: **Giacomo Fenza**

Coordinatore Dottorato **Prof. Natalino Mandas**

Tutor Prof. Massimiliano Pau

Esame finale anno accademico 2014 – 2015

“This page is intentionally left blank”

DEDICATION

"… to Alessandra"

© Giacomo Fenza 2015

“This page is intentionally left blank”

Abstract

Ground displacements such as landslides, fault movements, soil liquefaction which may be caused by seismic activity are one of the most dangerous phenomena that can involve buried pipelines, e.g. for oil and gas transportation, or water and sewage. This aspect is currently an important part of research and a challenge for lifelines owners that are interested in prevent or limit pipeline damages.

Within the framework of GIPIPE[1] research program (SAFETY OF BURIED STEEL PIPELINES UNDER GROUND-INDUCED DEFORMATIONS) new full-scale facilities have been developed and adopted in order to investigate pipe-soil interaction mechanism (in particular sand and 8" $^{5/8}$ X65 steel pipes). The new experimental facilities have been designed to perform two groups of tests: simple interaction tests (axial pullout and transversal pullout test) and complex interaction tests (reproducing a pipeline crossing landslide). A system of steel containers (stationary and fixed) in which pipe samples are buried within the sand, have been assembled. Numerical analyses have been performed using strength parameters of sand and steel obtained from laboratory testing and subsequently validated by means full-scale experimental results.

The outcomes of the experimental activity showed some differences in soil reaction on pipe by increasing the relative density of soil filling and using a smoother coating.

[1] A research project sponsored by European commission (Rfsr-ct-2011-00027)

Moreover peak soil resistances estimated with equations suggested by ASCE guidelines [4] cannot predict satisfactory measured axial and lateral soil reactions. This is a confirmation of previous studies in which was evidenced the effect of soil dilation in the annular soil zone around the pipe during axial relative movement between pipe and soil causes an increase of the normal stress at pipe soil interface, in particular the horizontal direction is significantly constrained by the surrounding soil mass leading to an higher increase in lateral soil stress in this direction respect to the vertical direction. Therefore this phenomenon leads to a lateral earth pressure coefficient K which is greater than K_0 (coefficient of pressure at rest) as suggested in the ASCE guidelines [4], therefore for a better estimation of soil response using that equation it is suggested to measure the ratio between horizontal stress and the vertical stress during a full-scale axial pullout test.

Pipes submitted to lateral soil displacement with a constrained uplifting show as expected a greater soil reaction than that estimated by ASCE [4] and PRCI [20].

As far as the landslide/fault test are concerned, the maximum soil relative density (D_r) achieved during experimental tests performed in this study was around 40%. This level of density led to a low stiffness of soil mass hence a limited global deformation of a 24 m embedded pipe during landslide/fault tests in which one caisson was moved up to 4 m respect to the initial position. These experimental findings confirm that sand with a low value of maximum achievable density may prevent from high loads developing on pipelines, in contrast to native soil which can apply higher loads.

Numerical analyses and their validation gave us a suitable instrument to estimate the pipe soil response for large ground displacements phenomena.

Table of contents

© *Giacomo Fenza 2015*

List of figures

“This page is intentionally left blank”

Nomenclature

α_{gw} = Girth weld factor

α_h = Yield strength to Tensile Strength ratio

D = Pipe outer diameter

D_A = Pipe axial displacement

D'_A = Normalized pipe axial displacement

D_L = Pipe lateral displacement

D'_L = Normalized pipe lateral displacement

δ_x = Horizontal displacement (referred to direct shear testing)

D_{max} = Maximum pipe outer diameter

D_{min} = Minimum pipe diameter

D_r = Relative density

D/t = Diameter to wall thickness ratio

ε_a = Axial strain

ε_b = Bending strain

ε_c = Critical strain

ε_+ = Compressive strain

ε_- = Tensile strain

f = coating dependent factor

ϕp = Peak internal friction angle

ϕr = Residual internal friction angle

γ = Soil density

γ^P = Plastic shear strain

H = Burial depth of the pipe springline

H/D = Overburden ratio

HDPE = High-density polyethylene

H_{FE} = Height of FE element

H_S = Height of soil specimen (referred to direct shear testing)

K = Coefficient of lateral pressure

K_0 = Coefficient of lateral pressure at rest

L = Pipe length

N_{qh} = Horizontal bearing capacity factor

OD = Pipe outer diameter

ψ = Dilation angle

P_L = Lateral soil resistance (ASCE [4] and PRCI [20])

P'_L = Normalized lateral soil resistance (referred to P_L)

R_A = Axial soil resistance

R'_A = Normalized axial soil resistance

R_L = Lateral soil resistance

R'_L = Normalized lateral soil resistance

R_{LP} = Peak lateral soil resistance

R_{LR} = Residual lateral soil resistance

R'_{LP} = Normalized peak lateral soil resistance

R'_{LR} = Normalized residual lateral soil resistance

T_A = Axial soil resistance (ASCE [4] and PRCI [20])

T'_A = Normalized axial soil resistance (referred to T_A)

w = Water content

WT = Pipe wall thickness

Acknowledgements

Giacomo Fenza gratefully acknowledges Sardinia Regional Government for the financial support of his PhD scholarship (P.O.R. Sardegna F.S.E. Operational Programme of the Autonomous Region of Sardinia, European Social Fund 2007-2013 - Axis IV Human Resources, Objective l.3, Line of Activity l.3.1.)

It is a great pleasure to express my gratitude to everyone who assisted and supported me through completing this thesis.

My sincere gratitude is extended to my supervisor, Professor Massimiliano Pau for his guidance during these years of work and for providing me the opportunity to freely choose my route.

In addition, I am grateful to Centro Sviluppo Materiali S.p.A. for giving me the opportunity to actively participate in the GIPIPE research program where full-scale tests on buried steel pipelines were performed, which are essential for the quality of this work. Especially I would like to thank Jan Ferino (Senior researcher at Centro Sviluppo Materiali) who has provided me with his invaluable experience and knowledge in pipeline research as well as his valuable time. Furthermore, his useful feedback played an important role to help me through my research program.

Moreover, I would like to express my deep and sincere gratitude to Professor George Gazetas (NTUA) who hosted me in his laboratory of soil mechanics for several months, to enhance my skills in numerical modeling of soil. I would also like to thank Angelos Tsatsis who helped me through his knowledge in those months of work.

I would also like to extend my thanks and appreciation to technical staff of the Centro Sviluppo Materiali laboratories, which includes Stefano Maddi, Luigi Piredda, Rossano Cabras, Nicola Secci, Nicola Corongiu, Andrea Granata, Stefano Monni, Marco Manunza, Aldo Lotta, Samuele Ennas, and Andrea Cannas.

Last but not least, I would like to thank my girlfriend, Alessandra, and my parents for their support during this period.

1. Introduction

1.1. Background

The safe transportation of fluids such as oil and gas by means pipelines is essential to justify this way of energy transmission. Citizens and environment must be protected as much as the technology can from possible accidents and pollution that can involve lifelines. Furthermore pipelines play an important role in our present economy, highlighted from the thousands of meters of pipes laid each year both onshore and offshore.

The extension of these transmission networks forces these lines to transit in areas with geological instabilities. Permanent ground displacements such as faulting, landslides, displacements due to liquefaction may undergo pipelines to high soil loads and hence unacceptably level of strains.

The modes of relative displacement between pipe and soil could be categorized as: horizontal lateral, longitudinal axial, vertical uplift and vertical bearing. The global deformations of pipelines may include two or more modes of relative displacements just described and due to the constrain applied on the pipe from the undeformed ground it is possible to have bending, shear, tension or compression and hence high levels of strains sometimes responsible of severe damage of the pipe section leading to a unserviceability and hazards for beings and environment.

Different global deformations of pipelines are shown in Fig. 1 ad Fig. 2, for landslide and fault phenomenon respectively. The restraints, stress, strains on the pipe section are function of pipeline orientation respect to the ground movement. When a pipe is perpendicular to the direction of landslide, the pipe is subjected mainly to bending and shear load Fig. 1 a). In case of pipe parallel to the landslide displacement, the pipeline is subjected both ten-

sion and compression combined with bending (Fig. 1 c)). The oblique interaction depicted in Fig. 1 b) is an intermediate condition between perpendicular interaction and parallel interaction.

A pipe involved in a fault event is subjected to bending moment and shear loads in any case, but the cross section is mainly subjected to tension in normal fault (Fig. 2 d)), compression in reverse fault (Fig. 2 e)) and either tension or compression in a strike slip fault depending on the pipe orientation respect to the fault plane as shown in Fig. 2 f).

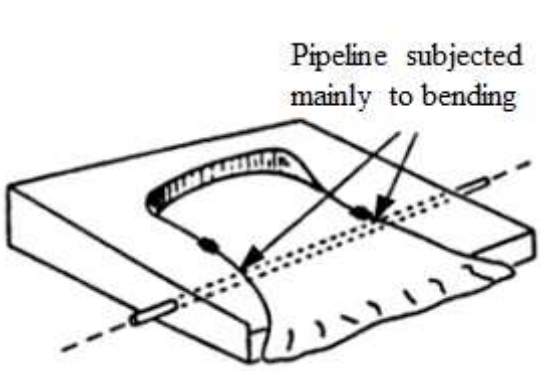

a). Perpendicular crossing interaction.

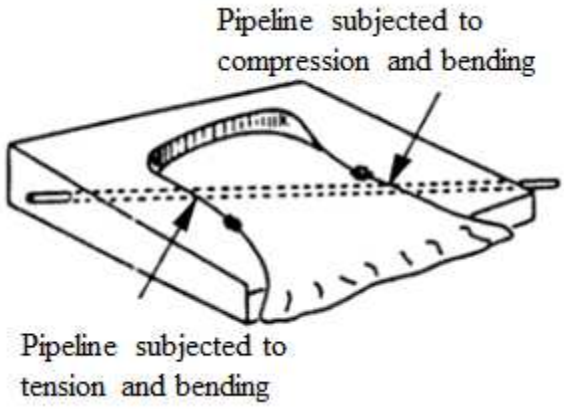

b). Oblique crossing interaction.

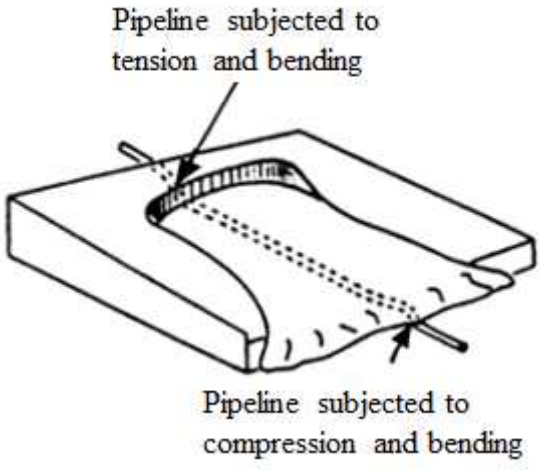

c). Parallel crossing interaction.

Fig. 1. Principal modes of pipeline-soil interaction during landslide phenomenon [17].

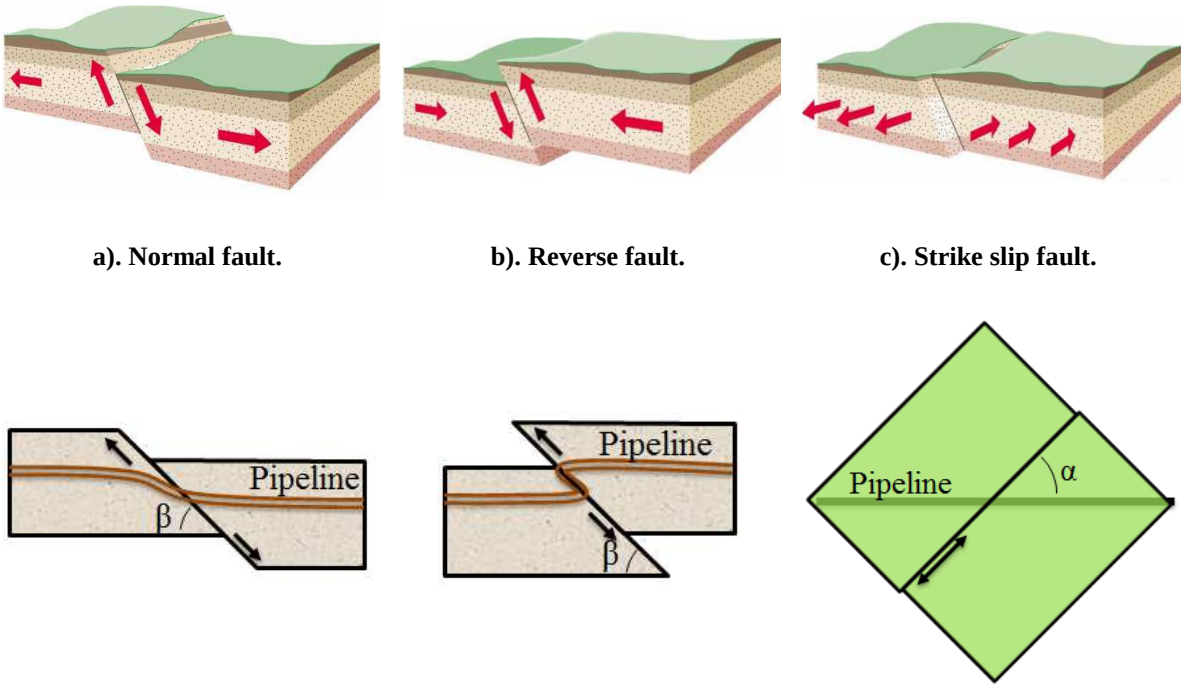

a). Normal fault. **b). Reverse fault.** **c). Strike slip fault.**

d). Normal fault. **e). Reverse fault.** **f). Strike slip fault.**

Fig. 2. Principal modes of pipeline-soil interaction during fault phenomenon [39].

In case of displacement due to liquefaction such as settlement the pipe may bend in the vertical plane and subjected to tension and shear stress mainly where the pipe is restrained by the undeformed ground.

1.2. Aim of this thesis

The purpose of this study has been to understand the soil-pipe behavior during horizontal relative displacements taking advantage of full-scale testing activity that Centro Sviluppo Materiali S.p.A. performed within the GIPIPE research program (SAFETY OF BURIED STEEL PIPELINES UNDER GROUND-INDUCED DEFORMATIONS). Besides, to de-

velop and validate reliable numerical models to be adopted in order to extend the results of experimental tests to different pipe-soil interaction conditions characterized by different pipe diameter and pipe burial depth.

Expressly the objective is:

- Study the response of a steel pipe embedded in a given soil subjected to axial displacement, the response of steel pipe subjected to lateral displacement and the response of a pipe exposed to landslide/fault scenario.

- Evaluate the analytical relations given from current guidelines for design of pipelines in areas with geological instabilities in comparison with full-scale results.

- Develop and validate numerical models of axial pipe soil interaction, lateral pipe soil interaction and pipeline exposed to landslide/fault.

To reach this goal several activities at laboratories of Centro Sviluppo Materiali were carried out:

- Realization of a steel caisson to perform axial and lateral pipe soil interaction housed within a stiff frame of the experimental devices equipped with a 2500 tons actuator.
- Realization of three caissons, two of which fixed and one movable to perform the landslide/fault tests in an area designed to perform bend test on 48” pipe.

- Performing axial and lateral pulling varying the pipe coating and the soil compaction.
- Performing four landslide/fault tests on a 24 m long buried pipeline, varying the soil compaction and the pipe internal pressure.
- Development of numerical models with finite element method, to capture full-scale testing results. This included calibration and validation of the model.
- Comparison of experimental result with ASCE guidelines [4], PRCI guidelines [20].

Preliminary geotechnical tests were performed on sand samples (the same used in the full-scale experiments) at the laboratory of NTUA (National Technical University of Athens) and at laboratory of University of Cagliari.

2. Literature review

2.1. Horizontal axial pipe soil interaction

Only few experimental studies on horizontal axial pipe soil interaction are published in literature. Those found have been performed on embedded pipes by means full-scale tests and carried out dealing with: maximum horizontal soil force and force-displacement relationship, effect of soil dilation in the increasing of normal stress at pipe-soil interface.

Paulin et al. [19] performed some full-scale axial tests on steel pipe embedded in sand and some other tests on steel pipe embedded in clay. The sand used during testing was well-graded with a maximum grain size of 4-5 mm, a uniformity coefficient of 4, and a coefficient of curvature equal to 0.8. Two level of soil compaction were tested relative density (D_r) around 0% and around 100%. To prepare the loose sand testbed the sand was slumped from a container; to prepare the dense sand testbed soil was placed in 100 mm layers and compacted with a vibratory tamper. The displacement rate used during sand tests was 10 mm/hour. Experimental findings have shown that the effect of difference in relative densities on the interaction was significant but load-displacement data value were omitted. Load displacement curve are expressed in percent, giving 100% to the maximum load achieved during tests in dense sand. All curves both for loose and for dense condition do not present a prominent peak load but a constant soil reaction after attainment the maximum reaction. The maximum soil reaction in loose conditions was 30% of maximum soil reaction reached in dense conditions. Dimensions of equipment and properties of soil were not published

Wijewickreme et al. [32] performed four axial pullout tests on a blasted-steel pipe with 457 mm outside diameter in loose and dense river sand. The pipes were subjected to axial

pullout with direct measurement of axial soil reaction and soil pressure at pipe soil interface. These authors presented the results from their experiments and interpretations with support from numerical modeling.

The test setup was mainly composed of a 3.8 to 5.0 m length x 2.5 m width x 2.5 height caisson, hydraulic actuator, and a data acquisition system. The length of the pipeline test specimen was kept longer than the length of the caisson so that the pipe extended through both ends of the soil caisson.

In all test configurations, the pipe was loaded in a displacement-controlled manner and the displacement rate chosen varied between 2 to 50 mm/s. Test results indicated that the loading rates selected had no noticeable effect on the results.

In some of these tests, the normal soil stress on the pipe was measured using five total-pressure transducers mounted at selected circumferential locations. The intent was to measure changes of normal soil stress acting on pipe cross section while filling the caisson, during compaction of the backfill soil and when subjecting the pipe to the axial loading.

Fraser river sand was used in their experiments with minimum and average grain size respectively of 0.074 and 0.23 mm, and a coefficient of uniformity equal to 1.5. A peak internal friction angle between 43.5° and 45.5° was measured through the tests conducted at a relative density of ~75% and vertical stress ranging from 15 to 50 kPa furthermore a constant volume friction angle in the range of about 31° and 33° were measured.

Steel pipe with outside diameter of 457 mm and a 12.7 mm wall thickness was used. the surface of the pipe was prepared by sand-blasting prior to testing.

The interface friction angle between sand-blasted steel and Fraser river sand was also measured giving values of 33° and 36° for loose and dense sand respectively.

Three tests were performed at relative density of 75% and one at 25%, with a buried pipe length of 3.8 m except for one test in dense sand that had a buried pipe length equal to 5.0 m. The H/D ratio was kept constant at 2.5 for tests performed with dense sand; test in loose sand was performed with H/D ratio of 2.7 to provide a vertical effective stress at the pipe level nearly the same as that for tests with dense sand.

Essentially identical load displacement response were obtained by two tests performed with dense sand and different length of buried pipe length suggesting that any affect arise from the boundary conditions. Moreover confirmation of this, earth pressure measurements conducted on the front and rear walls during axial pullout testing did not indicate any detectable change in pressure.

A slightly higher peak load soil resistance was obtained with axial pullout test in dense sand performed after 45 days from the date of specimen preparation.

Normalized value of soil reaction between 1.02 and 1.13 were reached in dense sand tests and 0.42 during tests in loose sand.

Authors of this study conducted also comparison of experimental results with ASCE [4] predictions showing that dense-sand tests exhibit much higher axial resistance than that predicted using equation suggested from ASCE. This is in contrast with the results of loose sand test that is in good agreement with the predictions made using the same approach.

Coefficient of lateral pressure at rest k_0 used in aforementioned equation has been object of analysis. A back calculation of K instead the use of K_0 was carried out and a value between 1.8 and 2.2 was necessary to obtain correspondence with peak axial resistance from tests conducted with dense sand.

Measurements with pressure transducers during experiments prove that the average normal stresses on the pipe with dense sand are significantly higher in comparison to the at-rest

values. The largest stress increase appears to have occurred at the springline, whereas the normal distribution on the pipe during pullout in test conducted with loose sand did not change significantly from those observed under at-rest conditions.

The values of K determined using these two approaches are compared show a general agreement.

The change in normal stress during pipe pullout was explained by the authors in terms of dilation of the annular soil zone around the pipe. Dense sand would exhibit a tendency to dilate as it undergoes shear deformations at the interface during pullout and the tendency to dilate in the horizontal direction is significantly constrained by the surrounding soil mass, leading to the observed increase in lateral soil stress at the springline of the pipe.

Using FLAC 2D a 2D plane strain model was developed to represent the effect of dilation in the shear zone at the pipe-soil interface can provide the means of determining suitable K values for use in ASCE equation under different soil dilation levels, pipe diameters, burial depths ratios, etc., instead of full-scale testing. In the numerical model, the dilation of the shear zone was simulated through expansion of the pipe in radial direction. The computed normal stresses on the pipe after applying such expansion to the interface were in good agreement with normal stress measurements during axial pullout of the pipe.

2.2. Horizontal lateral pipe soil interaction

Experimental studies have been performed on embedded pipes by means small scale tests, full-scale tests and centrifuge test. In particular full-scale of lateral pulling tests have been carried out dealing with: maximum horizontal soil force and force-displacement relation-ship. Several parameters were varied in order to investigate the variation of soil resistance, the burial depth, the outside diameter of pipe (hence the overburden ratio H/D), the soil

compaction, the shape of trench, material and coating of pipe. Trautmann and O'Rourke [24] tested full-scale steel pipe embedded in filter sand for H/D ranging from 1.5 to 11 and for each overburden ratio three levels of soil compaction were tested: loose 14.8 kN/m^3, medium 16.4 kN/m^3 and dense 17.7 kN/m^3. The effect of pipe surface friction have been assessed by covering the pipe with sandpaper and a plastic film in order to simulate rough and smooth surfaces. Summarizing their results, density has a small effect on peak normalized[2] soil resistance (R'_{LP}) for depths less than four diameters. As depth increase, R'_{LP} for dense sand increase significantly respect to loose and medium sand, moreover R'_{LP} for loose and medium sand reach a constant value at H/D around eight. The most significant result is that R'_{LP} for loose and medium sand is nearly equal at all depths tested. Increasing the overburden ratio residual normalized force (R'_{LR}) is nearly the same for all tested densities, there is only a constant increase in the difference between dense and medium density but never more than 12%. After H/D = 8 R'_{LR} for dense sand becomes to increase substantially respect to medium compaction.

The effect of surface roughness, determined as explained above, lead to a difference in R'_{LP} equal to 10% between rough pipe and smooth pipe. The effect of size implies a R'_{LP} 8% higher for tests on 324 mm diameter pipe when compared with 102 mm diameter pipe in condition of loose sand. Only one comparative test in dense sand has been performed and it showed a difference of 1%.

The dimensionless displacement (lateral displacement/diameter) associated with maximum force, is difficult to define for loose and medium sand because of the gradual increase in

[2] Normalized soil resistance will be defined later.

horizontal resistance with large displacement. For dense sand this ratio ranges from 0.1 to 0.25.

Karimian [13] tested full-scale steel pipe embedded in river sand for H/D ranging from 1 to 2.75 with one level of soil compaction equal to 15.7 kN/m^3, this level of compaction was associate with relative density equal to 75%. Uncovered sandblasted pipe surface was used for all tests conducted in a caisson mimicking a rectangular cross section trench. In all cases the peak of soil resistance was slightly greater than the residual resistance. Two dimension of pipe (457 mm and 324 mm) were used for the same H/D = 1.92 and the difference in residual resistance was around 14%. The other tests conducted with 324 mm diameter pipe with H/D equal to 1, 1.92 and 2.75 shows an increment of soil reaction equal to 17% from the first to the second overburden ratio and 42% from the first to the third overburden ratio. Also a pressure cell were placed around the pipe for one test showing clearly a peak of normal stress at about 0.075D of lateral displacement and a residual behaviour at 0.2D. Moreover tests on trapezoidal cross section caisson were performed, with native soil for the slope of the trench, rigid trench slope uncovered and covered with geotextile fabric. The pipe was placed near the slope and the reaction of soil shows a constant increasing after the yielding point of the curve. The geotextile layer lead to a reduction of soil reaction from 15% to 20%.

Finite element modeling using ABAQUS validate by large-scale test on pipe-soil lateral interaction are available in literature. The model of Jung et al. [12] is based on an elasto-plastic characterization of the soil, with Mohr Coulomb strength parameters and with strain softening adjustments proposed by Anastasopoulos et al. [2]. In this work plain-strain model strength parameters are obtained through the results of performed direct shear tests. The finite element analyses were performed with infinite elements and finite elements:

eight-node biquadratic plane strain quadrilateral, reduced integration elements (element type CPE8R) have been used for the soil around the pipe and five-node quadratic, plane strain, one way infinite quadrilateral elements (element type CINPE5R) have been used to represent the semi-infinite soil medium. The interface interaction is modelled through surface based contact, in which separation and slip between soil and pipe are allowed. Geostatic load was applied to the soil at the beginning of the analysis under K = 1. After the validation of the model Jung et. al. conducted a parametric analysis varying the overburden ratio from 3.5 to 100, with the diameter of the pipe held constant at 102 mm for dry medium, dense, and very dense sand. The simulated lateral pulling tests shows that the normalized peak soil resistance reaches a maximum value at H/D = 15÷20 and then decreases with increasing H/D. From H/D = 15 to 100 the peak soil resistance decreases approximately by 0.6, 3.3 and 3.1% for medium, dense and very dense sand respectively. Between H/D = 15 and 20, normalized peak soil reaction reaches its limiting values of approximately 15, 18 and 20 for medium, dense and very dense sand, respectively, also this work pointed out a steeply increase of peak soil reaction at shallower depths and remains relatively constant once H/D reaches a critical embedment ratio. Moreover the FE results show that at depths of 15 ÷ 23 H/D, the soil movement around the pipe becomes symmetric.

In the research of Yimsiri et. al. [34], lateral pulling finite element model have been validated by means Trautmann experiments [24]. Two different soil models are used for their simulations: Mohr Coulomb model and Nor-Sand model that allows better simulation of the stress dilatancy behaviour of soil than Mohr Coulomb. Models have been validated on two level of overburden ratio H/D = 2 and H/D = 11.5, with a 102 mm pipe diameter. The distance between the bottom boundary and the pipe were kept the same both for numerical mesh and tank experiments and the examinations showed that the interference by the bot-

tom boundary is insignificant. The soil and the pipe were represented by eight node bi-quadratic, reduced integration continuum elements. The analysis was performed in plane strain and dry conditions. FE analyses results showed a good agreement with experimental findings in which Nor-Sand model gives a stiffer response. It is noted that numerical results for the force-displacement curves from Nor-Sand agree very well with experimental data. Moreover peak dimensionless forces obtained from FE results were compared with the experimental data showing a good agreement for both Mohr Coulomb and Nor-Sand models. Additional FE analyses were performed for deeper overburden ratios from 14.5 to 100 to examine the transition of the peak dimensionless forces from the shallow to deep failure mechanisms. The FE results show that the peak dimensionless forces increase approximately linearly with the overburden ratio at shallow embedment conditions and reach their maximum values at a certain embedment ratio after which the peak dimensionless forces are approximately constant with the increasing of embedment ratio. The depth at which this transition occurs is called the critical embedment depth, and the constant peak dimensionless force is called the critical peak dimensionless force. In this study the critical embedment ratio for medium sand is H/D = 12 with the corresponding critical peak dimensionless force of 14, for dense sand H/D = 16 with the corresponding critical peak dimensionless force equal to 28. In conclusion Nor-Sand model is able to simulate the softening behaviour of the sand which cannot be achievable using Mohr Coulomb, but the peak forces of both models are reasonably similar.

2.3. Landslide/fault pipe soil interaction

The combination of aforementioned modes of relative displacement between pipe and soil may be originated by landslides, fault movements, liquefaction-induced lateral spreading, subsidences and so on.

Permanent ground deformations are arguably the most severe hazard for continuous buried pipelines and the major contribution of the research in this field focuses on fault movements. Several works have been conducted by means numerical analyses and small-scale tests but just few studies have been conducted by full-scale tests.

Experimental studies have been performed on embedded pipes by means small scale tests, full-scale tests and centrifuge test. Several conditions have been taken in to account in these studies such as angle of fault, material of embedment, moisture content, pipeline materials, pipe internal pressure.

Ha et al. [7] [8] performed centrifuge investigation on buried high-density polyethylene (HDPE) pipelines subjected to strike slip and 90° normal faulting. The first work [7] debate on the differences in behaviour of buried HDPE pipelines subjected to strike slip and 90° normal faulting. The fault offset was simulated using a split-box container having dimensions: 1.14 m x 0.76 m x 0.20 m. The pipes used has an outside diameter D = 33.4 mm and a wall thickness t = 1.96 m for a D/t = 17. All centrifuge tests were performed at gravity level of 12.2g, therefore the model pipe geometry simulates a prototype pipe with D = 407.5 mm and WT = 24 mm.

The two strike-slip faults were carried out with the pipe axis inclined of 85° respect the fault line (considering the plan view) and the two 90° normal faults were carried out with the pipe axis perpendicular to the fault plane. During the test the movable portion of the

container was offset horizontally of 1.06 m (in prototype scale) in the strike-slip tests and was offset vertically of 0.48 m in the normal faulting tests.

To monitor pipeline response during fault offset two types of measurement sensors were used in separate experiments. A specimen was instrumented with strain gauges along the pipe springline to measure the longitudinal strain distribution on both sides of the pipe for the first strike-slip experiment. On specimen used for the first normal fault testing, strain gauges were attached at crown and invert of the pipe to capture the longitudinal strains due to container offset in the vertical plane. The other specimens were instrumented with two tactile pressure sensor sheets manufactured by TEKSCAN. The sensor sheets were wrapped around the test pipes for a longitudinal distance of 0.25 m in model scale (3 m in prototype scale) on either side of the fault. The pressure sensor sheet measures the pressure at soil-pipe interface.

The pipeline was connected to the split container and walls using spherical bearings leaving free three dimensional rotations.

The soil used in these tests was a sieved and well-graded glaciofluvial sand that was placed at water content of about ~4% and compacted in layers to a dry unit weight of 14.7 kN/m^3 and to a depth H of 1.12 m (in prototype scale) having H/D equal to 2.8. The compacted sand has a relative density of about 82% and an internal peak friction angle of 40°. After the tests, analyses of data results showed that axial strains for strike-slip faulting are nominally symmetric with respect to the fault. Also beyond ~2 m from the fault, there is a linear decrease in axial strain with distance from the fault. The peak axial strain for the strike-slip case is located at around ±1 m from the fault at the maximum offset of 1.06 m. In contrast, for the normal faulting case the axial strain distribution is not symmetric. Axial strains are

larger on the up-thrown side and located at -1 m from the fault at the maximum box offset of 0.48 m.

For a given strike-slip fault offset, the bending strains are in agreement with double curvature bending, concave on one side of the fault and convex on the other. In contrast, as expected, the bending strain distribution is not symmetric for the case of normal faulting. Bending strains are larger on the up-thrown side with the peak value located at about -1 m from the fault at maximum offset, which is the approximate location of the peak axial strain at the same offset. For the normal faulting case, the peak bending strains on the up-thrown side are larger than those on the down-thrown side. For fault offsets larger than about 0.3 m, the peak bending strain in the strike-slip case is approximately equal to the average of the values for the up-thrown and down-thrown sides for the normal fault case.

It is noticeable that the peak axial strain versus fault offset plots for both the strike-slip test and the normal offset test more or less follow the same curve. On the other hand the peak bending strain versus fault offset plots for the strike-slip and normal tests do not follow the same curve.

The peak axial strain and the peak bending strain measured in the strike-slip test are respectively ~1% and ~1.5%, while the peak axial strain and the peak bending strain measured in the normal test are respectively ~0.75% and ~1.5%.

The pipe lateral force was measured using a tactile pressure sensor. The measured pipe lateral force distributions were in agreement with the strain gauge measurements. For the normal faulting case the pipe lateral force distribution is not symmetric and there is a concentration of lateral force on the up-thrown side of the pipe. For the strike-slip faulting case the pipe lateral force distribution is symmetric. The peak lateral forces per unit length at the soil–pipe interface are compared with the suggested values in the ASCE guidelines [4].

For strike-slip faulting the experimental p–y relation was softer than the ASCE relation; the difference being attributed to reduced compaction of soil near the pipe in the experimental models. On the other hand, the measured ultimate soil resistance (transverse horizontal) was generally consistent with that provided in the ASCE guidelines. For normal faulting both the ASCE suggested peak force and stiffness values (transverse vertical, downward) are much higher than those measured experimentally. It is believed that these differences are attributable to the fact that for normal faulting the soil deformation is three-dimensional while ASCE guidelines assume two-dimensional.

Vazouras et al. [28] performed an accurate analysis on the mechanical behaviour of buried steel pipes crossing active strike-slip faults. The investigation is based on numerical simulation of the nonlinear response of the soil pipeline system through finite elements using ABAQUS.

This work considered buried steel pipelines crossing the vertical fault plane at several angles. Moreover mechanical behaviour of buried steel pipelines was examined with respect to appropriate performance criteria, expressed in terms of local strain and cross sectional deformation. Pipes from two steel grades X65 and X80 are considered for typical values of diameter to thickness ratio D/t ranging from 57.6 to 144, in both cohesive and non-cohesive soils. The behaviour of internally pressurized pipes with respect to non-pressurized pipes is also examined.

The pipeline is embedded in an elongated soil prism. Four-node reduced integration shell elements are employed to modeling the pipeline segment and eight-node reduced integration brick elements are used to modeling the surrounding soil. The overburden ratio was chosen equal to 2, the prism length in the x direction is at least 65 pipeline diameters. The analysis was conducted in two steps gravity loading is applied first and subsequently then

fault movement is imposed, using a displacement-controlled scheme. For the case of pressurized pipelines an intermediate step of internal pressure application is considered (after the application of gravity and before the fault displacement is activated).

A large von Mises plasticity model with isotropic hardening is employed for the steel pipe material. Besides the mechanical behaviour of soil material is described through an elastic-perfectly plastic Mohr Coulomb constitutive model, characterize by cohesion, friction angle, elastic modulus and Poisson's Ratio. The dilation angle was assumed equal to zero for all cases.

The interface between the outer surface of the steel pipe and the surrounding soil is simulated with a contact algorithm, which allows separation of the pipe and the surrounding soil, and accounts for interface friction, through an appropriate friction coefficient.

Numerical results are obtained in this work using outer diameter equal to 914.4 mm and four values of the pipe wall thickness: 6.35 mm, 9.53 mm, 12.7 mm and 15.88 mm, corresponding to D/t values equal to 144, 96, 72 and 57.6 respectively. The soil-pipeline has dimensions of 60 m x 10 m x 5 m and the fault plane passes through the middle cross-section of the pipeline and crosses the pipeline axis at different angles, so that the value of angle between pipe axis and fault trace ranges between -10° to 45°, in which the minus sign indicates a configuration where the pipeline is subjected to global compression.

Non pressurized and pressurized pipelines are analysed with cohesive and non-cohesive soil conditions.

Most of the cases analysed show that local buckling is the governing mode of failure for non-positive values of the crossing angle. For pipelines under tension (i.e. positive values of crossing angle) local buckling is not dominant; in those pipelines the governing modes of failure are the 3% value of longitudinal tensile strain and the cross-sectional flattening.

However buckling may also occur for small positive values of crossing angle if the pipeline is thin-walled and the ground conditions are stiff.

The numerical results presented, indicate a strong dependence in terms of the pipeline diameter to thickness ratio D/t. It was also concluded that softer ground conditions result in a larger deformation capacity of the pipeline. Moreover the presence of internal pressure prevents cross-sectional distortion, and induces additional stresses leading to a reduced deformation capacity compared with non-pressurized pipelines. Results also showed the superior behaviour of high strength X80 steel pipelines with respect to that of X65 pipelines.

Yoshizaki et al. [38] in their research conducted large scale experiments of permanent ground deformation effects on steel pipelines with elbow.

Pipelines must often be constructed to change direction rapidly for several reasons; hence in such cases the pipeline is installed with an elbow that can be fabricated for change in direction from 90° to a few degrees. Since elbows are locations where flexural and axial pipeline deformations are restrained, concentrated strains can easily accumulate at elbows in response to permanent ground deformations. The response of pipeline elbows, deformed by adjacent ground rupture and subject to the constraining effects of surrounding soil, is a complex interaction problem.

For a global and reliable assessment of this problem laboratory experiments on elbows are required to characterize their three-dimensional response to axial and flexural loading and for such reasons Yoshizaki et al. performed full-scale experimental tests and numerical analysis that simulate soil structure interaction combined with three-dimensional elbow response.

Although lateral spreads and landslides involve complex patterns of soil movement, the most severe deformation associated with these phenomena occurs at the elbows and near

the margins between the displaced soil mass and adjacent, more stable ground. The deformation along this boundary is usually simplified as abrupt planar soil displacement that also represents the principal mode of deformation at fault crossing.

A pipeline outer diameter of 100 mm with 4.1 mm wall thickness was used in the tests. The system was composed of two straight pipes welded to a 90° elbow. The short section of straight pipe was 5.4 m long, whereas the longest section was 9.3 m. Both ends of the pipeline were bolted to reaction walls. The elbows were composed of STPT 370 steel with a specified minimum yield stress of 215 MPa and a minimum ultimate tensile strength of 370 MPa. The straight pipe was composed of SGP steel with a minimum ultimate tensile strength of 294 MPa.

The pipeline was installed at 0.9 m depth to the crown of pipe in each of two experiments, leading to an overburden ratio equal to 8.5. In each experiment soil was placed at a different water content and density. Both experiments were conducted to induce opening mode deformation of the elbow. Moreover they were conducted with an internal pipeline pressure of 0.1 MPa.

About 150 strain gauges were installed on the pipe to measure train during the tests.

Cornell sand was used as soil filling having D_{10} = 0.2 mm, D_{50} = 0.7 mm, D_{60} = 0.9 mm, a minimum dry unit weight of 17.4 kN/m^3 and an optimum water content of 10.1%.

Tests 1 and test 2 ware conducted with water content of 0.5% and 3.1% respectively. Test 2 was performed with sufficiently large water content to investigate the effects of partial saturation.

The sand was placed and compacted in 150 mm lifts with rigorous controls on water content and density. Internal friction angles between 40° and 51° were obtained through triaxi-

al tests with strain rates of 0.1%/min and 5%/min determined from dry unit weight. 5%/min was used in order to see the effect of dynamic loading on the results.

The rate of displacement imposed to the movable box was approximately 16 mm/s.

During test 1 leakage occurred at the connecting part between the elbow and the shorter straight pipe when the ground displacement was 0.78 m, and full circumferential rupture of the pipe occurred when the displacement was 0.94 m. Moreover leakage occurred during test 2 but a full circumferential rupture of the pipe did not occur.

The maximum longitudinal strain measured during the tests was around 11.6% at intrados line of the elbow

Authors of this work conducted also a finite element analysis. The pipeline was modelled with isotropic shell elements with reduced integration. ABAQUS was used as solver for the analyses with geometric nonlinearity and large strain formulation. von Mises criterion and associated flow rule were applied to the model. Soil-pipeline interaction was modeled with spring elements allocated at the top and at the bottom of pipeline. The force displacement relationship was modeled in accordance with JGA guideline [11] and the data presented by Trautmann and O'Rourke [25].

Comparison of the deformed pipeline shape and distribution of longitudinal strain between experimental findings and numerical analyses are in good agreement.

The soil deformation patterns adjacent to the pipeline were different for the dry and partially saturated sands. During test 1, dry sand tended to flow around the pipeline, in contrast the partially saturated sand in test 2 showed an apparent cohesion and relative movement of the pipe generated rupture surfaces rather than flow in the adjacent soil. The generation of rupture surfaces in partially saturated sand would be expected in lateral pipe forces larger than those related to the shear flow condition of test 1.

Using the calibrated numerical model, the authors of this work proposed recommendations for enhancing the resistance of buried pipelines with elbows against permanent ground deformations. As observed in past works [35] [36] [37] leakage occurred near the welds connecting the straight pipes to the elbow hence the resistance against permanent ground deformations can be improved effectively in this portion of the pipeline.

For this analysis an evaluation of different thickness combination among elbow and straight pipes was carried out. An effective method of reinforcement is to use straight pipe with wall thickness the same as or more than that of the elbow for a distance of 0.1 m from the elbow.

3. Experimental testing aspects

3.1. Testing program

A total of 10 full-scale tests have been performed within this work: three axial tests, three lateral tests and four landslide/fault tests as described in the
Table 1 in which the details of relative density, mass density, water content, pipe coating and internal pressure are pointed out. In all cases the outside diameter of the pipe specimens is equal to 219.1 mm (8"$^{5/8}$), the wall thickness is equal to 5.56 mm and the steel grade is API 5L X65.

The roughness of pipes coated with antioxidant paint may be considered very similar to a bare pipe. Moreover each test was carried out within 24 hours from the start of soil filling.

Various types of interaction aspects have been investigated:

- Axial pullout tests in order to investigate the horizontal longitudinal pipe-soil interaction mechanism;

- Lateral pullout tests in order to investigate the horizontal lateral pipe-soil interaction mechanism;

- Landslide/fault testings to investigate the complex interaction mechanism between a pipeline and surrounding soil in case of seismic/geological phenomena and deformations induced in pipe.

The effect of send compaction, pipe surface condition, and pipeline internal pressure were also investigated.

Test No.	Test	Relative density	Mass density	Water content	Pipe coating	Internal pres-sure	Overbur-den ratio
[-]	[-]	[%]	[kg/m^3]	[%]	[-]	[MPa]	[-]
1	Axial 1	35	1629	5.7	Antioxidant paint	0	3.4
2	Axial 2	23	1602	7.8	Antioxidant paint	0	3.4
3	Axial 3	30	1613	5.8	Apsacoat 104	0	3.4
4	Lateral 1	22	1601	7.6	Antioxidant paint	0	3.4
5	Lateral 2	35	1640	6.1	Antioxidant paint	0	3.4
6	Lateral 3	35	1645	7.3	Apsacoat 104	0	3.4
7	Landslide 1	40	1600	5	Bare pipe	0	3.1
8	Landslide 2	36	1688	8	Bare pipe	11.4	3.1
9	Landslide 3	21	-	8	Bare pipe	0	3.1
10	Landslide 4	29	-	8	Bare pipe	11.4	3.1

Table 1. Summary of full-scale tests performed.

3.1.1. Axial pulling testing

The purpose of this test is to investigate longitudinal interaction during relative displacement between soil and pipe. Basically the interaction is frictional and function of internal

friction angle of the soil, surface finish of pipe or pipe coating, and level of pressure at pipe soil interface.

The axial pullout tests have been performed adopting the testing equipment schematized in Fig. 7 composed by a steel caisson in which the specimen is embedded.

Quarry sand was used to fill the caisson and compacted at specific value using a vibratory plate. Starting from this configuration pipe is pulled in a controlled manner along its axis by a hydraulic actuator. During actuator stroke the buried pipe is subjected to soil reaction which causes at most negligible axial deformation.

More details of real setup are presented in the next section 3.2.

3.1.2. Lateral pulling testing

The purpose of this test is to investigate transversal interaction during relative displacement between soil and pipe. The forces exchanged by pipe and soil arise from pressure at pipe-soil interface and frictional action due to soil flux around pipe resulting from lateral displacement. The lateral pullout tests have been performed adopting the testing equipment schematized in Fig. 8 composed by a steel caisson in which the specimen is embedded.

Quarry sand was used to fill the caisson and compacted at specific value using a vibratory plate. Starting from this configuration pipe is pulled in a controlled manner perpendicular to its longitudinal axis by a hydraulic actuator. During actuator stroke the buried pipe is subjected to soil reaction which can causes pipe bend depending on the pipe wall thickness and the soil compaction level. In this study the forces involved are not enough to submit the pipe neither to a large elastic deformation nor a plastic deformation.

More details of real setup are presented in the next section 3.2.

3.1.3. Landslide/fault testing

The purpose of this test is to investigate a complex pipe-soil interaction representative as far as possible of a pipeline crossing a landslide. The proposed testing configuration is also an approximation of a pipeline crossing two strike slip faults with very close fault lines. However it is worth noting that these tests are mainly aimed to calibrate finite element models for subsequent analyses of more complex pipeline-soil interactions.

The displacement of sliding caisson mainly leads to a bending of the embedded pipe and a soil deformation providing indications on the effect of soil motion on pipeline integrity.

The forces exchanged by pipeline and soil arise from: pressure at pipe-soil interface and frictional action due to soil flux around pipe resulting from lateral component of relative displacement, besides a frictional action resulting from axial component of relative displacement.

The landslide/fault tests have been performed adopting the testing equipment presented in Fig. 10 composed by three communicating soil caissons in which the specimen is embedded. Quarry sand was used to fill the caissons and compacted at specific value using a vibratory plate. Starting from this configuration the central caisson was pulled perpendicular to the pipe axis by two hydraulic actuators up to 3600 mm, identified as maximum displacement to avoid pipe-box wall interferences. During caisson displacement the buried pipe is subjected to soil action which causes pipe deflection and plastic deformation. As described later, due to constraints applied at pipe ends the specimen is free to translate and rotate around its longitudinal axis.

More details of real setup are presented in the next section.

3.2. Experimental apparatus

Two experimental equipments were modified in order to perform the full-scale tests at Centro Sviluppo Materiali S.p.A. Both apparatus were already equipped with hydraulic actuators and control systems, the first (Fig. 3) currently used for combined loading on pipes and the second (Fig. 4) used for four points bend on 48” pipe diameter.

Fig. 3. Picture of testing machine frame #1.

A configurable steel caisson to conduct both axial and lateral full-scale tests on 8” $^{5/8}$ pipe diameter was designed and constructed. This steel caisson was placed and clamped on the testing machine frame (Fig. 5).

Three caissons to perform landslide/fault tests were designed and assembled, two of which were built with concrete walls and the central sliding caisson was built with a stiff frame usable also for diameters of pipe greater than 8” $^{5/8}$. A picture of test equipment is shown in Fig. 6.

Fig. 4. Picture of testing machine #2.

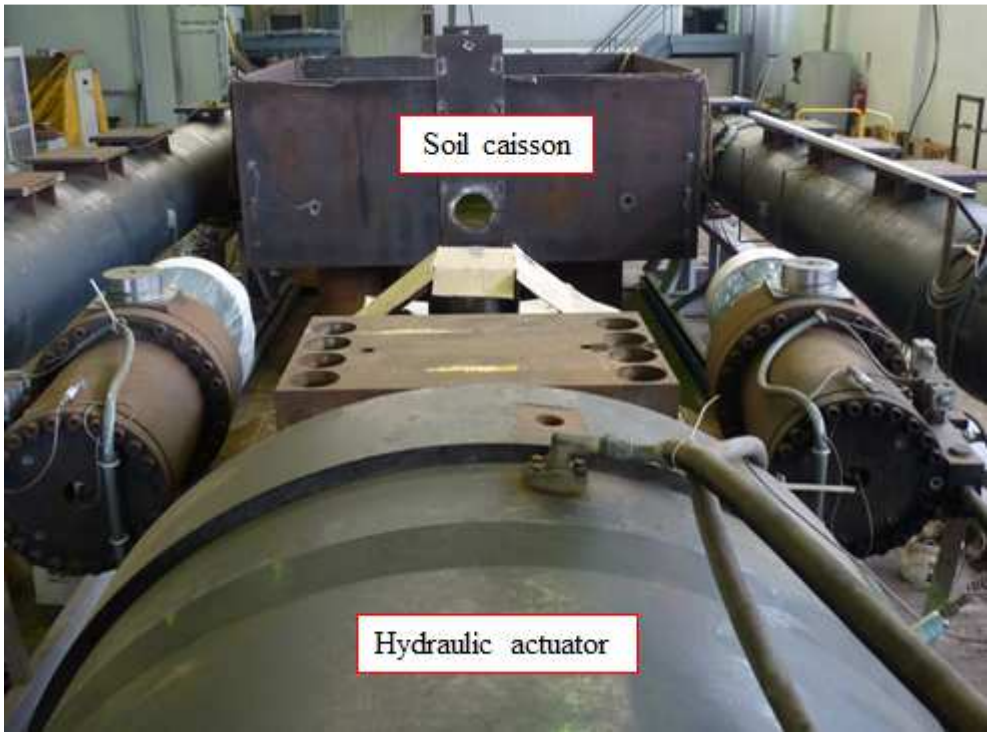

Fig. 5. Steel caisson for axial and lateral pullout testing placed and clamped on the testing machine frame #1.

Fig. 6. Testing equipment for landslide/fault experiments.

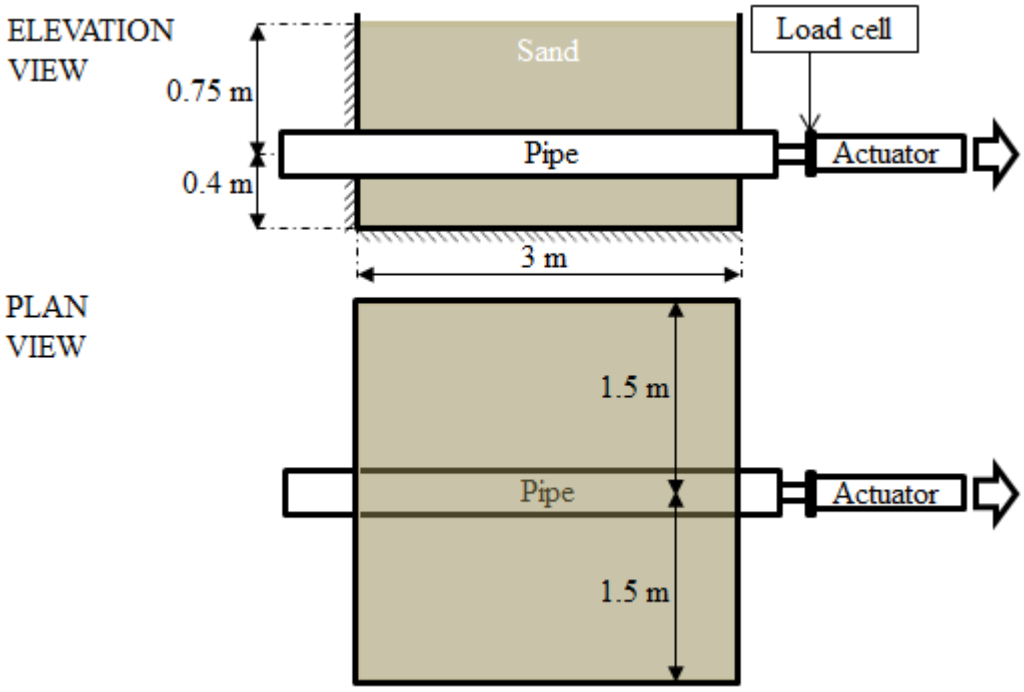

Fig. 7. Elevation view and plan view of testing equipment for axial pullout tests.

Fig. 7 and Fig. 8 show the layout of the test facility, respectively for axial pullout tests and transversal pullout tests in which the main components are shown.

As depicted in aforementioned figures, the rear wall and the bottom of the caisson were clamped for both typologies of tests.

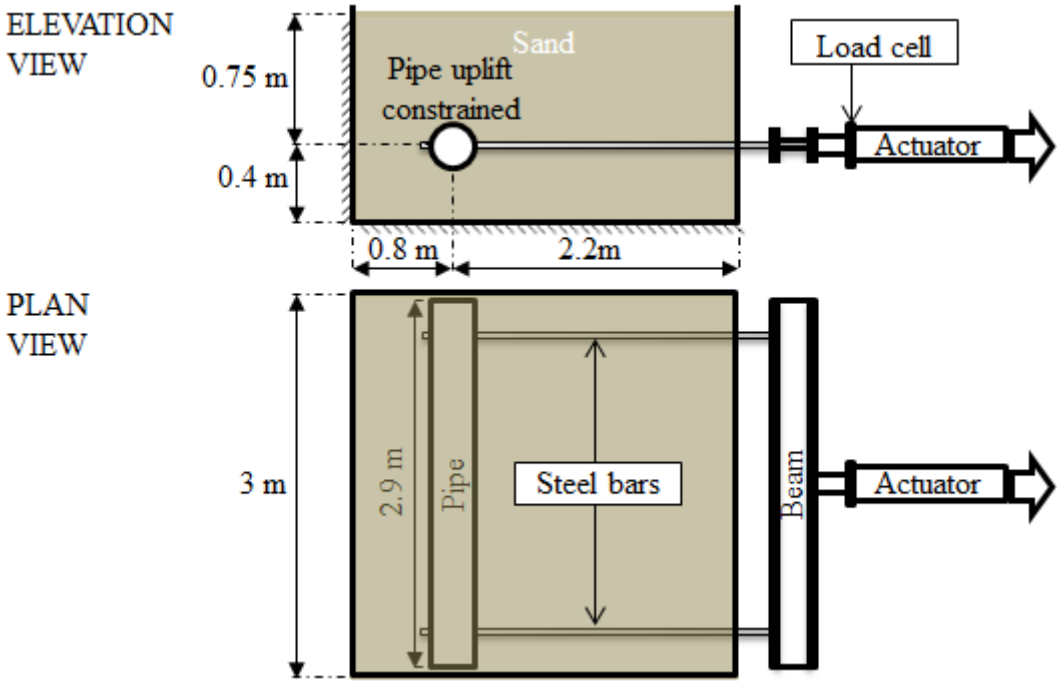

Fig. 8. Elevation view and plan view of testing equipment for lateral pullout tests.

The dimension of the internal caisson is fixed equal to 3 m x 3 m, for 1.25 m of depth, the pipes used for the axial tests were 6 m long to ensure a constant pipe-soil contact length of the buried pipe during pulling action. The pipes used for the lateral tests were 2.9 m long and were filled with concrete in order to minimize any deflection induced by soil action. Horizontal rails were positioned nearby the lateral walls to avoid specimen vertical motion,

in this case the pipe was pulled by means two steel bars designed for allow a negligible friction with the soil and axial deformation.

The configurations of the caisson permit a maximum burial depth of 0.75 m respect to the pipe axis.

a). Axial pullout configuration.

b). Lateral pullout configuration (with removed sand).

Fig. 9. Testing configurations caisson.

Perspective views of testing configurations are shown in Fig. 9 a) and Fig. 9 b) respectively for axial pullout test just before a test and for lateral pullout test.

Fig. 10 show the layout of the test facility for the landslide/fault tests in which are highlighted the main components: two fixed caissons made with concrete blocks with adequate weight force to avoid translation due to soil pressure applied during tests, one sliding caisson to simulate the ground displacement assembled with steel plates and beams: two actuators to pull the sliding caisson, a 36 m long pipeline of which 24.7 m embedded. The plan dimension of internal fixed caissons were 8.35 m long x 4.35 m wide and 8 m x 4 m for the sliding caisson (Fig. 12); the maximum depth of caissons were 1.5 m (Fig. 13).

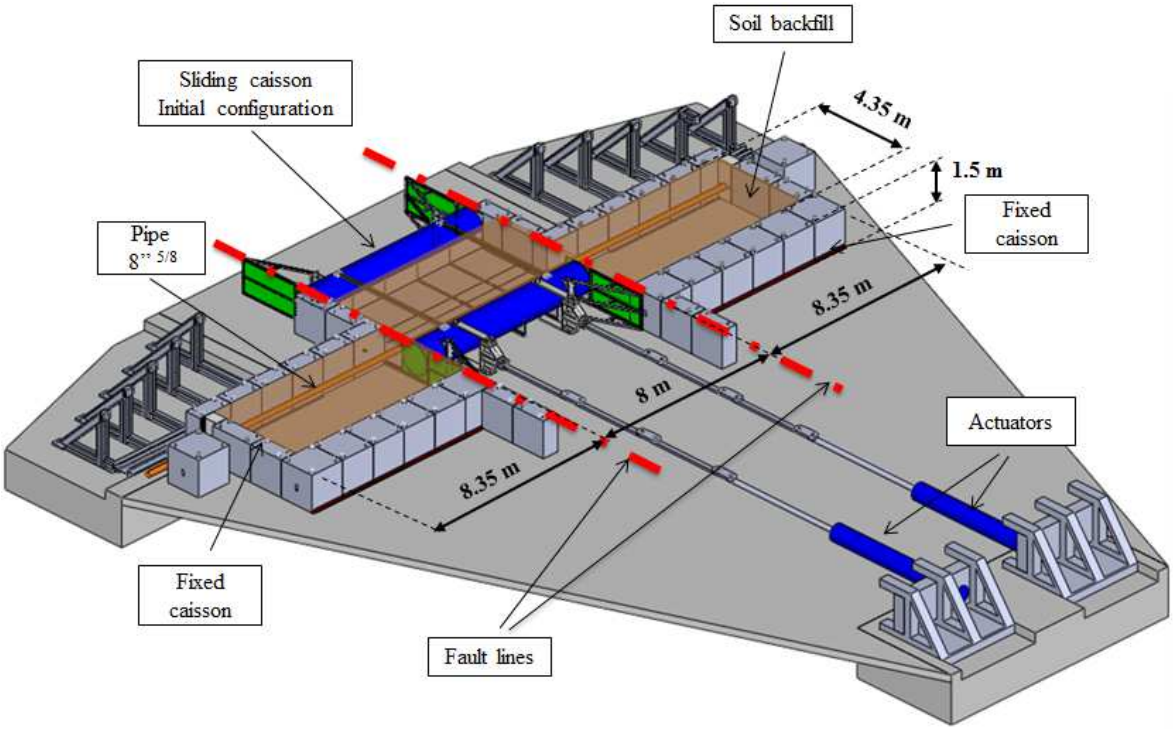

Fig. 10. View of testing equipment for landslide/fault tests – Initial configuration.

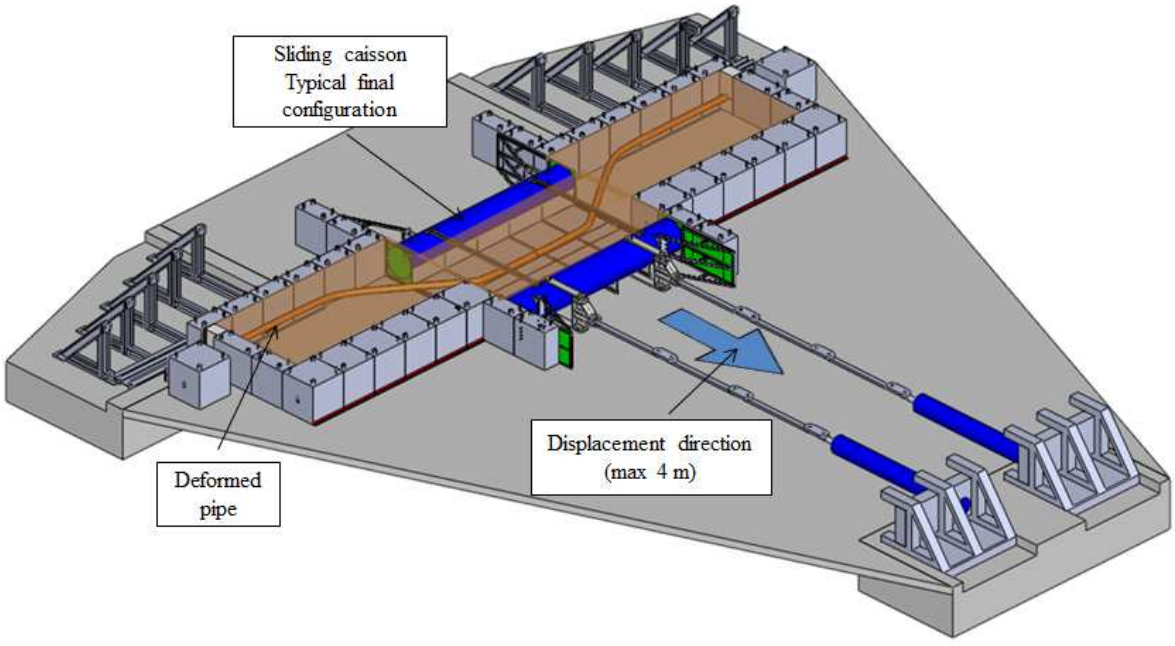

Fig. 11. View of testing equipment for landslide/fault tests – Typical final configuration.

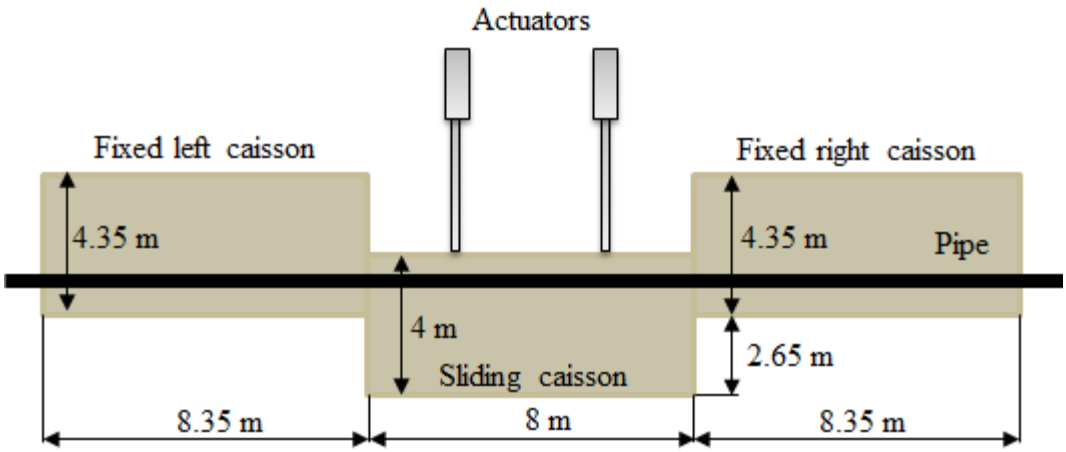

Fig. 12. Caissons internal dimensions – Plan view.

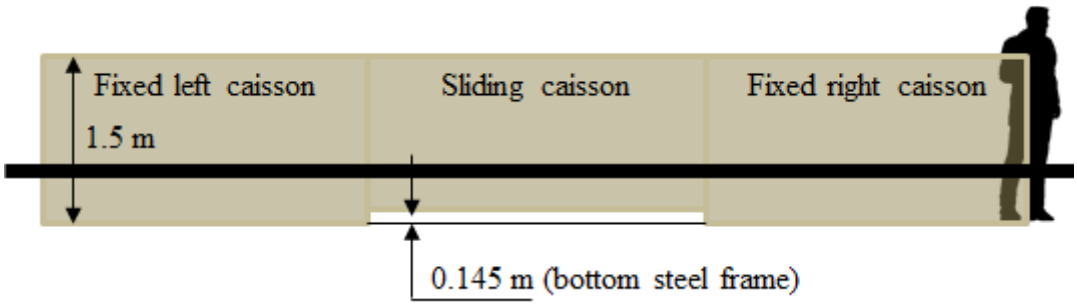

Fig. 13. Caissons internal dimensions – Elevation view.

The configurations of the caissons permit to adjust the burial depth within 1.5 m of embedment.

The pipe was also constrained at the ends allowing only rotation and translation along the pipe axis as schematized in Fig. 14 adopting pipe rollers (Fig. 15). This boundary conditions lead to an approximation of a real pipeline conditions.

Pipe position respect lateral walls and caisson bottom have been taken identical for all landslide/tests; distances from pipe axis and internal caissons are shown in Fig. 17 and Fig. 16 respectively in an elevation view and in a plan view.

The initial configuration of the equipment (Fig. 10) show a misalignment between sliding caisson and fixed caissons, this layout was used in order to allow a wider displacement

perpendicular to the pipe than the case with aligned caissons. The final configuration of the equipment is shown in Fig. 11

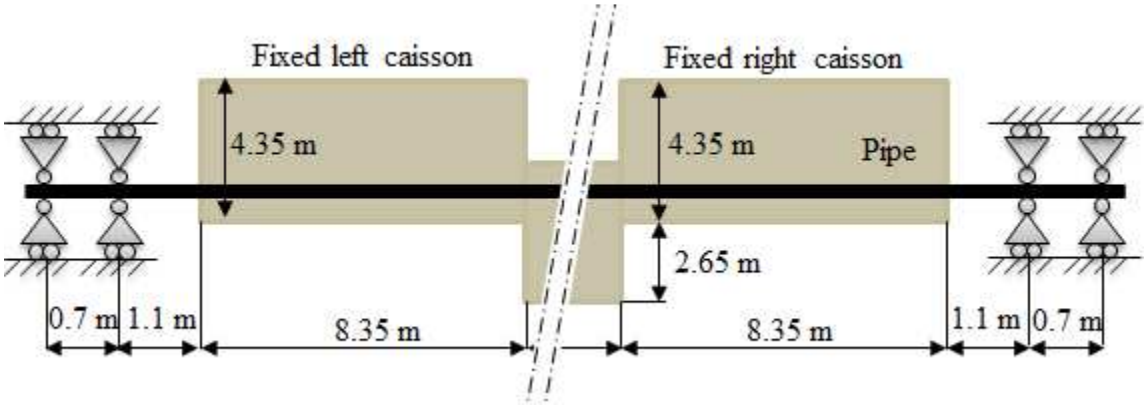

Fig. 14. Pipe ends constrains.

Fig. 15.Travitec® pipe roller.

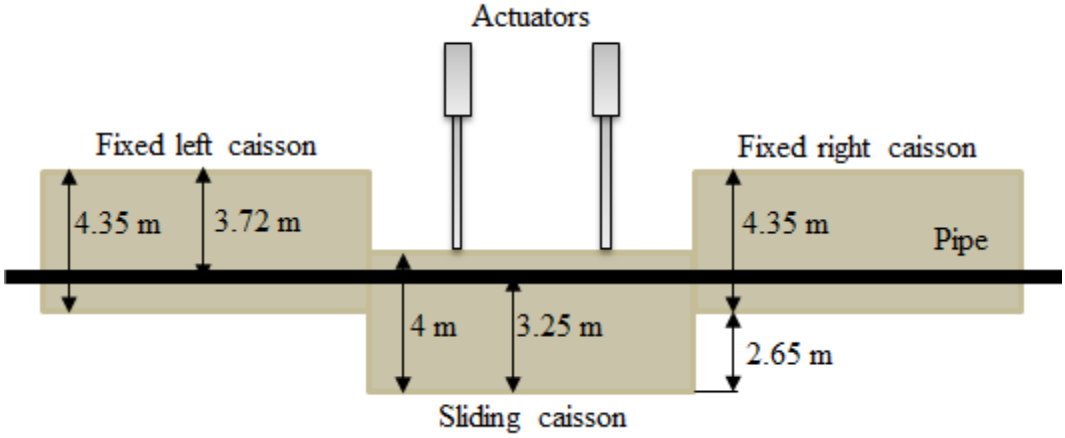

Fig. 16. Pipe position – Plan view.

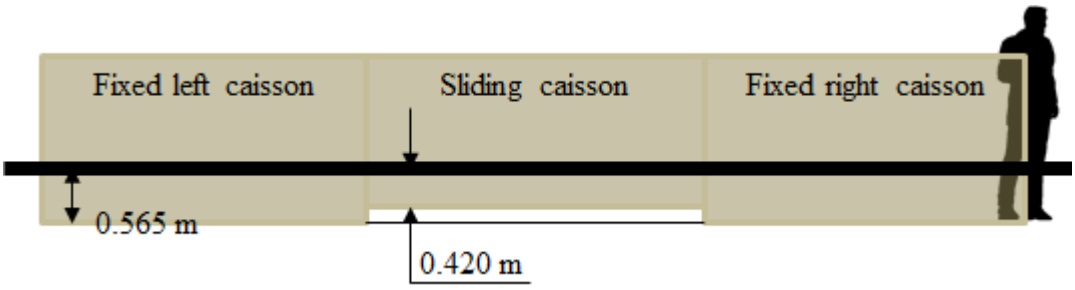

Fig. 17. Pipe position – Elevation view.

a). Global view of landslide fault equipment.

b). Fixed left caisson.

c). Sliding central caisson.

d). Fixed right caisson.

Fig. 18. Testing configuration caissons for landslide/fault tests.

A view of landslide fault testing configuration is shown in Fig. 18 a). Fig. 18 b) and Fig. 18 d) depict respectively the fixed left caisson and the fixed right caisson, Fig. 18 c) highlights the sliding central caisson.

In both cases axial pulling tests and landslide fault tests pipe ends were outside soil caissons and in order to avoid loss of sand from the holes. Polystyrene shapes were used to seal the gap between pipe and walls.

3.3. Backfilling material and density measurements

Pipelines may be laid with two technologies: excavated trench and trenchless technology. In case of trenchless technology the pipe goes in contact with the native soil, in case of excavated trench the pipeline may be laid and subsequently embedded with native soil or granular backfill materials, it depends on the site of installation.

In order to perform full-scale experimental test is more convenient to handle granular material such as sand than clayey soils, both for working conditions (e.g. fill and empty the caissons, work outdoor, level out layers of soil) and faster realization of geotechnical tests.

For these reasons the partners of the GIPIPE project decided to use a quarry washed sand for all experimental tests performed in this study.

About 11 m^3 was the first sand supply for axial and lateral tests, stored in a skip loader indoor, handled with a hopper and an overhead crane. Later the second sand supply, 180 m^3 of the same sand was stored outdoor in a concrete base in order to avoid contamination with the surrounding soil. In this case the sand was handled with an excavator.

3.4. Loading apparatus and force measurement

Axial and lateral pullout tests were performed in a displacement controlled manner. The displacement rate was varied from 0.5 mm/s to 2 mm/s during every single axial test and from 0.5 mm/s to 1 mm/s during lateral tests. This variation has not shown variation of soil load response. Also landslide/fault tests were performed pulling the sliding caisson in a displacement controlled manner with a single speed rate equal to 1 mm/s.

The hydraulic systems used for the tests were different, for axial and lateral tests a single hydraulic actuator have been used, with maximum displacement of 600 mm and a maximum load capacity of 25000 kN. For landslide fault tests two hydraulic actuators have been used, with maximum displacement equal to 5000 mm and a maximum load equal to 4000 kN each one.

Both hydraulic systems are integrated with linear variable displacement transducers.

The applied load on the pipeline segments in axial and lateral tests was measured using a HBM load cell with a maximum load capacity of 500 kN, besides the load on the sliding caisson used for landslide/fault tests was measured with an integrated load cell.

3.5. Pressure measurement at pipe soil interface

In order to measure the pressure distribution at soil-pipe interface during lateral pullout tests a 3150E pressure mapping sensor manufactured by Tekscan has been used (Fig. 19). As shown in Fig. 20 and Fig. 29 the pressure sensor was wrapped around the pipe for half circumference to measure the soil pressure on the side oriented toward the direction of pipe displacement. The maximum pressure expected during the pipe displacement was estimat-

ed around 300 kPa. The flexible sensor sheet used has dimension of 517 mm x 499 mm with a sensing region of 369 mm x 436 mm, the sensitive area contain 2288 sensels spaced in 8.4 mm in each direction, the operating pressure is 0 to 862 kPa. The data acquisition system developed from Tekscan allows observing and recording the distribution of pressure as a function of time. Previous works used successfully this sort of devices to measure pipe-soil pressure interaction, O'Rourke, T.D. et al. [18], Da Ha [8].

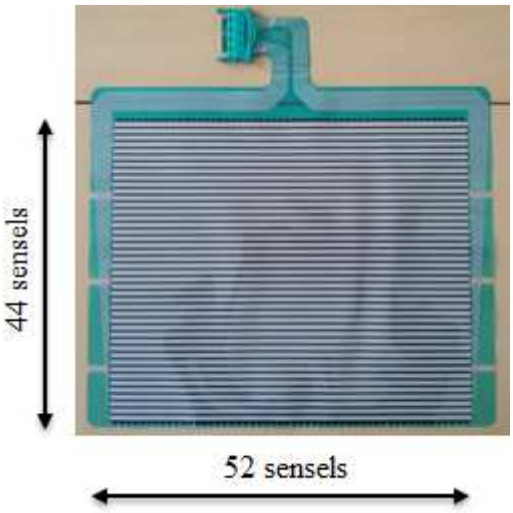

Fig. 19. Pressure mapping sensor.

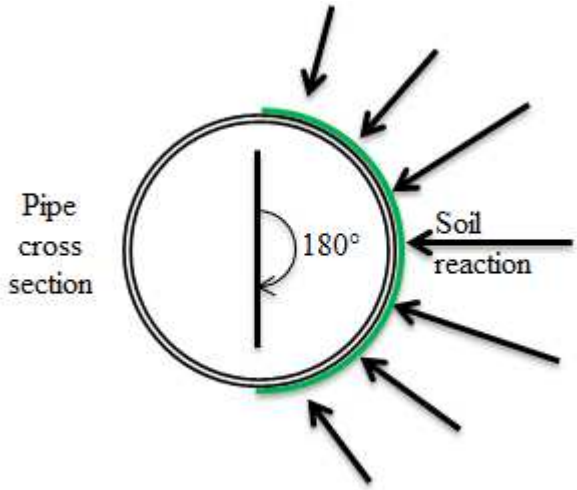

Fig. 20. Scheme of pressure sensor wrapping.

Fig. 21. Pressure sensor wrapped on pipe.

3.6. Monitoring instrumentation of landslide/fault tests

In order to measure the most important parameters that describe the pipeline-soil interaction the following instrumentation has been adopted:

- Pipe internal pressure monitored and controlled within specified values;
- Hydraulic jack displacements: monitored and controlled;
- Hydraulic jack loads: monitored;
- Soil surface displacement have been observed, by means of image recording;
- Pipe deformed configuration displacements, by means of strain gauges and laser LVDTs;
- Local strains on pipe with strain gauges.

3.6.1. Soil surface deformations

Soil surface deformation has been analysed by camera recording as shown in Fig. 22. This information is useful in order to study the size of the soil shear area at fault line and to compare results of full-scale test with finite element analyses.

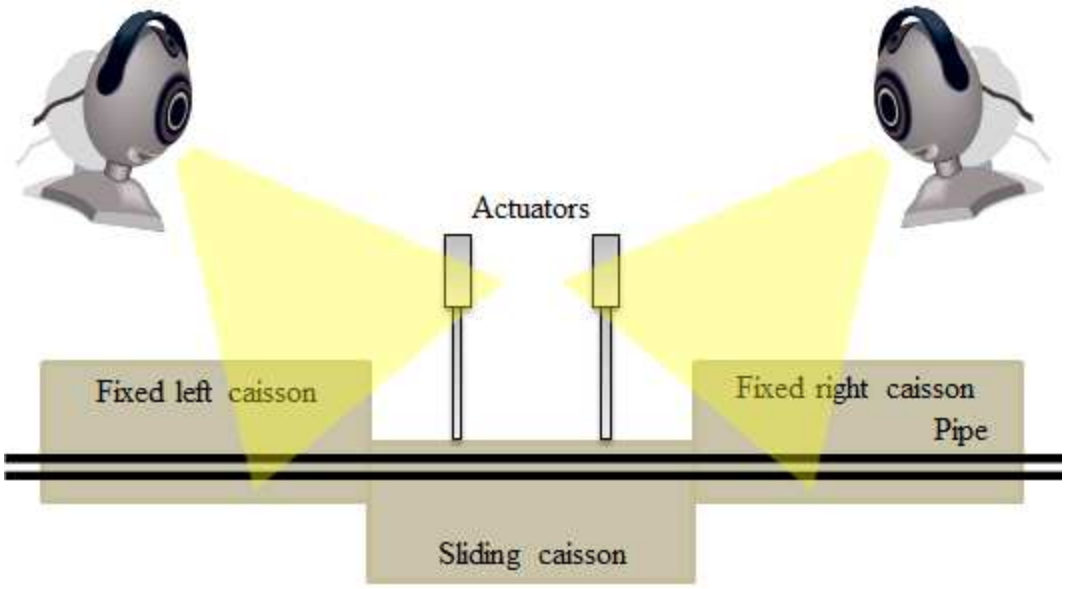

Fig. 22. Video recording of sand surface, to evaluate surface deformation.

3.6.2. Global pipe displacements and ovalization

Measurement of pipe displacement during landslide/fault testing is rather complicated due to the embedment conditions, in spite of that useful information will be obtained if pipe deformed configuration could be evaluated during caisson displacement and not only after test, at soil removal. This measurement is complicated due to the presence of soil which does not allow using laser LVDTs or wire LVDTs. To overcome such difficulties a measuring procedure employing longitudinal strain gauges at pipe intrados and extrados Fig. 23, and laser LVDTs (Fig. 24) has been employed. LVDTs are employed to measure the longitudinal displacement at pipe ends, while strain gauges are employed to evaluate global deformation by measuring the local strain distribution, Fig. 25, by applying the following formulation:

- Bending strain can be calculated according to (Eq. 1):

(Eq. 1) $$\varepsilon_{\text{bending}} = \frac{\varepsilon_{+} - \varepsilon_{-}}{2}$$

- Bending curvature is obtained by:

(Eq. 2) $$k_{\text{bending}} = \frac{2 \cdot \varepsilon_{\text{bending}}}{OD}$$

From the curvature and the initial pipe configuration it is possible to obtain by geometric construction the pipe global deformation. A dedicated finite element study has been performed shown the adequacy to measure the pipe global deformations applying the aforementioned formulation. Additionally pipe axial stretching can be calculated by:

(Eq. 3) $$\boldsymbol{\varepsilon_a} = \frac{\varepsilon_{+} + \varepsilon_{-}}{2}$$

The final pipe deformation has been measured after each test and compared with above calculations.

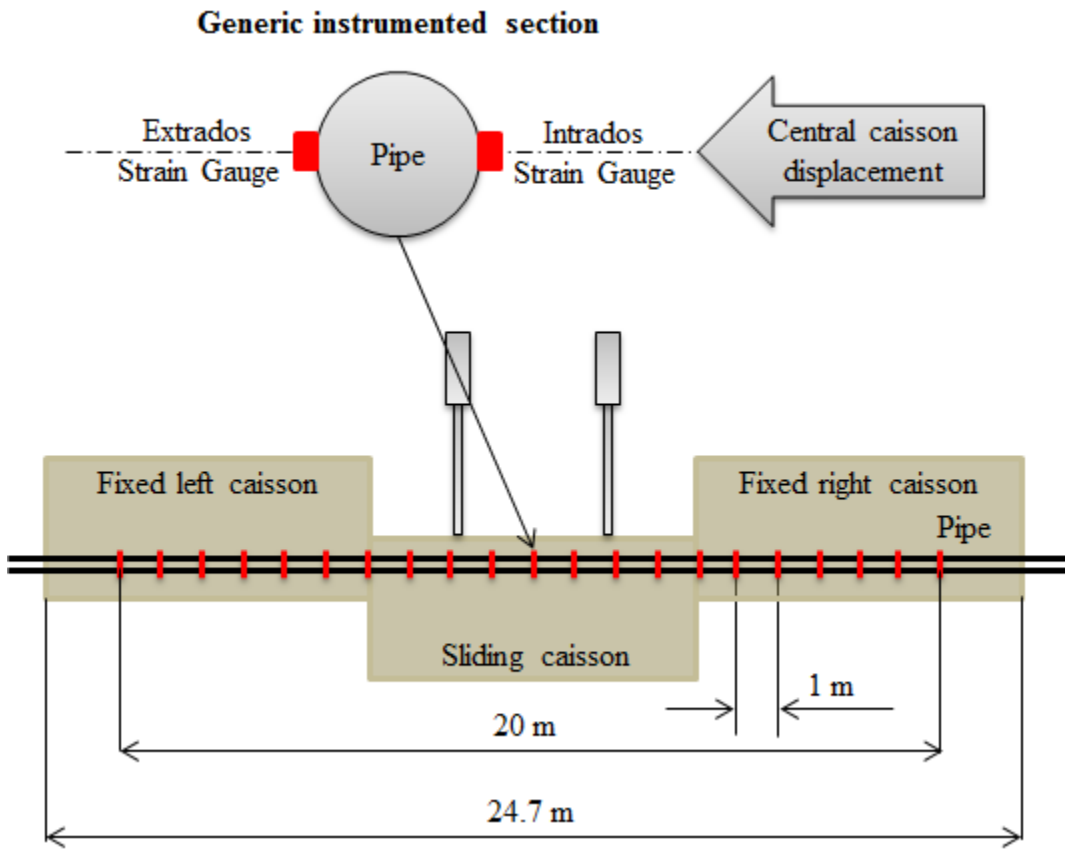

Fig. 23. Strain gauges positioning plan.

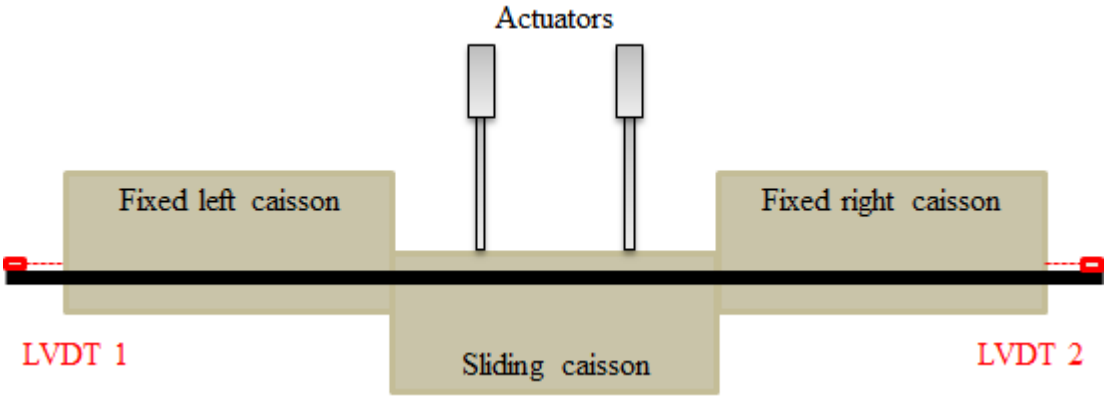

Fig. 24. Laser LVDTs positioning to evaluate pipe displacement at pipe ends.

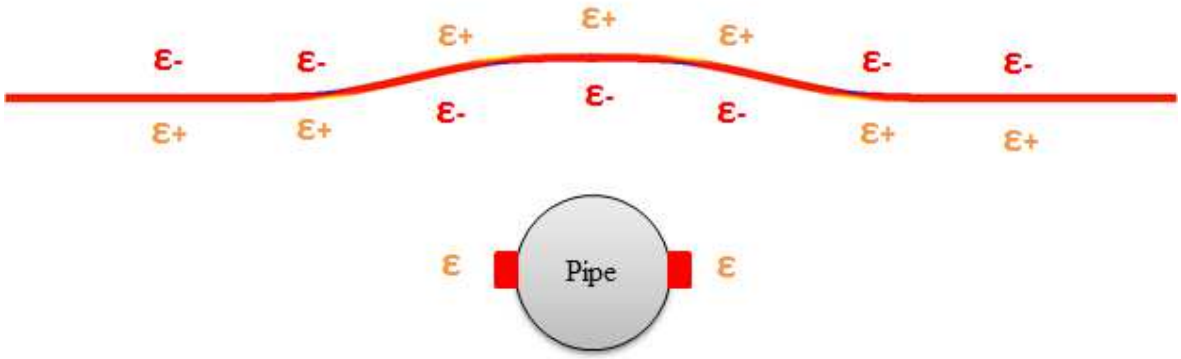

Fig. 25. Typical longitudinal strain distribution on pipe during landslide/fault bending test.

With reference to Fig. 26, pipe ovalization has been measured according to the following formula:

(Eq. 4) $$\text{Ovality} = \frac{\mathbf{OD_{max}} + \mathbf{OD_{min}}}{OD_{nominal}}$$

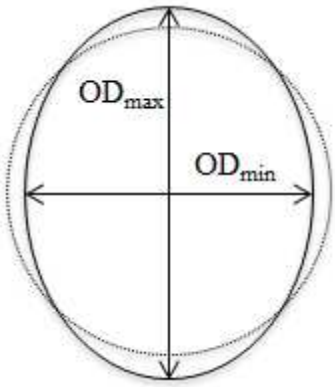

Fig. 26. Pipe ovalization scheme.

3.7. Data acquisition

The measurements of loads and displacements were recorded at 1 Hz.

3.8. Backfill preparation and density measurements

The caissons were filled up layer by layer (250 mm each lift) up to the established level. For each layer, sand was compacted to a target relative density with a vibrating plate compactor and density was controlled with a standard dynamic cone penetrometer (DCP). The relative density was estimated by means the relation D_r (%) = 189.93/(DPI)$^{0.53}$ reported in Mohammadi et al. [15]. In order to verify the relative density estimations, at the end of each tests embedded small containers of sand placed during the caisson filling at the pipe depth positions were extracted and weighed. A good agreement was achieved.

The moisture content was measured by weighing the sand contained in the aforementioned containers, before and after the drying in an oven.

Before each test, the caissons were emptied to the bottom level in order to remove any possible residual stresses in the soil.

3.9. Characterization of soil properties

In order understand the mechanical behavior of the soil several tests have been performed in geotechnical laboratories, grain size distribution, sand equivalent test, standard proctor test, several drained direct shear tests for two levels of relative density.

Also tensile tests were performed to characterize the steel of the pipes used for the tests.

Therefore this chapter provides more information about the materials used in this study and summarizes the findings from laboratory tests.

3.9.1. Sand used in the full-scale tests

The quarry sand used for the tests was the same in both supplies, to be sure of this, grain size distribution were measured. The results are shown in Fig. 27. This confirmation allows considering all the data obtained from geotechnical tests performed on the first sand supply suitable for the tests performed with the second sand supply.

Sand equivalent test confirms that the material is composed by 79.7% of sand and 20.3% of silt.

In order to know the maximum dry unit weight and the corresponding optimum moisture water content for a given compaction energy a standard proctor test was performed, the compaction curve (Fig. 28) shown that there is a slightly difference changing the moisture content from 2% up to 10% that is near the saturation.

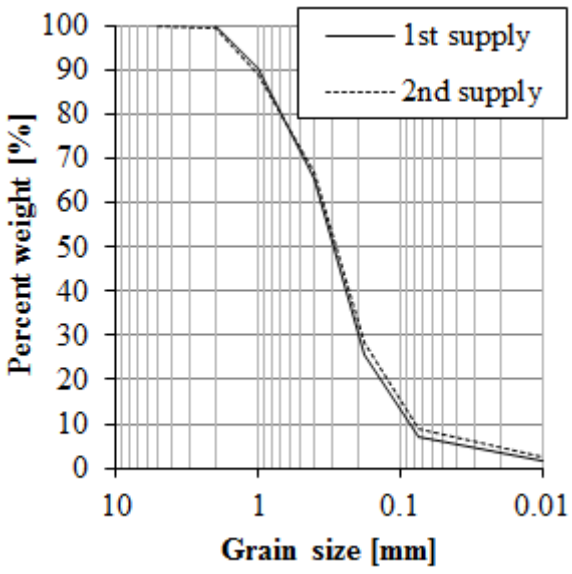

Fig. 27. Quarry sand grain size distribution. Measured for both supplies.

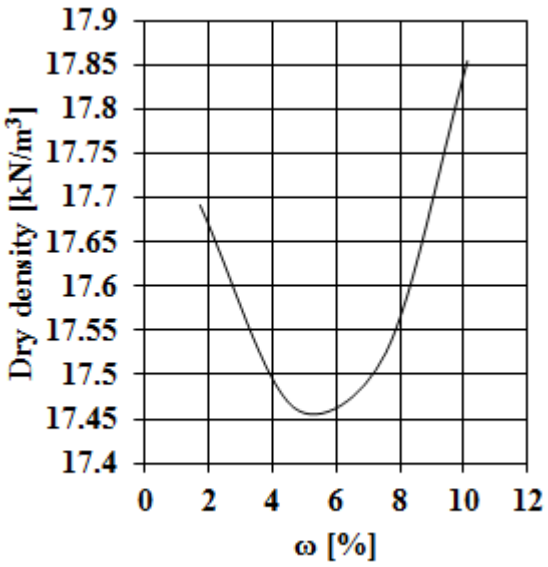

Fig. 28. Compaction curve.

The specific gravity, the minimum and maximum void ratios were determined and are reported in

Table 2 to be respectively G_s = 2.61, e_{max} = 0.692 e_{min} = 0.417. The minimum and maximum void ratios are determined in accordance with American society for testing and materials standards ASTM-4254 and ASTM-4253.

G_s	2.61
e_{max}	0.692
e_{min}	0.417

Table 2. Specific gravity and void ratios of the quarry sand.

Several direct shear tests have been performed with a vertical stress ranging from 17 kPa to 434 kPa both for D_r = 20% and D_r = 40%, values of density achieved during the full-scale

tests. In Fig. 29 and Fig. 30 are shown the direct shear test data that exhibits a slightly difference for the two levels of compaction tested.

The dilative sand response is detected during the shear tests will have a key role in the understanding of soil response during axial pulling tests.

Numerical simulations of pullout tests and experimental measurements on lateral pullout tests indicated that the maximum stress around the pipe section may range from 22 kPa to 300 kPa respectively for axial and lateral pulling experiments. The sand strength parameters among individual direct shear tests performed in this range varied as reported in Table 3. Therefore representative average values are assumed: peak friction angle equal to 42°, residual friction angle equal to 36° and a dilation angle of 10° used also for the numerical models presented in this work.

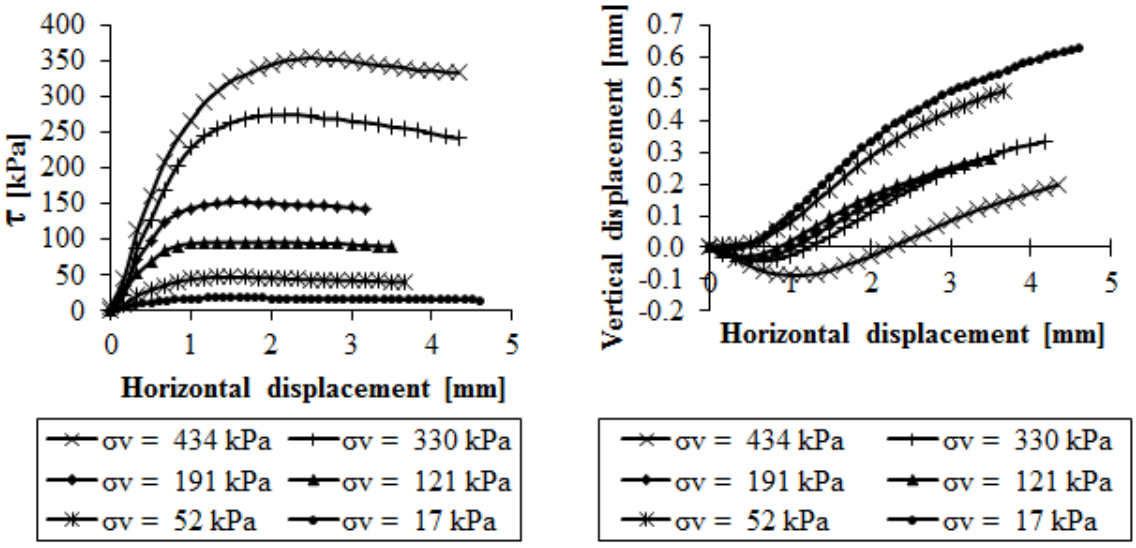

Fig. 29. Laboratory direct shear tests on quarry sand with D_r = 20%.

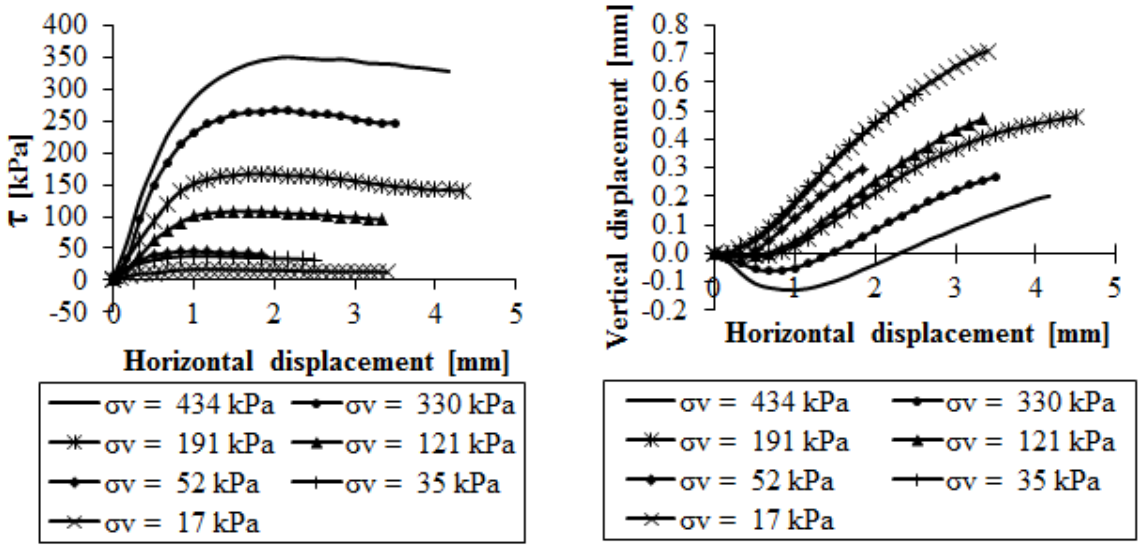

Fig. 30. Laboratory direct shear tests on quarry sand with D_r = 40%.

Soil parameters	
ϕ_p	39°-44°
ϕ_r	35°-38°
ψ_p	8°-13°

Table 3. Soil strength parameters washed quarry sand.

3.9.2. Pipeline material

The pipe adopted for testing is 8”$^{5/8}$ pipe diameter, 5.56 mm wall thickness, X65 grade, ERW; produced by Corinth Pipe Works. Extensive material characterization has been performed. Test specimens for landslide fault tests are composed by 5 pipes welded by manual SMAW welding adopting the WPS specifically developed for the project. Fig. 31 shows the tensile curves of the pipe material and

Table 4 the tensile mechanical properties.

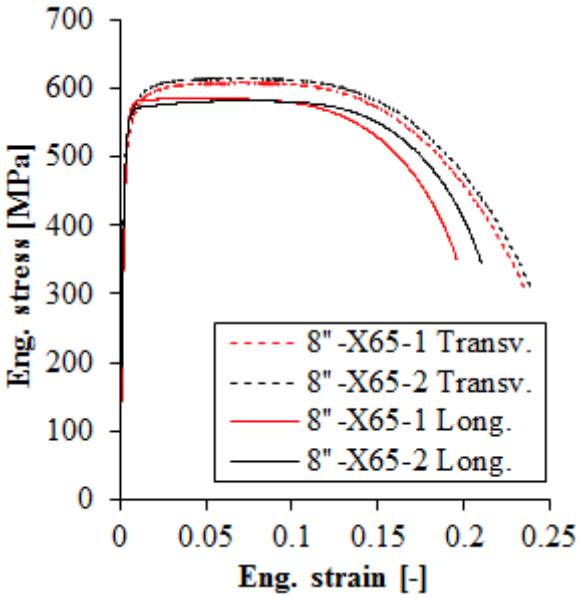

Fig. 31. Tensile curves of the pipe material adopted for OD = 8" $^{5/8}$, WT = 5.56 mm, X65 ERW pipes adopted in full-scale testing.

Pipe type		**OD = 8.625", WT = 5.56 mm, X65 grade, ERW**			
Specimen id.		**8L-1**	**8L-2**	**8-RB-T1**	**8-RB-T1**
Direction		**Longitudinal**		**Transversal**	
$R_{p0.2\%}$	Yield Strength (MPa)	551	540	519	537
R_m	Tensile Strength (MPa)	586	582	609	616
A%	Elongation (%)*	16	18	24	24

(*) calculated over a gauge length of 65mm

Table 4. X65 base material tensile mechanical properties.

4. Embedded pipes subjected to axial pulling action

4.1. Introduction

This chapter describes the experimental findings obtained from the three axial pulling tests on steel pipes and the results from the numerical analyses of the experiments. The results are discussed and also compared with currently recommended methods for prediction of axial loads on buried pipelines during ground movements.

In order to conform the results presented herein to the current practice the axial soil resistance is presented in the form of normalized axial soil resistance as defined below:

(Eq. 5) $$R'_A = R_A/(\gamma H \pi D L)$$

where:

- R_A: is the axial soil resistance;
- γ: is the soil density;
- H is the burial depth of the pipe springline;
- D is the pipe outer diameter;
- L is the pipe length;

while the displacement is normalized according the following relationship:

(Eq. 6) $$D'_A = D_A/D$$

where:

- D_A is the pipe axial displacement.

The concept of dimensionless load and normalized displacement has been used previously by Audibert and Nyman [6], Trautmann and O'Rourke [24], Paulin et al.[19].

The value of R'_A represents the average shear force around the pipe normalized with respect to the vertical effective stress given from the soil above the centreline of the pipe.

Test configuration	Axial longitudinal pullout
Soil type	Quarry sand
Average density	From 1600 to 1630 kg/m^3 respectively for Dr = 20% and Dr = 40%
Average moisture	From 5.7% to 7.8%
Average internal friction angle	ϕ_p = 42°, ϕ_r = 36%
Caisson size	3 m x 3 m x 1.25 m
Pipe size	OD = 8"$^{5/8}$ (219.1 mm), WT = 5.56 mm, length = 6 m
Pipe grade & Surface coating	API5L X65, antioxidant paint and Apsacoat 104
Overburden ratio	H/D = 3.4
Loading rate	Min = 0.1 mm/s, Max = 2 mm/s

Table 5. Summary of parameters in axial pullout testing.

4.2. Axial load vs. displacement response

In this section, results of horizontal soil reaction measurements during axial pullout tests are presented.

Test No.	Test	Relative density	Mass density	Water content	Pipe coating	Internal pres-sure	Overbur-den ratio
[-]	[-]	[%]	[kg/m^3]	[%]	[-]	[MPa]	[-]
1	Axial 1	35	1629	5.7	Antioxidant paint	0	3.4
2	Axial 2	23	1602	7.8	Antioxidant paint	0	3.4
3	Axial 3	30	1613	5.8	Apsacoat 104	0	3.4

Table 6. Summary of axial tests performed.

As summarized in Table 6 Test No. 1 and Test No. 2 performed with the same coating differ for the relative density level, 35% and 23% respectively, besides Test No. 1 and Test No. 3 performed with higher relative density level differ for the pipe coating. The compared normalized load displacement response is shown in Fig. 32 in which the first thing you may notice is the difference between soil level reaction obtained from Test No. 1 and Test No. 3 respect to the soil level reaction measured during Test No. 2 performed with D_r = 20%.

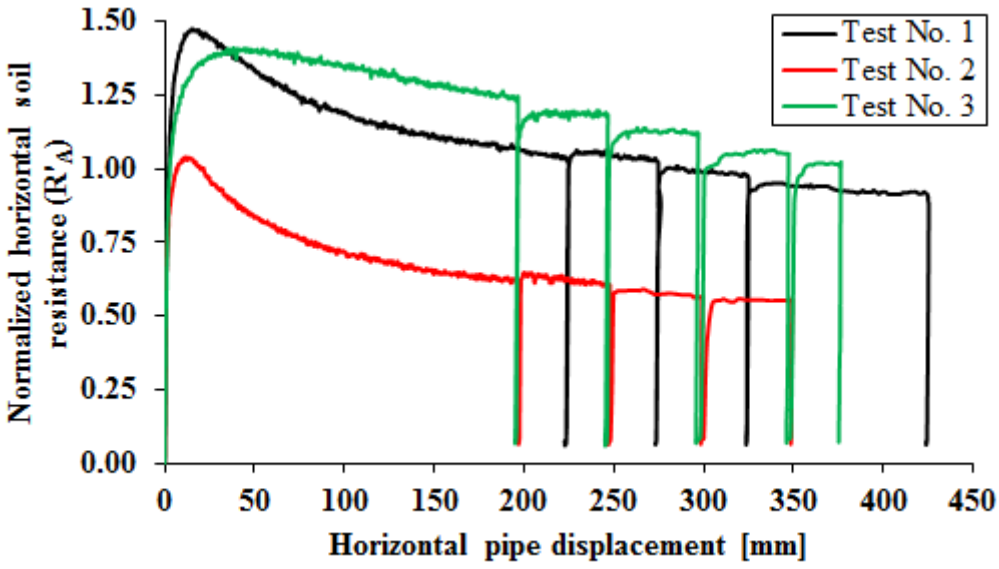

Fig. 32. Load displacement response, Tests Nos. 1, 2, 3, during subsequent loadings after first loading/unloading.

The second thing you may notice is the shape of each curve, that show the behavior of the different pipe coating, the load displacement response during the Test No. 3 show a more round shaped achievement of peak resistance compared to the tests performed with antioxidant paint coating, for which an abrupt decrease is observed; this difference show a different rate of decay of internal friction angle with respect the to the horizontal displacement.

In terms of peak soil resistance, considering tests at the same level of compaction, the two different surface finishes give a negligible difference.

In all cases the decay of load is achieved toward an asymptotic residual value.

As highlighted in Fig. 33 peak soil resistance is 1.47, 1.04 and 1.41 achieved in 15.4 mm, 11 mm and 38 mm for Tests Nos. 1, 2 and 3 respectively. The post peak R'_A values for a common displacement of 350 mm is 0.94, 0.55 and 1.05 for Tests Nos. 1, 2 and 3 respectively, which show again a lower rate decay of internal friction angle for Test No. 3 respect to the Test No. 1.

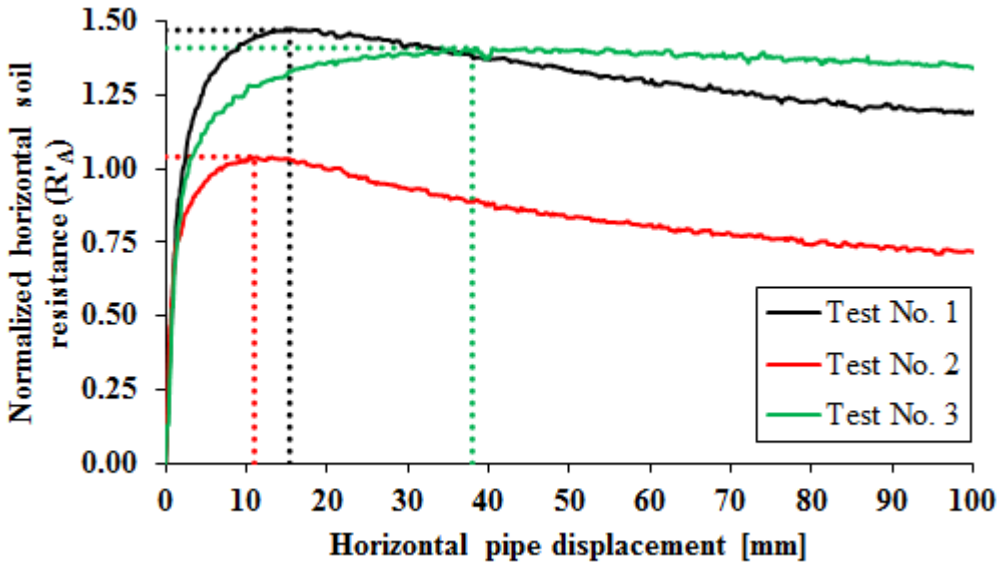

Fig. 33. Load peak response in the peak region for Tests Nos. 1, 2, 3.

4.2.1. Axial pulling Test No. 1

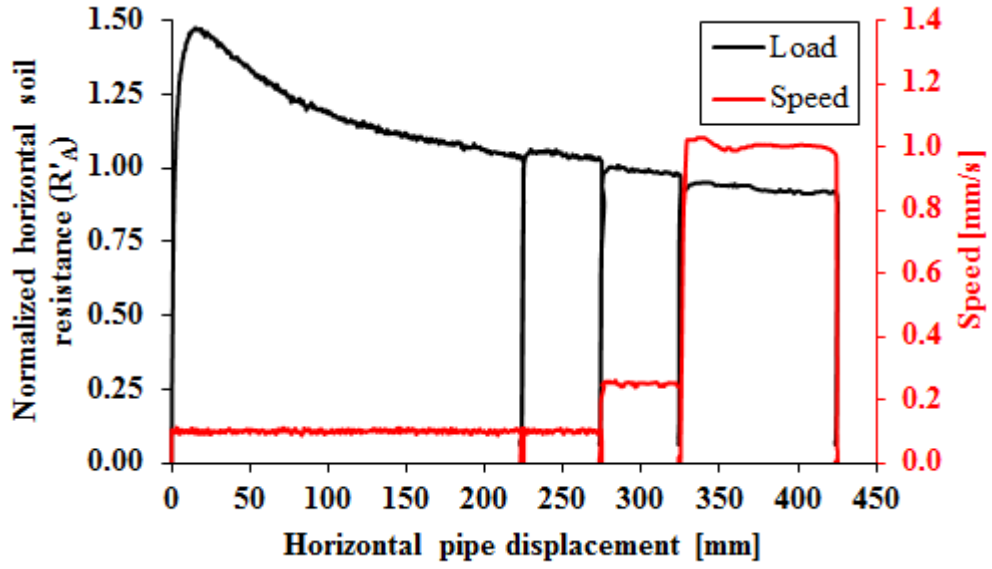

Fig. 34. Load displacement response, Test No. 1, during subsequent loadings after first loading/unloading.

The first axial pulling test was performed on a painted sample embedded in sand with relative density equal to 35%. The load displacement diagram is reported in Fig. 34. The pipe has been pulled in various stages along the longitudinal pipe axis.

Phase 1, a displacement up to 225 mm with an actuator speed of 0.1 mm/s was performed and then the load was reduced to zero. A normalized peak load of $R'_A = 1.47$ was recorded for a displacement of 15.4 mm. The load increases rapidly in the beginning, then a maximum in the load displacement curve is reached. After the initial peak, the load progressively decreases; the rate of decrease is much smaller than the initial load increase. At 225 mm the load has been removed, a slight displacement is observed in this unload phase.

Phase 2, from 225 mm to 275 mm displacement was applied again with 0.1 mm/s of speed. The load value returned very similar to the ones recorded before the unloading of the previous part and the initial loading did not exhibit a prominent peak load. During the whole axial displacement the load progressively reduces, being the rate of load reduction continuously decreasing. At 275 mm the load has been removed, very small displacement is observed in this unloading phase.

Phase 3, from 275 mm to 325 mm of displacement the speed was increased to 0.25 mm/s, no significant variations of load may be observed. Again the load decrease and start from a value closely to the ones of the last end phase. At 325 mm the load was reduced to zero.

Phase 4, from 325 mm to 425 mm, the actuator speed was increased again to 1mm/s, and alike results as the previous phase can be observed. At 425mm of displacement the load was reduced to zero.

4.2.2. Axial pulling Test No. 2

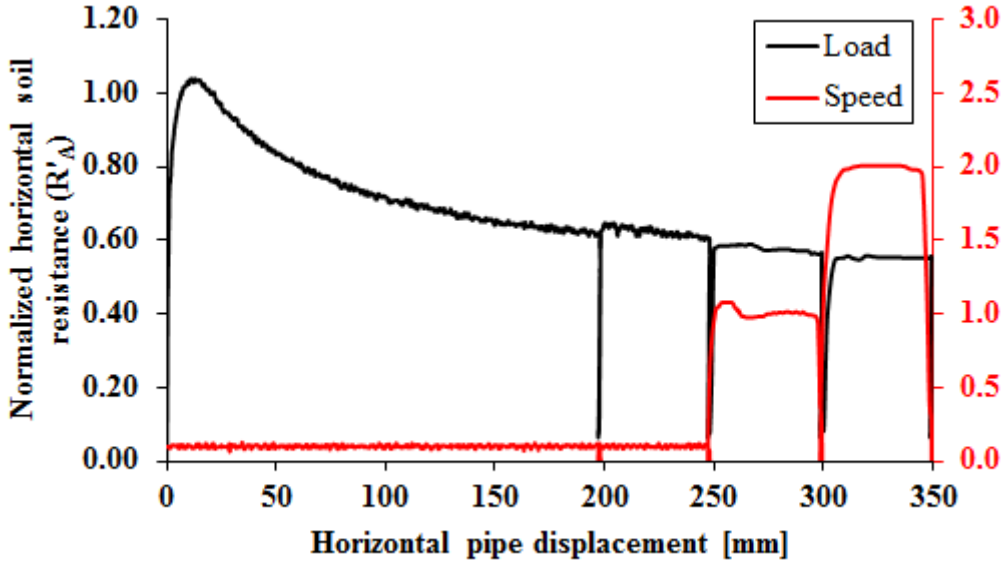

Fig. 35. Load displacement response, Test No. 2, during subsequent loadings after first loading/unloading.

The second axial pulling test was performed on a painted sample adopting the lowest level of density achieved in this study (D_r = 23%). The load displacement diagram is reported in Fig. 35. The pipe has been pulled in various stages along the longitudinal pipe axis.

Phase 1, a displacement up to 200 mm with an actuator speed of 0.1 mm/s was performed and then the load was reduced to zero. A normalized peak load of R'_A = 1.04 was recorded for a displacement of 11 mm. The load increases rapidly in the beginning, then a maximum in the load displacement curve is reached. After the initial peak, the load progressively decreases; the rate of decrease is much smaller than the initial load increase. At 200 mm the load has been removed, a slight displacement is observed in this unload phase.

Phase 2, from 200 mm to 250 mm of displacement a displacement was applied again with 0.1 mm/s of speed. The load value returned very similar to the ones recorded before the un-

loading of the previous phase and the initial loading did not exhibit a prominent peak load. During the whole axial displacement the load progressively reduces, being the rate of load reduction continuously decreasing. At 250 mm the load has been removed, very small displacement is observed in this unloading phase.

Phase 3, from 250 mm to 300 mm of displacement the speed was increased to 1 mm/s, no significant variations of loads may be observed. Again the load is seen to decrease and start from value closely to the ones of the last end phase. At 300 mm the load was reduced to zero.

Phase 4, from 300 mm to 350 mm, the actuator speed was increased again up to 2 mm/s, and alike results as the previous phase can be observed, while a slightly smoother transition up to the regime load is observed. At 350 mm of displacement the load was reduced to zero.

4.2.3. Axial pulling Test No. 3

The third axial pulling test was performed on a coated sample embedded in a sand with relative density equal to 30%. The load displacement diagram is reported in Fig. 36. The pipe has been pulled in various stages along the longitudinal pipe axis.

Phase 1, a displacement up to 200 mm with an actuator speed of 0.1 mm/s has been performed and then the load was reduced to zero. A normalized peak load of $R'_A = 1.41$ was recorded for a displacement of 38 mm. The load increases rapidly in the beginning, then a smooth transition to a maximum in the load displacement curve is reached. After the initial peak, the load progressively decreases, the rate of decrease being much smaller than the initial load increase. This rate of decrease is lower also to the ones observed for the previous

two tests, involving painted pipes. At 200 mm the load was removed, very little displacement is observed in this unload phase.

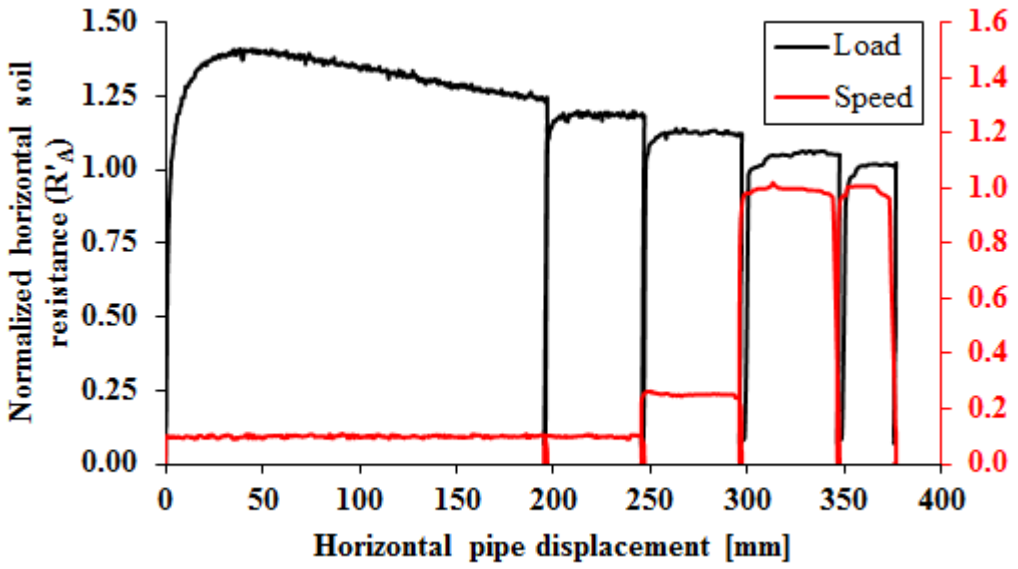

Fig. 36. Load displacement response, Test No. 3, during subsequent loadings after first loading/unloading.

Phase 2, from 200 mm to 250 mm of displacement the speed applied was again with 0.1 mm/s. The load value returned to slightly lower values compared to the ones recorder before the unloading of the previous phase and the initial loading did not exhibit a prominent peak load. The initial peak value it is not reached again. Nonetheless it appears evident that the upon reloading the diagram does not represent a simple continuation of the preceding load phase but rather reproduces, in a reduced scale, a similar behaviour as observed in the Phase 1, where a smooth transition to a load peak was present.

During the entire displacement of the Phase 2 the load does not reduce sensibly. At 250 m the load has been removed, very little displacement is observed in this unload phase.

Phase 3, from 250 mm to 300 mm of displacement the speed was increased up to 0.25 mm/s, slight decrease of the maximum loads may be observed. Again the load has a

smooth transition when approaching the maximum values. No significant load variations are observed through the 50 mm displacement. At 300 mm the load was reduced to zero. Phase 4 and Phase 5, from 300 mm to 375 mm, the actuator speed was increased again to 1 mm/s, and similar behaviour as in Phase 3 was observed. At the end of Phase 5 the load has been reduced to zero.

4.3. Prediction of axial soil resistance

The axial soil resistances obtained in this study for different soil compaction levels and pipe coating are compared herein with those computed using the formula given in ASCE [4], ALA [5], PRCI [20] guidelines for cohesionless soils as reported in (Eq. 7):

(Eq. 7) $$T_A = \pi D H \bar{\gamma} \left(\frac{1+K}{2}\right) tan\delta$$

where:

- D = pipe outside diameter;
- H = depth to pipe centerline;
- $\bar{\gamma}$ = effective unit weight of soil;
- K = K_0 = coefficient of pressure at rest for ASCE and ALA;
- K = effective coefficient of horizontal earth pressure which may vary from the value for at rest conditions for loose soil to values as high as 2 for dense dilative soils (Wijewickreme et al. [32]);
- δ = interface angle of friction for pipe and soil = f*ϕ;

- ϕ = internal friction angle of the soil;
- f = coating dependent factor relating the internal friction angle of the soil to the friction angle at the soil-pipe interface.

K can be determined experimentally as ratio between the effective horizontal stress and the effective vertical stress. K_0 in absence of experimental results it can be obtained through the empirical equation (Eq. 8) by Jaky (1944):

(Eq. 8) $$K_0 = 1-\sin\phi$$

Representative f values for various types of external pipe coatings are provided in the Table 7 ALA [5].

Pipe coating	f
Concrete	1
Coal tar	0.9
Rough steel	0.8
Smooth steel	0.7
Fusion bonded epoxy	0.6
Polyethylene	0.6

Table 7. Friction factor f for various external coatings [4] [5] [20].

In order to compare the results also the (Eq. 7) is used in normalized form:

(Eq. 9) $$T'_A = T_A/(\gamma H \pi D L)$$

Experimental findings obtained from Karimian [13] demonstrate that ASCE (Eq. 7) for cohesionless soils, in which $K = K_0 = 0.33$, cannot predict satisfactory the soil reaction when a pipe is embedded in a compacted sand. This behavior can be explained by the dilative behavior of the sand and due to the confinement of the soil around the pipe, the combination of these two conditions leads to a sensible increasing of the normal stress around the pipe, much higher than cases of nondilative soil or as placed soil compaction. The increasing of normal stresses on the pipe surface during the axial pullout test is well described and measured [13] in an increase of horizontal earth pressure coefficient (K) that after 10÷15 mm pipe axial displacement remain nearly constant. These findings are introduced in the (Eq. 7) by PRCI [20] in which is underlined that K may vary from the value at rest conditions for loose soil to values as high as 2 for dense dilative soils.

These findings are confirmed by the experimental data presented herein.

4.3.1. Axial pulling Test No. 1

Test No. 1 load displacement data compared with equations provided from aforementioned guidelines (Fig. 37) suggest an unsatisfactory level of prediction with an error of 65% using ASCE and a right prediction using $K = 2.8$ more than $K_{max} = 2$ suggested from PRCI. Friction factor suggested from

Table 7 for rough steel is 0.8, Karimian in his experiments measured 0.85, in the current study a reasonable value of 0.9 has been used as done for the numerical simulations.

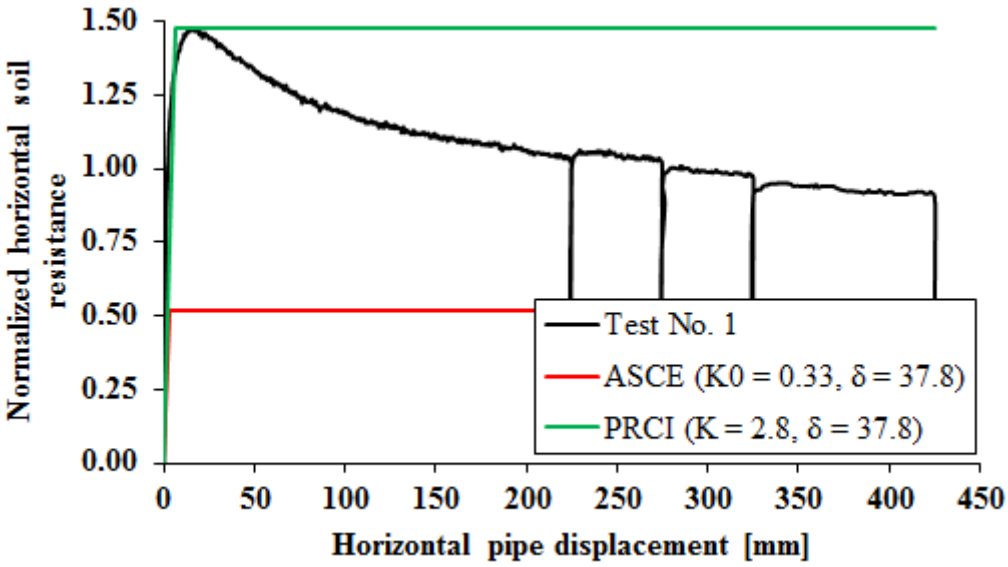

Fig. 37. Normalized load displacement response of Test No. 1 compared with normalized ASCE and PRCI predictions.

4.3.2. Axial pulling Test No. 2

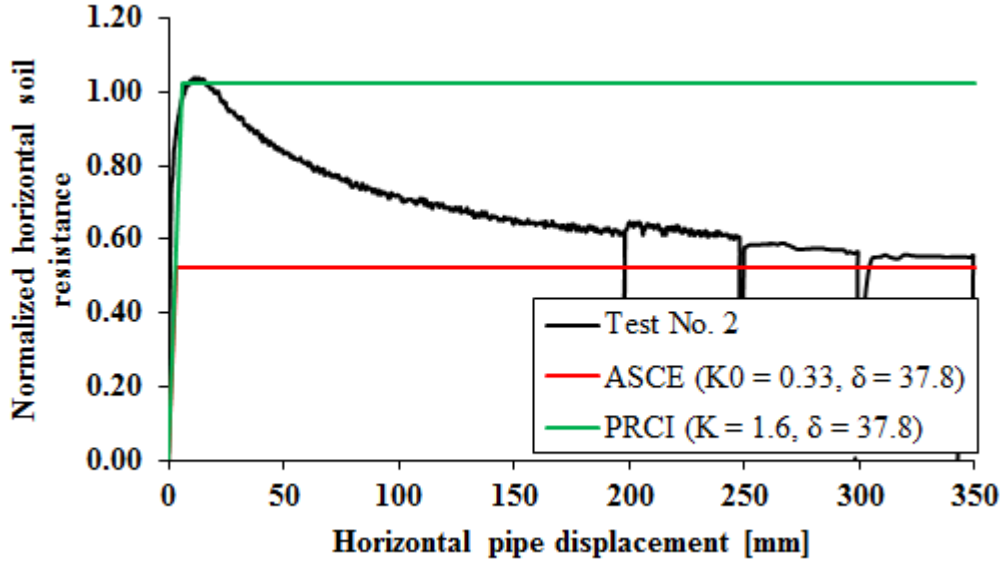

Fig. 38. Normalized load displacement response of Test No. 2 compared with normalized ASCE and PRCI predictions.

Also the comparison of Test No. 2 load displacement data (Fig. 38) with ASCE guidelines equation gives an unsatisfactory prediction with an error of 49%. A right prediction can be achieved using K = 1.6. Friction factor has been used equal to 0.9 also in this case.

4.3.3. Axial pulling Test No. 3

Test No. 3 load displacement data is compared with ASCE and PRCI in Fig. 39. In this case since peak soil resistance is only slightly less than the Test No 1 and the levels of soil compaction are nearly the same K should be the same in both cases.

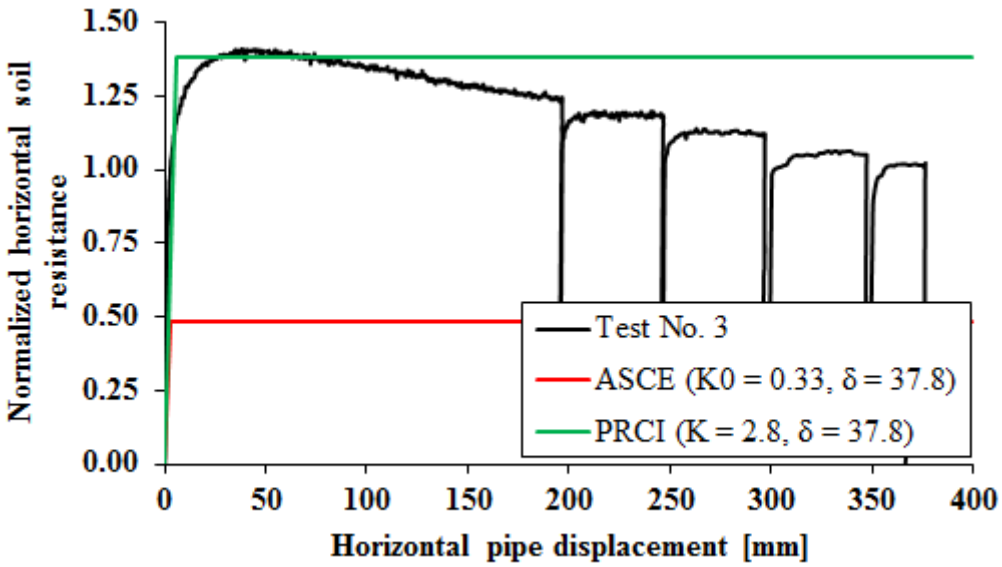

Fig. 39. Normalized load displacement response of Test No. 3 compared with normalized ASCE and PRCI predictions.

This suggests that friction factor equal to 0.6 recommended from
Table 7 for fusion bonded epoxy external pipe it is not suitable for APSACOAT 104. It has been assumed a friction factor equal to 0.85. Whit such considerations, using a K_0 = 0.33

the error of peak soil resistance prediction is equal to 66%, while K = 2.8 is a good value for predict satisfactorily the maximum value of soil resistance.

4.3.4. General comments

Back calculation of K is not supported by experimental measurements in this work, but the correlation between K back calculated and K measured from Karimian [13] is taken as a support of this procedure.

Value of K = 2.8 back calculated for Test No. 1 and Test No. 3 is higher than K_{max} = 2 suggested from PRCI, on the other hand is near K = 2.5 back calculate for a full-scale axial pulling test performed from Karimian [13] on blasted steel pipe embedded in high compacted rivers sand.

4.4. Numerical modeling

The results obtained from full-scale axial pullout tests performed on 8”$^{5/8}$ steel pipe with two different surface finish embedded in quarry sand has been carried out to understand the soil reaction during ground movements and as a preliminary test before to perform the landslide/fault full-scale tests that are main composed of two relative displacements between soil and pipe, axial and lateral movements.

The experimental findings have been used to compare the measurements with analytical approaches available in literature and validate numerical model developed to simulate these tests.

4.4.1. Finite element modeling

The numerical analysis was conducted using a commercial finite element program ABAQUS 6.14 version [1], accompanied from a subroutine[3] written in FORTRAN language in order to achieve the softening behavior of the soil.

A four-node doubly curved general-purpose shell, finite membrane strains (S4) are employed for modeling the cylindrical pipeline cross section and an eight-node linear brick (C3D8) are used to simulate the surrounding soil and the rear wall of the soil caisson. The model has the same dimension of the experimental tests as depicted in Fig. 40 also the pipe diameter and the wall thickness. The soil mesh is the result of sensitivity analysis conducted in order to reach a good compromise between accuracy of results and velocity of simulation, the dimension of the mesh is chosen finer around pipe with a constant increase towards the boundaries of the model. No plastic deformations are expected for the steel pipe therefore no particular refinement of the mesh is used, the size of shell elements in the circumferential direction has been chosen equal to 28.7 mm and 50 mm in the longitudinal direction. The distance from the pipe crown and the top surface is 2.9D, 1.32D from the pipe invert to the bottom of the soil prism, 6.8D the distance from the pipe axis and the lateral walls.

The top surface of the prism represents the soil surface, others surfaces were in contact with the internal surfaces of the soil caisson. The nodes of the bottom surface are constrained for all translational directions; normal direction is constrained for lateral surfaces except for the rear wall in which the constrain is provided with surface to surface contact

[3] Developed by Ioannis Anastasopoulos

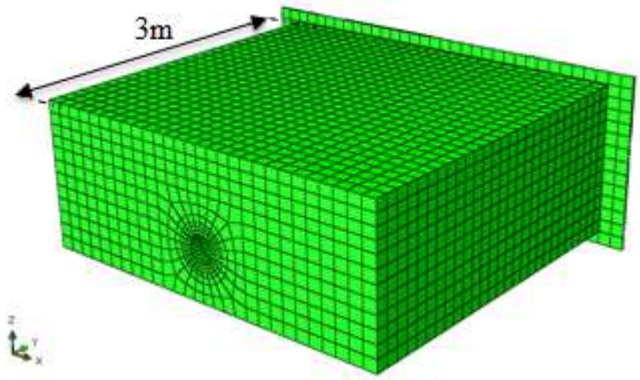

a) Finite element mesh of soil and rear wall.

b) Finite element mesh of pipeline.

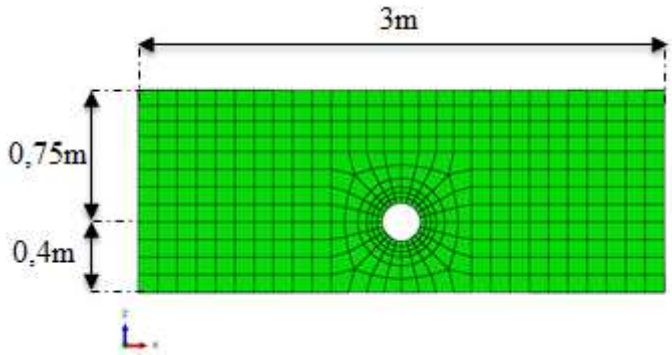

c) Finite element mesh of soil prism cross-section.

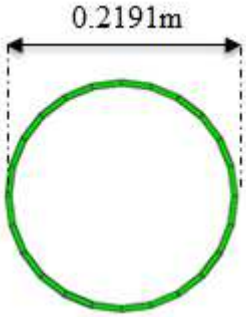

d) Finite element mesh of pipeline cross-section.

Fig. 40. Finite element model of the axial pullout test.

between soil surface and bulkhead surface in order to allow the separation. These boundary conditions are commonly used in models published in literature and represent a good approximation of experimental conditions. The interface interaction between the pipe and the surrounding soil is simulated with a contact algorithm that include normal contact and tangential friction coefficient in which separation after contact is allowed, a master-slave contact algorithm between external pipe surface and soil surface has been used. ASCE guidelines [4] suggest a friction angle equal to 0.8*ϕ between the soil and a rough steel pipe,

Karimian [13] for his rough steel specimens measured 0.85*ϕ with a direct shear test between soil and pipe. The numerical analysis conducted to simulate Test No. 1 and Test No. 2, 0.9*ϕ was used. Fusion bounded epoxy coating has been used for the specimen of Test No. 3 therefore ASCE guidelines suggest f = 0.6, this value also in the numerical model is too low to permit reaching a reasonable result in terms of soil reaction, for the same reasons aforementioned in the previous section friction factor was used equal to 0.85.

An elastic model is used for the steel pipe material because it is not expected plastic deformation on the other hand an elastic perfectly-plastic constitutive model with Mohr Coulomb failure criterion was used modified by means the aforementioned subroutine (USDFLD) that take into account the strain softening of the soil. This subroutine is based on strain softening adjustments proposed by Anastasopoulos et al. [2]. Referring on Fig. 41 the shear band in a direct shear test can be considered formed after the peak point, therefore up to this point the shear strain can be assumed uniformly distributed throughout the whole height of the soil specimen (H_s) hence the plastic shear strain at peak point will be $\gamma_p^p = \frac{\delta x_p - \delta x_y}{H_S}$. After formation of the shear band it is assumed that all plastic shear deformations take place within the shear band, while the rest of the soil remains elastic, in this case the use of finite element method may lead to mesh dependent solutions but defining a ratio between the real and the FE computed shear strain the scale effect can be incorporated into the model in a reasonably approximate manner and obtain the following relation: $\gamma_f^p = \gamma_p^p + \frac{\delta x_f - \delta x_p}{H_{FE}}$ in which H_{FE} is the height of the FE element.

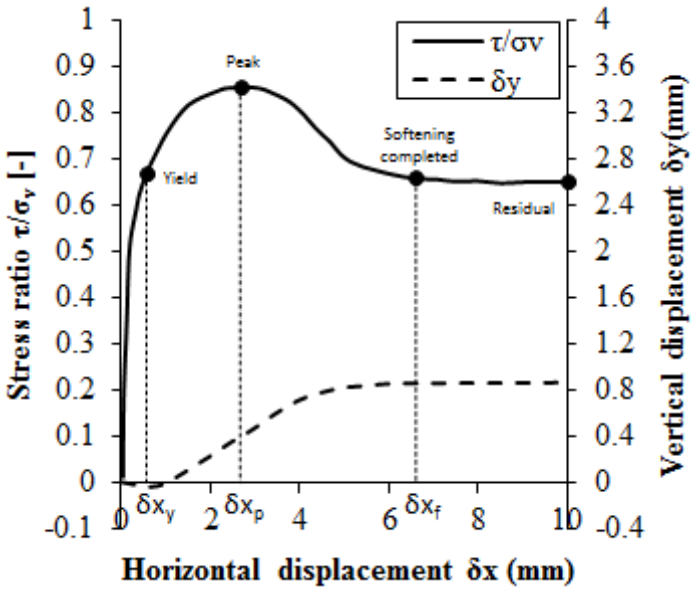

Fig. 41. Typical variation of stress ratio and volume change with respect to horizontal displacement in a direct shear test (Shibuya et al. [22])

In order to ease numerical stability, all simulations were performed with a slight cohesion equal to 0.1 kPa.

The analysis has been conducted in three steps as follow: geostatic stress is applied in the initial step, the gravity loading in the first step and maintained in the second step then the axial pipe displacement in the second step. A uniform axial controlled displacement of the pipe is imposed.

4.4.2. Axial pulling model of Test No. 1

The calculated soil loads on the pipe from the numerical model are compared with measured soil reaction Fig. 42 (Test No. 1).

Setting the model with the soil strength parameters aforementioned (i.e. peak friction angle equal to 42°, residual friction angle equal to 36° and a dilation angle of 10° used also for the other numerical models presented in this work), assuming 0.9 as friction factor then a parametric analysis has been carried out varying the initial value of K (not measured experimentally). This analysis demonstrates that a value of lateral earth pressure around K_0 (that means ~0.33 in this case) is inadequate to reach the peak soil reaction measured experimentally. For this reason and considering the compaction applied on the sand it is reasonable assume K = 1 as measured from Karimian in his tests with high level of compaction ad as assumed from Jung [12].

With this plausible assumption the load displacement obtained from the numerical simulation is in good agreement with experimental data for the first 50 mm of pipe displacement.

In experimental findings after the peak point reaction load progressively reduces as highlighted in a previous section, on the the contrary numerical model demonstrate the inability to describe that response introducing only the softening response by means the subroutine mentioned before.

The experimental results show a secondary phenomenon well known in the research. From large displacement interface shear tests it is known that after the initial soil dilation the normal stress will reduce with increase in displacement. This phenomenon is called frictional degradation behavior and it was observed by several soil element tests such as buried pipes from Weerasekara and Wijewickreme [30], pipe driving from White and Lehane [31]. The reduction in diameter due to Poisson's effect is not sufficient justify this stress reduction in axial pullout tests as experimented from Wijewickreme et al. [32].

This phenomenon can be explained as the contraction associated with wear and tear of grain asperities leading to particle rearrangement in particular under large shear displace-

ments (Luo et al. [14], Zeghal and Edil [33]). Price (1988) affirmed that with the increasing displacement, the finer particles may fill the space between larger particles increasing the contact area. This increase will reduce the inter-particle forces. With this mechanism, it is also debated that the rate of particle crushing will be reduced with the increasing displacement.

Although the frictional degradation behavior has been widely observed, only few studies have been performed to evaluate this phenomenon in detail Randolph et al. [21].

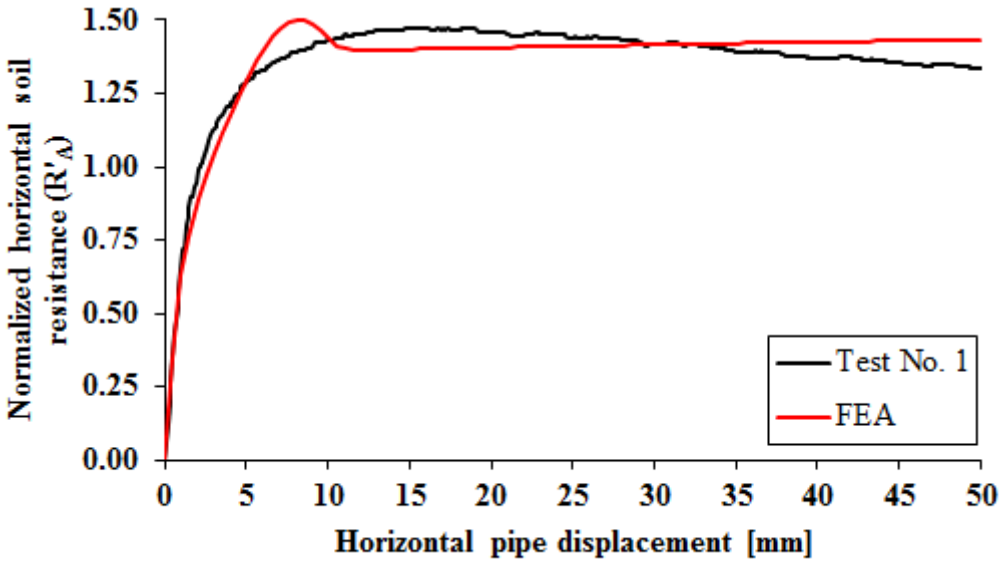

Fig. 42. Normalized load displacement response of Test No. 1 compared with normalized FEA analysis.

Therefore the model developed lack of this frictional degradation assumes a constant soil reaction after the point of softening. This result can be accepted as it goes in the direction of the caution and at the same time does not over predict too much the residual soil resistance. Horizontal and vertical stress results (Fig. 43 and Fig. 44 respectively) obtained with numerical analysis and extracted from a central section of soil prism show together an increasing of normal stress around the pipe, the ratio between horizontal stress and vertical stress at the springline depth give a value of K = 2.2.

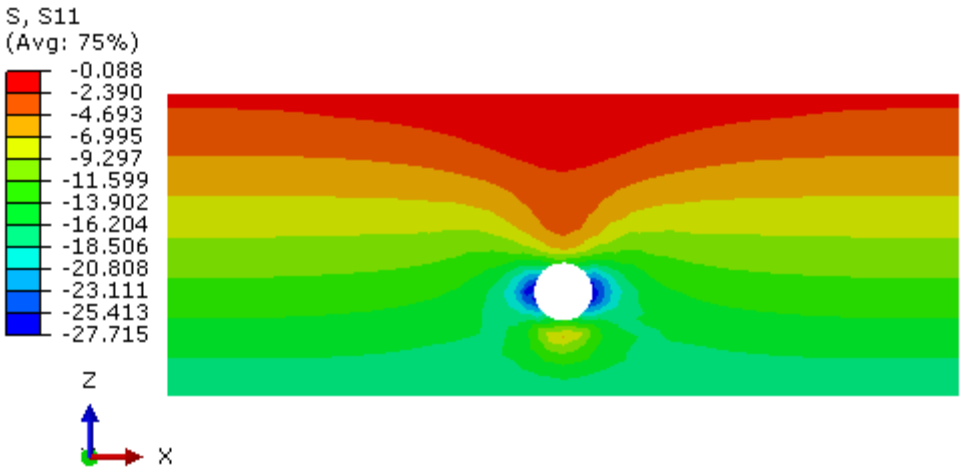

Fig. 43. Horizontal stresses contour after 50 mm of axial pipe displacement related to the model of Test No. 1.

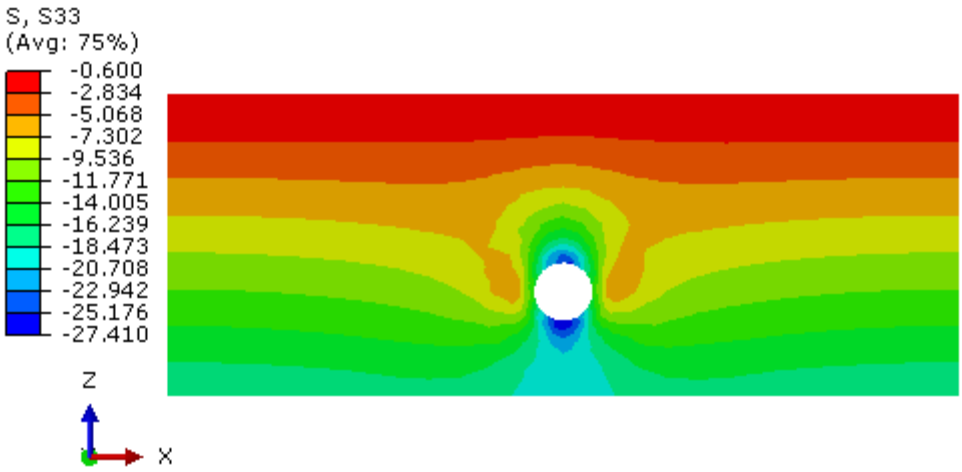

Fig. 44. Vertical stresses contour after 50 mm of axial pipe displacement related to the model of Test No. 1.

4.4.3. Axial pulling model of Test No. 2

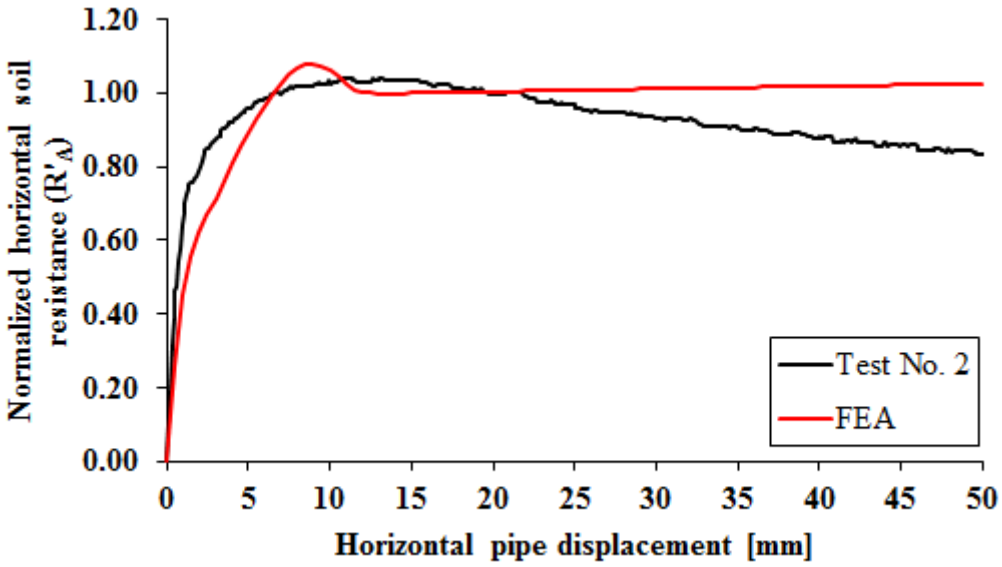

Fig. 45. Normalized load displacement response of Test No. 2 compared with normalized FEA analysis.

In this case the parameters used for the model (peak friction angle equal to 42°, residual friction angle equal to 36° and a dilation angle of 10°) are the same used for the Test No. 1 except for the initial value of K. Known the lower level of compaction of the Test No. 2 respect to the Test No. 1 and known that values of strength parameters are nearly the same in both cases the unique difference between the two cases can be summarized in a difference of initial coefficient of horizontal earth pressure. After a parametric analysis K = 0.5 has been determined as reasonable value. The result is shown in Fig. 45.

At 50 mm of pipe displacement the numerical analysis give a value of K = 1.8. Horizontal and vertical stresses are depicted in Fig. 46 and Fig. 47 for that displacement.

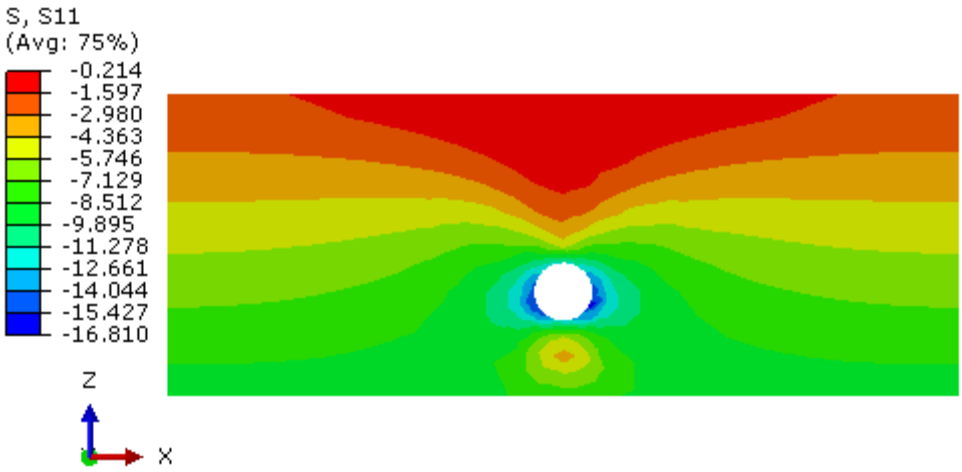

Fig. 46. Horizontal stresses contour after 50 mm of axial pipe displacement related to the model of Test No. 2.

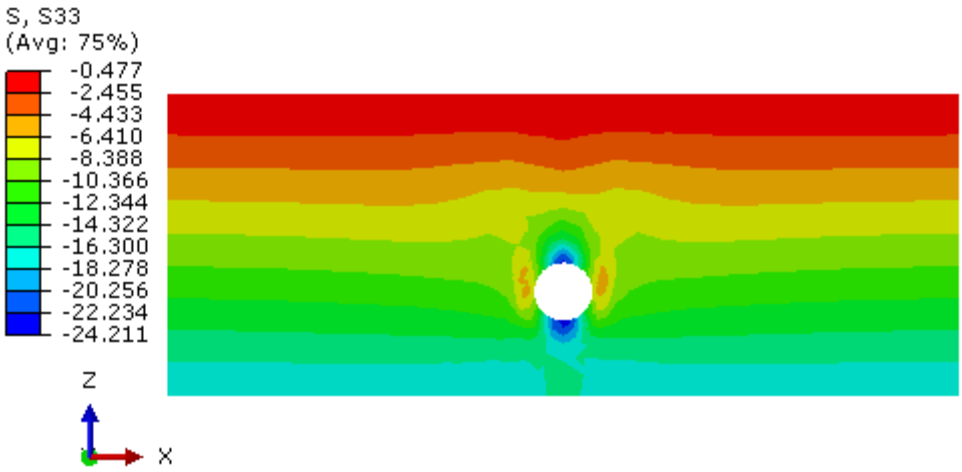

Fig. 47. Vertical stresses contour after 50 mm of axial pipe displacement related to the model of Test No. 2.

4.4.4. Axial pulling model of Test No. 3

Test No. 3 was performed in the same conditions of soil compaction achieved for the Test No.1. With this in mind the only parameter that should be varied into the model respect the numerical analysis conducted for the Test No. 1 is the coefficient of friction between pipe and soil. As discussed before for the prediction of soil resistance using ASCE [4] and PRCI [20] equations, suggested value of friction factor equal to 0.6 for fusion bonded epoxy coatings is not suitable for this case. Therefore it has been assumed a friction factor equal to 0.85 also for the numerical model. The load displacement result is shown in Fig. 48.

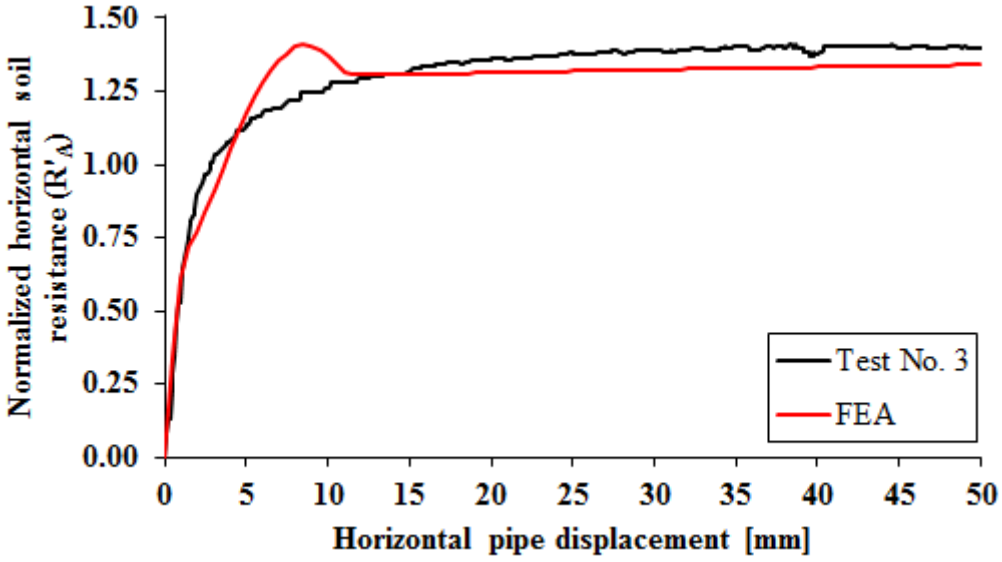

Fig. 48. Normalized load displacement response of Test No. 3 compared with normalized FEA analysis.

The numerical results of the horizontal and vertical stresses extracted at 50 mm of pipe displacement are shown in Fig. 49 and Fig. 50 This analysis give a value of K = 1.9 compatible with a slightly lower axial soil reaction respect the Test No. 1.

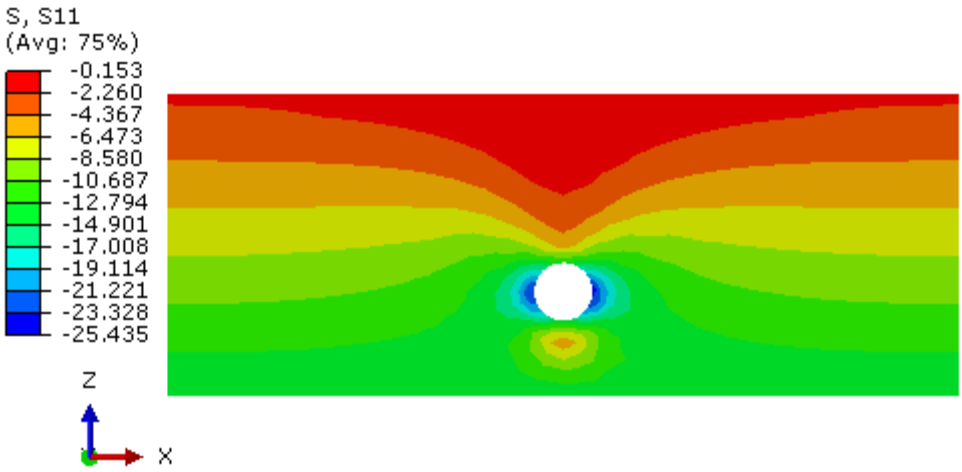

Fig. 49. Horizontal stresses contour after 50 mm of axial pipe displacement related to the model of Test No. 3.

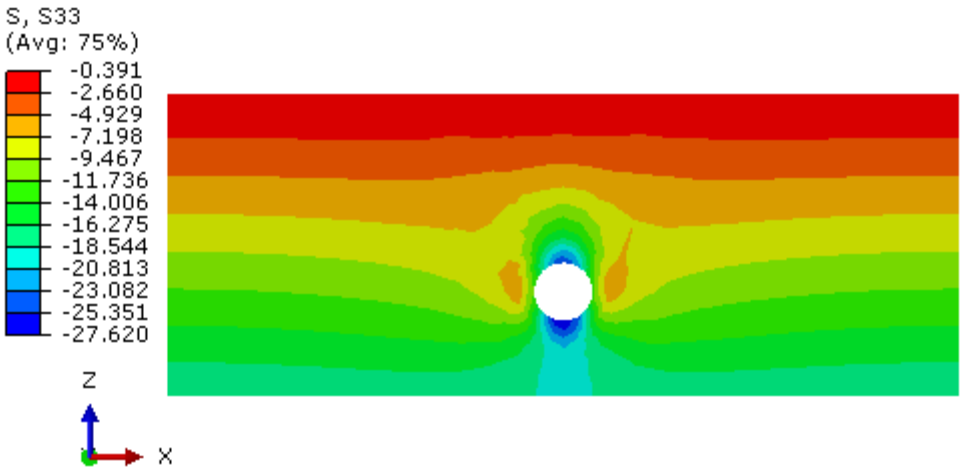

Fig. 50. Vertical stresses contour after 50 mm of axial pipe displacement related to the model of Test No. 3.

4.5. Discussion of the results

After the analyses conducted with analytical and then numerical approach is recommended during preparation and performing of full-scale assessments to determine the interface fric-

tion angle between soil and material of pipe and to measure experimentally variations of stresses around the pipe to determine with more accuracy:

- The friction factor between a specific soil and a specific pipe coating;
- The development of K during axial pullout test;
- The frictional degradation.

useful to perform more accurate numerical analysis on a longer pipeline embedded in such conditions.

5. Embedded pipes subjected to lateral puling action

5.1. Introduction

This chapter describes the experimental findings obtained from three lateral pulling tests on steel pipes, the results from numerical models. The results are discussed and also compared with current recommended methods for prediction of lateral loads on buried pipelines during ground movements.

In order to align the results presented in this study to the current practice the lateral soil resistance is presented in form of normalized lateral soil resistance as defined below:

(Eq. 10) $$R'_L = R_L/(\gamma HDL)$$

and in some cases also the displacement is used in normalized form:

(Eq. 11) $$D'_L = D_L/D$$

where:

- R_L: is the pulling load;
- γ: is the soil density;
- H: is the burial depth of the pipe springline;
- D: is the outside pipe diameter;
- L: is the pipe length;

- D_L: the pipe lateral displacement.

The concept of dimensionless load and normalized displacement has been used previously by Audibert and Nyman [6], Trautmann and O'Rourke [24], Paulin et al.[19].

The value of R'_L represents the average shear force around the pipe normalized with respect to the vertical effective stress given from the soil above the centreline of the pipe.

Test configuration	Horizontal lateral pullout
Soil type	Quarry sand
Average density	From 1600 to 1645 kg/m^3 respectively for D_r = 20% and D_r = 40%
Average moisture	From 6.1% to 7.6%
Average internal friction angle	ϕ_p = 42°, ϕ_r = 36°
Caisson size	3 m x 3 m x 1.25 m
Pipe size	OD = 8"$^{5/8}$ (219.1 mm), WT = 5.56 mm, length = 2.9 m
Pipe grade & Surface	API5L X65, antioxidant paint and Apsacoat 104
Overburden ratio	H/D = 3.4
Loading rate	Min = 0.5 mm/s, Max = 1 mm/s

Table 8. Summary of parameters in lateral pullout testing.

5.2. Lateral load vs. displacement response

Test No.	Test	Relative density	Mass density	Water content	Pipe coating	Internal pres-sure	Overbur-den ratio
[-]	[-]	[%]	[kg/m3]	[%]	[-]	[MPa]	[-]
4	Lateral 1	22	1600	7.6	Antioxidant paint	0	3.4
5	Lateral 2	35	1640	6.1	Antioxidant paint	0	3.4
6	Lateral 3	35	1645	7.3	Apsacoat 104	0	3.4

Table 9. Summary of lateral tests performed.

In this section, results of horizontal soil reaction measurements during lateral pullout tests are presented. As summarized in

Table 9 Test No. 4 and Test No. 5 with the same pipe coating differ for the relative density level, 22% and 35% respectively, besides Test No. 4 and Test No. 6 with the same relative density level (equal to 35%) differ for the pipe coating.

The normalized lateral soil resistance R'_L respect to the pipe displacement is shown in Fig. 51 for Test Nos. 4, 5 and 6. In each test the pipe has been pulled and unloaded in various stages and during these stages the velocity of pipe displacement was increased from 0.1 mm/s to 1 mm/s but no effects were noticed. The constant increasing of the soil reaction in all these tests is due to the constrained uplift of the pipe with the aforementioned rails.

The difference in soil relative density between Test No. 4 and Test No. 5 is detected in a small difference of soil reaction for the first 250 mm of pipe displacement (Fig. 51), after

this displacement there is an overlapping due to the achievement of the same soil compaction.

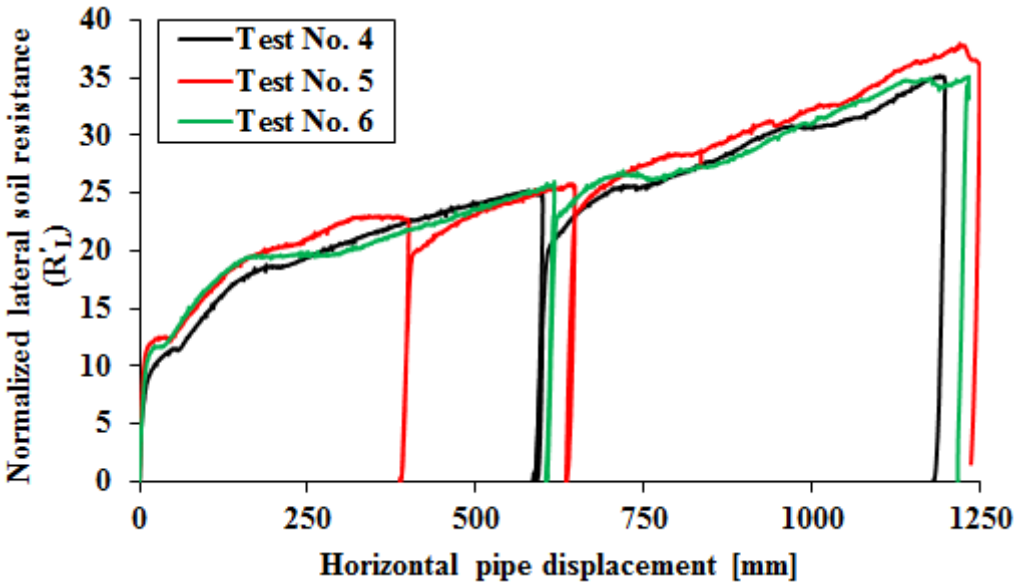

Fig. 51. Load displacement response, Tests Nos. 4, 5, 6, during subsequent loadings after first loading/unloading.

Moreover reducing the friction factor of external pipe surface by using a smoother coating on the Test No. 6 lead to a slightly lower soil reaction respect to the Test No. 5. This small difference detected also during axial pullout measurements confirm comparable interfacial friction angle among sand and two different pipe coating tested.

5.2.1. Lateral pulling Test No. 4

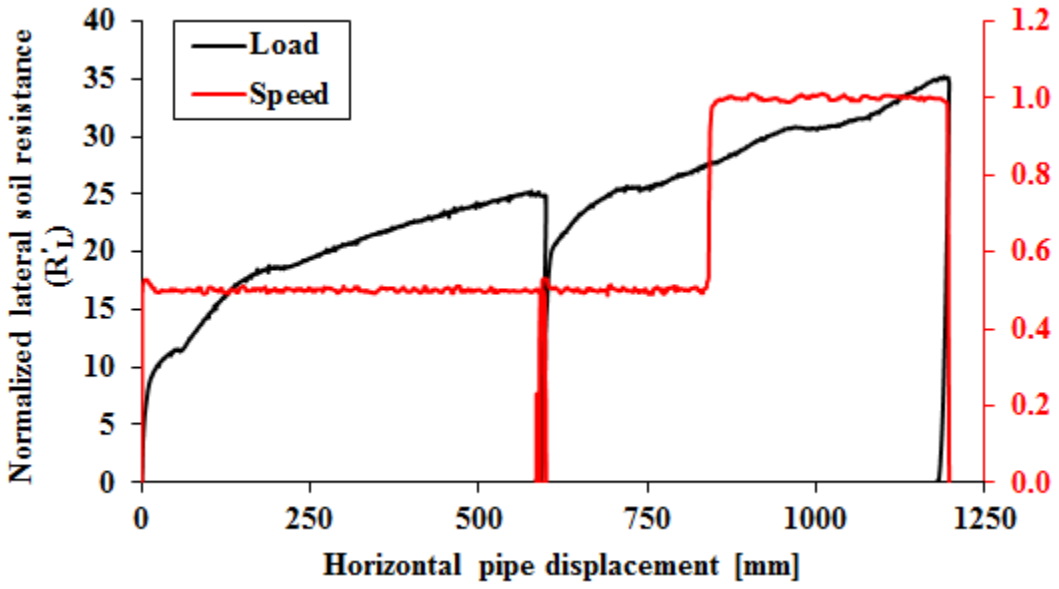

Fig. 52. Load displacement response, Test No. 4, during subsequent loadings after first loading/unloading.

The first transversal pulling was performed on a painted sample adopting the lowest level of soil relative density (D_r = 22%) tested in this study. The pipe has been pulled in two phases along a horizontal direction, transversal to the pipe axis:

- Phase 1, up to 600 mm of displacement with a speed of 0.5 mm/s;
- Phase 2, from 600 mm to 1200 mm, with a speed of 0.5 mm/s up to 800 mm then 1 mm/s to the end.

This variation of speed did not result in an appreciable variation of the soil reaction as clear from the load displacement response reported in Fig. 52.

Between Phase 1 and Phase 2 the load was reduced to zero and the load value returned significantly lower to the ones recorder before the unloading of the previous phase for about 20% less.

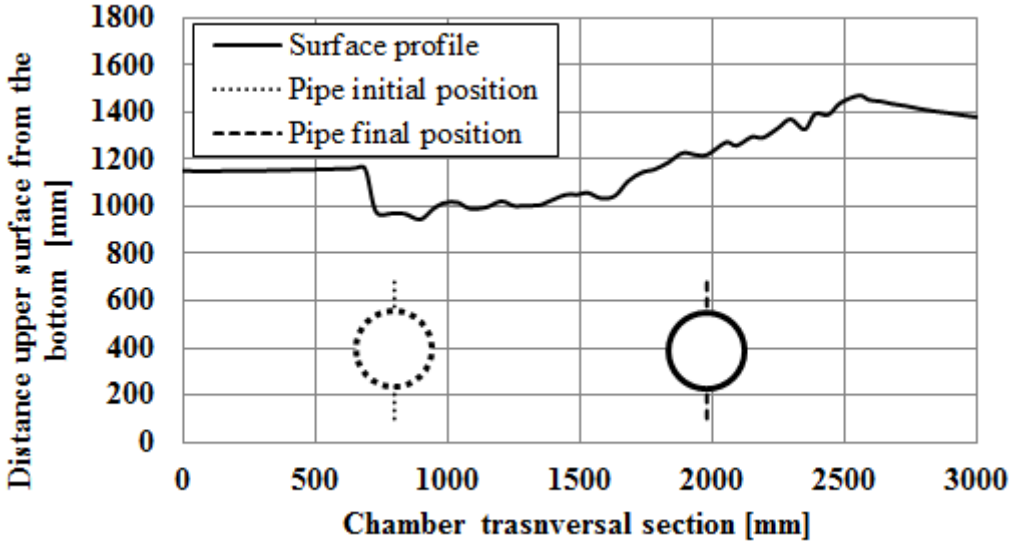

Fig. 53. Soil surface profile measured by laser scanning at the end of the transversal pulling test (Test No. 4).

In Fig. 53 is graphically reported the measurement of soil profile at the end of the test by a laser equipment. Significant amount of soil displaced in vertical direction can be observed. In general the soil subsidence left behind the pipe during its motion is lower than one pipe diameter.

5.2.2. Lateral pulling Test No. 5

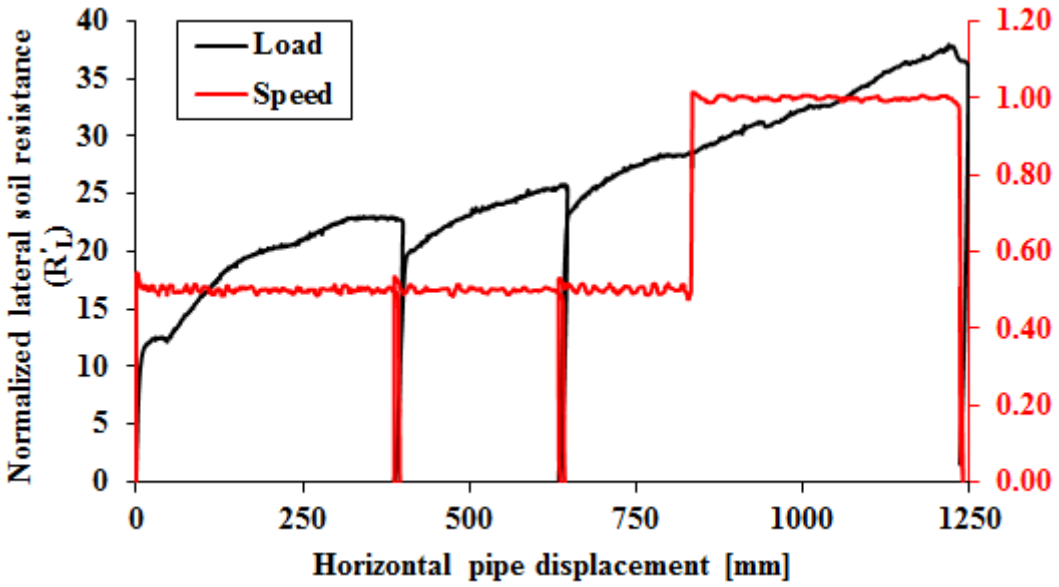

Fig. 54. Load displacement response, Test No. 5, during subsequent loadings after first loading/unloading.

The second transversal pulling test was performed on a painted sample adopting the level of soil relative density equal to 35%. The pipe has been pulled in three phases along a horizontal direction, transversal to the pipe axis:

- Phase 1, up to 400 mm of displacement with a speed of 0.5 mm/s;
- Phase 2, from 400 mm to 650 mm, with a speed of 0.5 mm/s;
- Phase 3, from 650 to 1250 mm, with speed of 0.5 mm/s up to 800 mm then 1 mm/s to the end.

Also in this case the variation of speed did not result in an appreciable variation of the soil reaction as visible from the load displacement response reported in Fig. 54.

Between Phase 1 and Phase 2 the load was reduced to zero and the load value returned significantly lower to the ones recorder before the unloading of the previous phase for about

14% less. Again between Phase 2 and Phase 3 the load was reduced to zero and the load value returned lower to the ones recorder before the unloading at about 7% less.

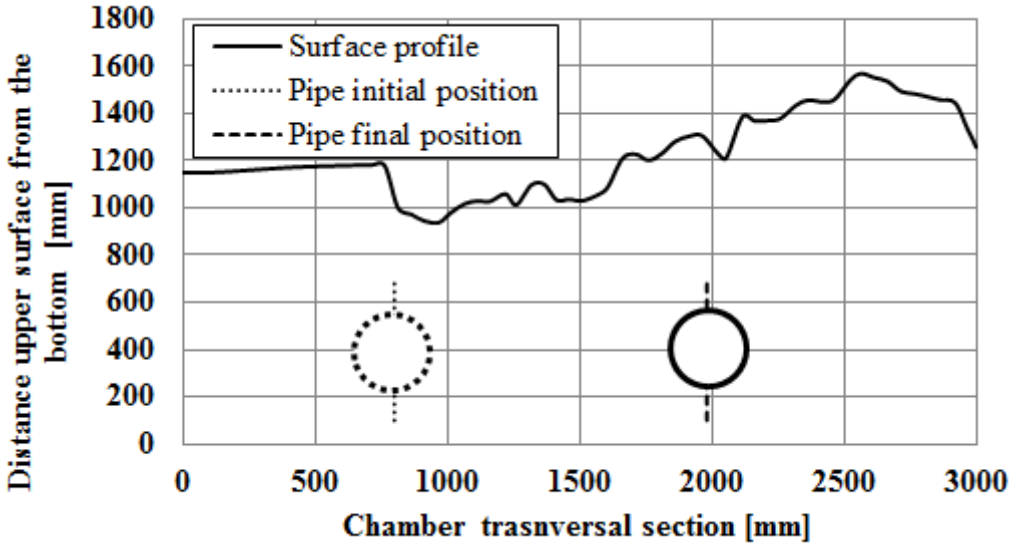

Fig. 55. Soil surface profile measured by laser scanning at the end of the transversal pulling test (Test No. 5).

In Fig. 55 is graphically reported the measurement of soil profile at the end of the test by a laser equipment. Significant amount of soil displaced in vertical direction can be observed. In general the soil subsidence left behind the pipe during its motion is lower than one pipe diameter.

5.2.3. Lateral pulling Test No. 6

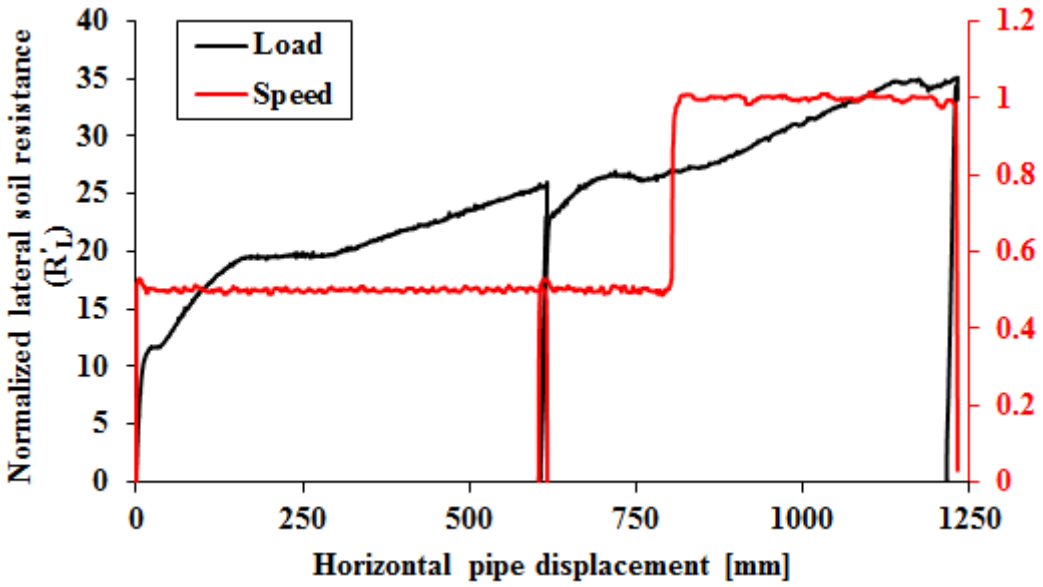

Fig. 56. Load displacement response, Test No. 6, during subsequent loadings after first loading/unloading.

The third transversal pulling was performed on a coated sample adopting the level of soil compaction equal to 35%. The pipe has been pulled in two phases along a horizontal direction, transversal to the pipe axis:

- Phase 1, up to 620 mm of displacement with a speed of 0.5 mm/s;
- Phase 2, from 620 mm to 1230 mm, with a speed of 0.5 mm/s up to 800 mm then 1 mm/s to the end.

The variation of speed did not result in an appreciable variation of the soil response, the load displacement response is reported in Fig. 56.

Between Phase 1 and Phase 2 the load was reduced to zero and the load value returned significantly lower to the ones recorder before the unloading of the previous phase for about 11% less.

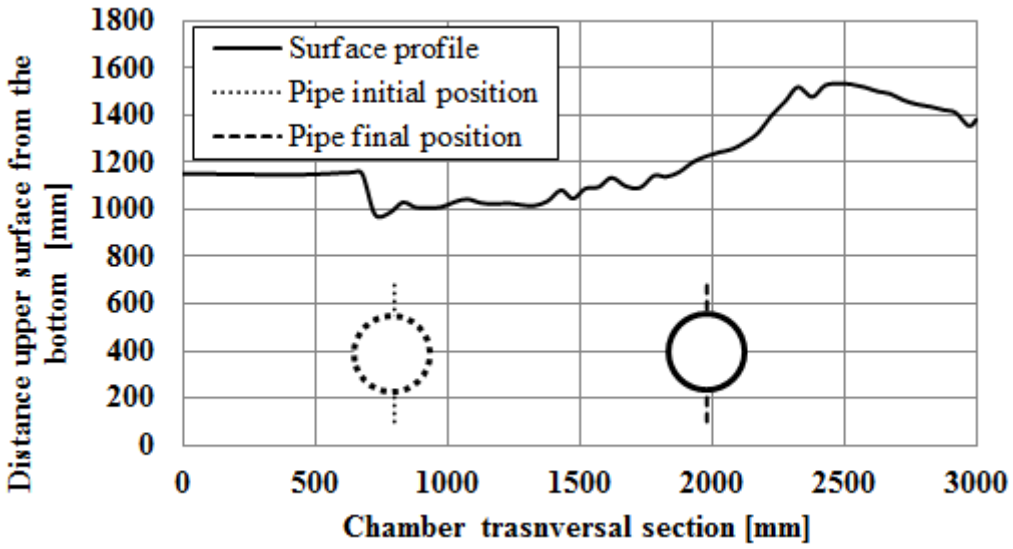

Fig. 57. Soil surface profile measured by laser scanning at the end of the transversal pulling test (Test No. 6).

In Fig. 57 is graphically reported the measurement of soil profile at the end of the test by a laser equipment. Significant amount of soil displaced in vertical direction can be observed. In general the soil subsidence left behind the pipe during its motion is lower than one pipe diameter.

5.3. Distribution of soil pressure around the pipe

Pipe soil interface pressures measured with the sensor Tekscan 3150E during the lateral pulling tests have been computed, plotted for several steps of pipe displacement and for each lateral full-scale test.

The distribution of soil pressure increase during the pipe displacement as expected and also there is clockwise rotation of the resultant pressure i.e. at the beginning the resultant pushes the pipe down, at around 30-50 mm of pipe displacement the resultant is in the opposite

direction of pipe movement, after 30-50 mm of pipe displacement the resultant push the pipe up. This rotation may be observed in Fig. 59, Fig. 72 and Fig. 85.

In accordance with analytical and numerical analysis presented in the next sections the small plateau pointed out in Fig. 58 is the peak of lateral soil resistance of a pipe in the same conditions tested herein but without vertical constrain. This affirmation is confirmed by the distribution of pressure presented in in this section.

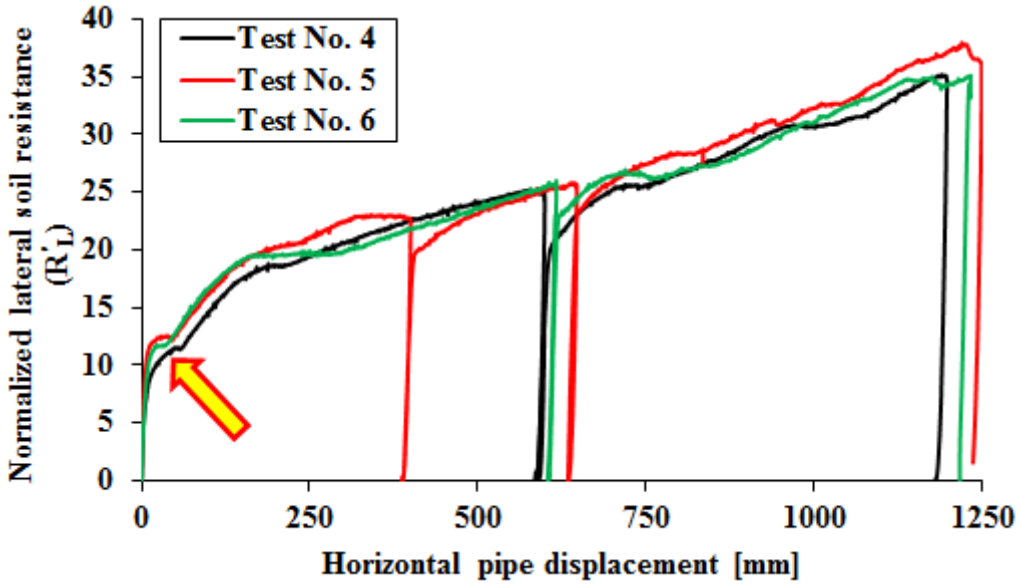

Fig. 58. Small plateau in the curves of load displacement response (Tests Nos. 4, 5, 6)

5.3.1. Lateral pulling Test No. 4

Fig. 59 shows the average of pressure distribution at the pipe soil interface for several steps of pipe displacement for the Test No. 4.

The maximum value of pressure increase during the pullout, from 120 kPa for 10 mm of pipe displacement to 275 kPa for 830 mm of pipe displacement.

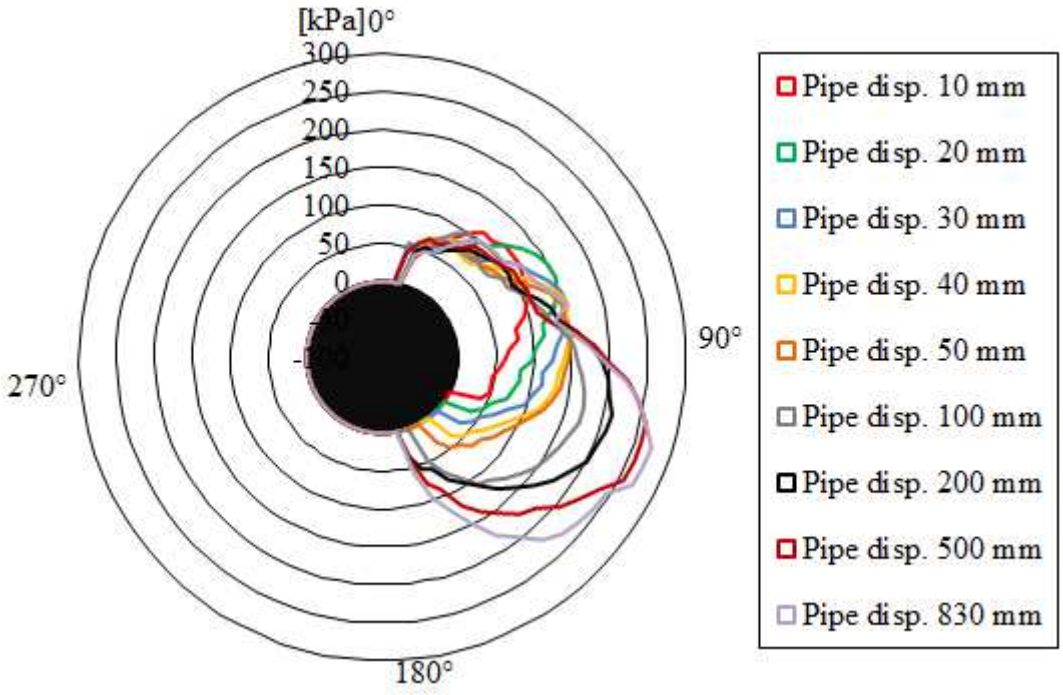

Fig. 59. Average pressure distribution at pipe-soil interface during Test No. 4.

In this case the distribution of pressure at pipe soil interface develops in three principal phases:

- Phase 1, before the yielding point (Fig. 60 and Fig. 61) the vertical component of pressure resultant pull the pipe down;
- Phase 2, at the small plateau just before the hardening behavior of the soil (Fig. 62 and Fig. 63) the vertical component of pressure resultant is nearly to zero around 50 mm of pipe displacement, therefore is right to assume at this displacement the soil resistance as the maximum lateral resistance of a pipe in the same conditions but without vertical constrain;
- Phase 3, the vertical component of pressure resultant start to push up the pipe but due to the vertical constrain the soil continue to increase its level of compaction in-

creasing constantly the horizontal reaction as show from Fig. 64 to Fig. 71 which highlights pressure distribution and respective load displacement value.

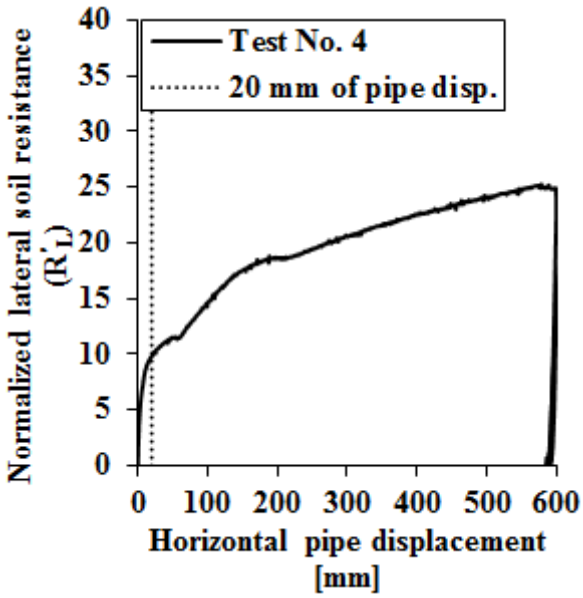

Fig. 60. Load displacement response Test No. 4. Highlight of 20 mm pipe displacement.

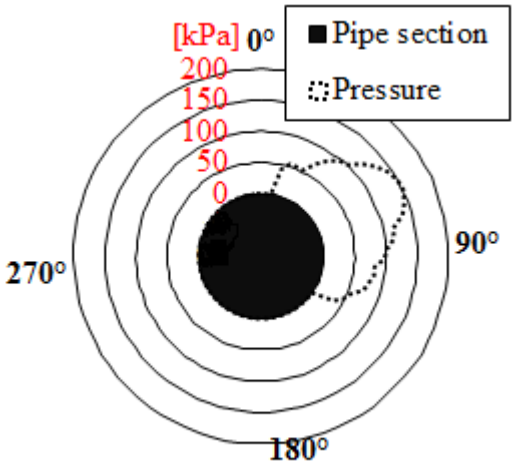

Fig. 61. Pipe soil interface pressure distribution at 20 mm of pipe displacement.

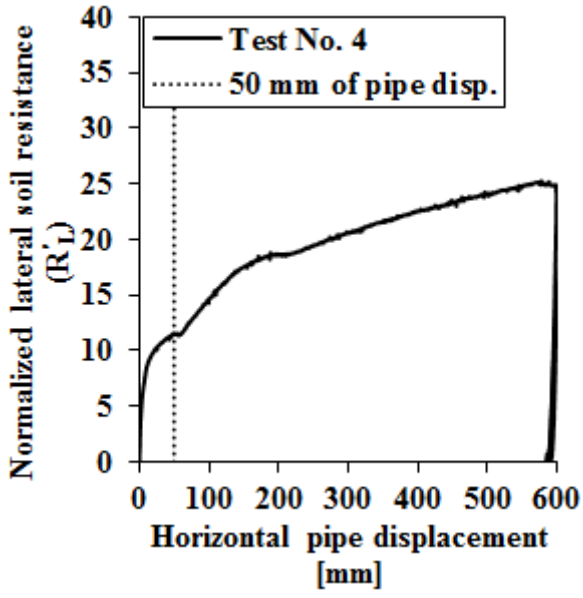

Fig. 62. Load displacement response Test No. 4. Highlight of 50 mm pipe displacement.

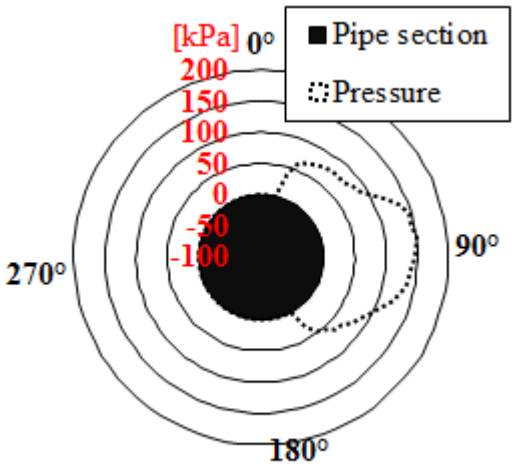

Fig. 63. Pipe soil interface pressure distribution at 50 mm of pipe displacement.

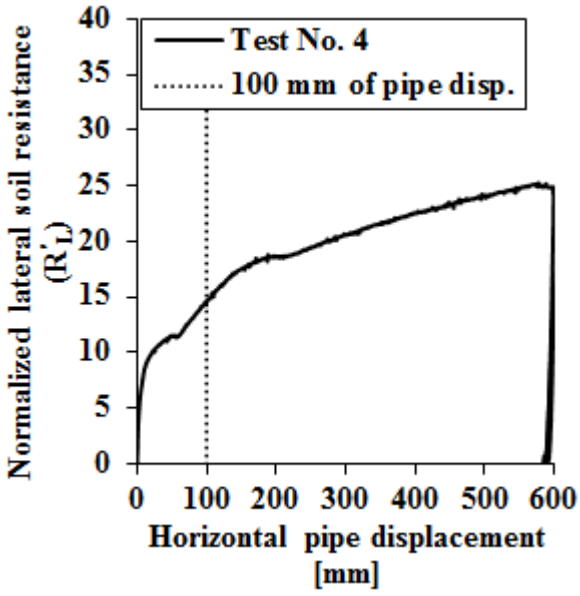

Fig. 64. Load displacement response Test No. 4. Highlight of 100 mm pipe displacement.

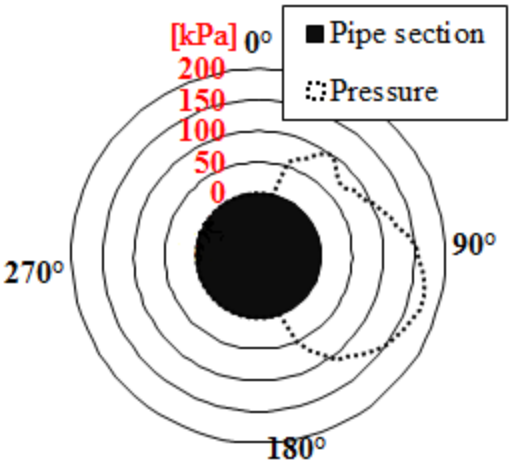

Fig. 65. Pipe soil interface pressure distribution at 100 mm of pipe displacement.

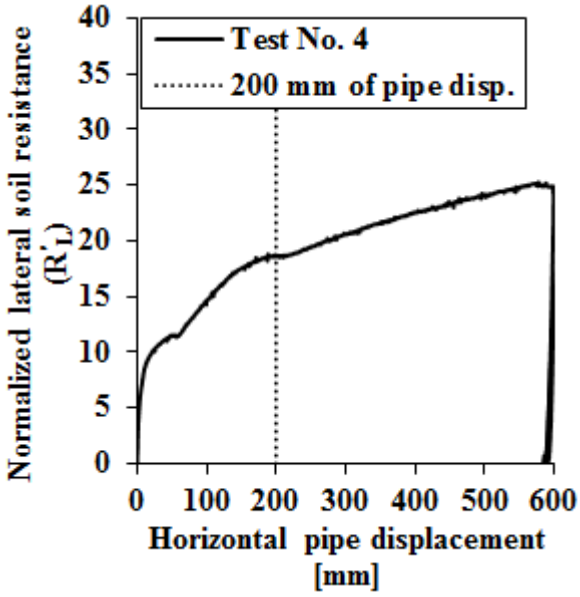

Fig. 66. Load displacement response Test No. 4. Highlight of 200 mm pipe displacement.

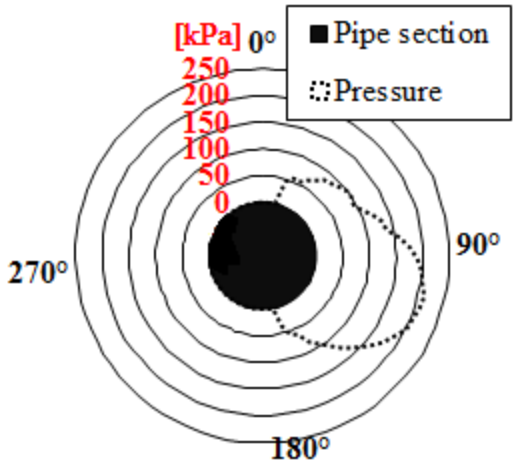

Fig. 67. Pipe soil interface pressure distribution at 200 mm of pipe displacement.

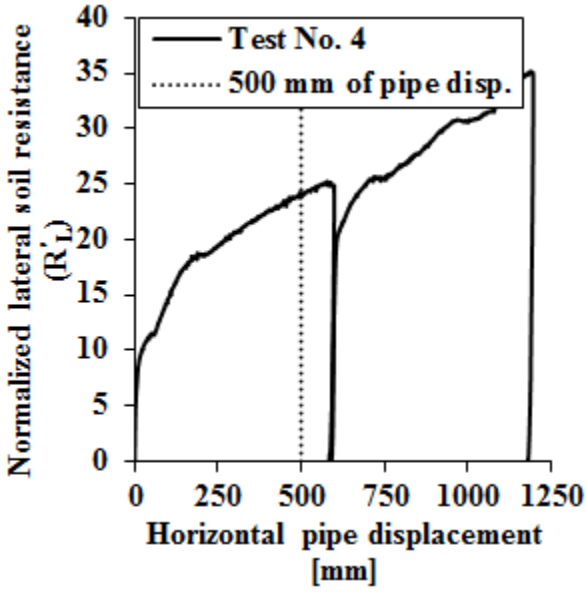

Fig. 68. Load displacement response Test No. 4. Highlight of 500 mm pipe displacement.

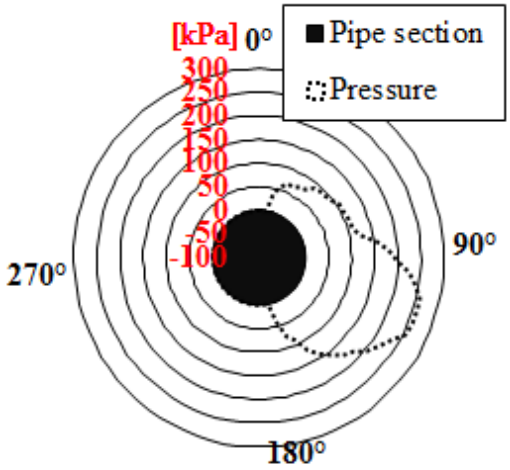

Fig. 69. Pipe soil interface pressure distribution at 500 mm of pipe displacement.

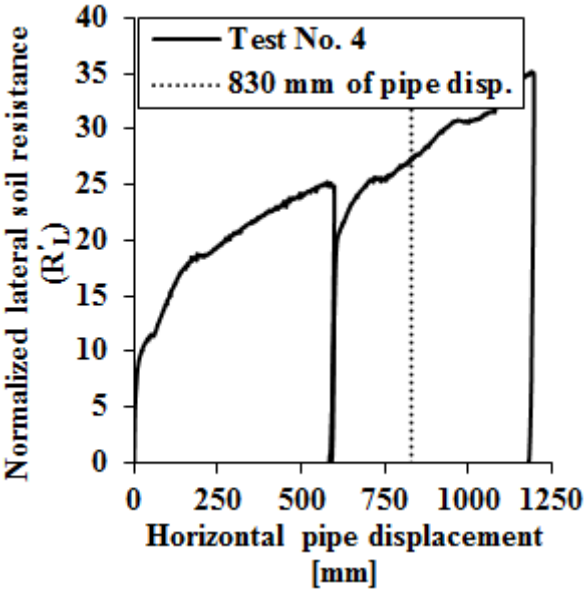

Fig. 70. Load displacement response Test No. 4. Highlight of 830 mm pipe displacement.

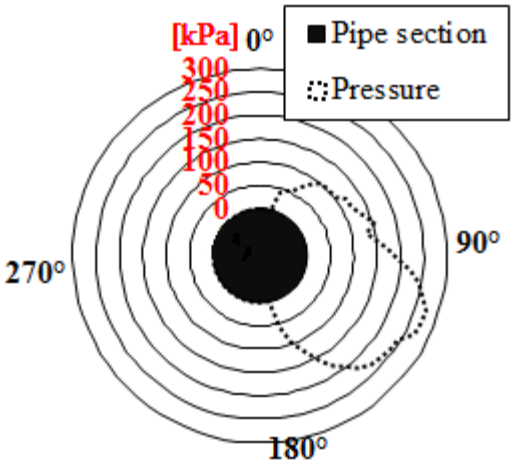

Fig. 71. Pipe soil interface pressure distribution at 830 mm of pipe displacement.

5.3.2. Lateral pulling Test No. 5

Fig. 72 shows the average of pressure distribution at the pipe soil interface for several steps of pipe displacement for the Test No. 5.

The maximum value of pressure increase during the pullout, from 150 kPa for 10 mm of pipe displacement to 320 kPa for 760 mm of pipe displacement.

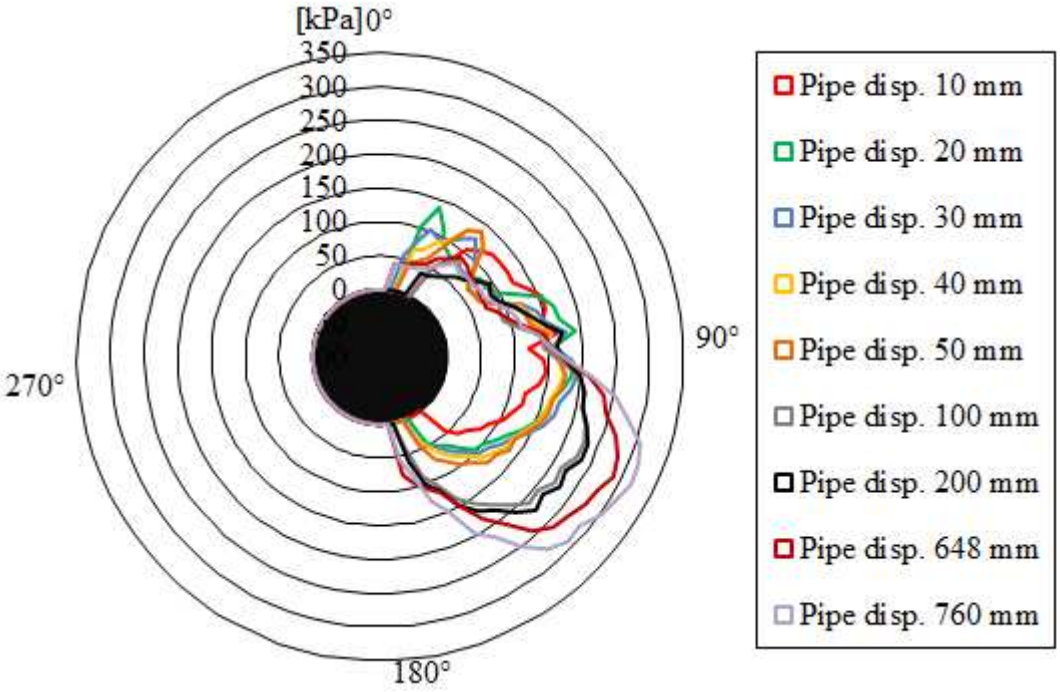

Fig. 72. Average pressure distribution at pipe-soil interface during Test No. 5.

Also in this case the distribution of pressure at pipe soil interface develops in three principal phases:

- Phase 1, before the yielding point (Fig. 73 and Fig. 74) the vertical component of pressure resultant pull the pipe down;
- Phase 2, at the small plateau for a pipe displacement equal to 30 mm Fig. 76 show that the vertical component of pressure resultant is nearly to zero, therefore also in

this case is right to assume at this displacement the soil resistance as the maximum lateral resistance of a pipe in the same conditions but without vertical constrain;

- Phase 3, the vertical component of pressure resultant start to push up the pipe but due to the vertical constrain the soil continue to increase its level of compaction increasing constantly the horizontal reaction as show from Fig. 77 to Fig. 84 which highlights pressure distribution and respective load displacement value.

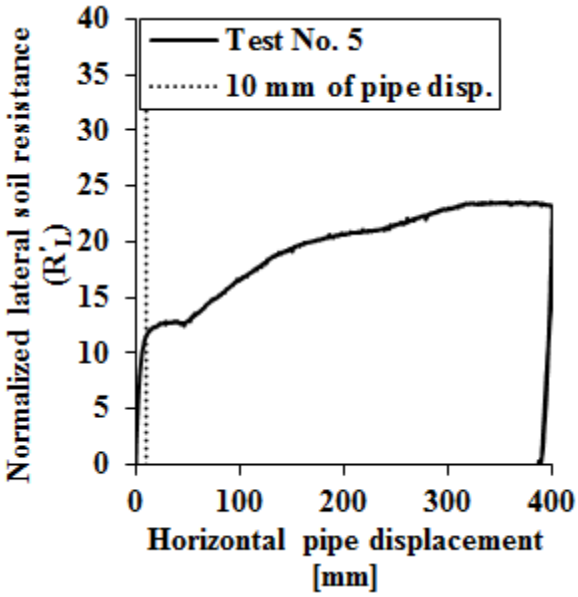

Fig. 73. Load displacement response Test No. 5. Highlight of 10 mm pipe displacement.

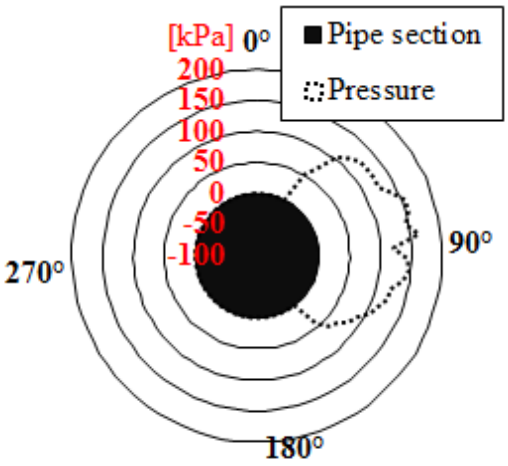

Fig. 74. Pipe soil interface pressure distribution at 10 mm of pipe displacement.

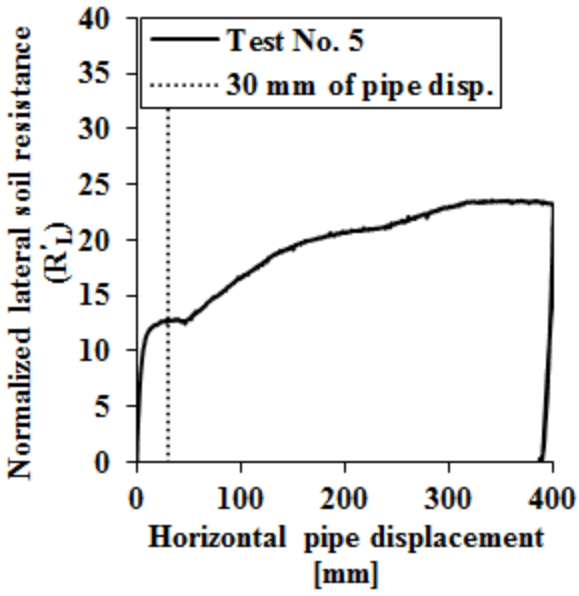

Fig. 75. Load displacement response Test No. 5. Highlight of 30 mm pipe displacement.

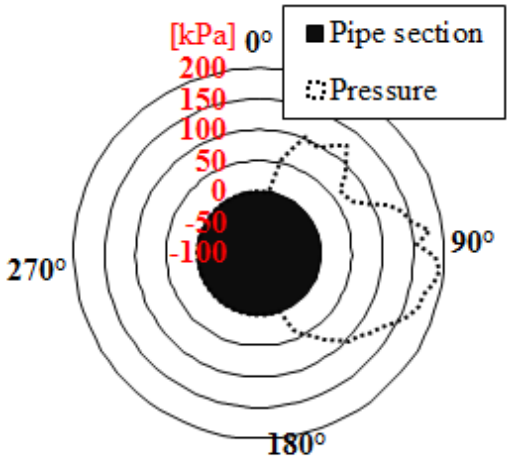

Fig. 76. Pipe soil interface pressure distribution at 30 mm of pipe displacement.

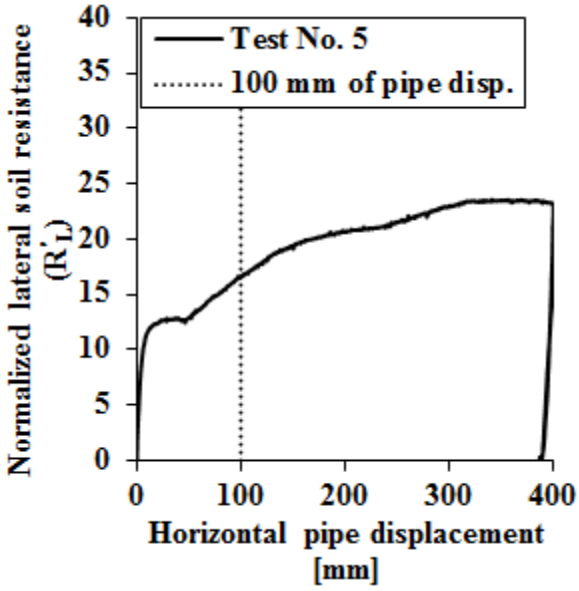

Fig. 77. Load displacement response Test No. 5. Highlight of 100 mm pipe displacement.

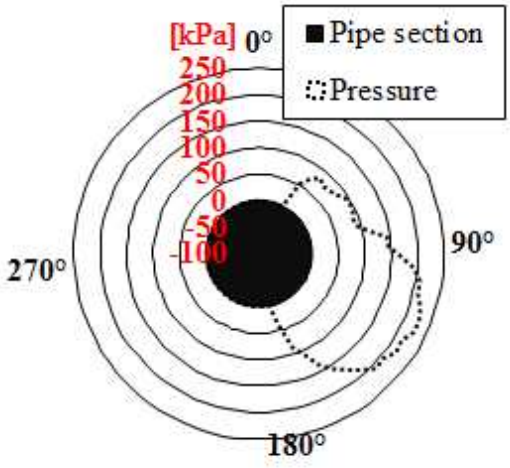

Fig. 78. Pipe soil interface pressure distribution at 100 mm of pipe displacement.

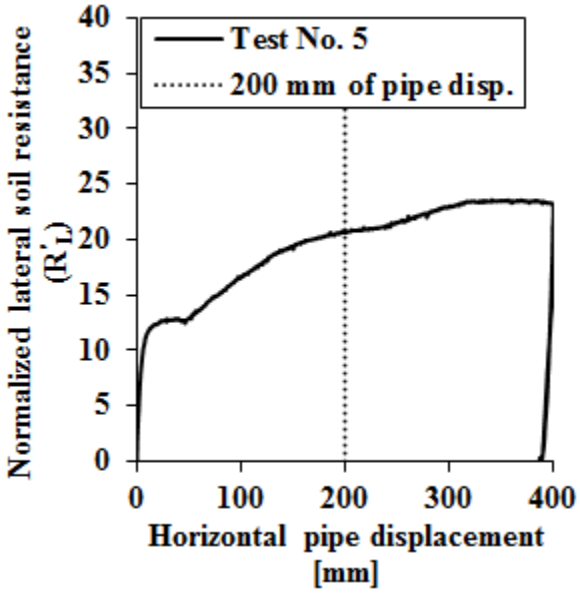

Fig. 79. Load displacement response Test No. 5. Highlight of 200 mm pipe displacement.

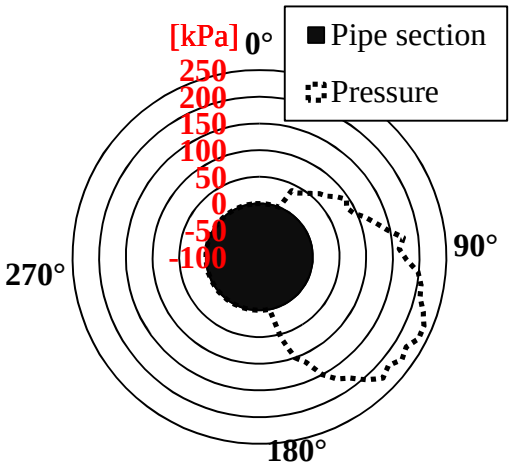

Fig. 80. Pipe soil interface pressure distribution at 200 mm of pipe displacement.

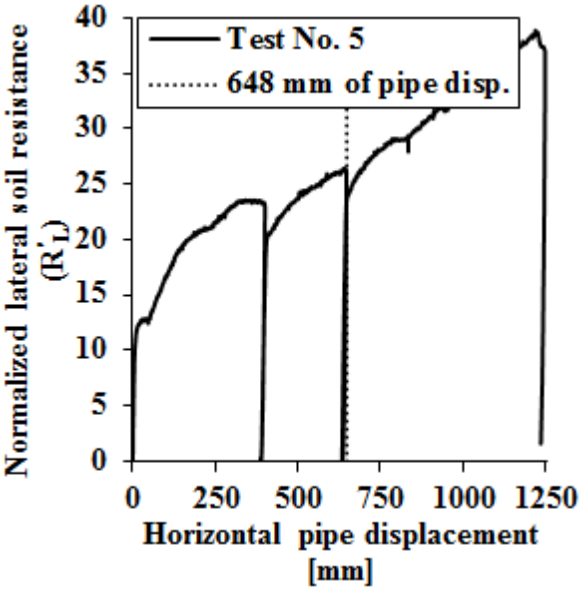

Fig. 81. Load displacement response Test No. 5. Highlight of 648 mm pipe displacement.

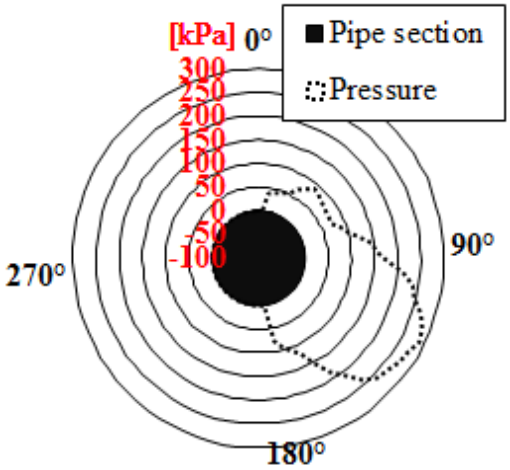

Fig. 82. Pipe soil interface pressure distribution at 648 mm of pipe displacement.

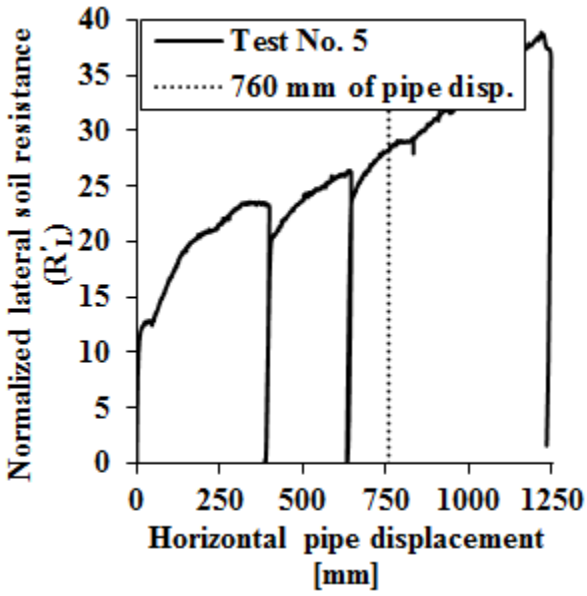

Fig. 83. Load displacement response Test No. 5. Highlight of 760 mm pipe displacement.

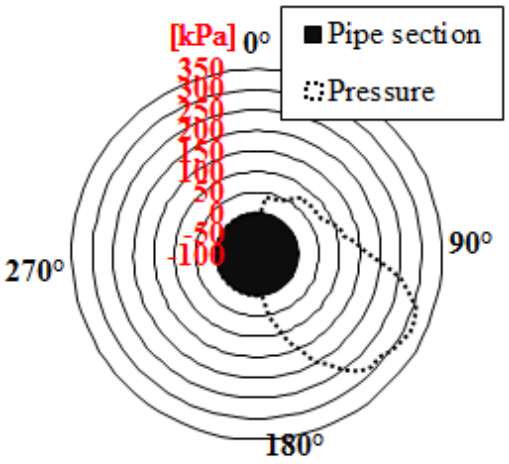

Fig. 84. Pipe soil interface pressure distribution at 760 mm of pipe displacement.

5.3.3. Lateral pulling Test No. 6

Fig. 85 shows the average of pressure distribution at the pipe soil interface for several steps of pipe displacement for the Test No. 6.

The maximum value of pressure increase during the pullout, from 110 kPa for 10 mm of pipe displacement to 250 kPa for 1150 mm of pipe displacement.

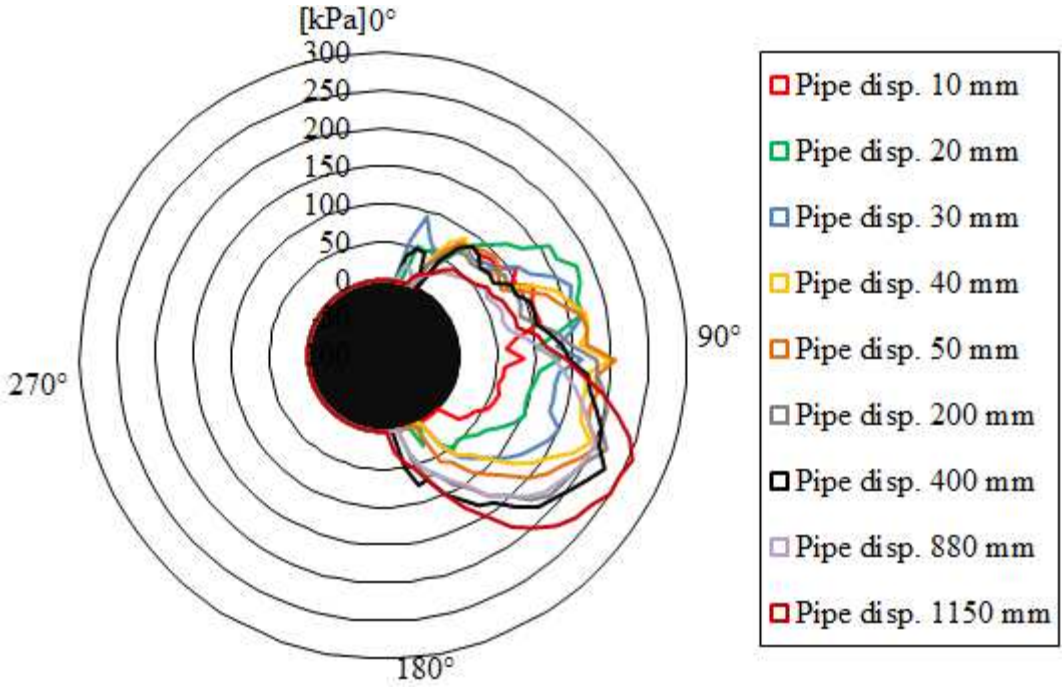

Fig. 85. Average pressure distribution at pipe-soil interface during Test No. 6.

Confirmation of soil pressure distribution at pipe soil interface come also in this tests developing in three principal phases:

- Phase 1, around the yielding point (Fig. 86 and Fig. 87) the vertical component of pressure resultant pull the pipe down;
- Phase 2, at the small plateau for a pipe displacement equal to 30 mm Fig. 89 show the vertical component of pressure resultant is nearly to zero, therefore also in this case is right to assume at this displacement the soil resistance as the maximum lateral resistance of a pipe in the same conditions but without vertical constrain;
- Phase 3, the vertical component of pressure resultant start to push up the pipe but due to the vertical constrain the soil continue to increase its level of compaction increasing constantly the horizontal reaction as show from Fig. 90 to Fig. 99 which highlights pressure distribution and respective load displacement value.

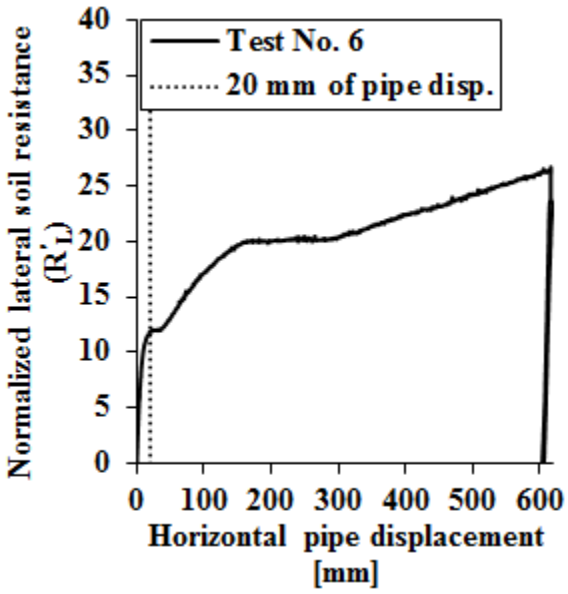

Fig. 86. Load displacement response Test No. 6. Highlight of 20 mm pipe displacement.

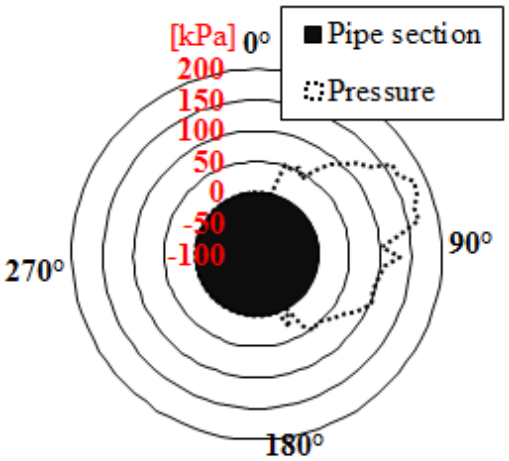

Fig. 87. Pipe soil interface pressure distribution at 20 mm of pipe displacement.

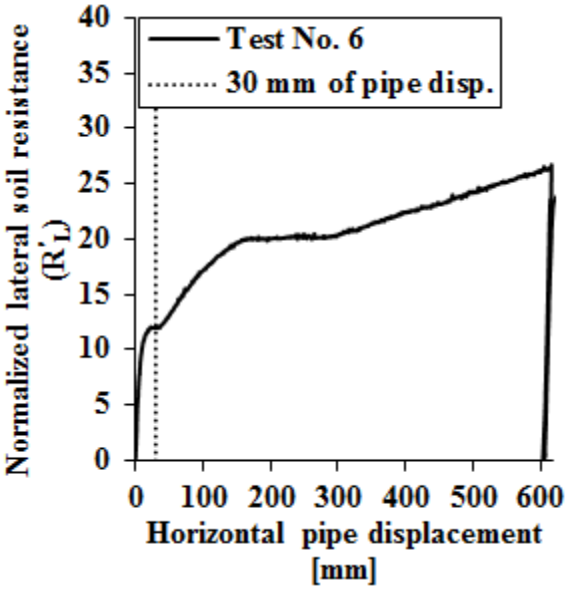

Fig. 88. Load displacement response Test No. 6. Highlight of 30 mm pipe displacement.

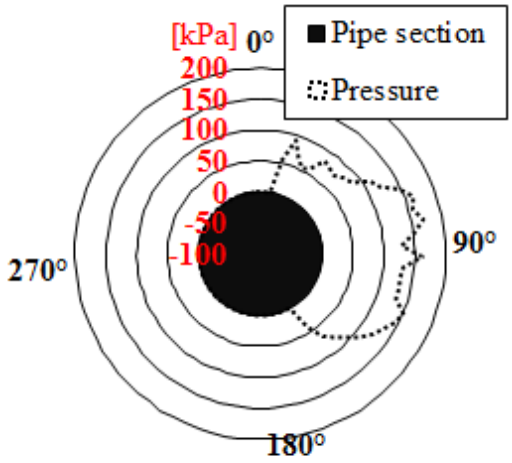

Fig. 89. Pipe soil interface pressure distribution at 30 mm of pipe displacement.

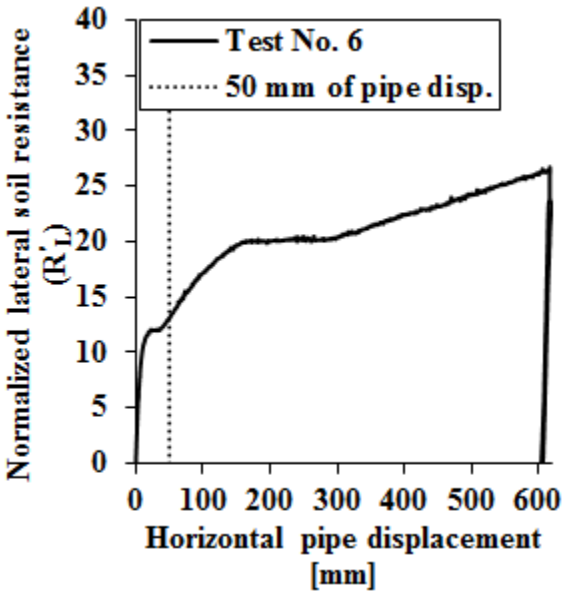

Fig. 90. Load displacement response Test No. 6. Highlight of 50 mm pipe displacement.

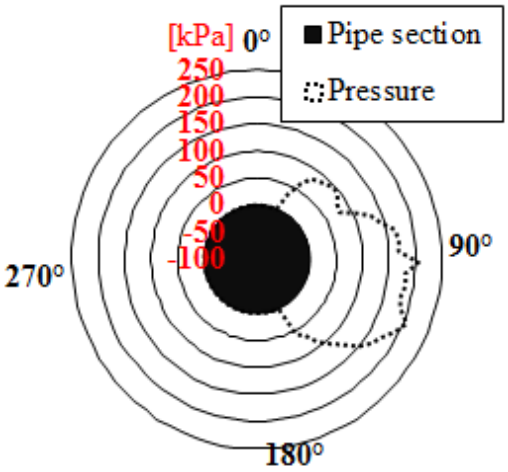

Fig. 91. Pipe soil interface pressure distribution at 50 mm of pipe displacement.

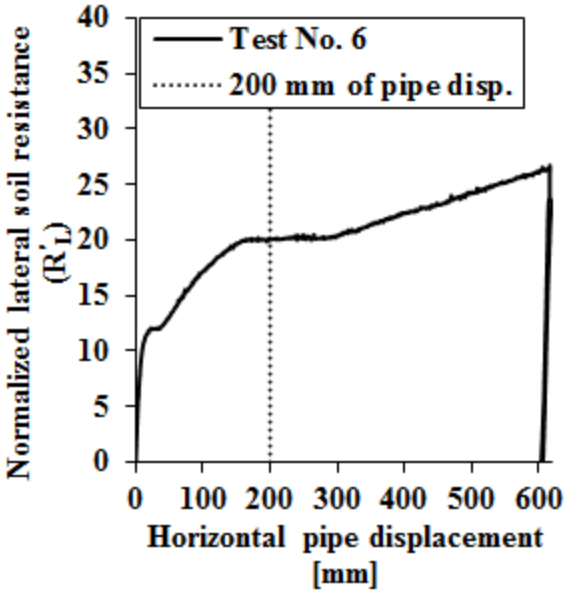

Fig. 92. Load displacement response Test No. 6. Highlight of 200 mm pipe displacement.

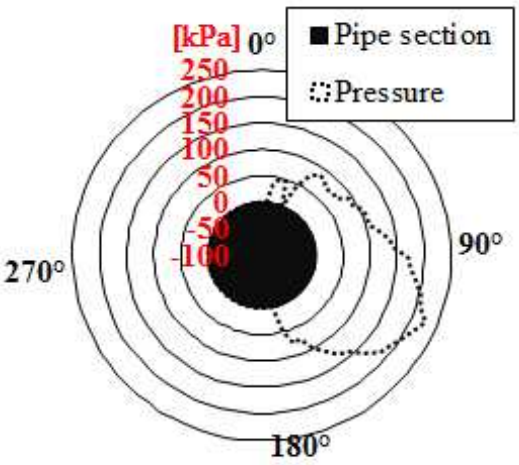

Fig. 93. Pipe soil interface pressure distribution at 200 mm of pipe displacement.

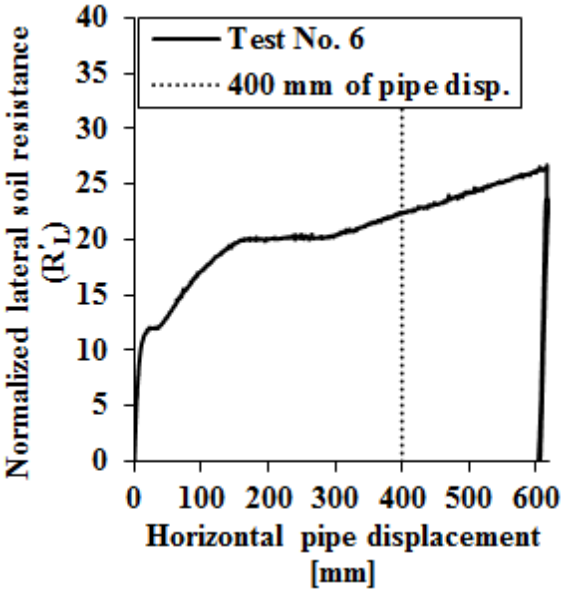

Fig. 94. Load displacement response Test No. 6. Highlight of 400 mm pipe displacement.

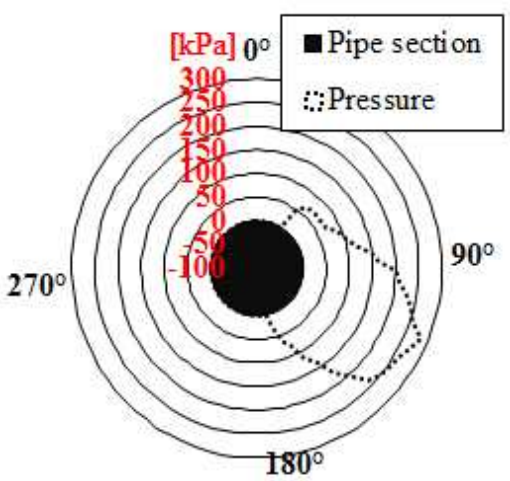

Fig. 95. Pipe soil interface pressure distribution at 400 mm of pipe displacement.

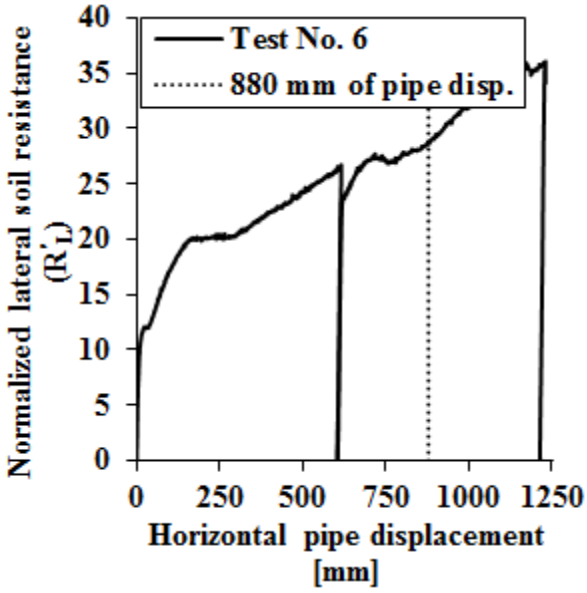

Fig. 96. Load displacement response Test No. 6. Highlight of 880 mm pipe displacement.

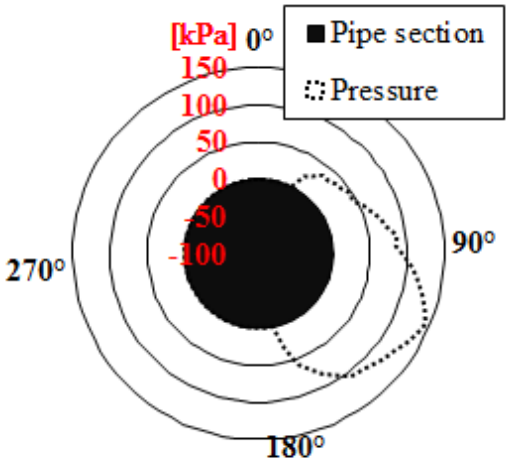

Fig. 97. Pipe soil interface pressure distribution at 880 mm of pipe displacement.

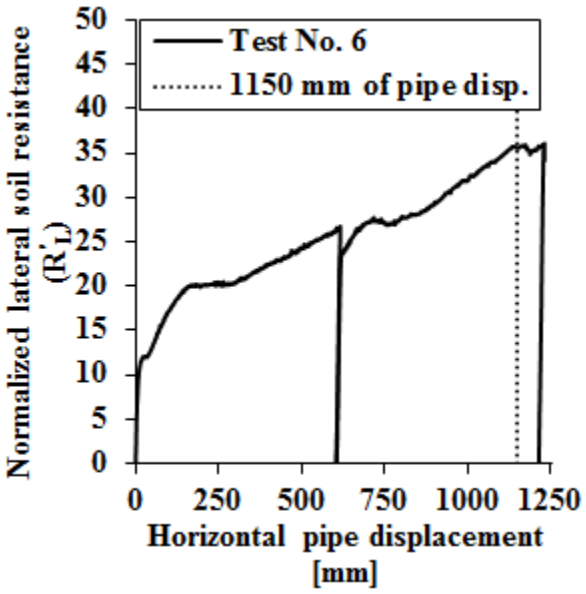

Fig. 98. Load displacement response Test No. 6. Highlight of 1150 mm pipe displacement.

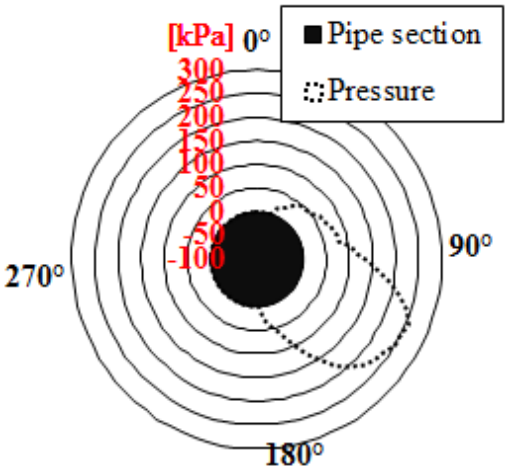

Fig. 99. Pipe soil interface pressure distribution at 1150 mm of pipe displacement.

5.4. Prediction of lateral soil resistance

The horizontal soil resistances obtained in this study for different soil compaction and pipe coating are compared herein with those computed using the formula given in ASCE [4], PRCI [20] guidelines for cohesionless soils. The formula is reported in (Eq. 12):

(Eq. 12) $$P_L = N_{qh}\bar{\gamma}HD$$

where:

D = pipe outside diameter;

H = depth to pipe centerline;

$\bar{\gamma}$ = effective unit weight of soil;

N_{qh} = Horizontal bearing capacity factor.

The two guidelines differ for the way to calculate N_{qh}:

- For PRCI [20] the horizontal bearing capacity factor for sand is equal to:

(Eq. 13) $$N_{qh} = a + b\frac{H}{D}$$

where *a* and *b* are given in the Table 10. *a* and *b* can be interpolated for intermediate values of ϕ between 35° and 45º and should not be taken less than 35º also if soil tests indicate lower ϕ values.

Then for H/D values greater than those indicated in the range, PRCI guidelines suggest a maximum value of N_{qh}: 15, 23 and 30 respectively for ϕ = 35°, 40° and 45°.

PRCI guidelines [20] affirm that as pointed out from O'Rourke [18] the horizontal soil resistance relationship can be applicate both for dry and moist sand.

ϕ	H/D range	*a*	*b*
35°	0.5 to 12	4	0.92
40°	0.5 to 6	5	1.43
	6 to 15	8	1
45°	0.5 to 7	5	2.17
	7 to 15	10	1.33

Table 10. Factors to calculate N_{qh}, PRCI [20].

- For ASCE [4] the horizontal bearing capacity factor for sand is equal to:

(Eq. 14) $$N_{qh} = a + bx + cx^2 + dx^3 + ex^4$$

Where *a, b, c, d, e* are given inTable 11.

ϕ	x	a	b	c	d	e
20°	H/D	2.399	0.439	-0.030	$1.059(10)^{-3}$	$-1.754(10)^{-5}$
25°	H/D	3.332	0.839	-0.090	$5.606(10)^{-3}$	$-1.319(10)^{-4}$
30°	H/D	4.565	1.234	-0.089	$4.275(10)^{-3}$	$-9.159(10)^{-5}$
35°	H/D	6.816	2.019	-0.146	$7.651(10)^{-3}$	$-1.683(10)^{-4}$
40°	H/D	10.959	1.783	0.045	$-5.425(10)^{-3}$	$-1.153(10)^{-4}$
45°	H/D	17.658	3.309	0.048	$-6.443(10)^{-3}$	$-1.299(10)^{-4}$

Table 11. Factors to calculate N_{qh}, ASCE [4].

In order to compare the lateral soil predictions with experimental the results also the (Eq. 12) is used normalized:

(Eq. 15) $$P'_L = P_L/(\gamma HDL)$$

As discuss before, in this study the lateral full-scale tests have been performed constraining the pipes along the vertical direction. Therefore these analytical relationships shouldn't be used in this case as comparison. But from the load displacement chart presented in Fig. 51 it can be noticed that for all experiments a small plateau is present at around $R'_L = 12$, before the constant increasing of the soil resistance. This suggest to be the maximum soil resistance before the effect of vertical constrain as confirmed from the distribution of soil

pressure around the pipe in the previous section and it seems confirmed from PRCI equation and numerical analysis with free uplift, presented in the next sections.

5.4.1. Lateral pulling Test No. 4

Test No. 4 load displacement normalized data compared with normalized predictions (Fig. 100) show that PRCI give a peak soil reaction that is slightly lower than the small plateau registered experimentally. ASCE relationships gives a prediction of soil resistance double respect to PRCI and compared with the experimental results seems to reach a value too high since the same value of soil resistance was achieved during the test after a displacement of 380mm when it is reasonable to assume an extra stress due to the increase of soil compaction considering the blocked uplift.

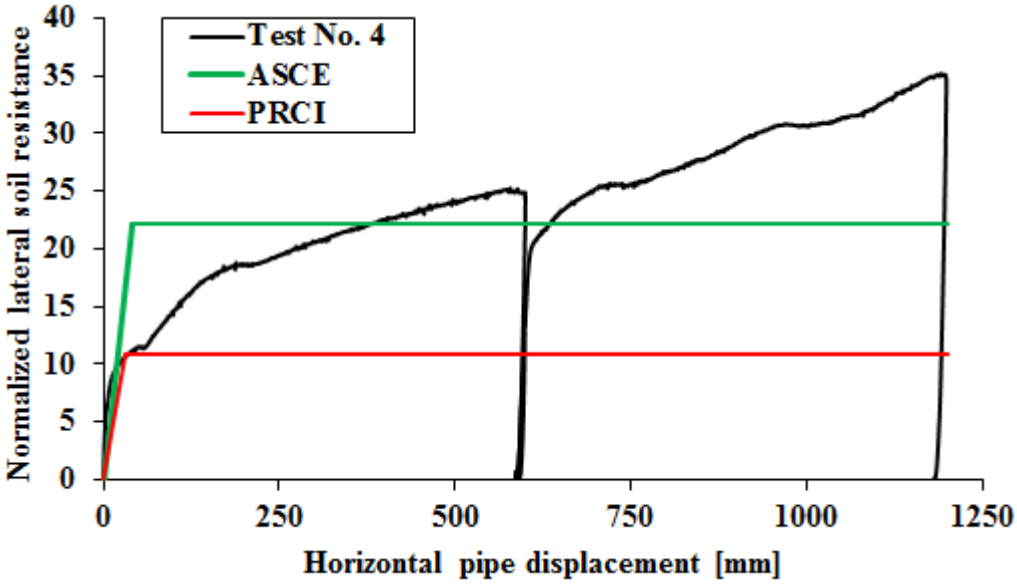

Fig. 100. Normalized load displacement response of Test No. 4 compared with normalized ASCE and PRCI predictions.

5.4.2. Lateral pulling Test No. 5

Test No. 5 performed at level of compaction greater than that achieved for the Test No. 4 show a load displacement response quite similar, this confirm the main dependence from the internal friction angle and from the effective unit weight of soil as suggested from ASCE and PRCI formula, that for all tests were measured equal to 42° and $\bar{\gamma}$ in a range of 15.7 ÷ 16 kN/m^3.

After this consideration it is possible to observe in Fig. 101 that also in this case PRCI give a peak soil reaction that is slightly lower than the small plateau registered experimentally and ASCE relationships gives a prediction of soil resistance double respect to PRCI.

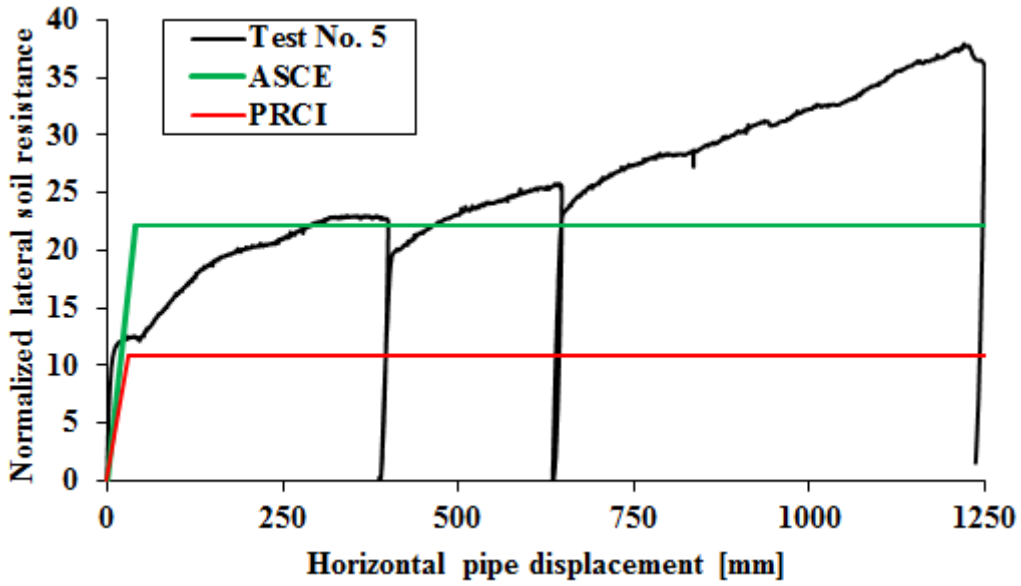

Fig. 101. Normalized load displacement response of Test No. 5 compared with normalized ASCE and PRCI predictions.

5.4.3. Lateral pulling Test No. 6

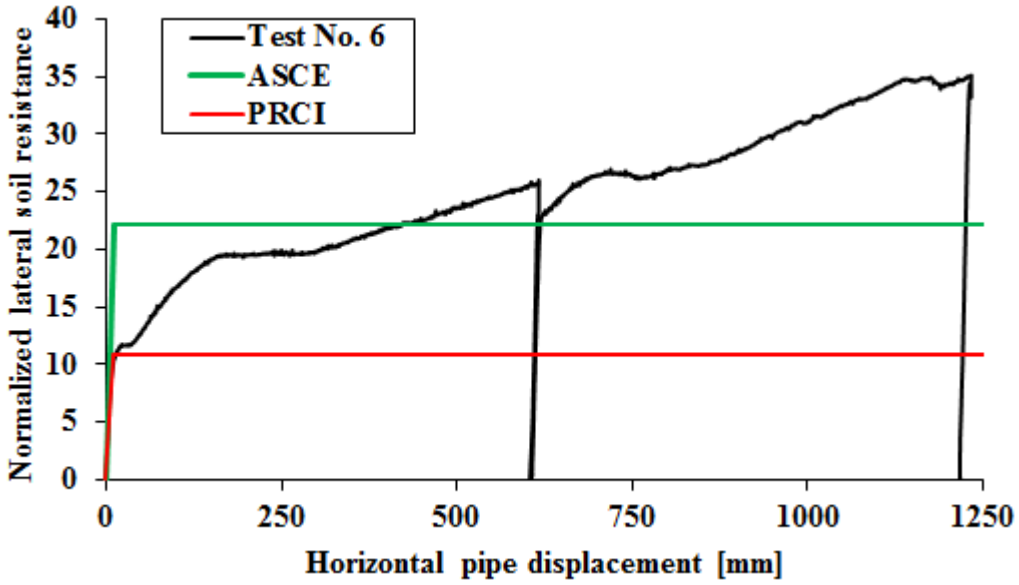

Fig. 102. Normalized load displacement response of Test No. 6 compared with normalized ASCE and PRCI predictions.

Test No. 6 performed at the same level of compaction of test Test No. 5 but with a different pipe coating. Despite this it is possible to neglect the effect of surface finish and comparing the experimental data with guidelines prediction extrapolate the same conclusions mentioned for the previous test.

5.5. Numerical modeling of lateral pullout tests

The results obtained from full-scale lateral pullout tests performed on 8”$^{5/8}$ steel pipe with two different surface finish embedded in quarry sand has been carried out to understand the soil reaction during ground movements and as a preliminary test before to perform the landslide/fault full-scale experiments.

The experimental findings have been used to compare the measurements with analytical approaches available in literature and validate a numerical model developed to simulate these tests.

5.5.1. Finite element modeling

The numerical analysis was conducted using a commercial finite element software ABAQUS 6.14 version [1], accompanied from a subroutine written in FORTRAN language in order to achieve the softening behavior of the soil, the same used with axial pullout finite element model.

The lateral pulling tests performed can be considered in a plane strain condition, for this reason the model was made in two-dimensional (2D) conditions. Two-node linear beam in a plain elements (B21) are employed for modeling the cylindrical pipeline cross section and four-node bilinear plain strain quadrilateral elements (CPE4) are used to simulate the surrounding soil. The model has the same dimension of the experimental tests as depicted in Fig. 103. The soil mesh is the result of sensitivity analysis conducted in order to reach a good compromise between accuracy of results and velocity of simulation, the dimension of the mesh is chosen finer around pipe with a constant increase towards the boundaries of the model. No plastic deformations are expected for the steel pipe therefore no particular refinement of the mesh is used, the section is composed of 32 elements. The distance from the pipe crown and the top surface is 2.9D, 1.32D from the pipe invert to the bottom of the soil prism, 3.13D the distance from the left side of the pipe to the lateral wall, 9.5D the distance from the right side of the pipe to the lateral wall.

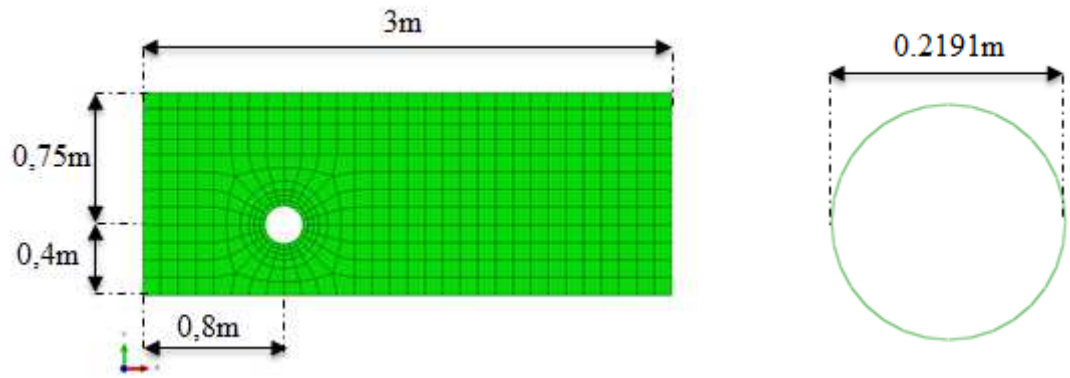

a) 2D finite element mesh of soil.

b) Finite element mesh of pipe cross section.

Fig. 103. Finite element model of the lateral pullout test.

Top surface of the prism represents the soil surface, others surfaces were in contact with internal surfaces of the caisson. Nodes of the bottom surface are constrained for all translational directions; normal direction is constrained for lateral surfaces. These boundary conditions are commonly used in models published in literature and represent a good approximation of experimental conditions. In addition, the pipe is constrained to move vertically. The interface interaction between the pipe and the surrounding soil is simulated with a contact algorithm that include normal contact and tangential friction coefficient in which separation after contact is allowed, the master-slave contact algorithm between external pipe surface and soil surface has been used. ASCE [4] and PRCI [20] guidelines suggest a friction angle equal to 0.8*ϕ between the soil and a rough steel pipe, Karimian [13] for his rough steel specimens measured 0.85*ϕ with a direct shear test between soil and pipe. The numerical analysis conducted in order to simulate Test No. 4 and Test No. 5, 0.9*ϕ was used but the same analysis conducted with 0.8*ϕ showed that the force decrease by ap-

proximately 2%. Fusion bounded epoxy coating was used for the specimen of Test No. 6, hence following suggestion of the aforementioned guidelines a friction factor equal to 0.6 was used for the numerical analysis to simulate this test. Using a friction factor equal to 0.85 as did for numerical model of Test No. 3 the soil reaction increase only of 5%.

An elastic model is used for the steel pipe material because it is not expected plastic deformation on the other hand an elastic perfectly-plastic constitutive model with Mohr Coulomb failure criterion was used and modified by means the USDFLD subroutine explained in a previous section.

In order to avoid numerical instability, all simulations were performed with a slight cohesion equal to 0.1kPa.

The analysis has been conducted in three steps as follow: geostatic stress is applied in the initial step, the gravity loading in the first step and maintained in the second step then the axial pipe displacement in the second step. A uniform lateral controlled displacement of the pipe is imposed.

In all cases i.e. Tests Nos.: 4, 5 and 6 strength parameters equal to: $\phi_p = 42°$, $\phi_r = 36°$ and $\psi_p = 10°$ has been used.

The load-displacement response obtained from numerical simulations are in good agreement with the experimental findings. In all cases at about 50 mm of pipe displacement each experimental test present the same decreasing of the gradient resistance before the hardening behavior called small plateau (Fig. 58), this behavior has been properly confirmed through the numerical analyses.

The model can well describe the phenomenon up to the first 250÷350 mm of pipe displacement. After that the distortion of the soil mesh makes a wrong influence of the results that are not in agreement with the experimental results. However in real cases the pipe it is

not constrained to avoid uplift as did in this experimental study, therefore the model is able to describe the development of the phenomenon (hardening – softening) in less than 300 mm on completion of which there is a steady soil reaction as obtained from several authors, Trautmann [24], Karimian [13] and in most of cases 100 mm or 200 mm horizontal pipe displacement is enough although displacement at peak force is a function of pipe embedment depth, this findings derives from database of various research works of pipes or anchor plate ([24] [25] [26] [16]). To evaluate numerically this behavior a simulation without vertical constrain has been carried out and results are shown below.

Fig. 104 shows the flux of the surrounding sand due to the pipe displacement, the advancing front push the soil mass upward and behind there is a subsidence, this was also observed in the experimental tests (Fig. 105).

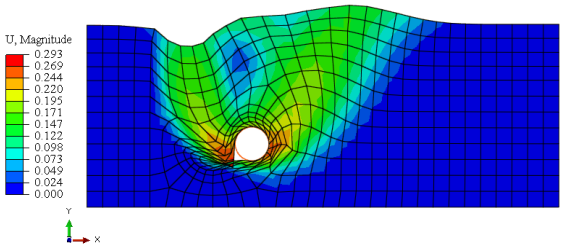

Fig. 104. FEA result of pipe movement in sand after 300 mm of pipe displacement.

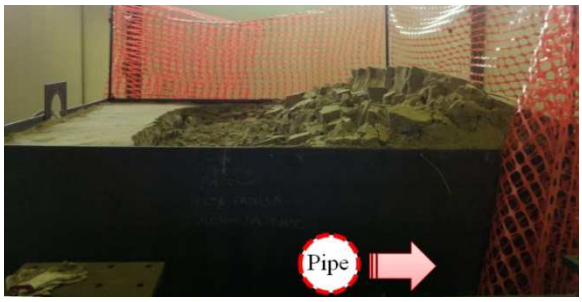

Fig. 105. Experimental result of pipe movement in sand after 1200 mm of pipe displacement.

5.5.2. Lateral pulling model of Test No. 4

Relative density measured for this test was 20% close to 22% measured during the preparation of the second axial test (Test No. 2) hence for consistency of analyses K = 0.5 has been used.

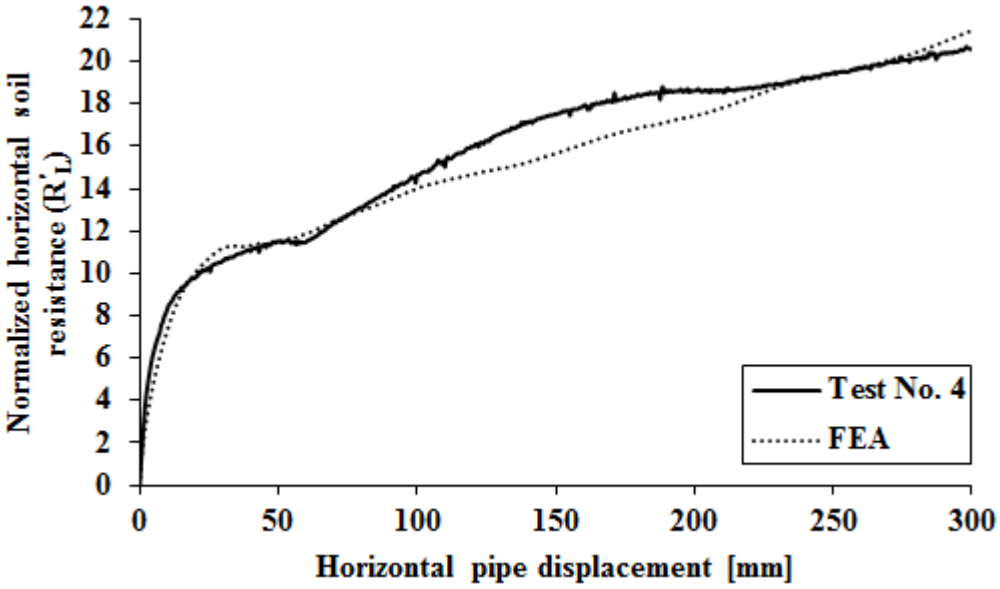

Fig. 106. Normalized load displacement response of Test No. 4 compared with normalized FEA analysis.

The load displacement computed with numerical analysis is compared herein with measured soil reaction of Test No. 4 (Fig. 106) showing a good agreement.

A parametric analysis was carried out and varying the coefficient of lateral pressure from 0.5 to 1 led to a negligible difference equal to 2%. This result demonstrates that initial K does not affect results as for axial pullout tests.

In order to evaluate the soil response with pipe free to rise up a numerical analysis was performed removing vertical constrain. The result is presented in Fig. 107 and the value of peak soil resistance correspond with the small plateau measured experimentally at around 50 mm of pipe displacement, supporting assertions made in this work by interface pressure analysis, i.e. this small plateau may be considered the peak soil resistance of a pipe in the same operating condition except for vertical constrain.

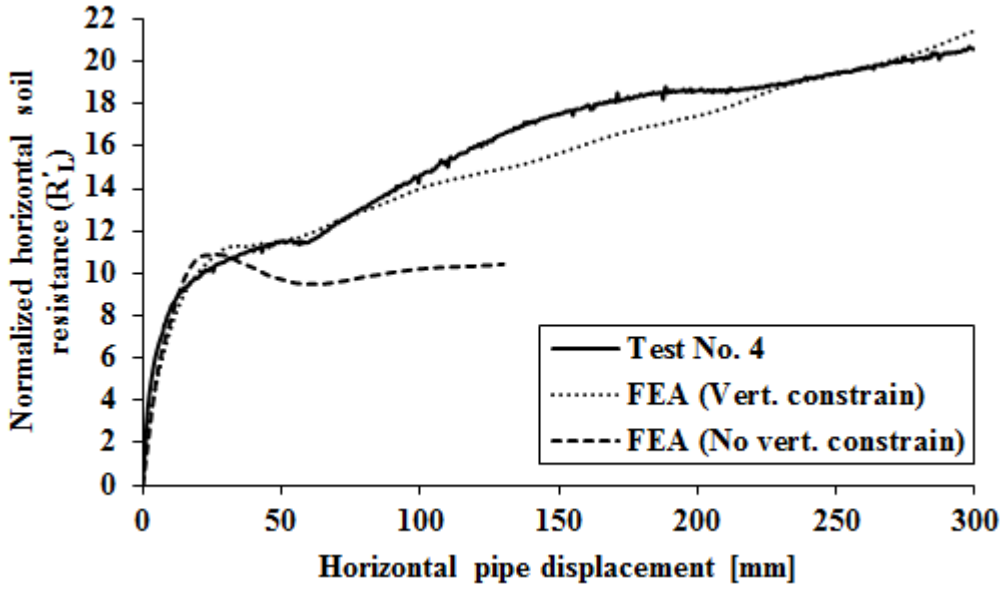

Fig. 107. Normalized load displacement response of Test No. 4 compared with normalized FEA analyses.

5.5.3. Lateral pulling model of Test No. 5

Test No. 5 was conducted at relative density equal to 35%, the numerical analysis of this experiment was conducted with initial K = 1 as for axial tests performed at the same soil compaction level. The good agreement between experimental data and numerical results are shown in Fig. 108.

For this test the numerical analysis conducted removing the pipe vertical constrain give a level of peak soil resistance slightly less than the small plateau measured experimentally. Normalized responses are compared in Fig. 109.

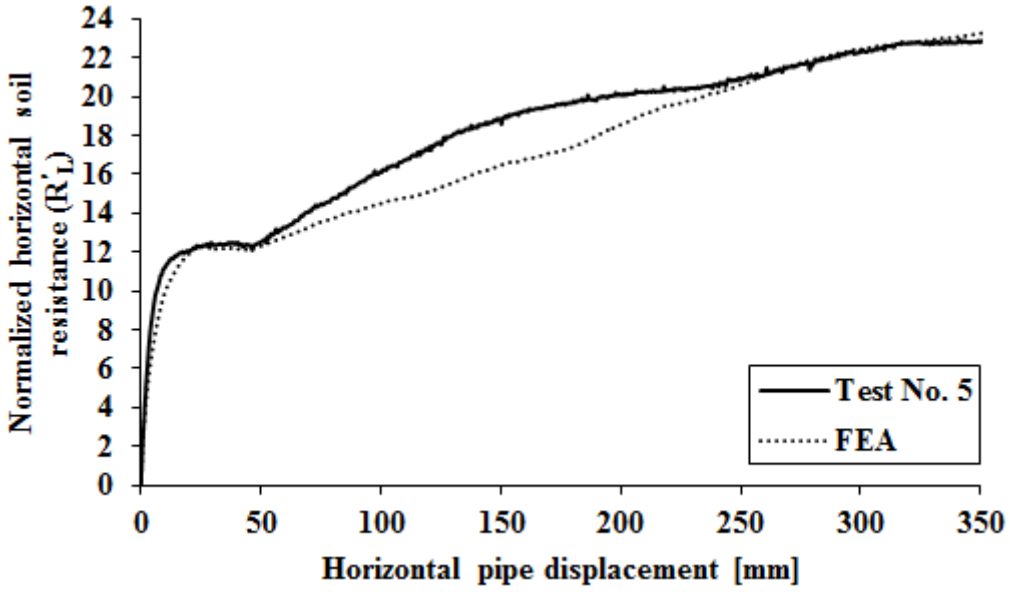

Fig. 108. Normalized load displacement response of Test No. 5 compared with normalized FEA analysis.

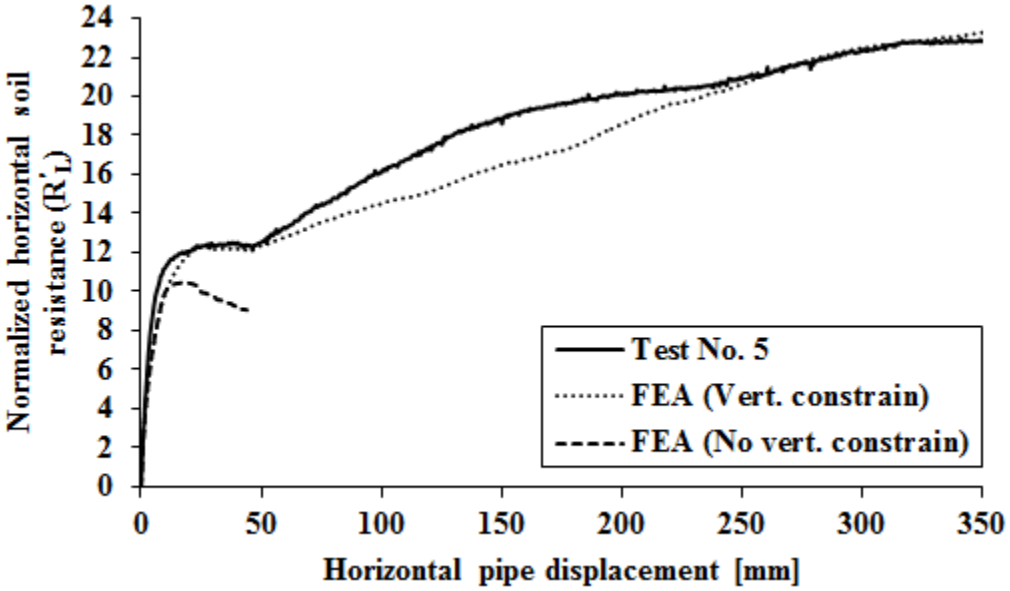

Fig. 109. Normalized load displacement response of Test No. 5 compared with normalized FEA analyses.

5.5.4. Lateral pulling model of Test No. 6

Test No. 6 was conducted at relative density equal to 35%, the numerical analysis of this experiment was conducted with initial K = 1 as for Test No. 5 and axial tests performed at the same soil compaction level. Friction factor equal to 0.85 was used in order to be coherent with axial simulation conducted for the Test No. 3 and a negligible influence respect to use 0.6 was found. The good agreement between experimental data and numerical results are shown in Fig. 110.

For this test the numerical analysis conducted removing the pipe vertical constrain give a level of peak soil resistance slightly less than the small plateau measured experimentally. Normalized responses are compared in Fig. 111.

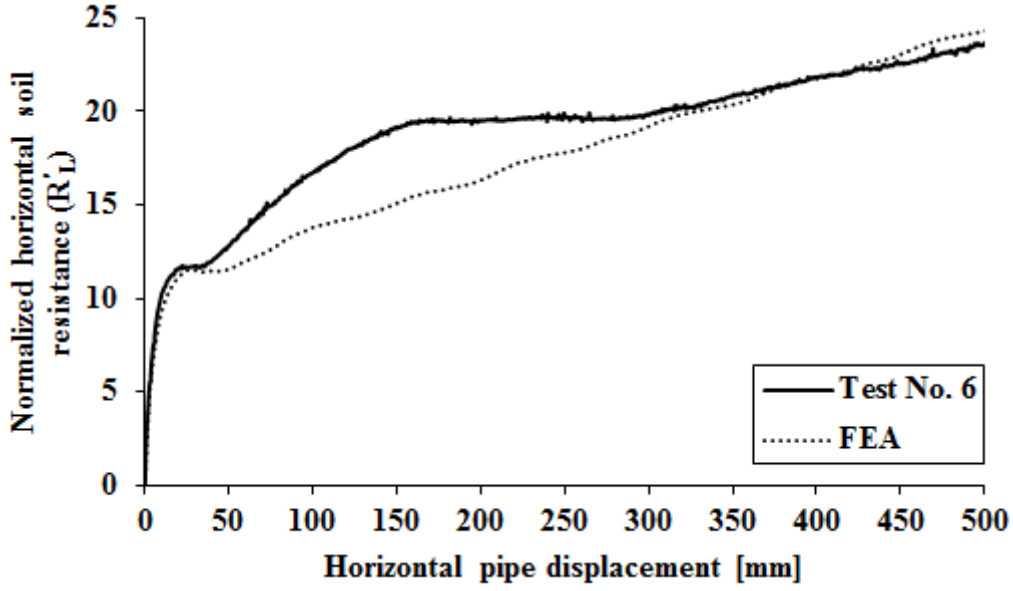

Fig. 110. Normalized load displacement response of Test No. 6 compared with normalized FEA analysis.

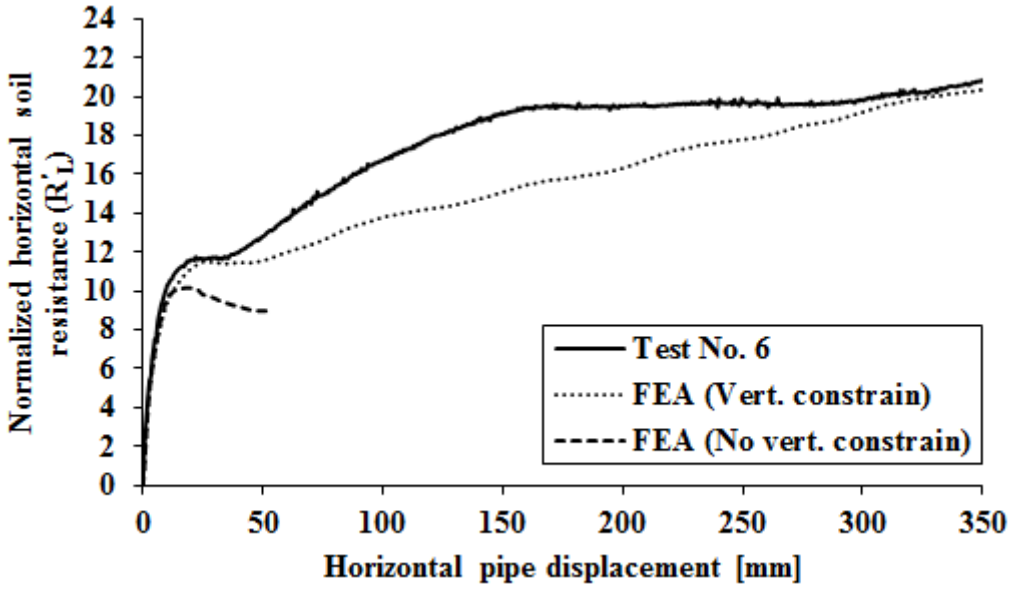

Fig. 111. Normalized load displacement response of Test No. 6 compared with normalized FEA analyses.

5.6. Experimental data compared with FEA analyses and PRCI predictions

The comparison among experimental data, finite element analyses conducted with and without vertical constrain, PRCI predictions are summarized in Fig. 112, Fig. 113 and Fig. 114. Peak soil resistance of PRCI predictions coincide with numerical analyses performed without pipe vertical constrain, for all lateral tests.

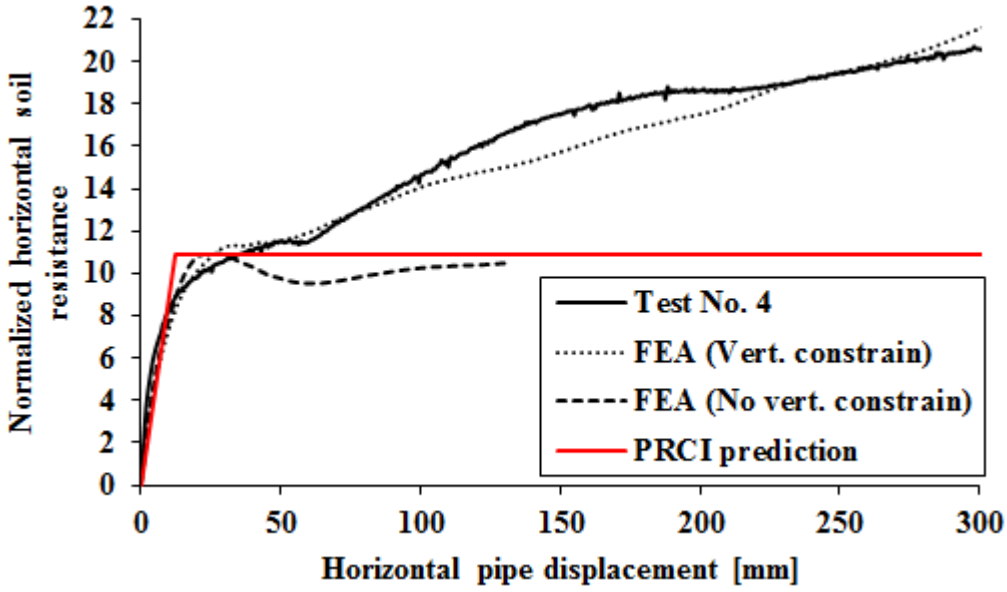

Fig. 112. Normalized load displacement response of Test No. 4 compared with normalized FEA analyses and PRCI prediction.

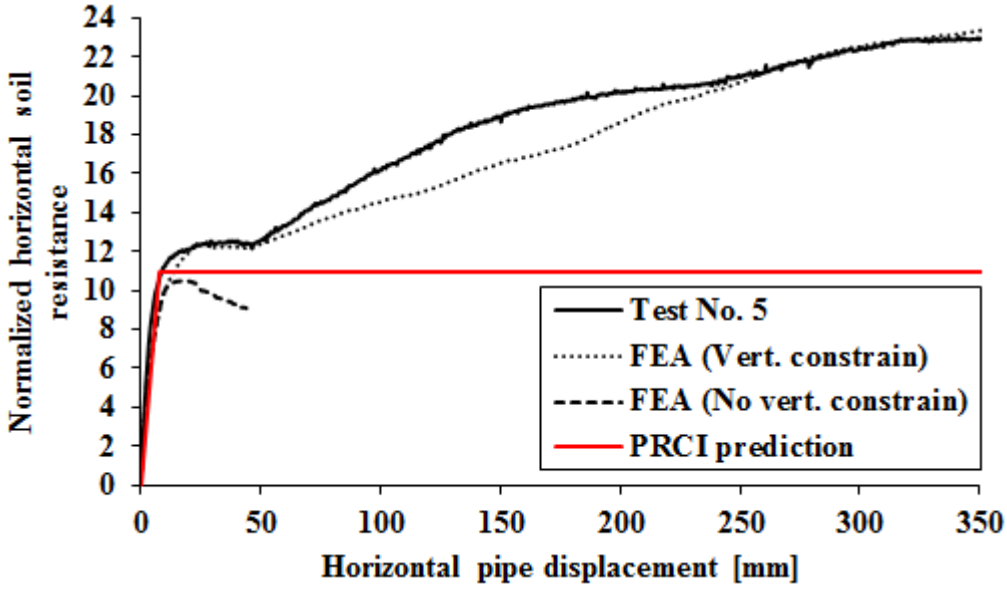

Fig. 113. Normalized load displacement response of Test No. 5 compared with normalized FEA analyses and PRCI prediction.

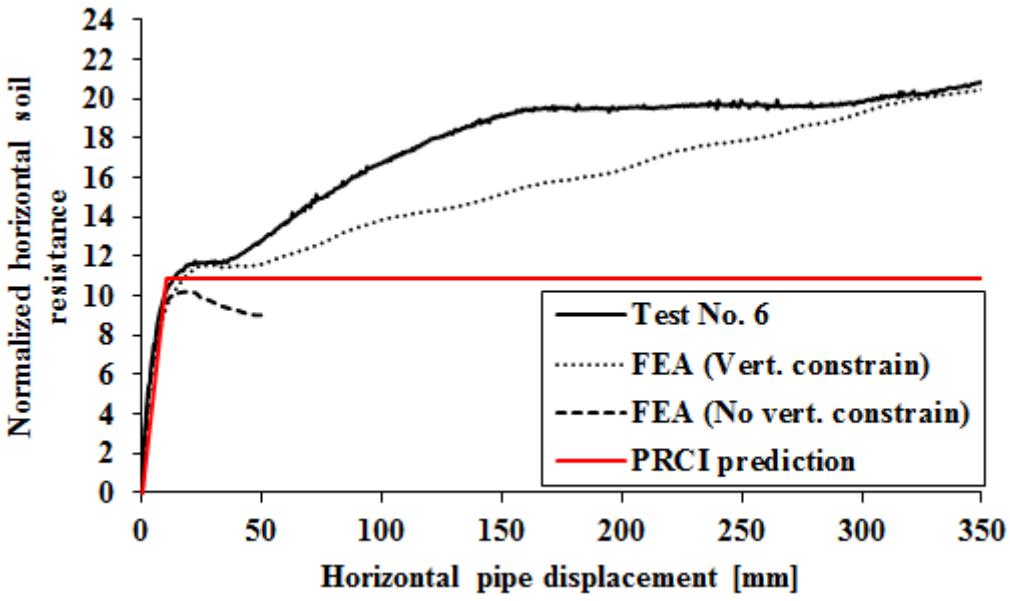

Fig. 114. Normalized load displacement response of Test No. 6 compared with normalized FEA analyses and PRCI prediction.

6. Embedded pipes subjected to landslide/fault tests

6.1. Introduction

This chapter describes the experimental findings obtained from four landslide/fault tests on steel pipes and results obtained from numerical models. The experimental and numerical results are discussed and compared in terms of longitudinal strains. The following table reports a summary (Table 12).

Test configuration	Landslide/fault
Soil type	Quarry sand
Average density	From 1600 to 1688 kg/m^3 for 1st and 2nd experiments. No mass density values are available for 3rd and 4th experiment. D_r from 21% to 40%
Average moisture	From 5% to 8%
Average internal friction angle	$\phi_p = 42°$, $\phi_r = 36°$
Caisson size	Whole length = 24.7 m, caisson width ~4 m, depth = 1.5 m
Pipe size	OD = 8"$^{5/8}$ (219.1 mm), WT = 5.56 mm, length = 36 m
Pipe grade & Surface coating	API5L X65, antioxidant paint and Apsacoat 104
Overburden ratio	H/D = 3.1
Loading rate	1 mm/s

Table 12. Summary of parameters in the landslide/fault testing.

Tests differ for internal pressure and relative density of soil, the first two tests were performed with D_r = 40% and 36% respectively, the second two tests performed with D_r = 21% and 29% respectively. Furthermore levels of pressure were tested, 0 MPa and 11.4 MPa corresponding to a usage factor of 50% of SMYS. All tests were performed with uncoated pipes.

6.2. Bending strain response

Test No.	Test	Relative density	Mass density	Water content	Pipe coating	Internal pressure	Overburden ratio
[-]	[-]	[%]	[kg/m^3]	[%]	[-]	[MPa]	[-]
7	Landslide 1	40	1600	5	Bare pipe	0	3.1
8	Landslide 2	36	1688	8	Bare pipe	11.4	3.1
9	Landslide 3	21	ND	8	Bare pipe	0	3.1
10	Landslide 4	29	ND	8	Bare pipe	11.4	3.1

Table 13. Summary of landslide/fault tests performed.

As described before, each pipe used for landslide/fault test was instrumented with strain gauges on 21 cross sections along the pipe springline to measure the longitudinal strain distribution on both the sides of the pipe i.e. extrados line and intrados line.

The difference in soil relative density between Test No. 7 and Test No. 9 (unpressurized pipes) is detected in a significant difference both for extrados and intrados longitudinal strains. The maximum difference is detected at the pipe middle length as shown in Fig. 115

and Fig. 116. Furthermore Test No. 8 and Test No. 10 conducted again with difference in soil relative density but with pressurized pipes (11.4 MPa) show once again a significant difference both for extrados and intrados longitudinal strains.

Comparison shows also lower strain values for tests conducted at the same relative density but with pressurized pipes. This means that for this level of internal pipe pressure the pipeline opposes the global deformation due to the horizontal soil displacement more than an unpressurized pipe.

No buckling were detected during tests therefore was not possible to assess the beneficial effect of the internal pressure that tends to counteract the ovalization, resulting in an increase of the critical bending strain at buckling.

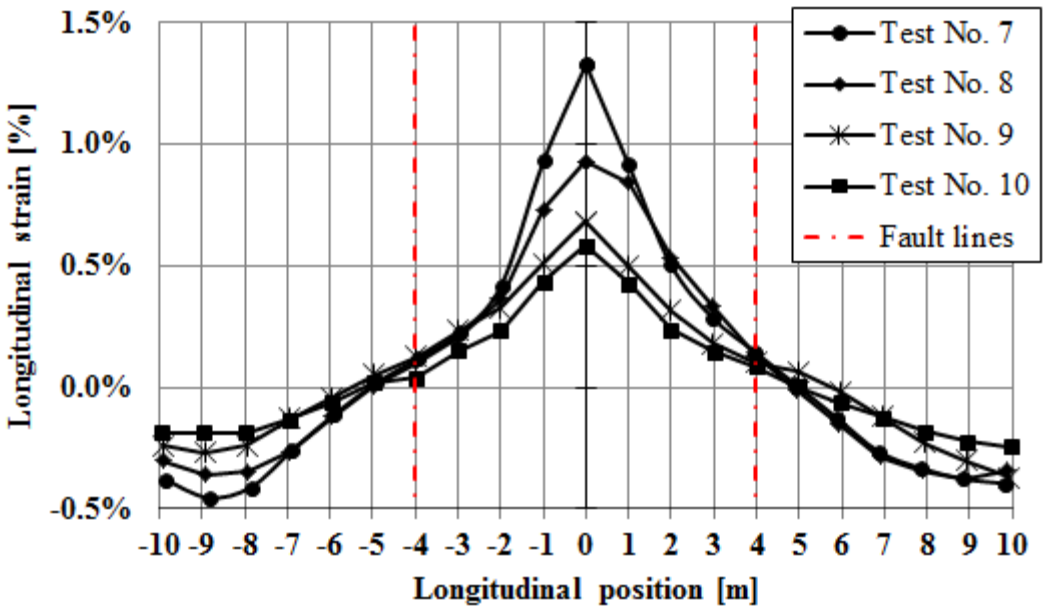

Fig. 115. Extrados strains along pipe for 3200 mm central caisson displacement, Test Nos. 7, 8, 9, 10.

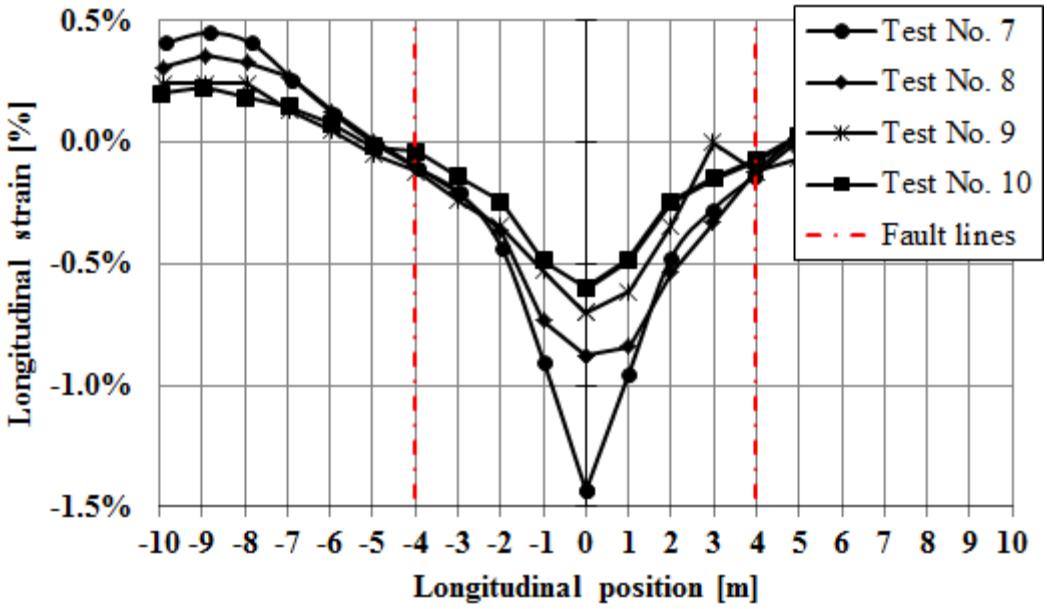

Fig. 116. Intrados strains along pipe for 3200 mm central caisson displacement, Test Nos. 7, 8, 9, 10.

6.3. Experimental tests

Several pictures of the first landslide/fault test are presented herein with particular focus on soil deformation during lateral displacement of central caisson pulled through two actuators in a controlled displacement manner. Fig. 117 a) shows the upper surface of soil at

a) Upper soil surface before the test.

b) Upper soil surface at 1800 mm of caisson displacement.

c) Upper soil surface at 2800 mm of caisson displacement.

d) Upper soil surface at 3650 mm of caisson displacement.

Fig. 117. Soil deformation during lateral displacement of central caisson.

1800 mm of pipe displacement (Fig. 117 b)) deformation of soil was detected in a slight subsidence due to the pipe bending and horizontal displacement. At 2800 mm (Fig. 117 c)) in addition to the subsidence at one side surficial heaving is noticeable. At the end of the test (3650 mm of caisson displacement) considerable accumulation of soil at the opposite direction of pipe movement can be appreciated.

After soil removal from the caisson a significant pipe deflection was observed and measured (Fig. 118). The horizontal pipe deformation is the result of soil displacement applied by the sliding caisson and the uplift is the result of the vertical component of soil reaction (a scheme is presented in Fig. 119 and in Fig. 120). Vertical component of soil reaction is confirmed from pressure measurements at pipe soil interface during lateral pullout tests (section 5.3).

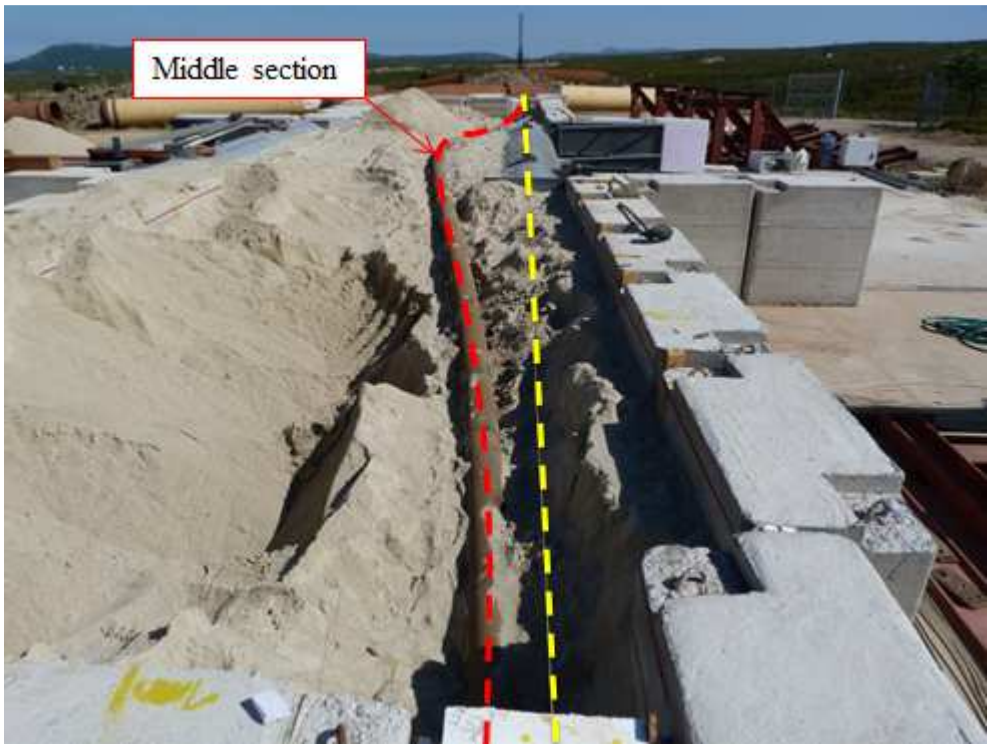

Fig. 118. Deformed pipe at the end of landslide/fault test after soil removal, Test No. 7.

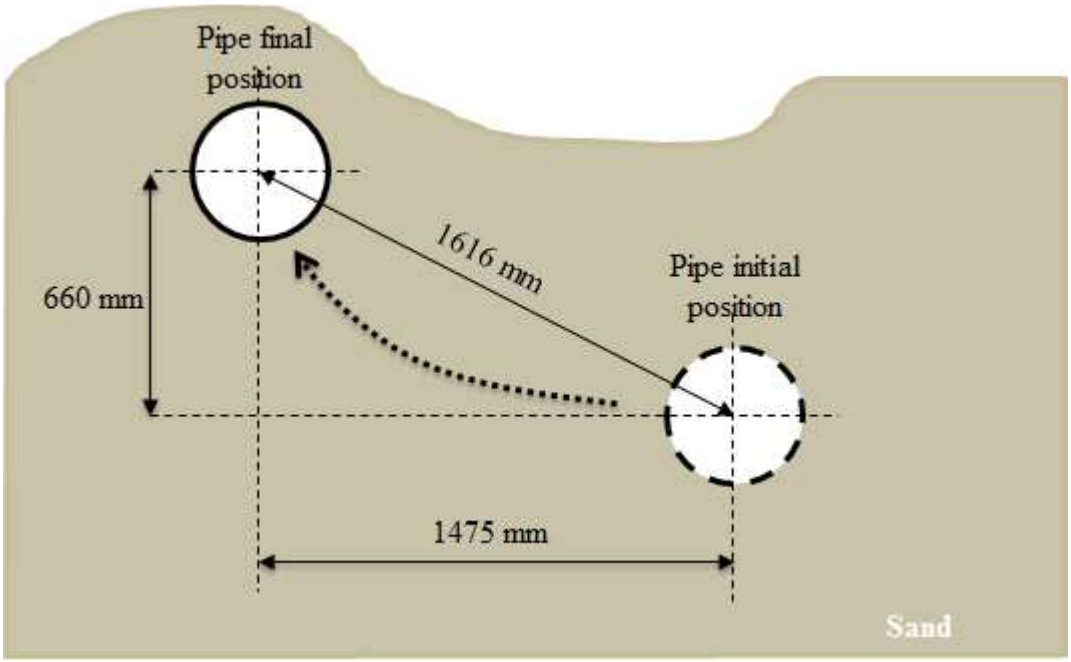

Fig. 119. Section scheme of maximum pipe displacement at middle section, Test No. 7.

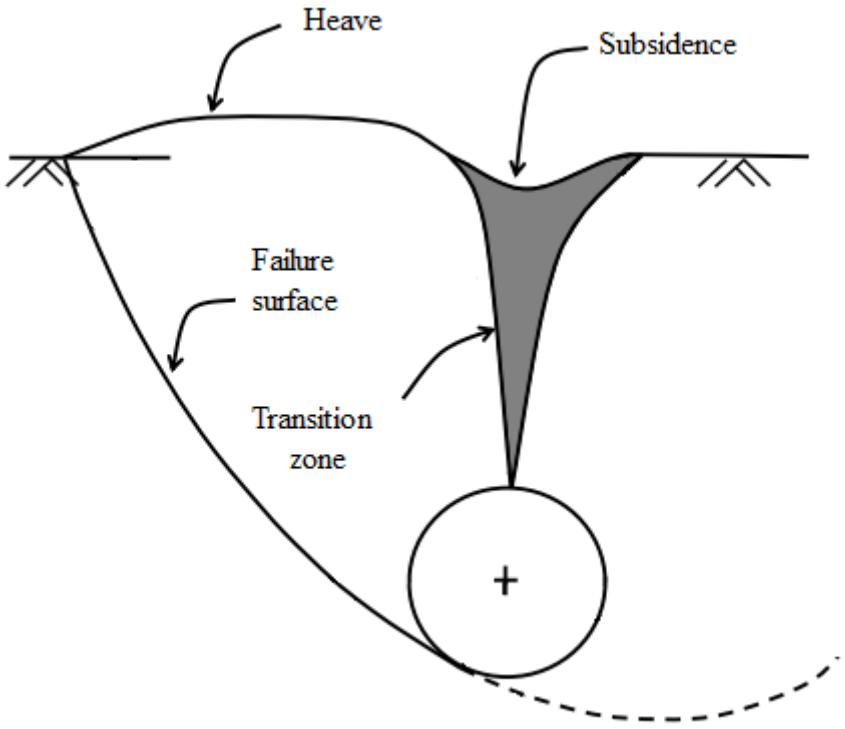

Fig. 120. Schematic surface failure [23].

At the end of first landslide test 1475 mm and 660 mm were measured as maximum pipe displacement at the middle section for horizontal plane and vertical plane respectively (Fig. 119). This uplift motion is maximum at pipe middle section and zero at constrained pipe ends.

6.3.1. Landslide/fault Test No. 7

Pipe specimen (for Test No. 7) assembled with 5 pipe segments welded by manual SMAW welding adopting the WPS specifically developed for the project is schematically presented in Fig. 121.

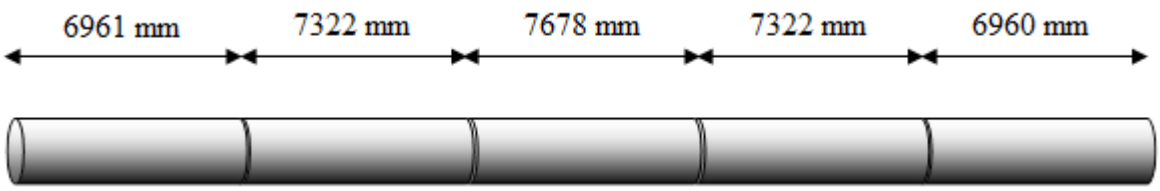

Fig. 121. Schematic assembly of pipe segments for specimen of Test No. 7.

Test No. 7 performed with an uncoated pipe, without internal pressure and relative density of sand equal to 40% have been subjected to significant bending, achieving plastic deformation mainly along the longitudinal direction in the range of ± 1.5%.

No buckling or tensile rupture was observed and slight cross section deformations were measured at the end of the test.

Several charts of strain distribution at extrados generatrix line, intrados generatrix line and axial line are presented for various steps of caisson displacement from Fig. 122 to Fig. 125. Some strain gauges failed during the test and the strain values for failed strain gauges have been interpolated by the values of neighboring sections. Analyzing the results it can be observed that in addition to a primary high strain spot (at pipe middle section) a secondary (lower) spot is located aside from the fault lines (dashed lines in plots). The distance of this secondary strain spot moves from an initial distance of about 3000 mm towards the pipe ends (for 600 mm of caisson displacement), to 5000 mm from fault lines (for maximum

caisson displacement attained of 3650 mm). The curvature inversion point (zero longitudinal strains) is located close to the fault lines and again is seen to move towards pipe ends for an increasing applied caisson displacement.

Starting from 600 mm of caisson displacement the range of strains was ± 0.5% and as reported in Fig. 126 the maximum calculated deflection was around 400 mm.

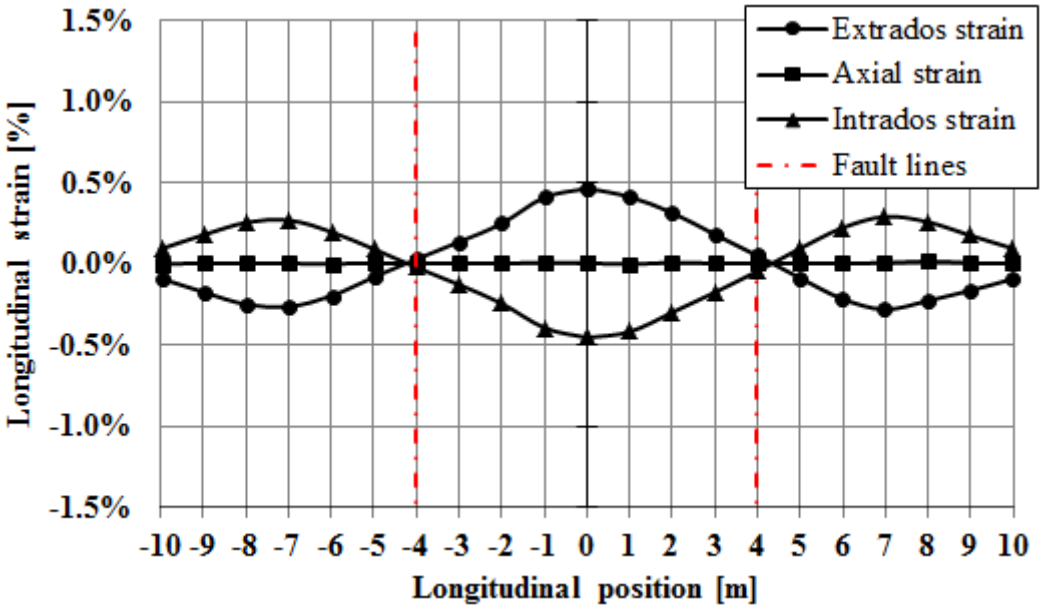

Fig. 122. Distribution of strains along pipe for 600 mm central caisson displacement, Test No. 7.

At 1200 mm of caisson displacement the range of strains was nearly ± 0.75% for a maximum deflection of pipe slightly less than 1200 mm. Then a range of strains was equal to ± 1.25% was detected at 2400 mm of caisson displacement with a maximum pipe deflection slightly more than 1400 mm.

At the end of the test, a pipe displacement of 3650 mm was achieved with a range of maximum strains from +1.3% to -1.5% and a maximum pipe deflection calculated as 1800 mm. In all cases the calculated axial strain is nearly to zero.

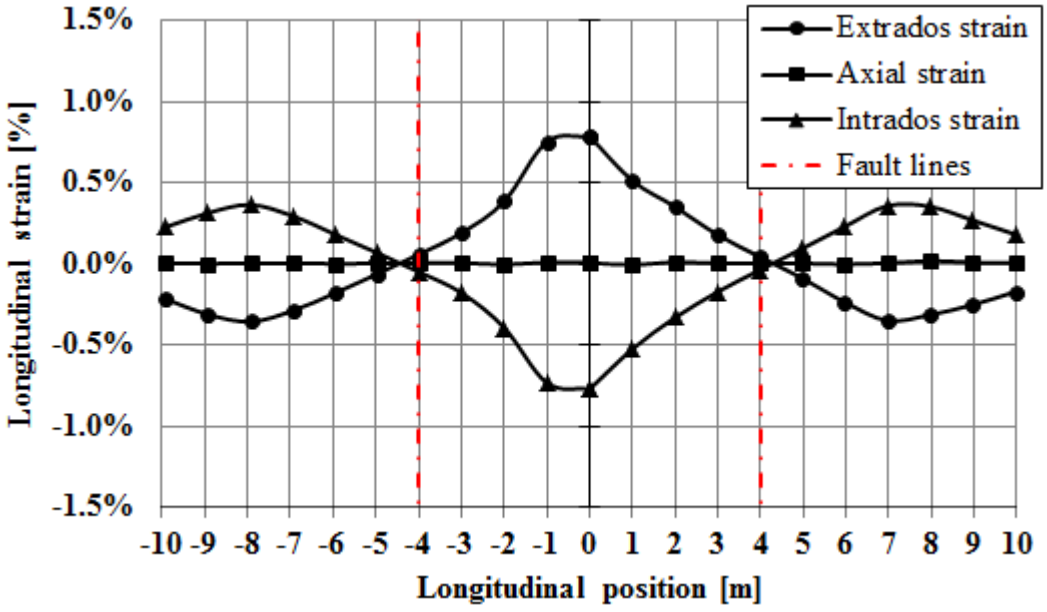

Fig. 123. Distribution of strains along pipe for 1200 mm central caisson displacement, Test No. 7.

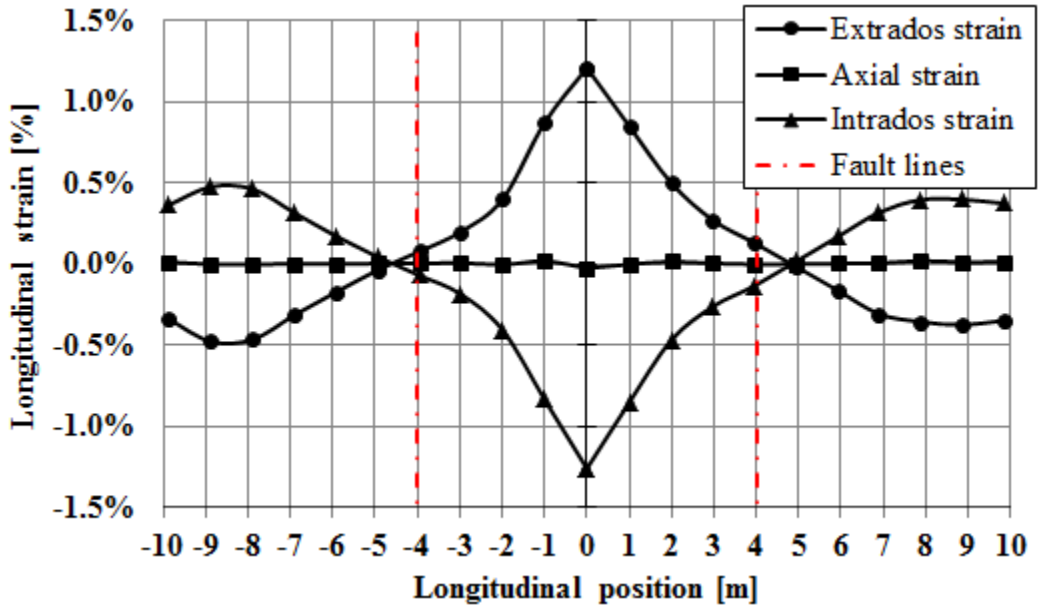

Fig. 124. Distribution of strains along pipe for 2400 mm central caisson displacement, Test No. 7.

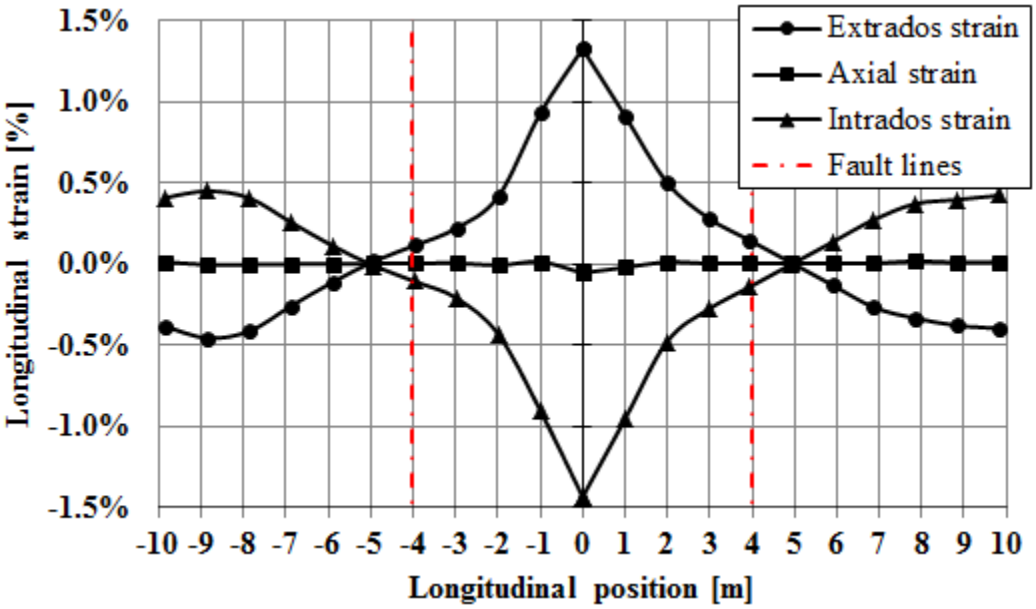

Fig. 125. Distribution of strains along pipe at maximum caisson displacement of 3650 mm, Test No. 7.

Fig. 126 shows the evolution of pipe deflection at various steps of pipe caisson displacement calculated from the longitudinal strains values according to the procedure presented in section 3.6.2. The pipe deflection initially grows quickly and tends to slow down and stabilize for high caisson displacements.

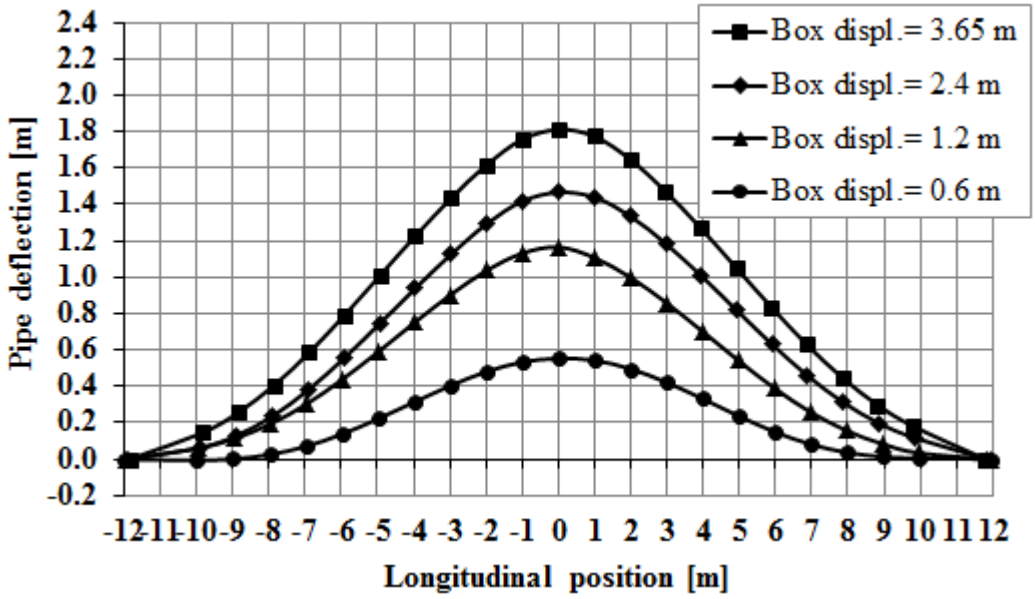

Fig. 126. Evolution of pipe deflection calculated by strains, Test No. 7.

Fig. 127 shows the calculated deflection of the middle section during the caisson displacement in which is clear the trend of pipe deformation.

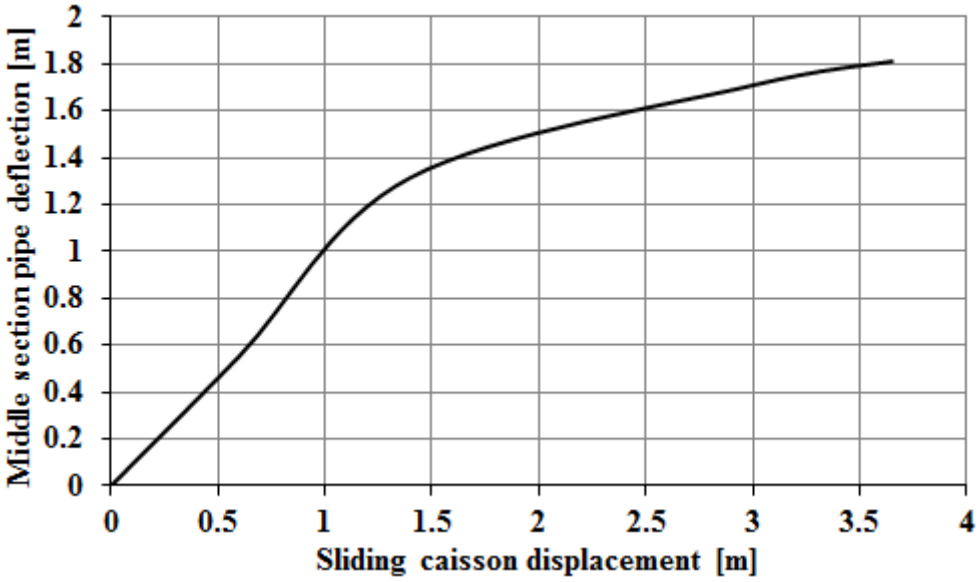

Fig. 127. Evolution of pipe deflection at middle section calculated by strains, Test No. 7.

At the end of the test after soil removal a spring back of the specimen was observed. Afterwards measurements of horizontal and vertical deflection were carried out. In Fig. 128 the comparison between calculated and measured pipe deformation is presented showing a good agreement. Also a relevant uplift is presented in the vertical deflection diagram (Fig. 129) in which it can be observed that the middle section reached the initial sand level.

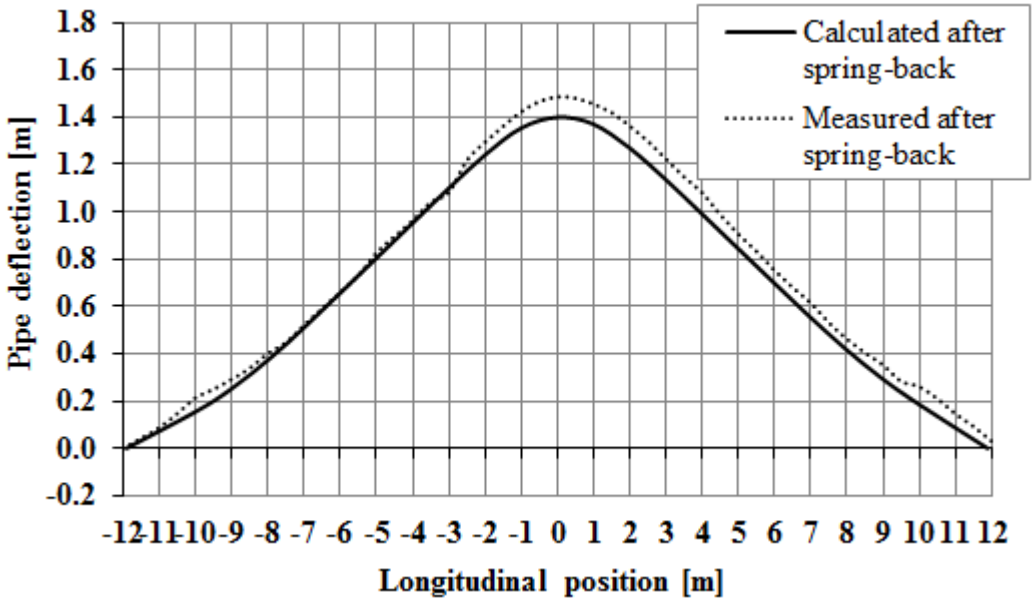

Fig. 128. Pipe deflection on the horizontal plane after soil removing calculated by strains and measured on field, Test No. 7.

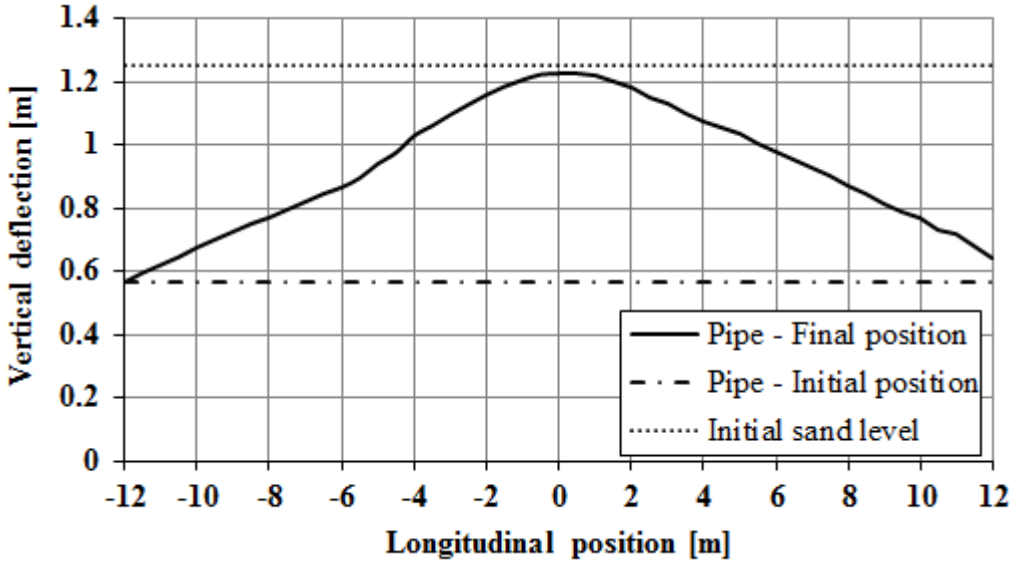

Fig. 129. Pipe deflection on the vertical plane measured on field after soil removing, Test No. 7.

Using two LVDTs applied at the ends of pipe, the longitudinal displacement was also measured, showing a symmetric shortening up to 1700 mm of caisson displacement and a

slight divergence after this point. The maximum pipe axial displacement measured was 130 mm and 160 mm respectively for left pipe end and right pipe end.

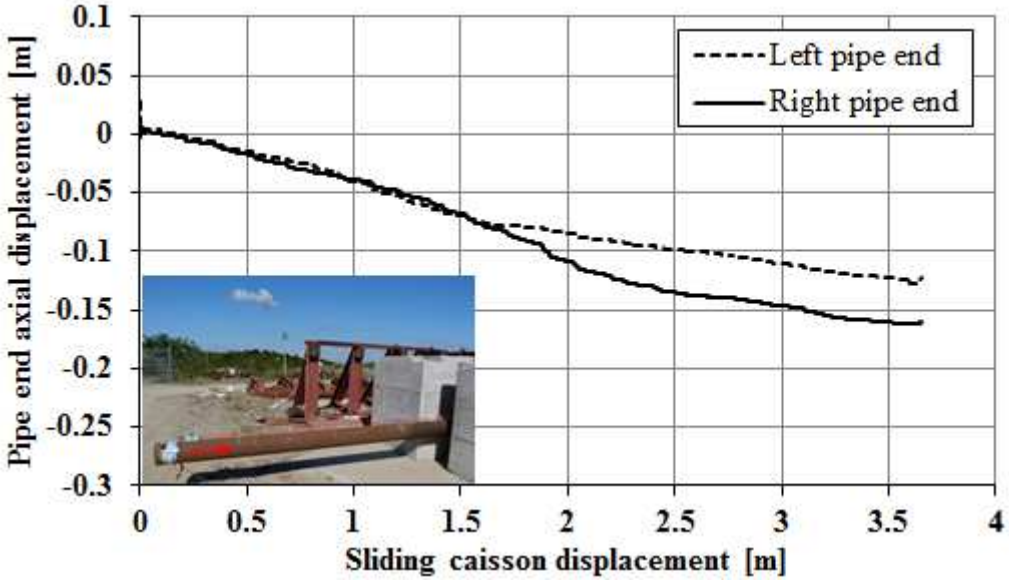

Fig. 130. Pipe ends shortening vs central caisson displacement, Test No. 7.

Removed the specimen from the caissons the ovalization of instrumented cross sections was measured and computed as ratio of $\frac{D_{max}-D_{min}}{D}$.

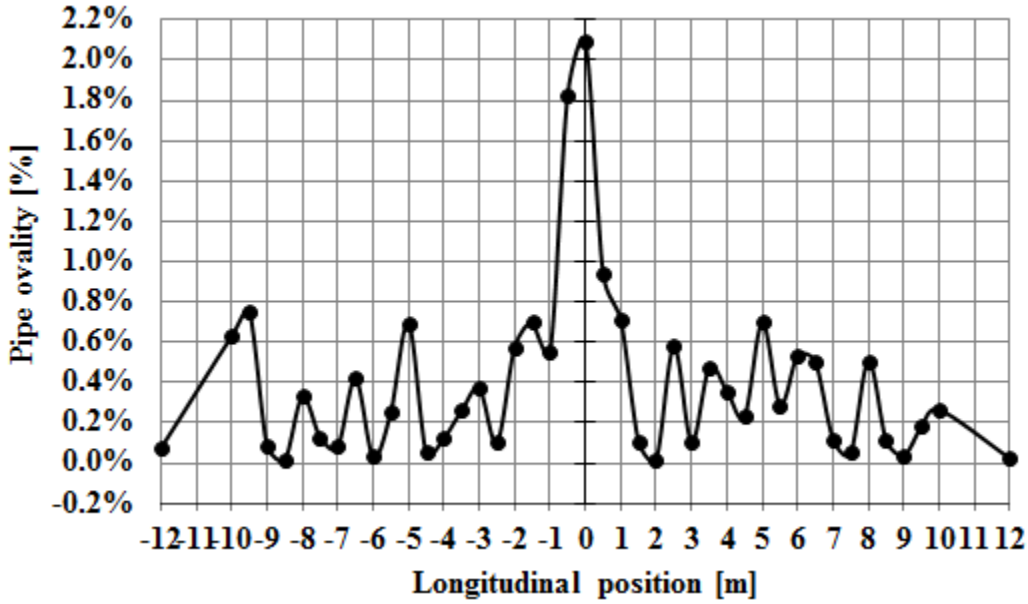

Fig. 131. Pipe cross section ovalization after the experiment, Test No. 7.

Some variations along the pipe can be observed in Fig. 131 and a maximum value of 2.1% at the middle section can be noticed.

6.3.2. Landslide/fault Test No. 8

Pipe specimen (for Test No. 8) assembled with 5 pipe segments welded by manual SMAW welding adopting the WPS specifically developed for the project is schematically presented in Fig. 132.

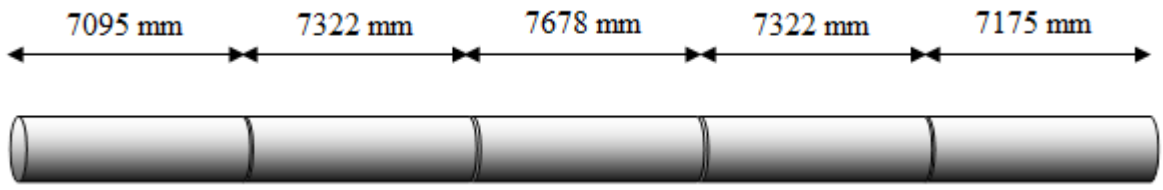

Fig. 132. Schematic assembly of pipe segments for specimen of Test No. 8.

Test No. 8 performed with uncoated pipe, with internal pressure equal to 11.4 MPa and relative density of sand equal to 29% have been subjected to significant bending, achieving plastic deformation mainly along the longitudinal direction in the range of ± 0.9%.

No buckling or tensile rupture was observed and slight cross section deformations were measured at the end of the test.

A picture of soil deformation at the end of the test is shown in Fig. 133. Besides in Fig. 134 the comparison between pipe final deformation after Test No. 8 and Test No. 7 is shown.

Fig. 133. Soil deformation occurred for 3200 mm of central caisson displacement, Test No. 8.

Fig. 134. Pipe final deformation after the Test No. 7 and Test No. 8.

Several charts of strain distribution at extrados generatrix line, intrados generatrix line and axial line are presented for various steps of caisson displacement from Fig. 135 to Fig. 138. The strain values for failed strain gauges have been interpolated by the values of neighboring sections. Analyzing the results it can be observed that in addition to a primary high strain spot (at pipe middle section) a secondary (lower) spot is located aside from the fault lines (dashed lines in plots). The distance of this secondary strain spot moves from an initial distance of about 3000 mm towards the pipe ends (for 600 mm of caisson displacement), to 4000÷5000 mm from fault lines (for maximum caisson displacement attained of 3200 mm). The curvature inversion point (zero longitudinal strains) is located close to fault lines and again is seen to move towards pipe ends for an increasing applied caisson displacement.

Starting from 600 mm of caisson displacement the range of strains was ± 0.45% and as reported in Fig. 135 the maximum calculated deflection was around 400 mm.

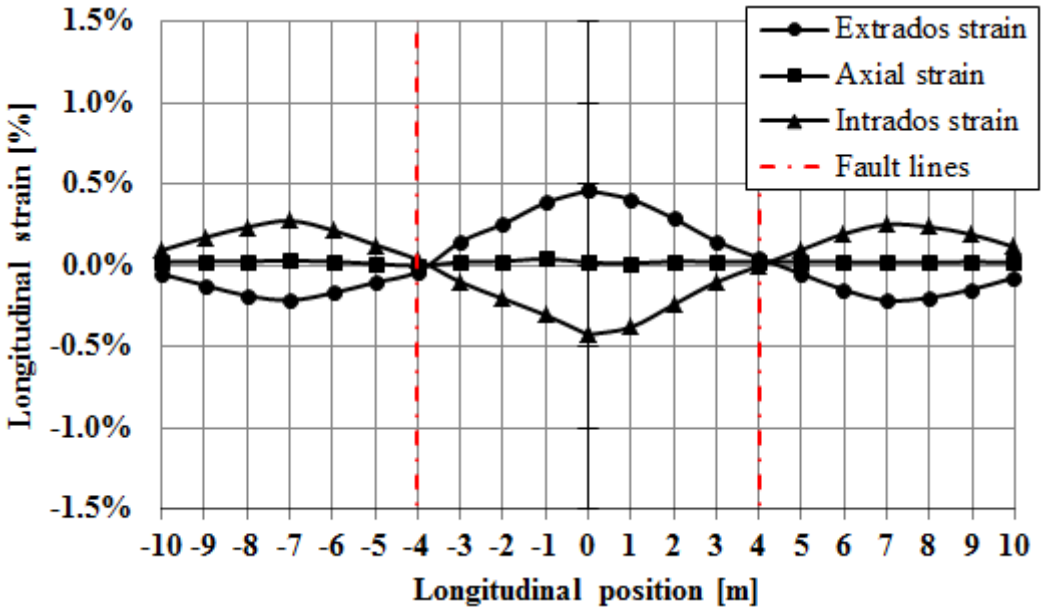

Fig. 135. Distribution of strains along pipe for 600 mm central caisson displacement, Test No. 8.

At 1200 mm of caisson displacement (Fig. 136) the range of strains was nearly ± 0.7% for a maximum deflection of pipe around 800 mm. Then a range of strains was equal to ± 0.9% (Fig. 137) was detected at 2400 mm of caisson displacement with a maximum pipe deflection slightly more than 1400 mm.

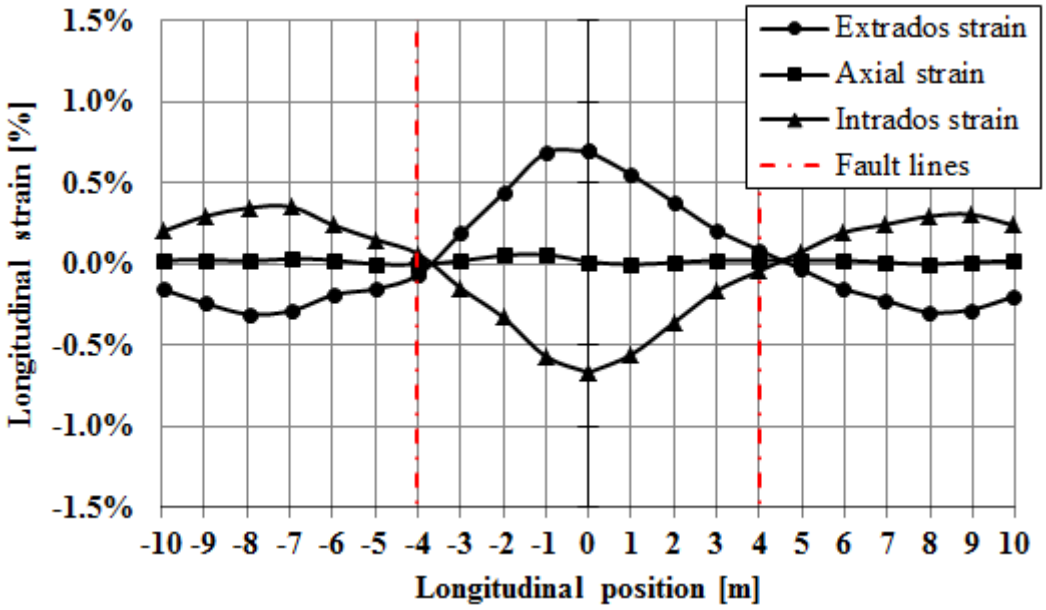

Fig. 136. Distribution of strains along pipe for 1200 mm central caisson displacement, Test No. 8.

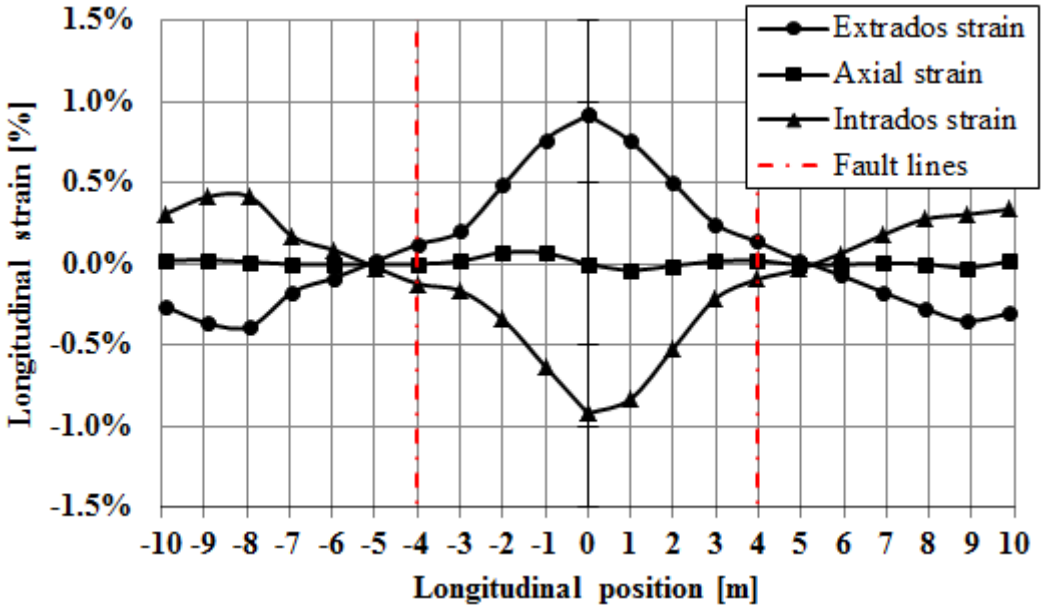

Fig. 137. Distribution of strains along pipe for 2400 mm central caisson displacement, Test No. 8.

At the end of the test, a pipe displacement of 3200 mm was achieved with a range of maximum strains equal to ± 0.9% and a maximum pipe deflection calculated as 1300 mm.

In all cases the calculated axial strain is nearly to zero.

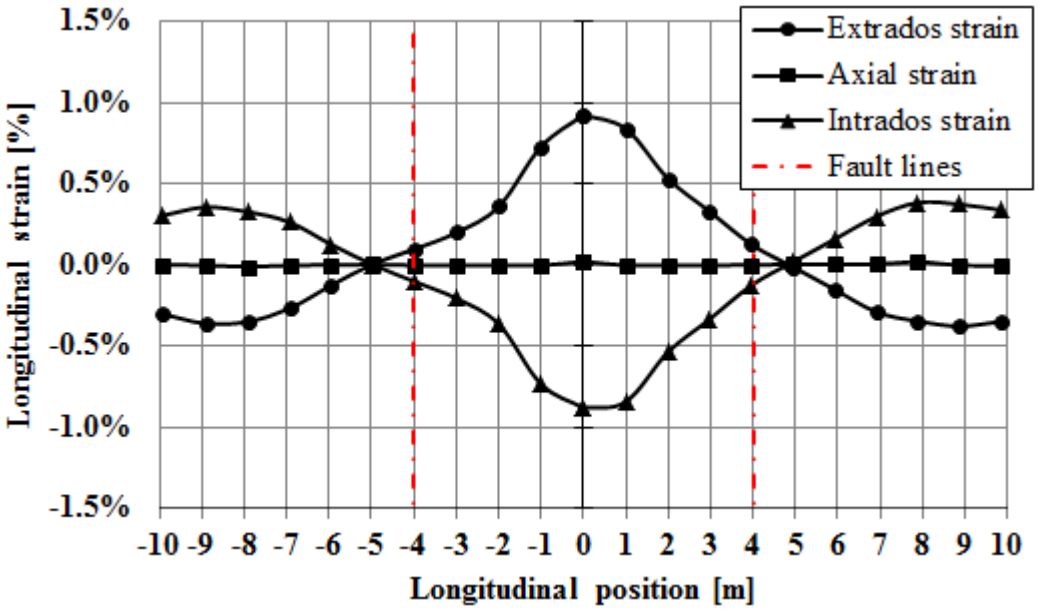

Fig. 138. Distribution of strains along pipe for 3200 mm central caisson displacement, Test No. 8.

Fig. 139 shows the evolution of pipe deflection at various steps of pipe caisson displacement calculated from the longitudinal strains values according to the procedure presented in section 3.6.2. The pipe deflection initially grows quickly and tends to slow down for high caisson displacements and in this experiment has been detected an inversion of pipe deflection going from 2400 mm to 3200 mm of pipe displacement. This behavior can be explained with the spring back of the pipe when the uplift leads the pipe towards the surface of the soil with lower resistance. Fig. 140 shows the calculated deflection of the middle section during the caisson displacement in which is clear the trend of pipe deformation.

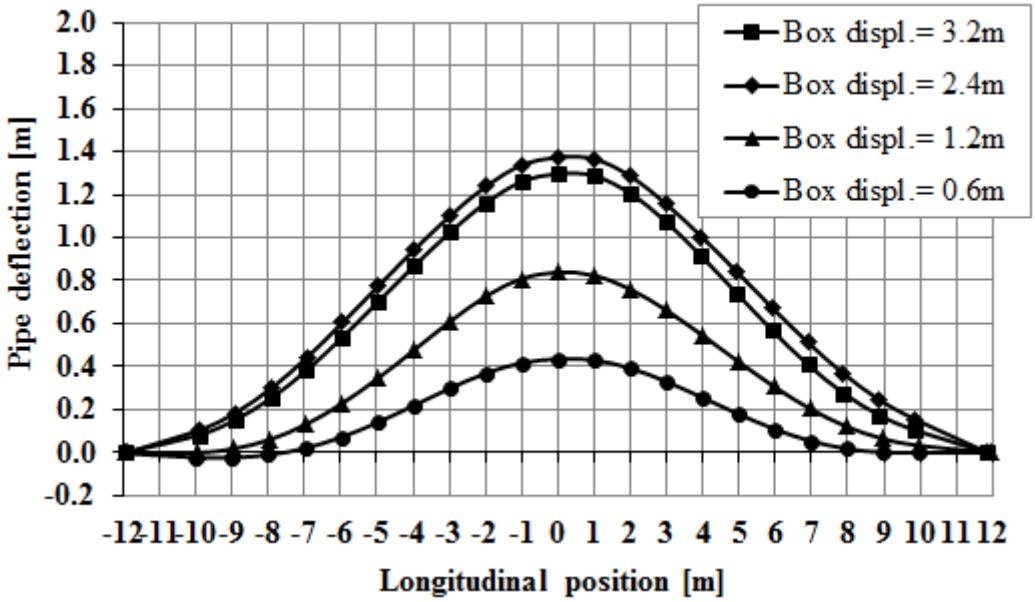

Fig. 139. Pipe deflection calculated by strains, Test No. 8.

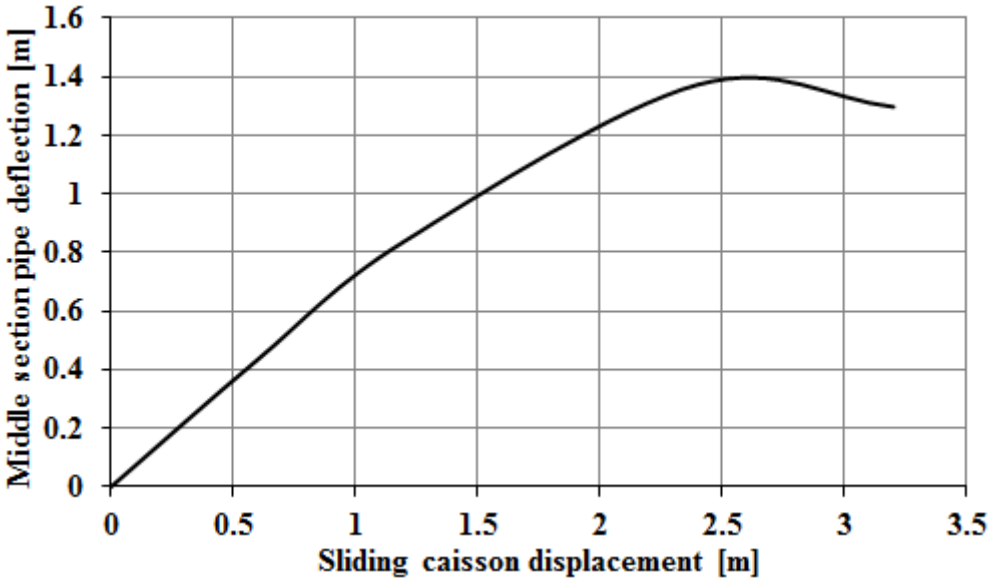

Fig. 140. Evolution of pipe deflection at middle section calculated by strains, Test No. 8.

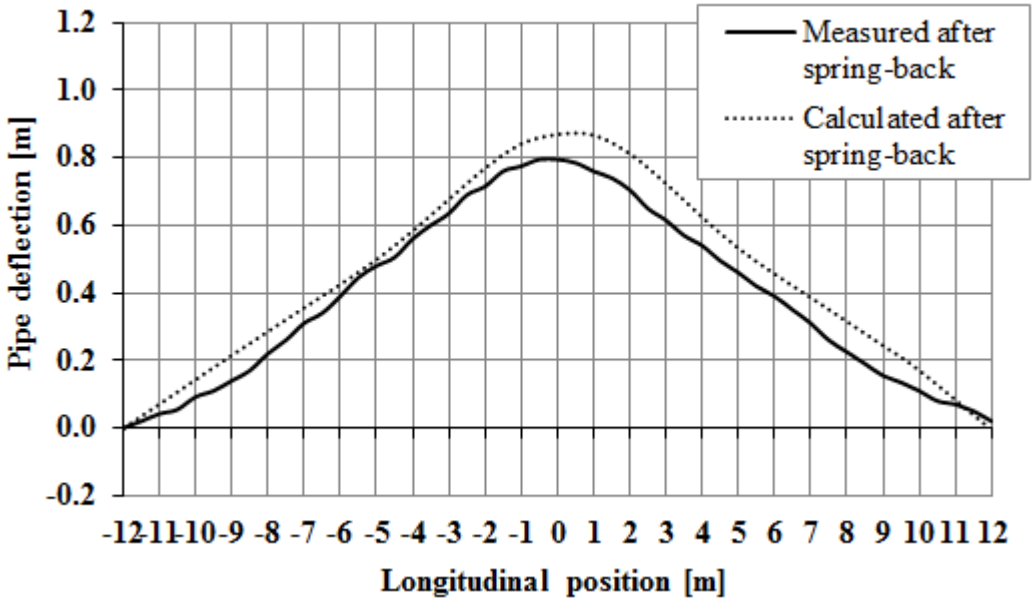

Fig. 141. Pipe deflection on the horizontal plane after soil removing calculated by strains and measured on field, Test No. 8.

At the end of the test after soil removal a spring back of the specimen was observed. Afterwards measurements of horizontal and vertical deflection were carried out. In Fig. 141 the comparison between calculated and measured pipe deformation is presented, showing a good agreement.

Using two LVDTs applied at the ends of pipe, the longitudinal displacement was also measured, showing a symmetric shortening up to 400 mm of caisson displacement and a sensitive divergence after this point. The maximum pipe axial displacement measured was 240 mm and 40 mm respectively for left pipe end and right pipe end.

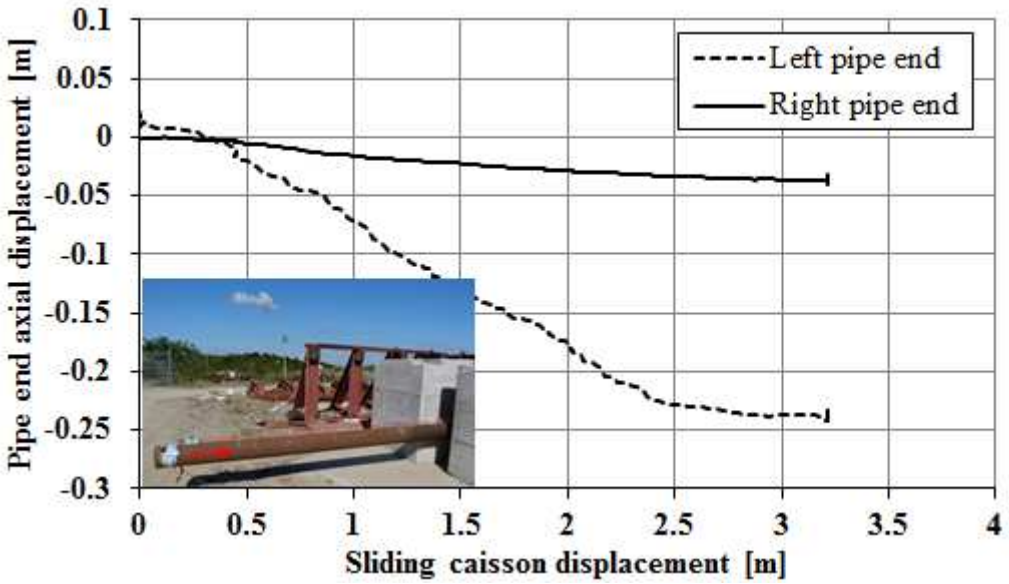

Fig. 142. Pipe ends shortening vs central caisson displacement, Test No. 8.

Removed the specimen from the caissons the ovalization of instrumented cross sections was measured and computed as ratio of $\frac{D_{max}-D_{min}}{D}$. Some variations along the pipe can be observed in Fig. 143 and a maximum value of 1.15% at the middle section can be noticed.

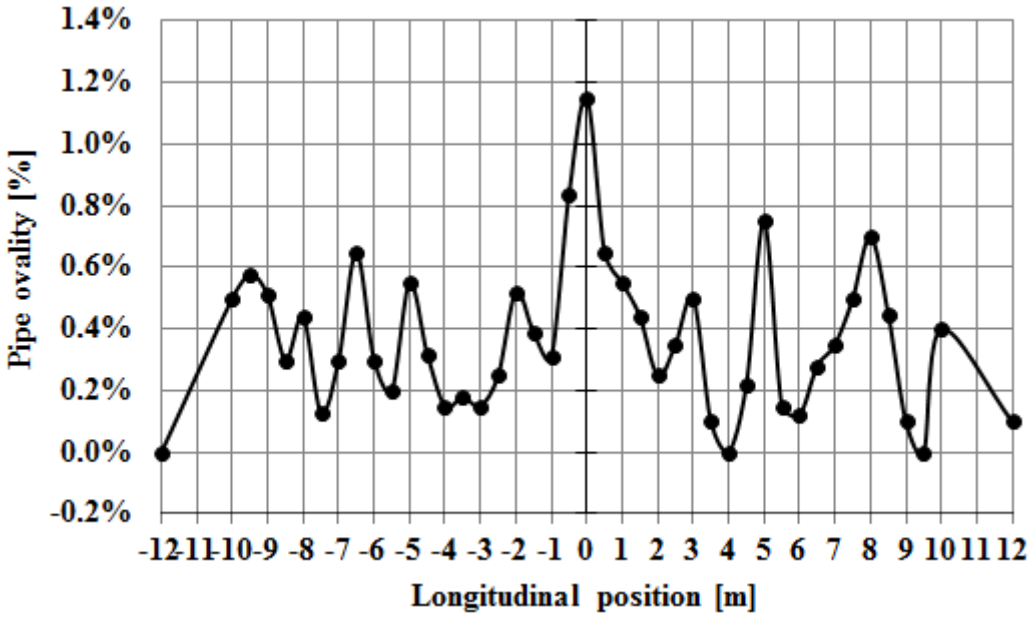

Fig. 143. Pipe cross section ovalization after the experiment, Test No. 8.

6.3.3. Landslide/fault Test No. 9

Pipe specimen (for Test No. 9) assembled with 5 pipe segments welded by manual SMAW welding adopting the WPS specifically developed for the project is schematically presented in Fig. 144.

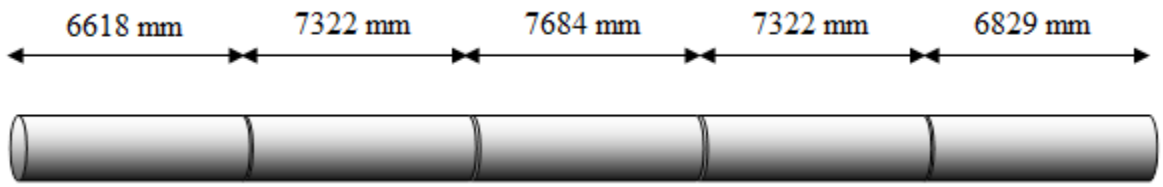

Fig. 144. Schematic assembly of pipe segments for specimen of Test No. 9.

Test No. 9 performed with uncoated pipe, without internal pressure and relative density of sand equal to 21% have been subjected to bending, achieving plastic deformation mainly along the longitudinal direction in the range of ± 0.7%.

No buckling or tensile rupture was observed and slight cross section deformations were measured at the end of the test.

A picture of soil deformation at the end of the test is shown in Fig. 145. Besides in Fig. 146 the comparison among pipe final deformation after Test No.9, Test No. 8 and Test No. 7 is shown.

Fig. 145. Soil deformation occurred for 3290 mm of central caisson displacement, Test No. 9.

Fig. 146. Pipe final deformation after the Test No. 9, Test No. 8 and Test No. 7.

Several charts of strain distribution at extrados generatrix line, intrados generatrix line and axial line are presented for various steps of caisson displacement from Fig. 147 to Fig. 150. The strain values for failed strain gauges have been interpolated by the values of neighboring sections. Analyzing the results it can be observed that in addition to a primary high strain spot (at pipe middle section) a secondary (lower) spot is located aside from the fault lines (dashed lines in plots). The distance of this secondary strain spot moves from an initial distance of about 4000 mm towards the pipe ends (for 600 mm of caisson displacement), to 6000 mm from fault lines (for maximum caisson displacement attained of 3290 mm). The curvature inversion point (zero longitudinal strains) is located close to fault lines and again is seen to move towards pipe ends for an increasing applied caisson displacement.

Starting from 600 mm of caisson displacement the range of strains was ± 0.35% and as reported in Fig. 147 the maximum calculated deflection was around 500 mm.

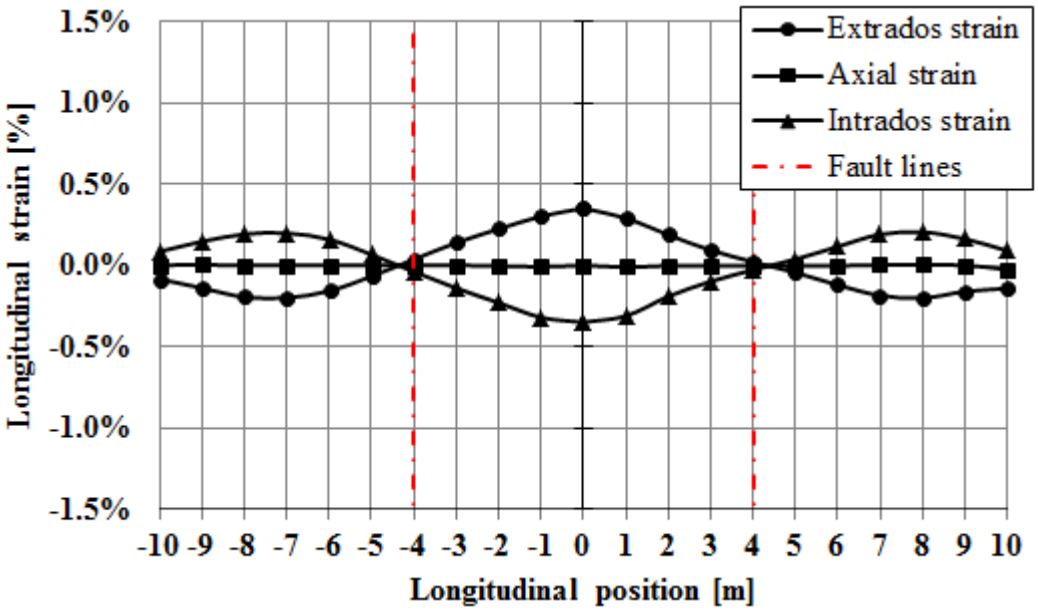

Fig. 147. Distribution of strains along pipe for 600 mm central caisson displacement, Test No. 9.

At 1200 mm of caisson displacement (Fig. 148) the range of strains was nearly ± 0.5% for a maximum deflection of pipe around 840 mm. Then a range of strains was equal to ± 0.7% (Fig. 149) was detected at 2400 mm of caisson displacement with a maximum pipe deflection slightly more than 1200 mm.

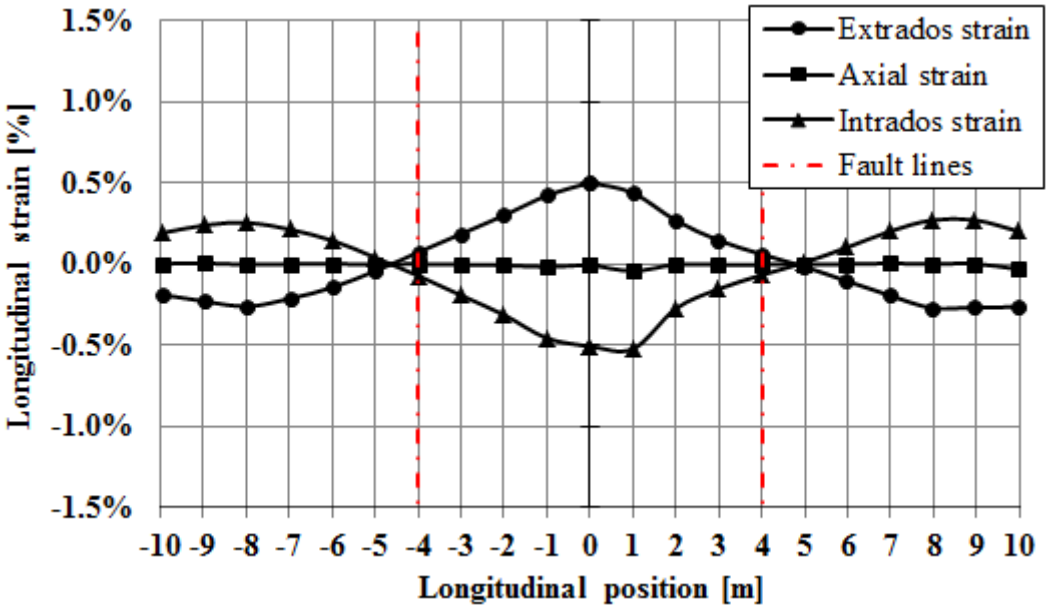

Fig. 148. Distribution of strains along pipe for 1200 mm central caisson displacement, Test No. 9.

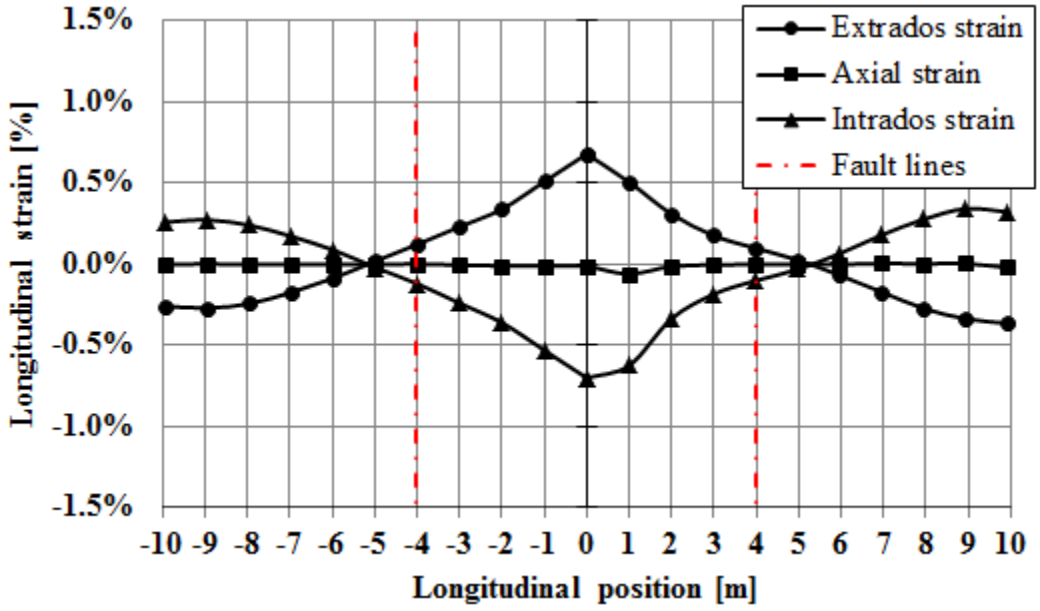

Fig. 149. Distribution of strains along pipe for 2400 mm central caisson displacement, Test No. 9.

At the end of the test, a pipe displacement of 3200 mm was achieved with a range of maximum strains equal to ± 0.7% and a maximum pipe deflection calculated as 1250 mm.

In all cases the calculated axial strain is nearly to zero.

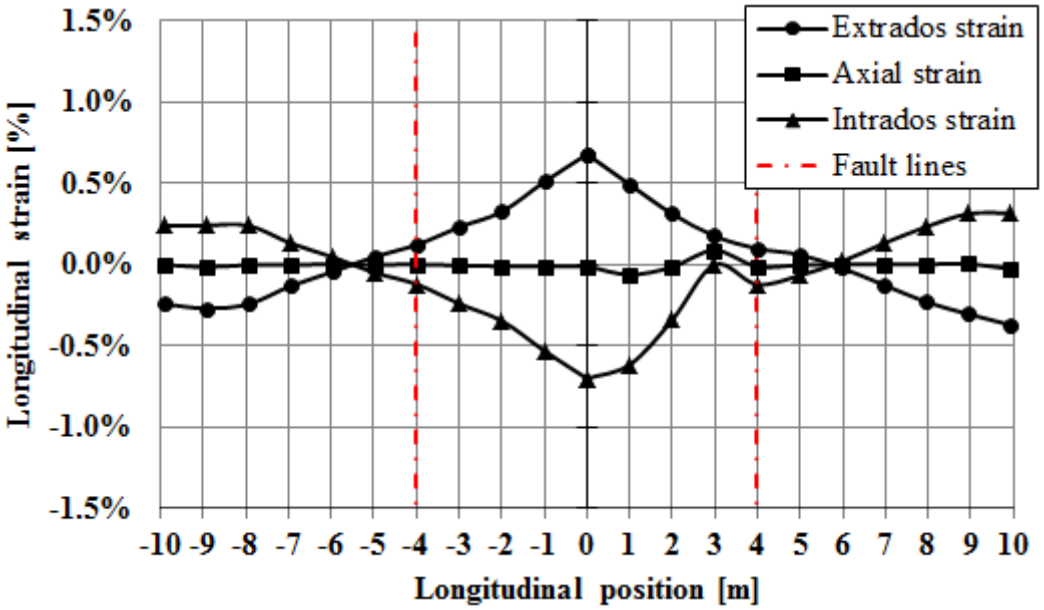

Fig. 150. Distribution of strains along pipe for 3290 mm central caisson displacement, Test No. 9.

Fig. 151 shows the evolution of pipe deflection at various steps of pipe caisson displacement calculated from the longitudinal strains values according to the procedure presented in section 3.6.2. The pipe deflection initially grows quickly and tends to slow down for high caisson displacements. Fig. 152 shows the calculated deflection of the middle section during the caisson displacement in which is clear the trend of pipe deformation.

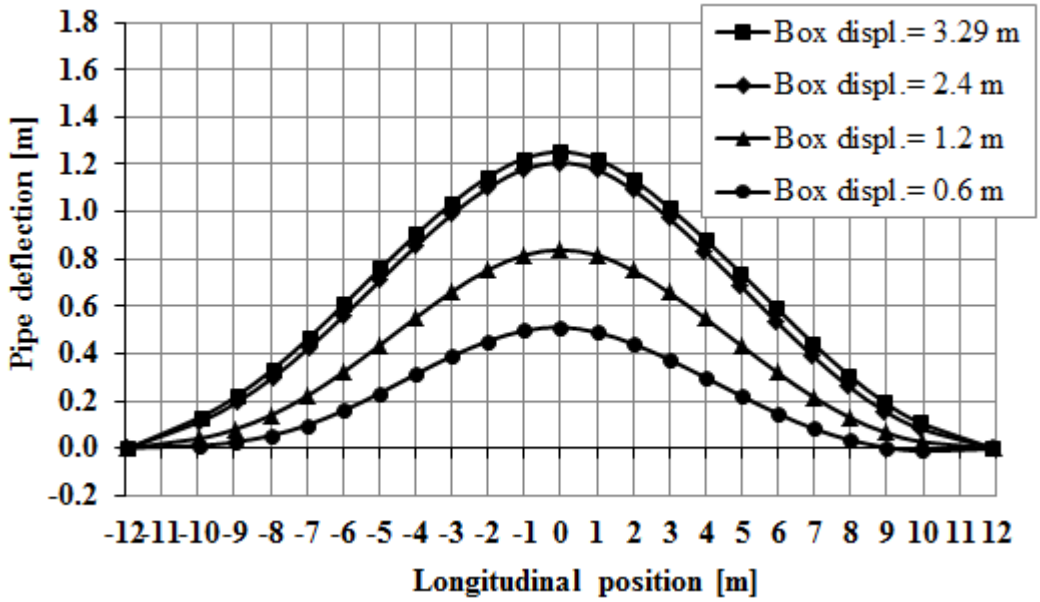

Fig. 151. Pipe deflection calculated by strains, Test No. 9.

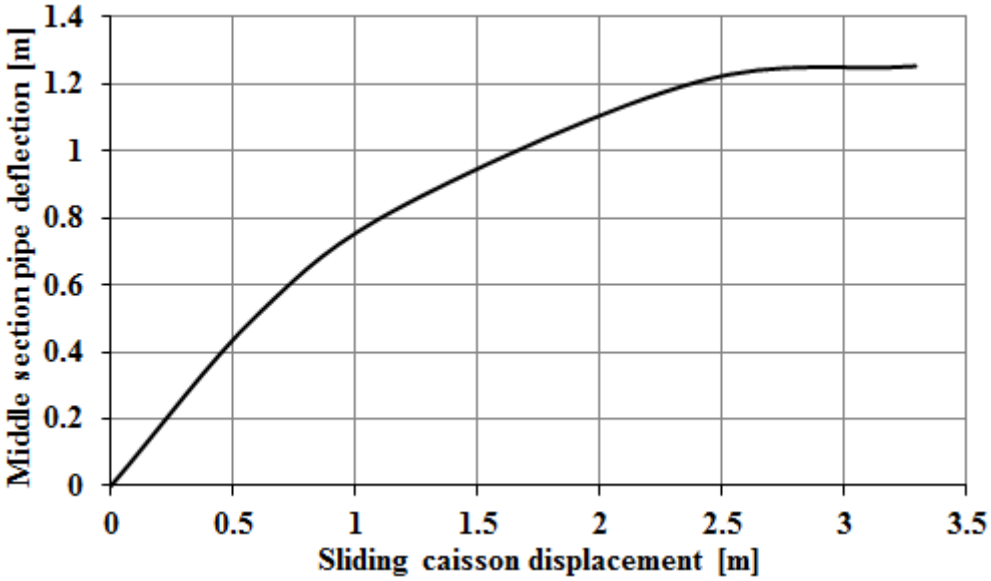

Fig. 152. Evolution of pipe deflection at middle section calculated by strains, Test No. 9.

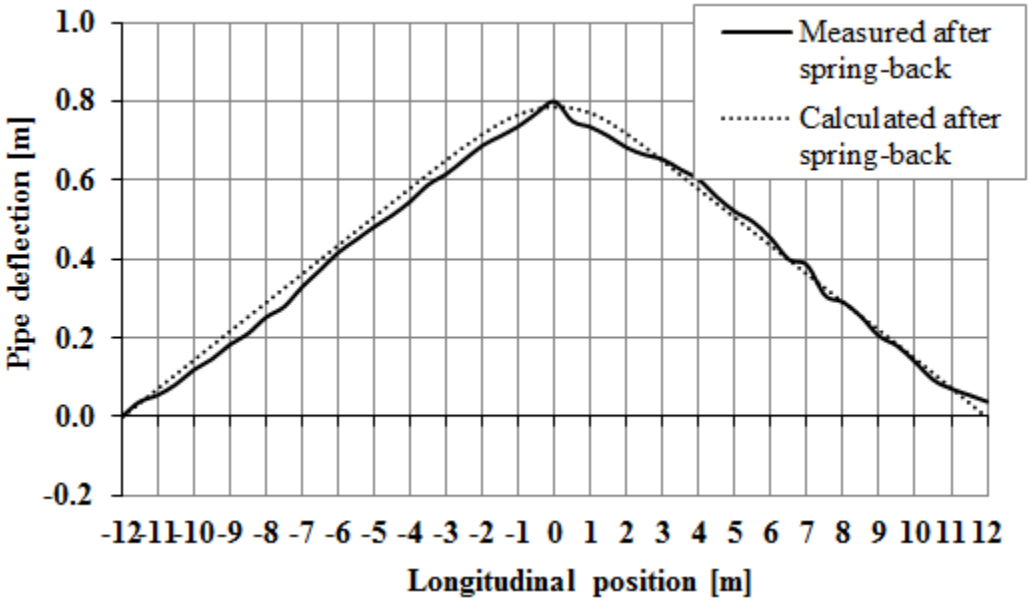

Fig. 153. Pipe deflection after soil removing calculated by strains and measured on field, Test No. 9.

At the end of the test after soil removal a spring back of the specimen was observed. Afterwards measurements of horizontal and vertical deflection were carried out. In Fig. 153 the comparison between calculated and measured pipe deformation is presented, showing a good agreement.

Using two LVDTs applied at the ends of pipe, the longitudinal displacement was also measured, showing a symmetric shortening up to 1000 mm of caisson displacement and a sensitive divergence after this point. The maximum pipe axial displacement measured was 106 mm and 30 mm respectively for left pipe end and right pipe end.

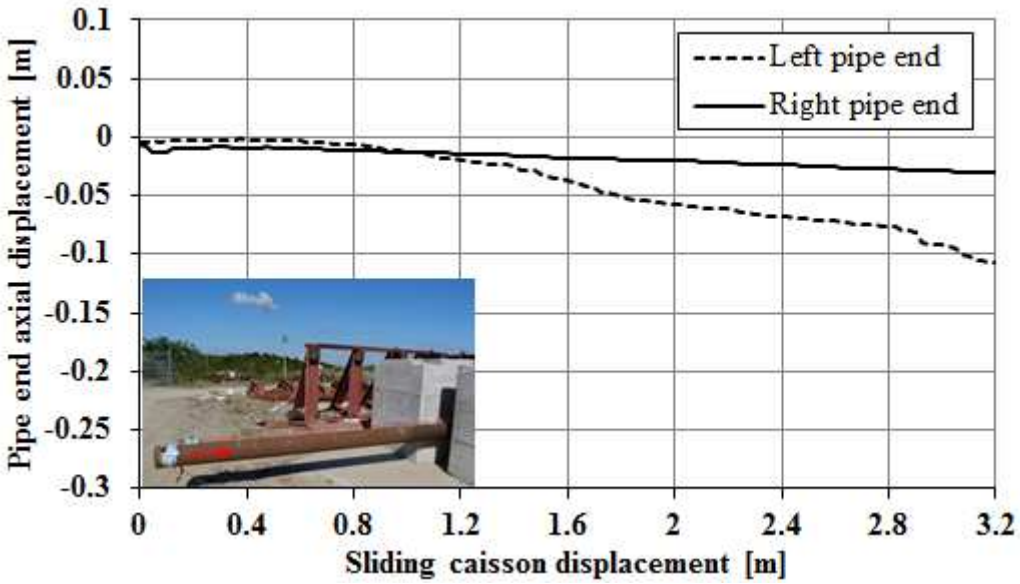

Fig. 154. Pipe ends shortening vs central caisson displacement, Test No. 9.

Removed the specimen from the caissons the ovalization of instrumented cross sections was measured and computed as ratio of $\frac{D_{max}-D_{min}}{D}$. Some variations along the pipe can be observed in Fig. 155 and a maximum value of 0.8% at middle section can be noticed.

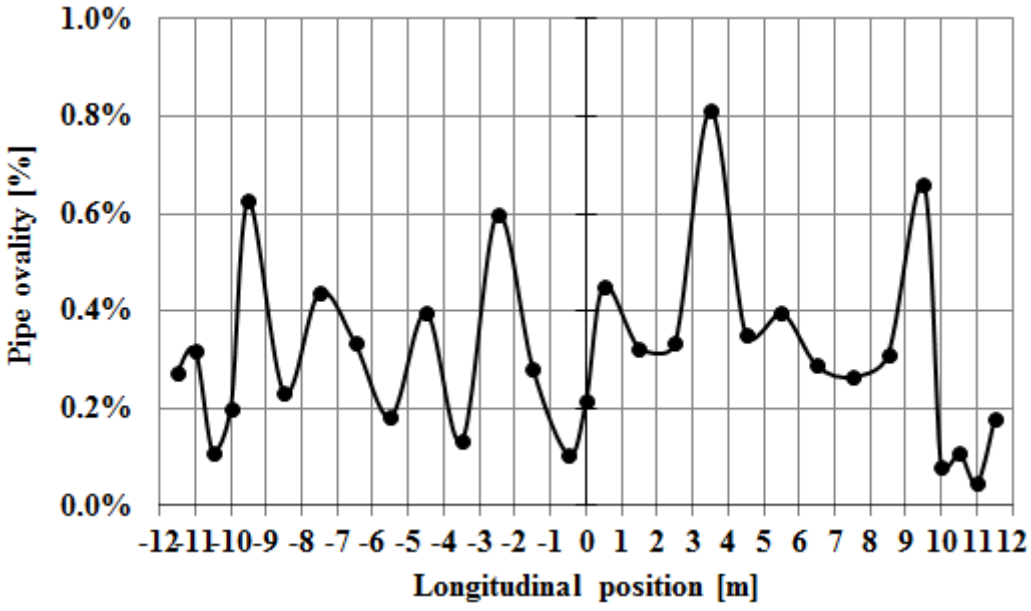

Fig. 155. Pipe cross section ovalization after the experiment, Test No. 9.

6.3.4. Landslide/fault Test No. 10

Pipe specimen (for Test No. 10) assembled with 5 pipe segments welded by manual SMAW welding adopting the WPS specifically developed for the project is schematically presented in Fig. 156.

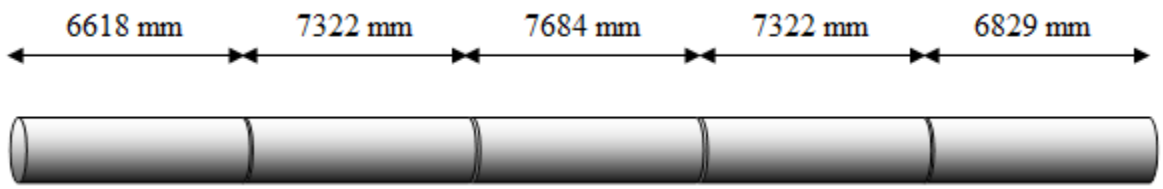

Fig. 156. Schematic assembly of pipe segments for specimen of Test No. 10.

Test No. 10 performed with uncoated pipe, with internal pressure equal to 11.4 MPa and relative density of sand equal to 35% have been subjected to significant bending, achieving plastic deformation mainly along the longitudinal direction in the range of ± 0.6%.

No buckling or tensile rupture was observed and slight cross section deformations were measured at the end of the test.

Several charts of strain distribution at extrados generatrix line, intrados generatrix line and axial line are presented for various steps of caisson displacement from Fig. 157 to Fig. 160. The strain values for failed strain gauges have been interpolated by the values of neighboring sections. Analyzing the results it can be observed that in addition to a primary high strain spot (at pipe middle section) a secondary (lower) spot is located aside from the fault lines (dashed lines in plots). The distance of this secondary strain spot moves from an initial distance of about 3000 mm towards the pipe ends (for 600 mm of caisson displacement), to 5000÷6000 mm from fault lines (for maximum caisson displacement attained of

3220 mm). The curvature inversion point (zero longitudinal strains) is located close to fault lines and again is seen to move towards pipe ends for an increasing applied caisson displacement.

Starting from 600 mm of caisson displacement the range of strains was ± 0.25% and as reported in Fig. 157 the maximum calculated deflection was around 300 mm.

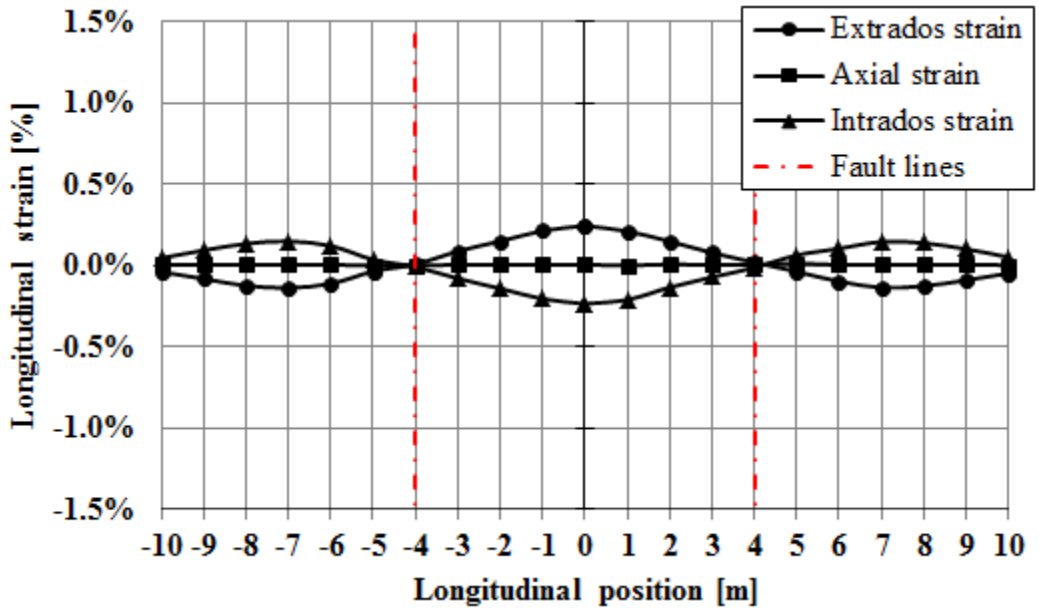

Fig. 157. Distribution of strains along pipe for 600 mm central caisson displacement, Test No. 10.

At 1200 mm of caisson displacement (Fig. 158) the range of strains was nearly ± 0.4% for a maximum deflection of pipe around 570 mm. Then a range of strains was equal to ± 0.6% (Fig. 159) was detected at 2400 mm of caisson displacement with a maximum pipe deflection equal to 870 mm.

At the end of the test, a pipe displacement of 3220 mm was achieved with a range of maximum strains equal to ± 0.6% and a maximum pipe deflection calculated as 950 mm.

In all cases the calculated axial strain is nearly to zero.

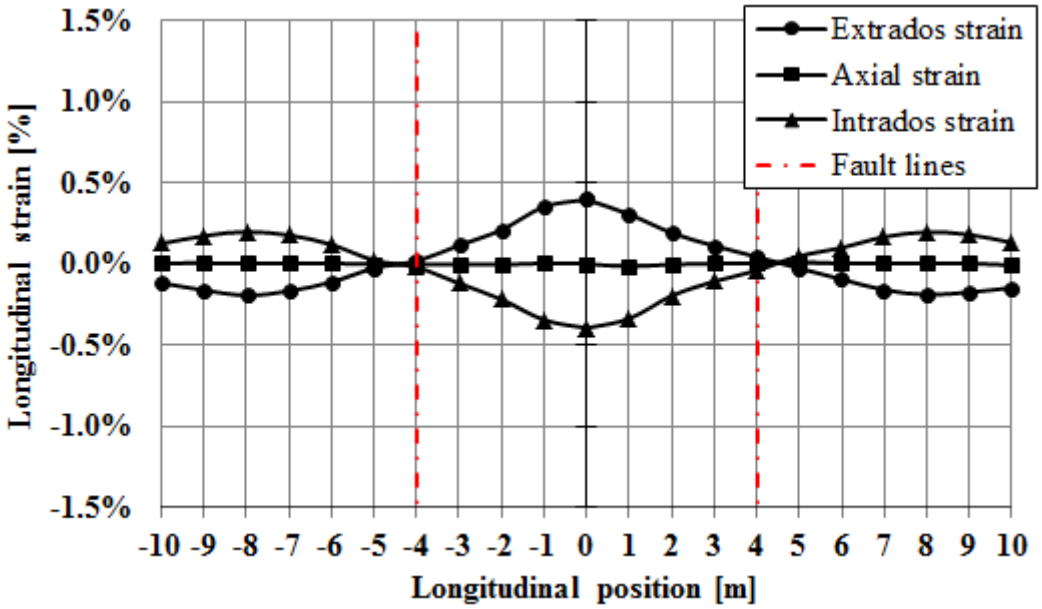

Fig. 158. Distribution of strains along pipe for 1200 mm central caisson displacement, Test No. 10.

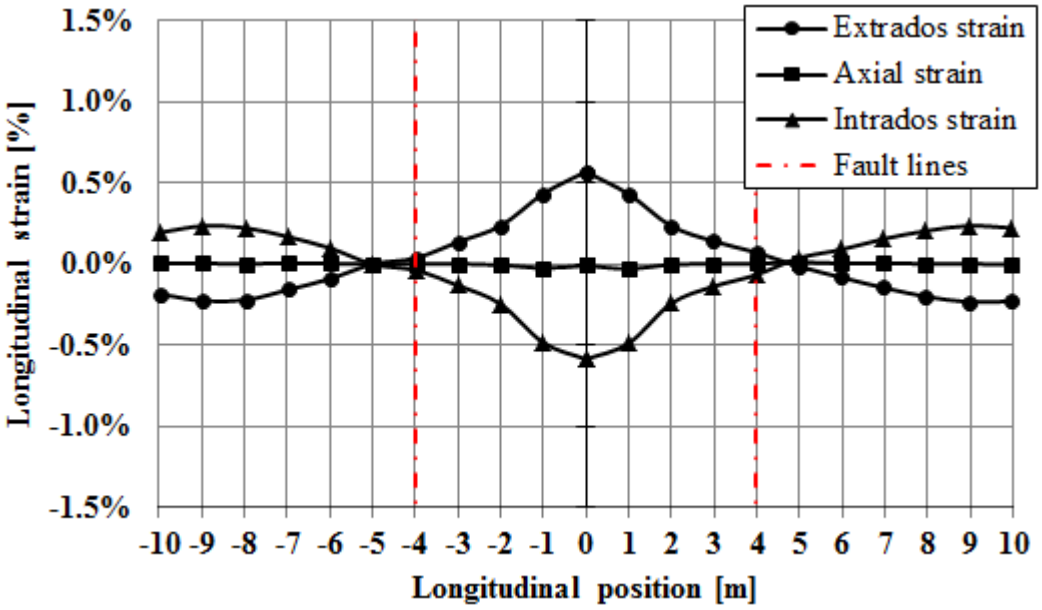

Fig. 159. Distribution of strains along pipe for 2400 mm central caisson displacement, Test No. 10.

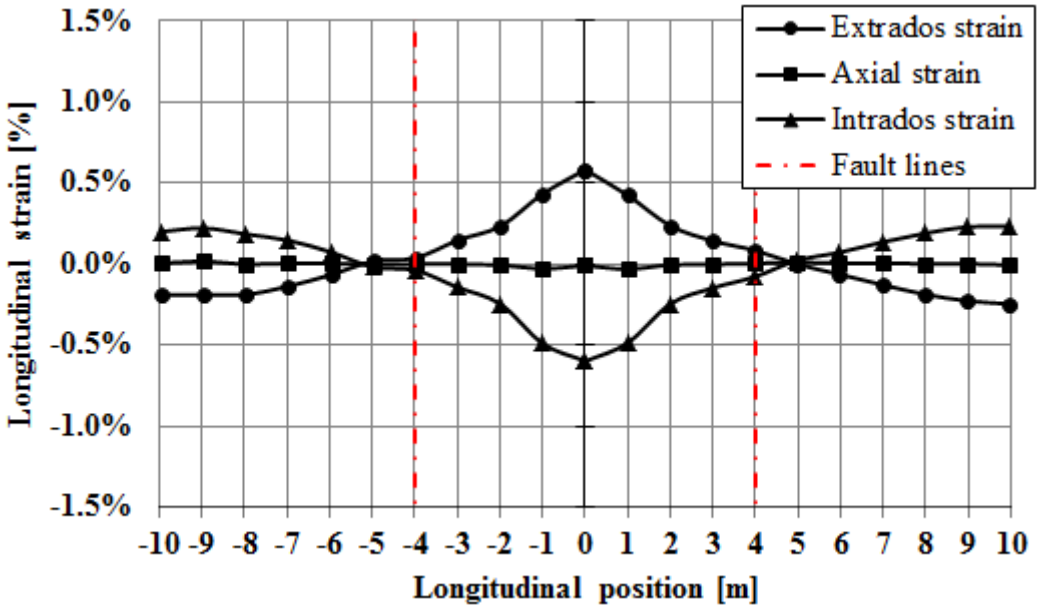

Fig. 160. Distribution of strains along pipe for 3220 mm central caisson displacement, Test No. 10.

Fig. 161 shows the evolution of pipe deflection at various steps of pipe caisson displacement calculated from the longitudinal strains values according to the procedure presented in section 3.6.2. The pipe deflection initially grows quickly and tends to slow down for high caisson displacements.

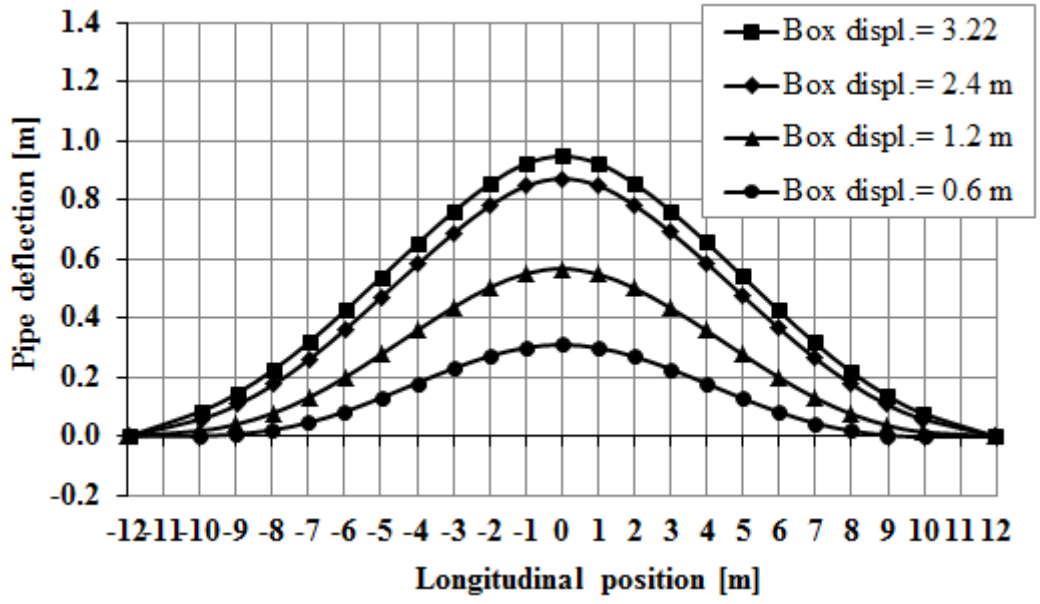

Fig. 161. Pipe deflection calculated by strains, Test No. 10.

Fig. 162 shows the calculated deflection of the middle section during the caisson displacement in which is clear the trend of pipe deformation.

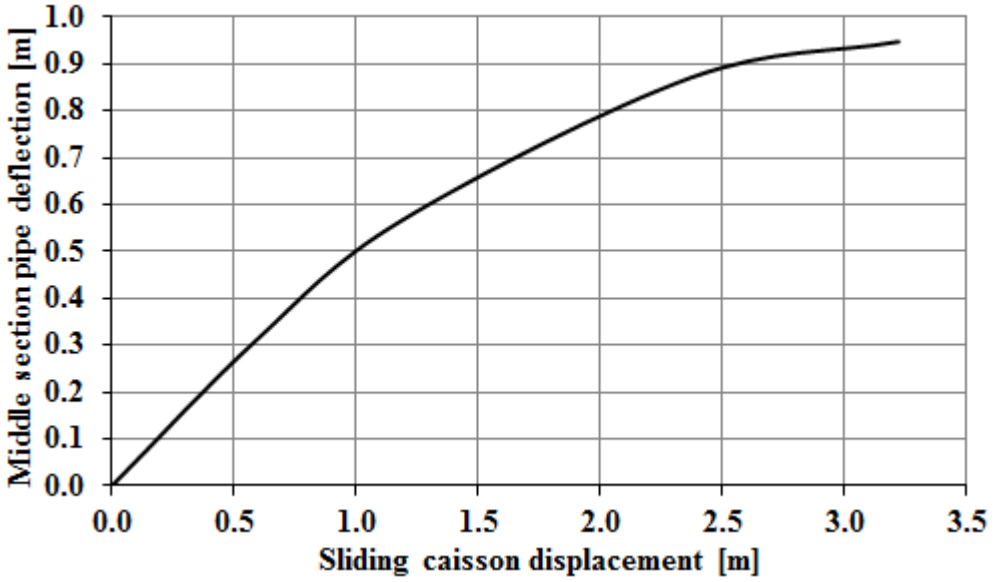

Fig. 162. Evolution of pipe deflection at middle section calculated by strains, Test No. 10.

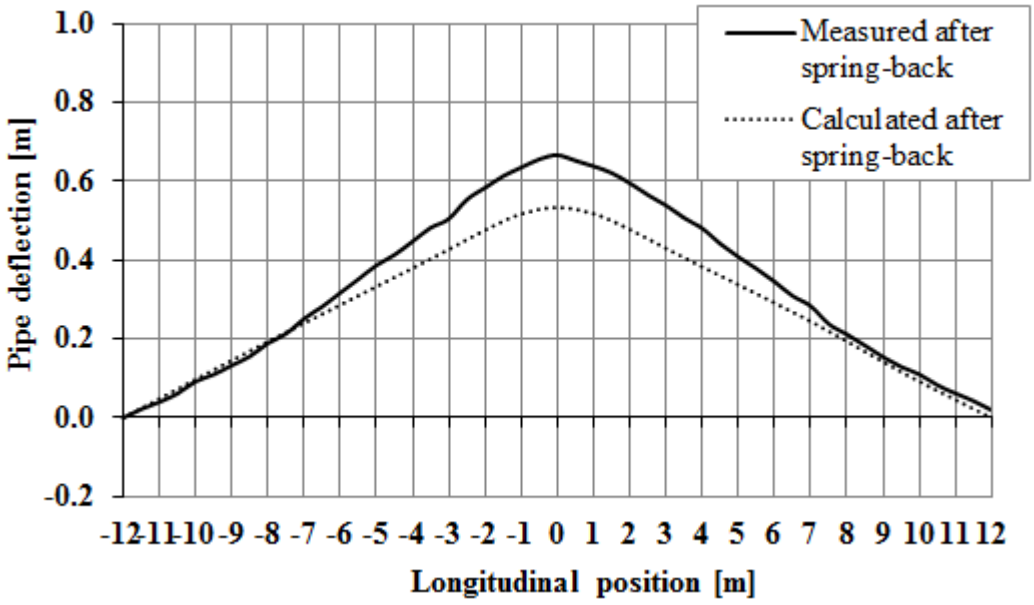

Fig. 163. Pipe deflection on the horizontal plane after soil removing calculated by strains and measured on field, Test No. 10.

At the end of the test after soil removal a spring back of the specimen was observed. Afterwards measurements of horizontal and vertical deflection were carried out. In Fig. 163 the comparison between calculated and measured pipe deformation is presented, showing a good agreement.

Using two LVDTs applied at the ends of pipe, the longitudinal displacement was also measured, showing a symmetric shortening up to 500 mm of caisson displacement and a sensitive divergence after this point. The maximum pipe axial displacement measured was 100 mm and 55 mm respectively for left pipe end and right pipe end.

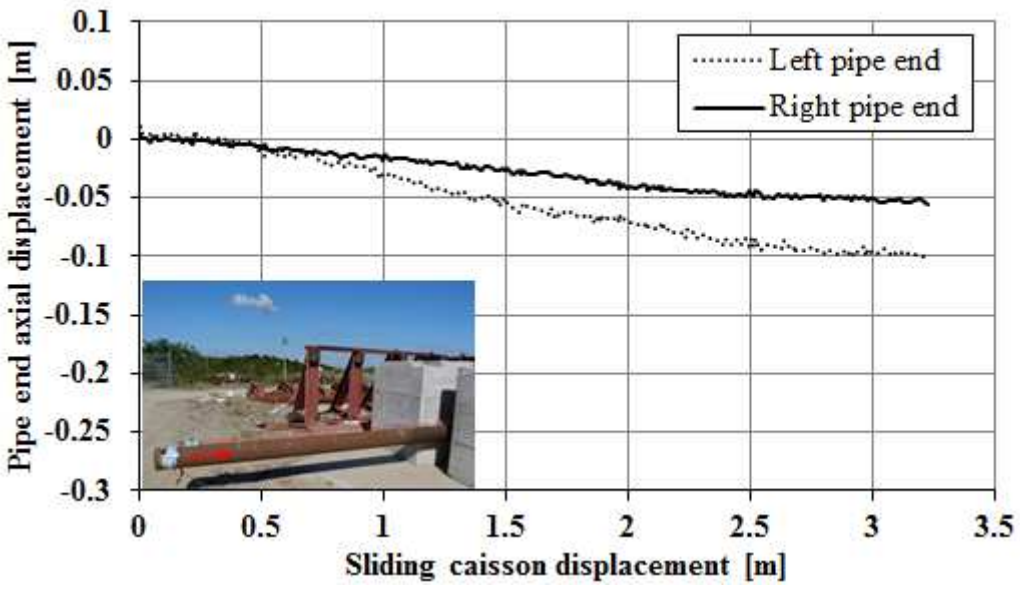

Fig. 164. Pipe ends shortening vs central caisson displacement, Test No. 10.

Removed the specimen from the caissons the ovalization of instrumented cross sections was measured and computed as ratio of $\frac{D_{max}-D_{min}}{D}$. Some variations along the pipe can be

observed in Fig. 165 and a maximum value of 0.52% nearly the middle section can be noticed.

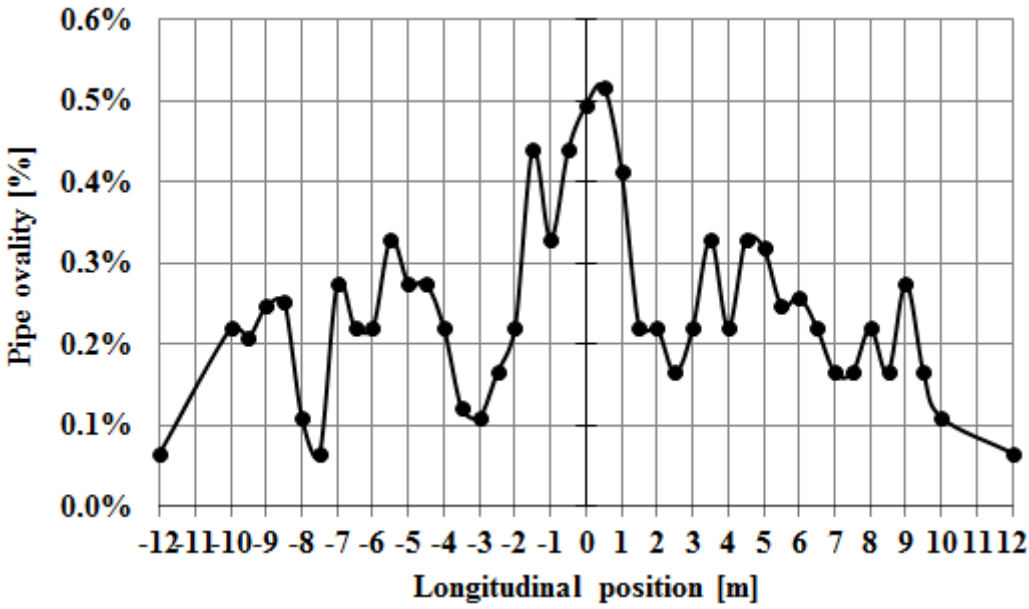

Fig. 165. Pipe cross section ovalization after the experiment, Test No. 10.

6.4. Finite element modeling of landslide/fault testing

The numerical analysis was conducted using a commercial finite element program ABAQUS 6.14 version [1], accompanied from a subroutine written in FORTRAN language in order to achieve the softening behavior of the soil.

A four-node doubly curved general-purpose shell finite membrane strains (S4) are employed for modeling the cylindrical pipeline cross section and an eight-node linear brick (C3D8) are used to simulate the surrounding soil. The model has the same dimension of the experimental tests as depicted in Fig. 166 also the pipe diameter and the wall thickness. The soil pipeline mesh is the result of sensitivity analysis conducted in order to reach a good compromise between accuracy of results and velocity of simulation, the dimension of

the mesh is chosen finer around pipe with a constant increase towards the boundaries of the model. A total of 34 shell elements around the cylinder circumference have been found adequate to achieve convergence in the solution. The size of shell elements in the circumferential direction has been chosen equal to 20.3 mm and 20 mm in the longitudinal direction equal to 1/11of the pipeline outer diameter.

The distance from the pipe crown and the top surface is 2.63D, 2.07D from the pipe invert to the bottom of the soil prism, 2.57D the distance from one side of the pipe to the same side lateral wall, 16.2D the distance from the other side of the pipe to the adjacent lateral wall. The overburden ratio was chosen equal to 3.1 as done with experimental tests.

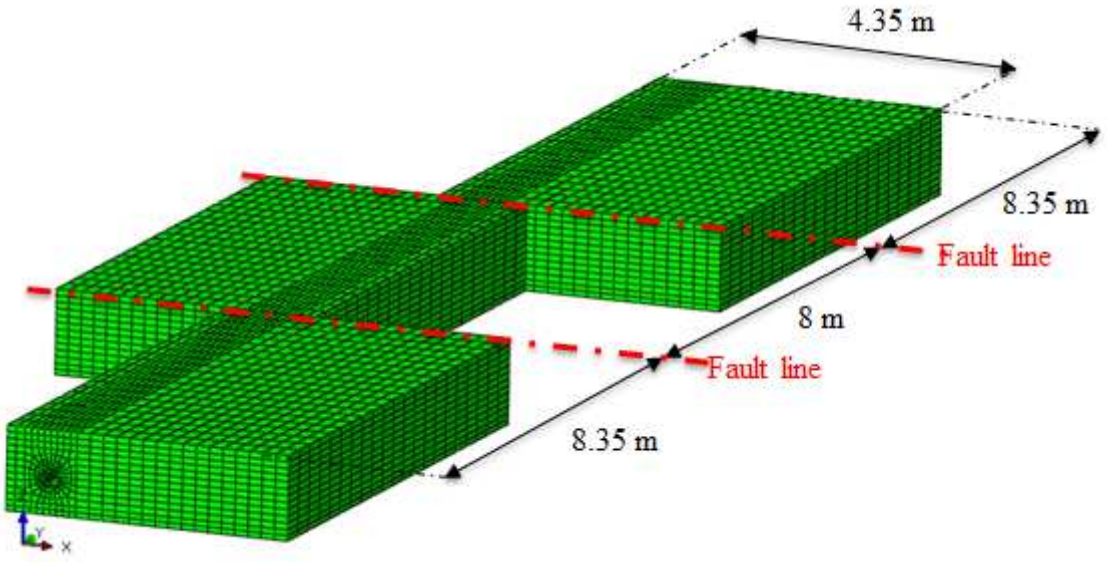

Fig. 166 a). Finite element mesh of soil prisms.

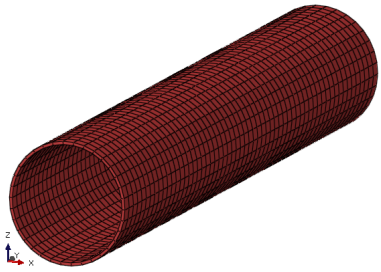

b). Finite element mesh of steel pipeline (segment).

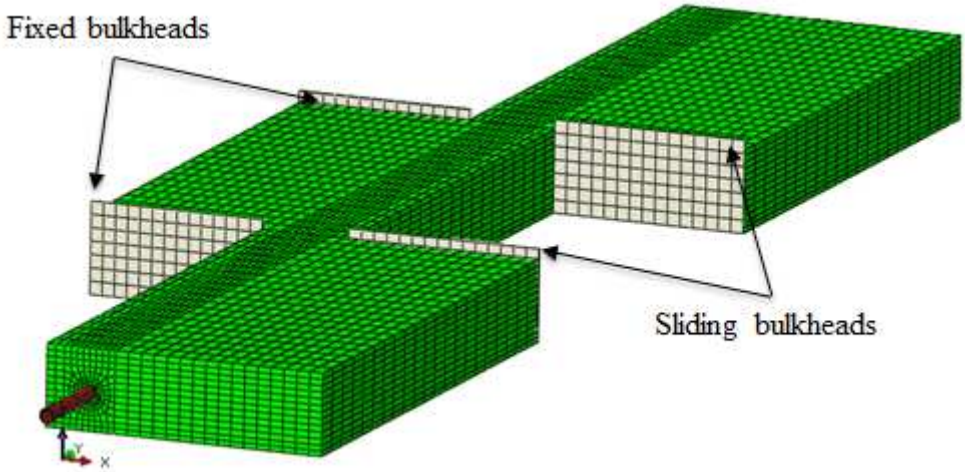

c). Finite element mesh of steel bulkheads.

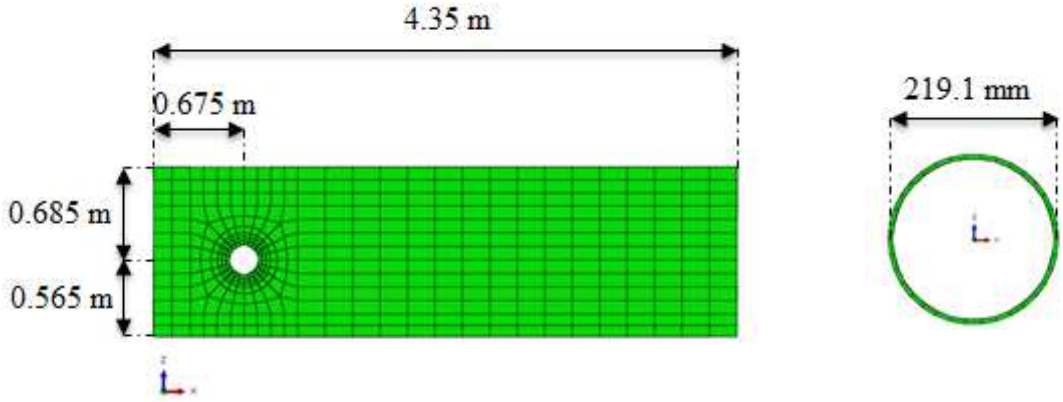

d). Finite element mesh of soil prism cross section.

e). Finite element mesh of steel pipeline cross section.

Fig. 166. Finite element model of landslide/fault testing.

Top surface of the prisms represent the soil surface, free to move in all directions. Nodes of lateral surfaces of the fixed soil prisms are fixed in the normal direction; the nodes of the bottom blocked prisms are fixed in x-y-z directions. Fault surfaces are in contact with bulkhead elements modeled with eight node brick elements (type C3D8). Two bulkheads are fixed and two free to slide on soil surface simultaneously to the central caisson (Fig. 166 c)).

Besides displacement of central soil prism in x direction (Fig. 166 a)) is imposed on lateral surface nodes and on bottom nodes. Bottom nodes are also fixed in y and z directions.

In addition, the pipe ends are constrained as schematically reported in Fig. 14 for experimental testing, leaving free pipe longitudinal translation and rotation. The interface interaction between the pipe and the surrounding soil is simulated with a contact algorithm that include normal contact and tangential friction coefficient in which separation after contact is allowed, the master-slave contact algorithm between external pipe surface and soil surface has been used. Different roughness between uncoated pipes tested in landslide/fault experiments and painted pipes tested in axial and lateral pullout experiments were negligible, therefore tangential friction coefficient was used equal to $0.9*\phi$ as done for axial and lateral models.

The interface interaction between soil surfaces at fault line is simulated with a contact algorithm include normal contact and tangential friction. Tangential friction was used equal to the peak internal friction angle i.e. tan 42°.

Lastly the interface interaction between bulkhead and fault surfaces include only normal contact and neglect tangential friction because it is not crucial for the purposes of the study.

The mechanical behaviour of the steel is described through a large strain von Mises plasticity with isotropic hardening and the behaviour of the soil is described through an elastic perfectly-plastic constitutive model with Mohr Coulomb failure criterion modified by means the USDFLD subroutine explained in previous sections.

In order to avoid numerical instability, all simulations were performed with a slight cohesion equal to 0.1 kPa.

The analysis has been conducted in three steps as follow: geostatic stress is applied in the initial step, the gravity loading in the first step and maintained in the second step then the central soil prism displacement in the second step. A uniform lateral controlled displacement of the soil prism is imposed by displacing the basement and sidewalls.

For the case of pressurized pipeline an intermediate step of internal pressure application is considered (after application of gravity and before the soil prism displacement is activated).

For modeled Tests Nos.: 7, 8 strength parameters equal to: $\phi_p = 42°$, $\phi_r = 36°$, $\psi_p = 10°$ has been used.

Longitudinal strains obtained from numerical analyses are in good agreement with the experimental findings. Detailed comments are presented in the next sections.

6.4.1. Landslide/fault model of Test No. 7

Relative density measured in the experimental Test No. 7 was 40% hence for consistency of the analysis K = 1was used. Pipe internal pressure in this test was zero.

Fig. 167 and Fig. 168 shows the soil deformation of the finite element model for a caisson displacement of 1000 mm in which surface heaving and depression are in agreement with

the experimental results. Fig. 169 and Fig. 170 present pipe stress and longitudinal strain distribution respectively for 1000 mm of central caisson displacement, showing a maximum von Mises stress value equal to 572 MPa and a maximum strain value of 0.8%, the highest stress and strain distribution are concentrated at around the middle section and at around three meters from the fault lines towards pipe ends. No local buckling or tearing rupture can be observed.

Comparison between experimental data and numerical results of longitudinal strain distribution is presented for several steps from Fig. 171 to Fig. 174. At 200 mm of middle caisson displacement there is a good agreement both for extrados strains and intrados strains for a range of ±0.15%. At 400 mm of caisson displacement a range of strains around ±0.3% can be observed, then from 800 mm of caisson displacement strains of numerical model start to be slightly higher than experimental measurement as shown in Fig. 173 to be more evident for 1000 mm of displacement (Fig. 174). The reason of this discrepancy is the lower pipe uplift determined with the numerical simulation than the uplift measured during the experiment, so that lead to a higher soil resistance and hence a higher pipe deformation of the numerical model. Despite this, differences in results are negligible and numerical analyses are conservative.

© *Giacomo Fenza 2015*

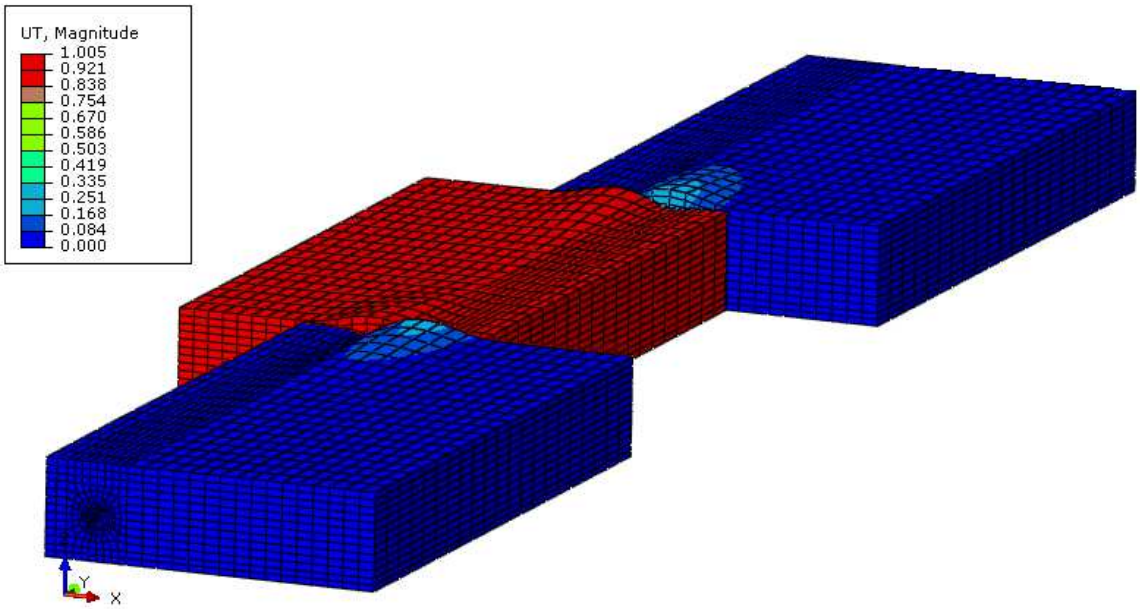

Fig. 167. Landslide/fault finite element model - soil deformation. Sliding caisson displacement equal to 1000 mm. Simulation of Test No. 7.

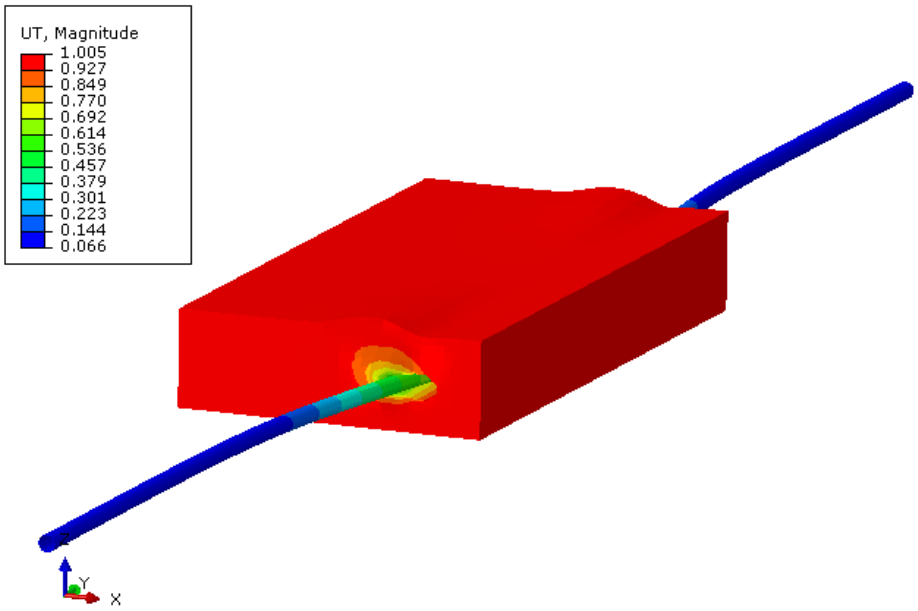

Fig. 168. Landslide/fault finite element model - pipe and middle soil prism deformation. Sliding caisson displacement equal to 1000 mm. Simulation of Test No. 7.

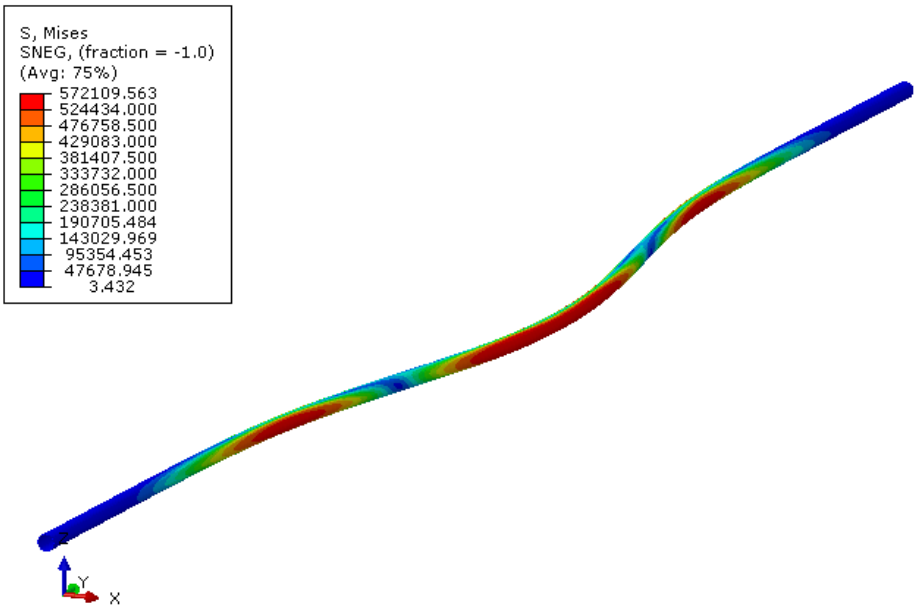

Fig. 169. Landslide/fault finite element model - pipeline stress distribution. Sliding caisson displacement equal to 1000 mm. Simulation of Test No. 7.

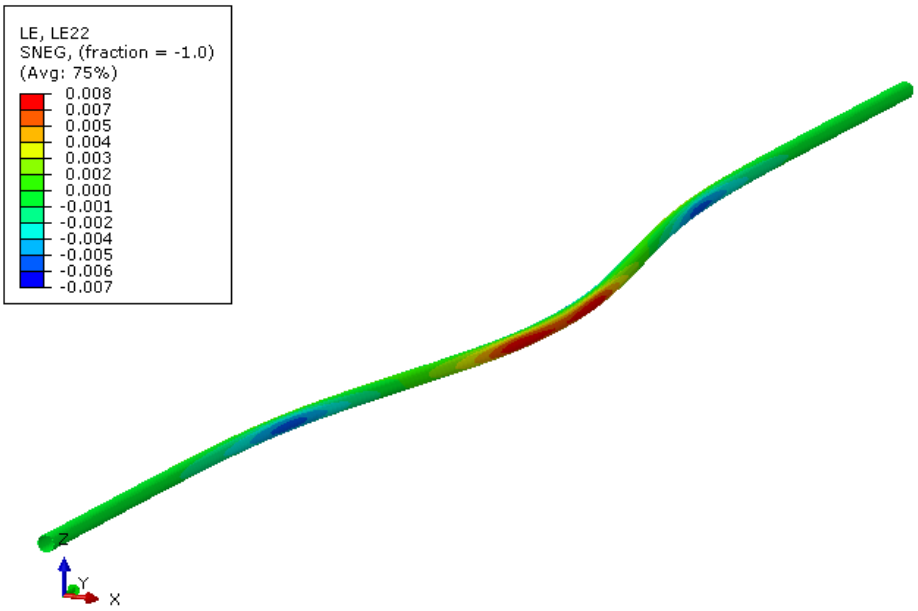

Fig. 170. Landslide/fault finite element model - pipeline longitudinal strain distribution. Sliding caisson displacement equal to 1000 mm. Simulation of Test No. 7.

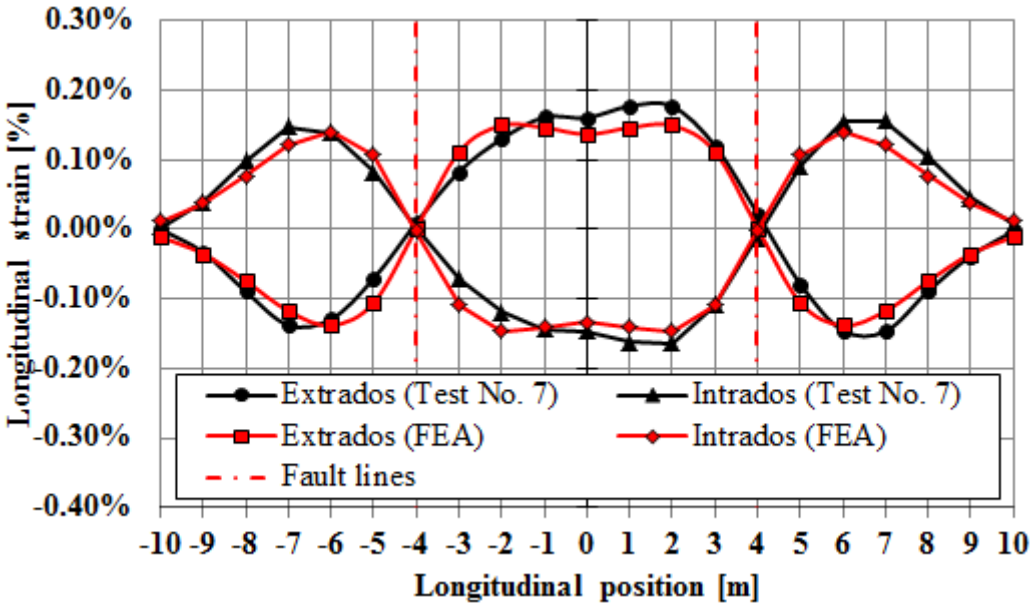

Fig. 171. Distribution of strains along pipe for 200 mm central caisson displacement, Test No. 7.

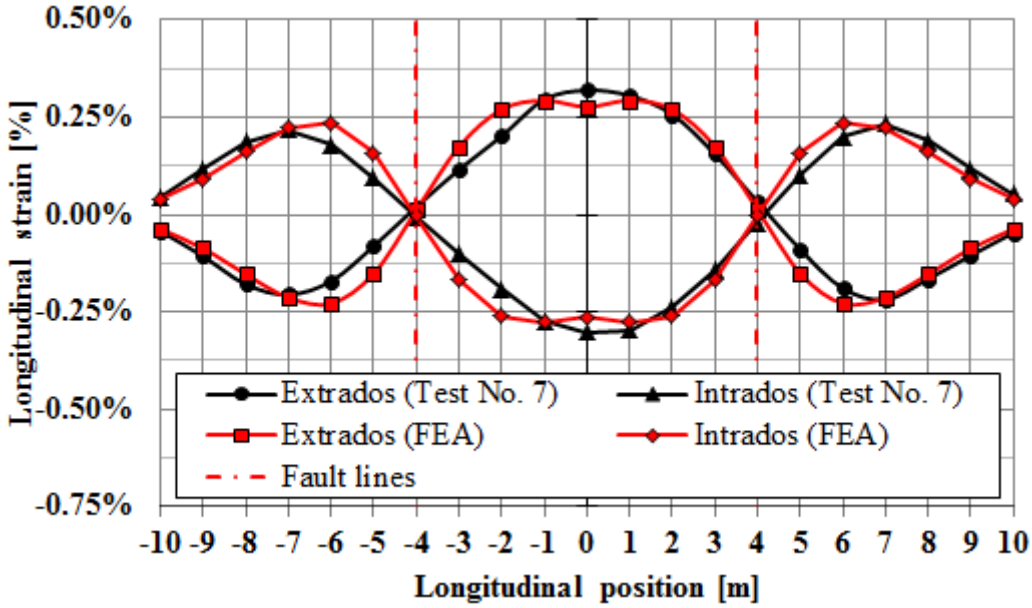

Fig. 172. Distribution of strains along pipe for 400 mm central caisson displacement, Test No. 7.

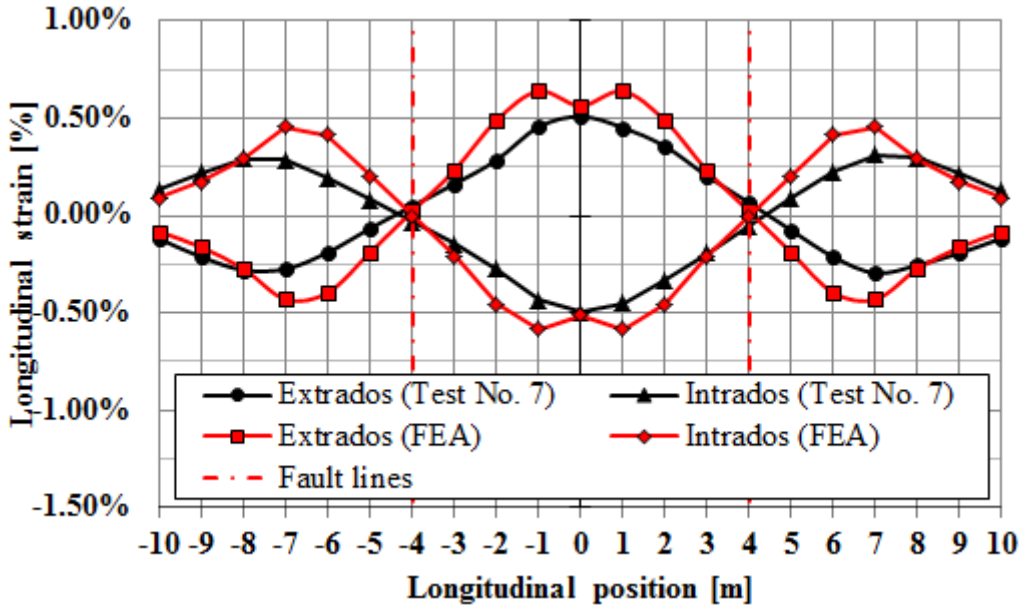

Fig. 173. Distribution of strains along pipe for 800 mm central caisson displacement, Test No. 7.

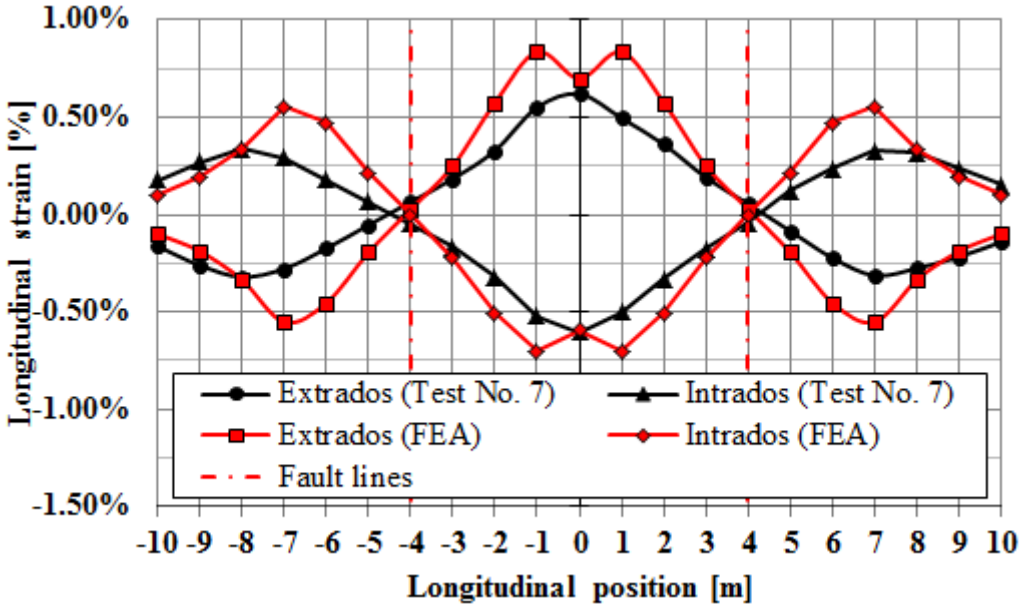

Fig. 174. Distribution of strains along pipe for 1000 mm central caisson displacement, Test No. 7.

Comparison between experimental and numerical pipe end shortening is depicted in Fig. 175, showing a divergence after 500 mm of caisson displacement leading to a slightly difference after this point. This behavior confirm that the numerical model is more severe that experimental.

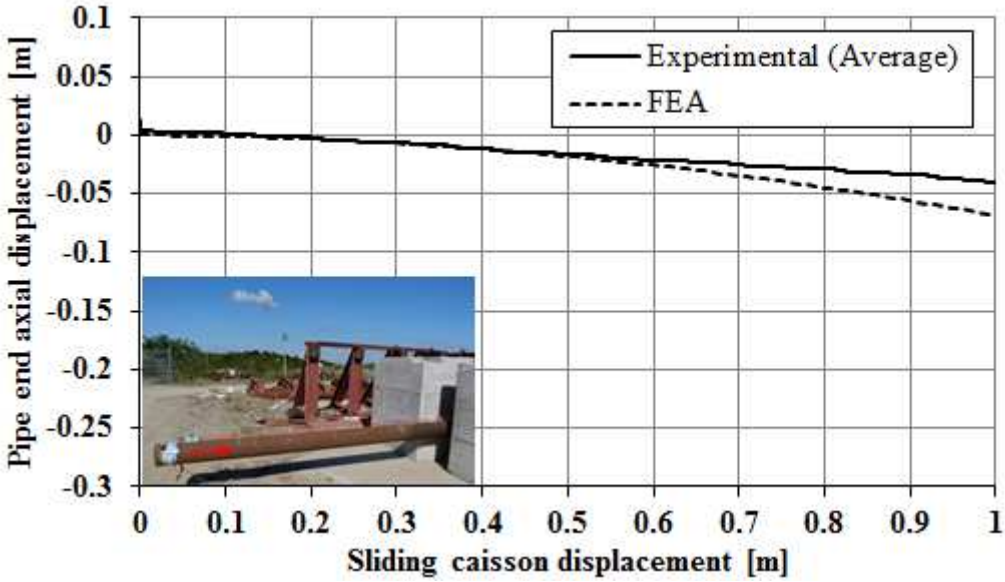

Fig. 175. Pipe ends shortening vs central caisson displacement. Comparison between experimental and numerical results. Test No. 7.

6.4.2. Landslide/fault model of Test No. 8

Relative density measured in the experimental Test No. 8 was 29%, also in this case the coefficient of lateral pressure was assumed equal to 1. Pipe internal pressure in this test was 11.4 MPa.

Fig. 176 and Fig. 177 shows the soil deformation of the finite element model for a caisson displacement of 1000 mm in which surface heaving and depression are in agreement with the experimental result. Fig. 178 and Fig. 179 present pipe stress and longitudinal strain distribution respectively for 1000 mm of central caisson displacement, showing a maximum von Mises stress value equal to 586 MPa and a maximum strain value of 0.9%, highest stress and strain distribution are concentrated at two meters from the middle section and

at around three meters from the fault lines towards pipe ends. No local buckling or tearing rupture can be observed also in this case.

Comparison between experimental data and numerical results of longitudinal strain distribution is presented for several steps from Fig. 180 to Fig. 183. At 200 mm of caisson displacement extrados strains of numerical model are slightly lower than measured strains, on the other hand intrados strains of numerical model are slightly higher than those measured. At 400 mm of caisson displacement numerical and experimental extrados strains are in good agreement, while numerical intrados strains are slightly higher than those measured. From 800 mm of caisson displacement strains of numerical model start to be significantly higher than experimental measurement at intrados line as shown in Fig. 182. At 1000 mm of displacement (Fig. 183) also numerical strains at extrados line start to concentrate the divergence respect measured strains at around two meters from the middle section and at around three meters from the fault lines towards pipe ends. The reason of this discrepancy is the lower pipe uplift determined with the numerical simulation than the uplift measured during the experiment, so that lead to a higher soil resistance and hence a higher pipe deformation of the numerical model. Moreover properties of soil used in the numerical model are the same used in the previous model although relative density achieved during the preparation of the Test No. 8 was lower than that reached during Test No.7.

© *Giacomo Fenza 2015*

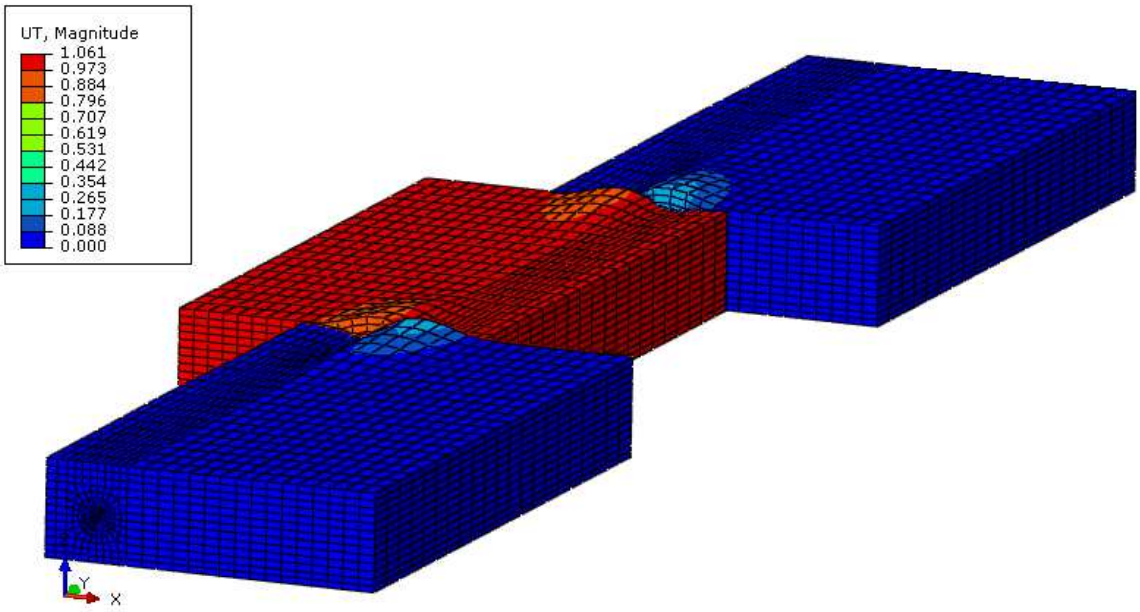

Fig. 176. Landslide/fault finite element model - soil deformation. Sliding caisson displacement equal to 1000 mm. Simulation of Test No. 8.

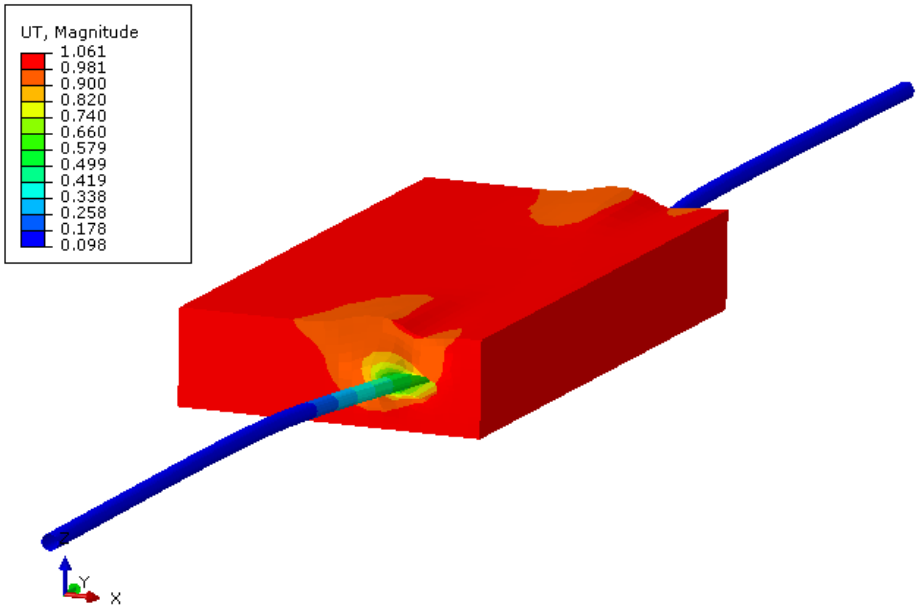

Fig. 177. Landslide/fault finite element model - pipe and middle soil prism deformation. Sliding caisson displacement equal to 1000 mm. Simulation of Test No. 8.

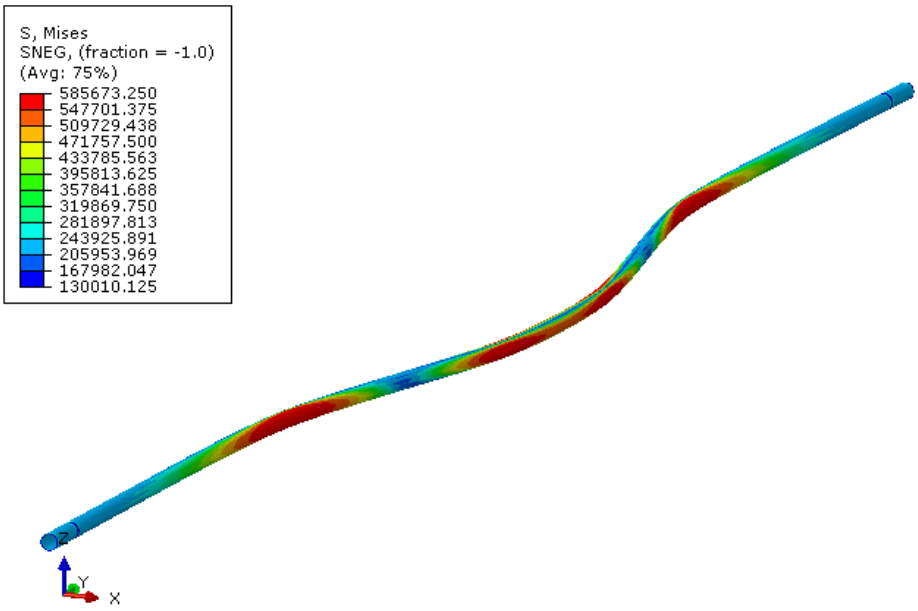

Fig. 178. Landslide/fault finite element model - pipeline stress distribution. Sliding caisson displacement equal to 1000 mm. Simulation of Test No. 8.

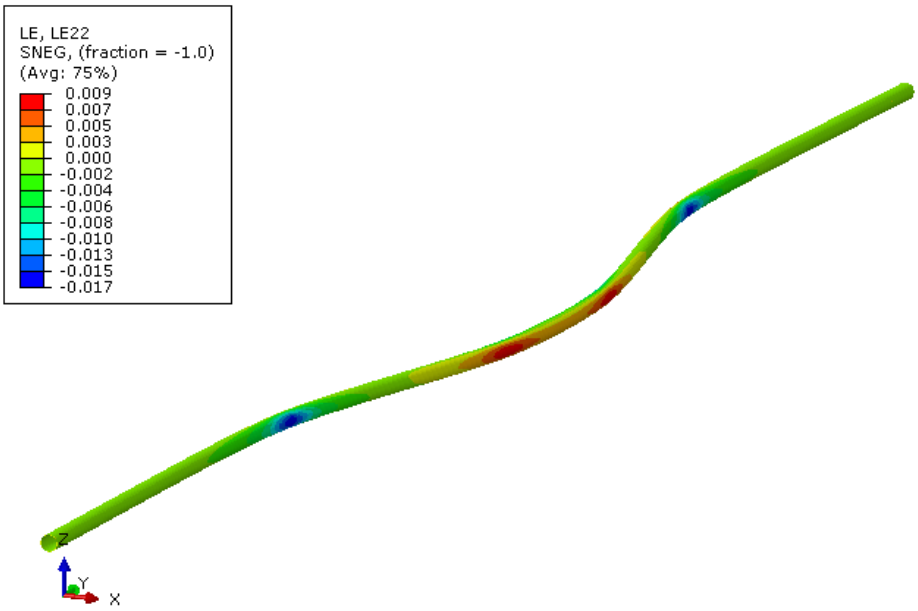

Fig. 179. Landslide/fault finite element model - pipeline longitudinal strain distribution. Sliding caisson displacement equal to 1000 mm. Simulation of Test No. 8.

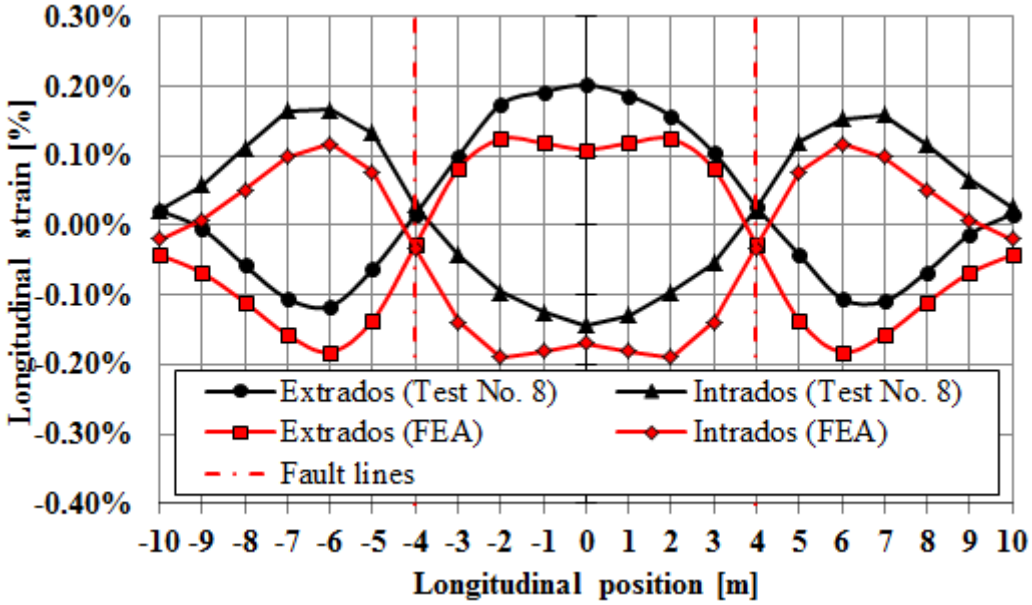

Fig. 180. Distribution of strains along pipe for 200 mm central caisson displacement, Test No. 8.

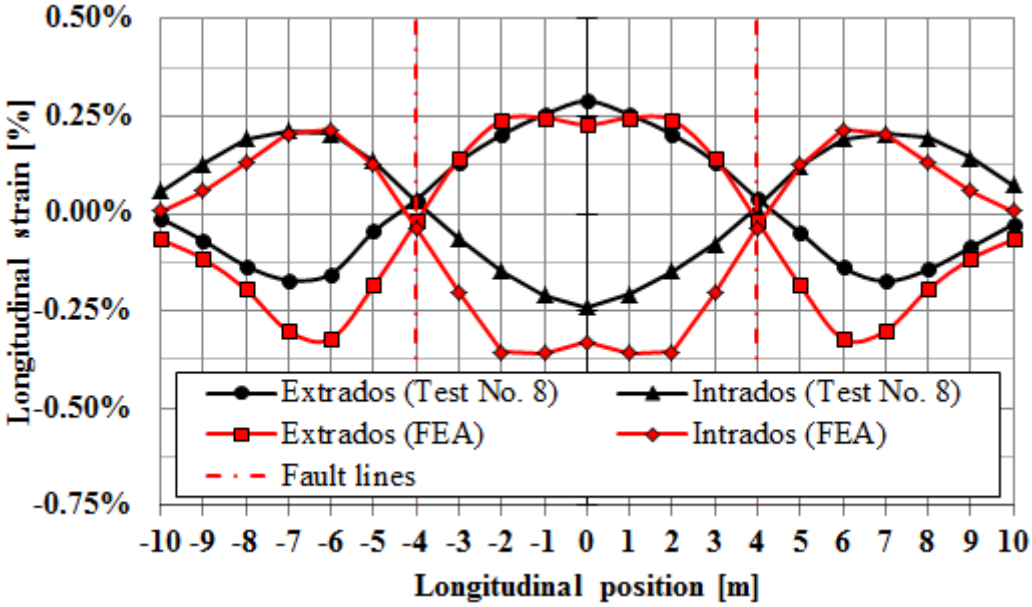

Fig. 181. Distribution of strains along pipe for 400 mm central caisson displacement, Test No. 8.

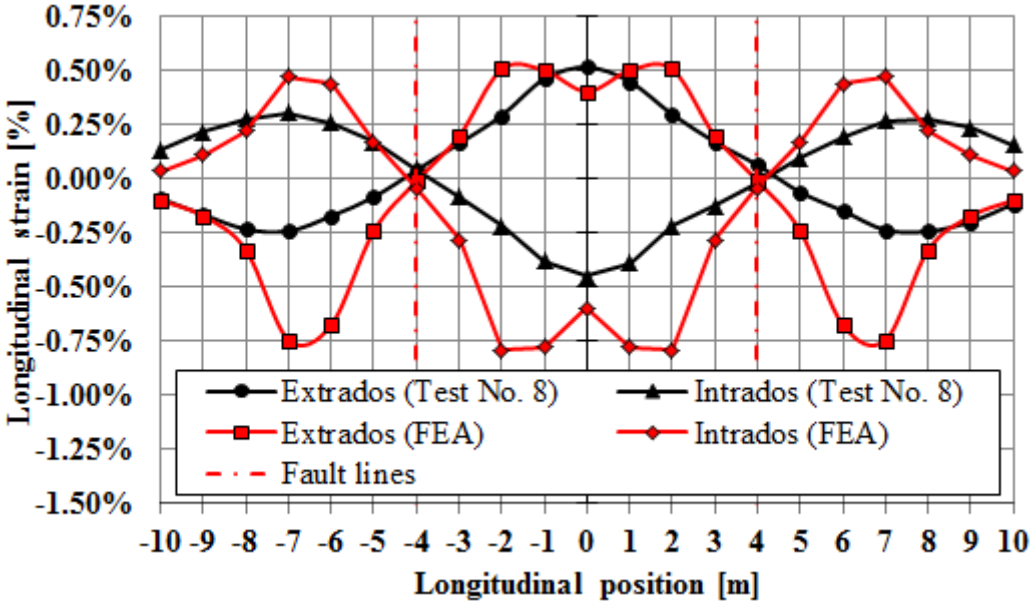

Fig. 182. Distribution of strains along pipe for 800 mm central caisson displacement, Test No. 8.

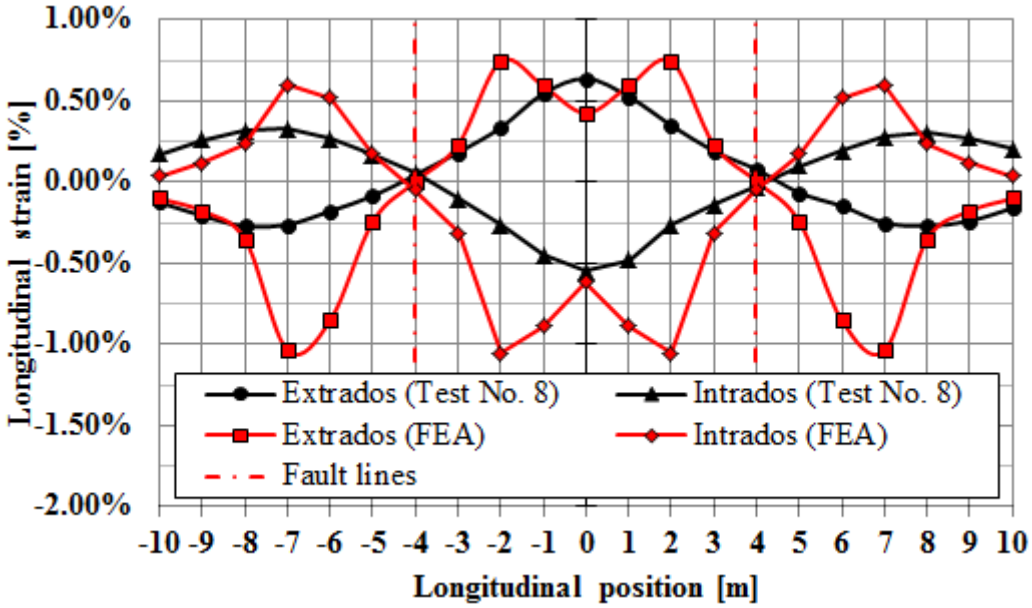

Fig. 183. Distribution of strains along pipe for 1000 mm central caisson displacement, Test No. 8.

Comparison between experimental and numerical pipe end shortening is depicted in Fig. 184, showing a divergence after 350 mm of caisson displacement leading to a sensitive difference reaching 50 mm of difference at 1000 mm of caisson displacement.

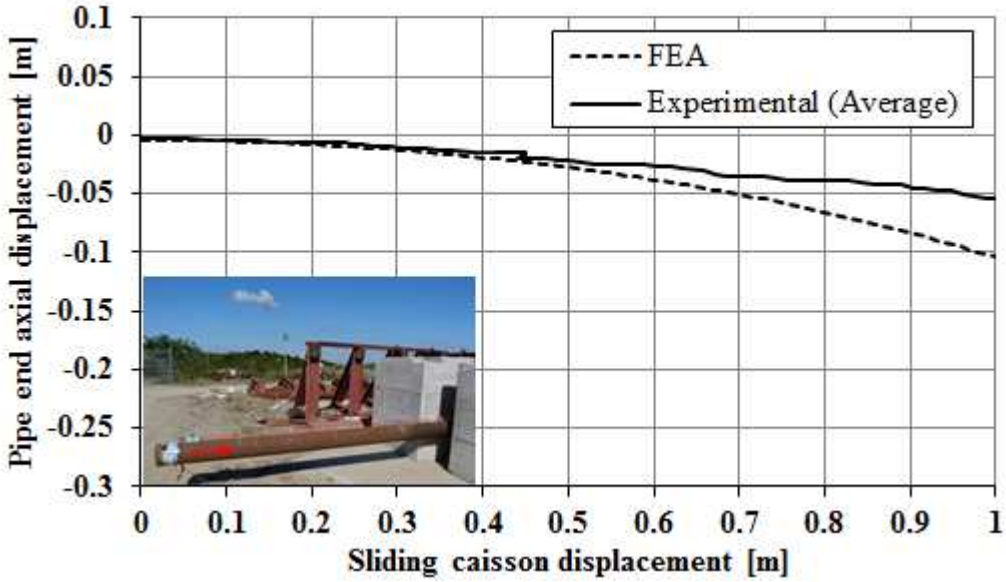

Fig. 184. Pipe ends shortening vs central caisson displacement. Comparison between experimental and numerical results. Test No. 8.

6.4.3. Discussion of results

Full-scale tests performed didn't show any kind of rupture such as buckling or tearing. Loads applied from soil have been able to bend the pipe over elastic strains reaching maximum values nearly 1.5% at the middle section, after a soil mass offset of ~3600 mm. Moreover a cross section ovalization with a maximum value of 2.1%.

In all tests the most critical part of the pipeline in terms of strain was the middle section while low strains were detected close to the fault lines.

Larger strains were measured in tests with the highest level of relative density tested that was around 40%.

Strain levels reached during tests have been compared with several equations present in literature i.e. DNV-OS- F101 [1[9], API RP 1111 [3] and Gresnigt [10] for unpressurized cases:

(Eq. 16) **DNV:** $\boldsymbol{\varepsilon_c = 0.78\left(\frac{WT}{OD} - 0.01\right)\frac{\alpha_{gw}}{\alpha_h^{1.5}}}$

Where α_{gw} = 0.8 (girth weld factor) and α_h = 0.93 (maximum Yield strength to Tensile strength ratio of the steel)

(Eq. 17) **API:** $\boldsymbol{\varepsilon_C = 0.5\left(\frac{WT}{OD}\right)}$

(Eq. 18) **Gresnigt:** $\boldsymbol{\varepsilon_C = 0.5\left(\frac{WT}{OD}\right) - 0.0025}$

In the current case aforementioned formulas give the following values:

- DNV ε_c = 1.07%
- API ε_c = 1.27%
- Gresnigt ε_c = 1.02%

Despite these predictions no local buckling were observed neither in experimental tests nor in the numerical analyses. Pressure tends to contrast the ovalization hence to oppose buckling, increasing the threshold of critical strain higher than the case without internal pressure. Experiments did not undergo on buckling, so that did not permitted to appreciate the effect of pressure.

General experimental findings show from strain plots that upon reaching a certain displacement the strain growth rate reduces almost to zero, a condition that can be associated

to the maximum soil force applied on pipe during relative displacement. Under these conditions the pipe starts to move through the soil.

As result of soil movement applied on the specimen, pipe deformed laterally and subjected to uplift, reaching the maximum vertical displacement at middle section (~650 mm) and zero at constrained pipe ends. These results are consistent with the vertical reaction measured by means pressure sensors sheet wrapped around the pipe in lateral tests.

Axial pipe ends displacement was also measured as consequence of pipe deflection.

Numerical analyses of landslide/fault testing demonstrate a general agreement with experimental findings but it can be observed a more severe action of the soil on the pipe during the entire relative displacement because the low pipe uplift measured undergo the pipe to interact with a more stiff soil, hence a bigger pipe deflection.

Numerical model can be considered reliable and with a slight conservative prediction.

7. Summary and conclusions

The aim of this thesis was to study the response of buried steel pipes subjected to horizontal ground movements. The work has been carried out including experimental full-scale testing, numerical analysis for the investigation and evaluation of the response of embedded pipeline in sand under relative ground movements.

The most of research conducted in this field concern lateral soil pipe interaction conducted with small relative displacement and with relatively small diameter pipelines. Besides axial soil pipe interaction experiments published in literature are just few despite the complexity of such relative movement needs a better understanding of the mechanism interactions at pipe soil interface.

For the reasons mentioned above soil testing facilities have been designed and assembled. The first one is able to subject pipes under large axial or lateral displacement whereas the second one is able to expose a pipeline to a landslide/fault movement.

Numerical models were developed in order to simulate axial, lateral and landslide/fault full-scale testing. A finite element software, ABAQUS 6.14, has been used in this study. Parameters to characterize the soil used in the numerical models were obtained from geotechnical laboratory testing.

The steps followed during the work may be summarized in:

- Development of a facility able to perform both axial and lateral full-scale testing on 8”$^{5/8}$ pipe diameter.

- Development of a facility composed by three caissons able to expose the pipeline under a landslide/fault phenomenon.
- Measurement of pressure distribution at pipe soil interface during lateral full-scale tests.
- Longitudinal strain measurements at extrados and intrados line during landslide/fault testing.
- Development of numerical models to simulate the response of buried pipes subjected to axial, lateral displacement and landslide/fault phenomenon.
- Evaluation of different levels of soil compaction, pipe coating and internal pipe pressure.
- Evaluation of analytical equation suggested from current guidelines used to predict axial and lateral soil resistance for design of pipeline laid in areas subjected to permanent ground deformations.

7.1. Full-scale testing facilities

The first test facility consist of a 3 m length, 3 m width, 1.25 m high (internal dimensions) placed within a rigid steel frame equipped with a hydraulic actuator of 25000 kN load capacity. This caisson allow to change the configuration to conduct axial soil pipe interaction and lateral soil pipe interaction.

The second test facility consist of three caissons: two fixed having 8.35 m length, 4.35 m width, 1.50 m high (internal dimensions) and one central caisson having 8 m length, 4 m width, 1.35 m high (internal dimensions) placed on a horizontal concrete basement. Two hydraulic actuator of 4000 kN load capacity (each one) have been used.

Steel pipes having 8"$^{5/8}$ outside diameter and 5.56 mm wall thickness have been used in each test.

The measurements during experimental testing included load and displacement of each actuator, pressure distribution at soil-pipe interface during lateral pullout testing, longitudinal strain during landslide/fault testing. Observation of soil surface deformation has been carried out using cameras.

Density of quarry sand was controlled through a dynamic cone penetrometer during soil filling and compaction. The overburden ratio for axial and lateral testing was taken equal to 3.4, and 3.1 for landslide fault testing.

The tests were conducted to simulate: embedded bare pipes in sand and embedded coated pipes. On the whole three axial tests, three lateral tests and four landslide /fault tests have been performed using the aforementioned facilities.

7.2. Axial pullout findings

A considerable difference in axial soil resistance was measured considering the first test conducted with $D_r \approx 20\%$ and the second test conducted with $D_r \approx 40\%$. Whereas a slightly difference in peak soil resistance was detected changing the pipe coating and maintaining the same relative density although the frictional degradation led to a different axial soil resistance decreasing.

The variation of speed from 0.5 mm/s to 2 mm/s did not result in an appreciable increase or decrease of soil reaction.

Axial soil resistance measured during experimental tests are compared with peak soil resistance predicted from current guidelines (ASCE [1] and PRCI [20]). The ASCE formula cannot predict satisfactory the peak axial soil load giving a value ~0.5 times less than the

experimental result obtained with relative density of soil equal to ~20% and ~0.33 times less than the experimental results obtained with relative density of soil equal to ~40% for both external surface finish. The PRCI formula is able to predict the peak axial soil load using a value of K equal to 1.6 for test with $D_r \approx 20\%$ and 2.8 for tests with $D_r \approx 40\%$.

A three dimensional numerical model was developed in order to simulate the experimental axial full-scale tests using soil strength parameters determined during geotechnical laboratory tests. The effect of soil dilation has been observed and values of K determined numerically are close to those back calculated with PRCI formula. From the numerical analysis it can be seen that the annular sand zone around the pipe is subjected to an increasing of normal stress at the pipe soil interface during pipe axial displacement as results of soil dilation and annular soil confinement. This soil behavior is responsible of an extra axial soil reaction respect to a non-dilative sand and it is a confirmation of experimental stress measurements conducted by Karimian [13] [32].

The developed model is able to predict the axial soil resistance up to the peak of load, afterward become constant instead of follow the same decreasing of soil reaction measured experimentally. Numerical model can be considered reliable and with a slight conservative prediction.

7.3. Lateral pulling findings

A negligible difference in lateral soil resistance was detected during the three lateral pullout tests performed although two levels of soil compaction ($D_r \approx 20\%$ and $D_r \approx 40\%$) and two different pipe coating (antioxidant paint and fusion bonded epoxy) have been tested.

The variation of speed from 0.5 mm/s to 1 mm/s did not result in an appreciable increase or decrease of soil reaction.

Lateral soil resistances measured during experimental tests are compared with the peak soil resistance predicted through current guidelines (ASCE [1] and PRCI [20]). Although the pipe vertical uplift was constrained in the experiments and aforementioned guidelines suggest a formula for pipes free to rise during horizontal lateral movements of surrounding soil, the comparison allow doing some remarks. Peak soil reaction predicted through PRCI formula coincide with the first peak soil reaction measured, that is the maximum soil resistance of a pipe in the same condition tested herein but without vertical constrain. This affirmation is confirmed by the distribution of pressure at pipe soil interface measured during each test and also with numerical analyses. Peak soil reaction predicted through ASCE formula is double respect the value predicted with PRCI formula and compared with the experimental results seems to reach a value too high.

Pipe soil interface pressure measured with the Tekscan 3150E sensor shows an increase of pressure distribution and a clockwise rotation of the resultant pressure starting from +45° and reaching -45°considering a pipe cross section with the crown positioned at 90° respect a horizontal plane.

A two dimensional numerical model was developed in order to simulate the experimental lateral full-scale tests using soil strength parameters determined during geotechnical laboratory tests. The model is able to predict the lateral soil resistance with a remarkable precision up to 300/350 mm of pipe displacement.

7.4. Landslide/fault findings

Two levels of soil relative density (~20% and ~40%) have been tested both for unpressurized and pressurized pipes during landslide/fault testing.

Soil loads applied through the central caisson displacement were able to produce inelastic bending deflection and a slightly cross section ovalization of the pipe but not any ruptures. No buckling was detected despite higher level of strains reached during tests than critical strains predicted by formulae for local buckling prognostication.

In all these tests the most critical portion of the pipe in terms of maximum strain is located at the middle length section and the smallest value of strain is located at the section close to the fault line.

As a result of the four full-scale tests performed, the increasing of soil compaction from the lowest to the highest level tested led to an appreciable increasing of longitudinal strain if we consider the same offset of the central caisson. Moreover tests conducted with pressurized pipes respect to unpressurized pipes present a lower level of longitudinal strains considering the same level of soil compaction and the same central caisson offset.

A three dimensional numerical model was developed in order to simulate the experimental landslide/fault tests using soil strength parameters and tensile mechanical properties of the steel pipe determined through laboratory tests. Numerical analyses have shown a general agreement with experimental findings but with a more severe soil load on the pipe during the caisson displacement since the small pipe uplift simulated undergo the pipe to interact with a stiffer soil than the shallower soil.

Developed numerical model can be considered reliable and with a slight conservative prediction.

7.5. Recommendations for future research

Further research to understand the complex behavior of the pipeline soil system involved in permanent ground deformations would be necessary.

- Additional longitudinal full-scale tests would be indispensable to determine the evolution of the frictional degradation after the peak soil resistance in relation to: the soil dilation angle, the soil relative density, the pipe surface finish and the pipe outside diameter.

- Determine lateral earth pressure evolution at pipe soil interface during axial pipe displacement in longitudinal full-scale tests in relation to: the dilation angle of the soil, relative density of the soil, surface finish of the pipe and pipe outside diameter. A range of lateral earth pressure values for different operating conditions would be a good contribution for the reliability of numerical and analytical calculations.

- Additional full-scale landslide/fault tests in order to assess more severe condition of pipe soil interaction, increasing the level of soil relative density respect the maximum value reached in this study.

References

[1] ABAQUS. Users' Manual. Simulia, Providence, RI, USA; 2014.

[2] Anastasopoulos, I., Gazetas, G., Bransby, M. F., Davies, M. C. R., El Nahas, A. (2007) Fault Rupture Propagation through Sand: Finite-Element Analysis and Validation through Centrifuge Experiments, Journal Of Geotechnical And Geoenvironmental Engineering., 133 (8): 943–958.

[3] API RP 1111 (1999) "Design, Construction, Operation, and Maintenance of Offshore Hydrocarbon Pipelines (Limit State Design)", American Petroleum Institute.

[4] ASCE, (1984) "Guidelines for the seismic design of oil and gas pipeline systems." Committee on Gas and Liquid Fuel Lifelines, ASCE, New York.

[5] American Lifelines Alliance, (July 2001), Guidelines for the Design of Buried Steel Pipe, ASCE.

[6] Audibert, J. M. E. and Nyman, K. J. (1975), Coefficient of subgrade reaction for the design of buried piping. Proceedings, 2nd Specialty Conference on Structural Design of Nuclear Plant Facilities, ASCE, Vol. IA, 109-141.

[7] Da Ha, Abdoun, T.H., O'Rourke, M.J., Symans M.D., O'Rourke, T.D, Michael C. Palmer; and Harry E. Stewart (2008), Buried high-density polyethylene pipelines subjected to normal and strike-slip faulting - a centrifuge investigation, Can. Geotech. J. 45: 1733–1742 (2008).

[8] Da Ha, Abdoun, T.H., O'Rourke, M.J., Symans M.D., O'Rourke, T.D, Michael C. Palmer; and Harry E. Stewart (2008), Centrifuge modelling of earthquake effects on buried

high-density polyethylene (HDPE) pipelines crossing fault zones. Journal of geotechnical and geoenvironmental engineering, ASCE, October 2008, 134(10) 1501-1515.

[9] Det Norske Veritas (DNV), 2013, "Submarine Pipeline Systems", DNV Offshore Standard, DNV-OS-F101.

[10] Gresnigt, A.M. (1986) "Plastic Design of Buried Pipelines in Settlement Areas" HERON, Volume 31, No 4.

[11] Japan Gas Association: Recommended Practice for Earthquake Resistant Design of High Pressure Gas Pipelines, Japan Gas Association, Tokyo, Japan, 2000.

[12] Jung, J.K., O'Rourke, T.D., and Olson, N.A. (2013), Lateral soil-pipe interaction in dry and partially saturated sand. Journal of geotechnical and geoenvironmental engineering, Vol. 139, No. 12, December 1, 2013.

[13] Karimian, H. (2006) Response of buried steel pipelines subjected to longitudinal and transverse ground movement. Ph.D. thesis, Department of Civil Engineering, The University of British Columbia, Vancouver, B.C.

[14] Luo, S. Q., Tan, S. A. and Yong, K. Y. (2000) Pull–out resistance mechanism of a soil nail reinforcement in dilative soils, Soils and Foundations,40 (1): 47-56.

[15] Mohammadi, S.D., Nikoudel, M.R., Rahimi, H., Khamehchiyan, M. (2008), Application of the Dynamic Cone Penetrometer (DCP) for determination of the engineering parameters of sandy soils, Engineering Geology, 195–203.

[16] Oversen, N. K., and Strømann, H. (1972) Design method for vertical anchor slabs in sand. Proc., Specialty Conf. on Performance of Earth and Earth-Supported Structures, ASCE, New York, Vol. 1, 1481–1500.

[17] O' Rourke, T. D., (1998). An Overview of Geotechnical and Lifeline Earthquake Engineering. Geotechnical Special Publication No. 75, ASCE, Pakoulis, P., Yegian, M. and D. Holtz, Eds, Reston, VA, 1998, II, 1392-1426.

[18] O'Rourke, T.D., Jezerski, J. M., Olson, N. A., Bonneau, A.L., Palmer, M.C., Stewart, H.E., O'Rourke, M. J., and Abdoun, T., (2008), Geotechnics of pipeline system response to earthquakes, Proceedings of Geotechnical Earthquake Engineering and Soil Dynamics IV, May.

[19] Paulin, M.J., Phillips, R., Clark, J.L, Trigg, A. and Konuk, I. (1998), A full-scale investigation into pipeline/soil interaction, Proceedings, International Pipeline Conference, Calgary, AB , ASME, 779-788.

[20] Pipeline Research Council International, (January 2009), Guidelines for constructing natural gas and liquid hydrocarbon pipelines through areas prone to landslide and subsidence hazards, Prepared by: C-CORE, D.G. Honegger Consulting, SSD, Inc.

[21] Randolph, M. F., Dolwin, J. and Beck, R. D. (1994) Design of driven piles in sand, Géotechnique, 44 (3): 427–448.

[22] Shibuya, S., Mitachi, T., and Tamate, S. (1997), Interpretation of direct shear box testing of sands as quasisimple shear." Geotechnique, 47(4), 769–790.

[23] O'Rourke, T. D., Stewart, H.E., Palmer, M.C. Bond , T.K., Jezerski, J.M., O'Rourke, M.J., Symans, M.D, Abdoun, T., Ha, D. (2008), NEESR-SG Final Report, Prepared by Cornell University, Rensselaer Polytechnic Institute and The Sciencenter Discovery Center.

[24] Trautmann, C. H., and O'Rourke, T. D. (1983) Behaviour of pipe in dry sand under lateral and uplift loading, Geotechnical Engineering Report 83-7, Cornell University, Ithaca, N.Y.

[25] Trautmann, C. H., and O'Rourke, T. D. (1985) Lateral force–displacement response of buried pipe. J. Geotech. Eng., 111(9) 1077–1092.

[26] Trautmann, C. H., O'Rourke, T. D., and Kulhawy, F. H. (1985). Uplift force–displacement response of buried pipe. J. Geotech. Eng., 111(9), 1061–1076.

[27] Vazouras, P., Karamanos, S., A., Dakoulas, P. (2010). Finite element analysis of buried steel pipelines under strike-slip fault displacements. Soil Dynamics and Earthquake Engineering 30 (2010) 1361–1376.

[28] Vazouras, P., Karamanos, S., A., Dakoulas, P. (2012). Mechanical behavior of buried steel pipes crossing active strike-slip faults. Soil Dynamics and Earthquake Engineering 41 (2012) 164–180.

[29] Vazouras, P., Dakoulas, P., Karamanos, S., A. (2015). Pipe–soil interaction and pipeline performance under strike–slip fault movements. Soil Dynamics and Earthquake Engineering 72 (2015) 48–65.

[30] Weerasekara, L. and Wijewickreme, D. (2008) Mobilization of soil loads on polyethylene natural gas pipelines subject to relative axial ground displacements, Canadian Geotechnical Journal, 45 (9):1237-1249.

[31] White, D. J. and Lehane, B. M. (2004) Friction fatigue on displacement piles in sand, Geotechnique, 54 (10): 645-658.

[32] Wijewickreme, D., Karimian, H., and Honegger, D., 2008, Response of buried steel pipelines subject to relative axial loading, Canadian Geotechnical Journal, in press.

[33] Zeghal, M. and Edil, T.B. (2002) Soil structure interaction analysis: Modeling the interface, Canadian Geotechnical Journal, 39 (3): 620–628.

[34] Yimsiri, S., Soga, K., Yoshizaki, K., Dasari, G. R. and O'Rourke, T. D. (2004), Lateral and upward soil-pipeline interactions in sand for deep embedment conditions. Journal

of Geotechnical and Geoenvironmental Engineering, Vol. 130, No. 8, August 1, 2004. ©ASCE, ISSN 1090-0241/2004/8-830.

[35] Yoshizaki, K., Hamada, M. and O'Rourke, T. D., (1999). Large Deformation Behavior of Pipelines with Elbows, Proceedings, 5th U.S. Conference on Lifeline Earthquake Engineering, ASCE, Reston, VA.

[36] Yoshizaki, K., Hosokawa, N., Ando, H., Oguchi, N., Sogabe, K. and Hamada, M., (1999). Deformation behaviour of buried pipelines with elbows subjected to large ground deformation, Journal of Structural Mechanics and Earthquake Engineering, JSCE, No. 626/I-48, pp. 173-184. 1999.

[37] Yoshizaki, K., O'Rourke, T. D. and Hamada, M.,(2001). Large Deformation Behavior of Buried Pipelines with Low-angle Elbows Subjected to Permanent Ground Deformation, Journal of Structural Mechanics and Earthquake Engineering, Vol. 18, No. 1, No. 675/I-55, pp. 41-52.

[38] Yoshizaki, K., O'Rourke, T., D. and Hamada, M., (2003), Large scale experiments of buried steel pipelines with elbows subjected to permanent ground deformation. Journal of structural mechanics and earthquake engineering, JSCE, Vol. 20, No. 1, No. 724/I-62, 1-11.

[39] http://www.yourdictionary.com/fault